

**SUPPORTED METAL CATALYSTS
FOR THE PRODUCTION OF
CHEMICAL PRECURSORS**

Thesis submitted in accordance with the requirements of Cardiff
University for the degree of Doctor of Philosophy

James Hayward

2013

Abstract

Supported metal catalysts have applications across a broad range of industrial processes. The metal species are often the active catalysts in these processes, but supporting these materials upon a different material can produce desirable characteristics in the overall catalyst. These effects can include, but are not limited to, increased dispersion of active material, increased stability of the active material, and, depending on the supporting material, beneficial metal-support interactions can be generated.

The production of benzaldehyde from benzyl alcohol is a reaction with high commercial value. Gold-palladium catalysts have been shown to be effective at production of benzaldehyde from benzyl alcohol under relatively mild, solvent-free conditions. It has also been shown that the selectivity of this reaction is dependent upon the acidic or basic character of the support material.

Perovskites are a class of highly stable minerals with a general formula of ABO_3 , with A being a cation with a larger ionic radius than B. The acidic and basic character of a perovskite is strongly determined by the nature of the A cation, which allows for the possibility of adjusting this character by metal substitution. This study investigates the effects of gradual substitution of lanthanum for strontium in vanadate perovskites, and showed that incorporation of the substituted metal is effective up to a certain point, beyond which the material switches to two separate perovskite phases. The substitution of the metal ions was shown to have an effect on the acidic and basic properties of the perovskite materials using the Isopropyl Alcohol (IPA) reaction, which forms different products on acidic or basic sites.

Following this, substitution with a wider range of group II metals was investigated and tested, both in the IPA reaction and as supports for precious metals in the production of benzaldehyde.

A separate series of investigations were performed on Fischer-Tropsch (FT) catalysts. Fischer-Tropsch is a name given to a wide range of catalytic processes involving the production of hydrocarbons from a mixture of carbon monoxide and hydrogen, known as syngas. The formation of products is generally believed to proceed through a chain-lengthening process using single-carbon units. This leads to a broad distribution of products

as opposed to a single highly selective product, and the selectivity pattern is often described using the Shulz-Florey-Anderson distribution. Much of the work on FT catalysts is involved in modifications of the catalyst system to produce a tighter distribution of products.

In this study a series of investigations have been made into the effects that variations of the preparation method of CoMnO_x supported on activated carbon. The basic preparation is an impregnation method, and several changes in catalyst activity and selectivity were observed following changes to this. An investigation into the effects of altering the amount of manganese relative to cobalt in the system also highlighted several trends, leading to a greater understanding of the factors affecting the conversion and selectivity of the catalyst system.

A separate area of research in FT-style reactions is the production of alcohols from syngas, typically at higher pressures. As in the previous section, an attempt was made to improve the activity and selectivity of these catalysts by alterations to the preparation methods, and also by alteration of the amount of secondary metal relative to cobalt. The catalysts used in these investigations consisted of CoMoO_x supported on activated carbon. The standard preparation used a coprecipitation method based upon a similar method used for the production of CoMoS_2 catalysts, which were also investigated in this study. Later investigations, notably those in which the amount of molybdenum relative to cobalt was altered, were prepared using an impregnation method.

A series of improvements to a base catalyst were achieved by alteration to the preparation conditions, but more substantial improvements were observed when the alteration of the metal ratios was investigated.

With regards to the use of activated carbon as a support material, it was also observed that it was possible to bring about the reduction of the cobalt species, and to a lesser extent the manganese and molybdenum species, by heating the catalysts to a high temperature in an inert atmosphere, namely helium.

Acknowledgements

I would like to thank my Supervisor, Professor Graham Hutchings, for giving me the opportunity to conduct this work, and also for all his support and advice.

I would like to thank SABIC, and in particular Dr Khalid Karim, for providing both funding and direction in this project.

I would like to thank all the following CCI staff for their unending help, advice, guidance, and most importantly, patience:

Dr Stuart Taylor

Dr Jonathan Bartley

Dr Thomas Davies

Dr Albert Carley

Dr Nicholas Dummer

Dr Sankar Meenakshisundaram

Dr Sarwat Iqbal

Edwin N Ntainjua

I would like to thank all of the people in both the workshop and in stores, for keeping everything going. In particular, thanks to Steve Morris and Dr Thomas Davies (again), for fixing everything that ever broke.

Contents

Chapter 1: Introduction

| | | |
|--------|---|----|
| 1.1. | Aims of study | 1 |
| 1.2. | Heterogeneous catalysis | 3 |
| 1.3. | The Fischer-Tropsch Synthesis | 4 |
| 1.4. | Products of Fischer-Tropsch | 8 |
| 1.5. | Mechanism of Fischer-Tropsch | 11 |
| 1.6. | Catalytically active metals for Fischer-Tropsch | 16 |
| 1.6.1. | Cobalt for Fischer-Tropsch | 17 |
| 1.7. | Fischer-Tropsch for higher alcohols synthesis | 19 |
| 1.8. | References | 21 |

Chapter 2: Experimental

| | | |
|-------|---|----|
| 2.1 | Catalyst preparation | 24 |
| 2.1.1 | Fischer-Tropsch catalyst preparation | 25 |
| 2.1.2 | Alcohols catalyst preparation | 29 |
| 2.1.3 | Perovskite preparation | 32 |
| 2.2 | Product analysis | 33 |
| 2.2.1 | Gas chromatography | 33 |
| 2.3 | Catalyst testing | 37 |
| 2.4 | Catalyst characterisation | 38 |
| 2.4.1 | Brunauer, Emmett and Teller (BET) method surface area Measurements | 38 |
| 2.4.2 | X-Ray Diffraction (XRD) | 39 |
| 2.4.3 | Scanning Electron Microscopy (SEM) | 41 |

| | | |
|-------|--|----|
| 2.4.4 | Energy Dispersive X-Ray Spectroscopy (EDX) | 42 |
| 2.4.5 | Thermogravimetric Analysis (TGA) | 42 |
| 2.5 | References | 43 |

Chapter 3: Effect of preparation on Co-Mn Fischer-Tropsch catalysts

| | | |
|-------|---|-----|
| 3.1 | Introduction | 44 |
| 3.2 | Catalyst preparation | 45 |
| 3.3 | Preparation method variations | 46 |
| 3.3.1 | Variations in heat treatment temperature | 46 |
| 3.3.2 | Mechanical mixing of catalyst and support | 55 |
| 3.3.3 | Variation in heat treatment duration | 67 |
| 3.3.4 | Variations of drying step | 70 |
| 3.3.5 | Variations of reduction step | 79 |
| 3.4 | Variation of catalyst composition | 93 |
| 3.4.1 | Variation of metal-support ratio | 93 |
| 3.4.2 | Variation of cobalt-manganese ratio | 98 |
| 3.5 | References | 106 |

Chapter 4: Cobalt-molybdenum catalysts for the production of alcohols from syngas

| | | |
|-------|---|-----|
| 4.1 | Introduction | 108 |
| 4.2 | Preparation details | 109 |
| 4.3 | Reproduction of cobalt-molybdenum on activated carbon support | 110 |
| 4.3.1 | Previous results | 111 |
| 4.3.2 | Reproduction of CoMo/C produced by deposition precipitation | 112 |
| 4.3.3 | Reproduction of CoMo/C produced by impregnation | 113 |
| 4.4 | Reproduction of Co-MoS ₂ + 0.2% wt Cu | 131 |

| | | |
|-----|------------------------------------|-----|
| 4.5 | Variations of catalyst composition | 132 |
| 4.6 | References | 140 |

Chapter 5: Catalytic properties and support effects of perovskites

| | | |
|-------|---------------------------------|-----|
| 5.1 | Introduction | 141 |
| 5.2 | Preparation details | 144 |
| 5.3 | Isopropyl alcohol test reaction | 145 |
| 5.3.1 | Results and discussion | 146 |
| 5.4 | Benzyl alcohol oxidation | 166 |
| 5.4.1 | Results and discussion | 167 |
| 5.5 | Perovskites for Fischer-Tropsch | 177 |
| 5.6 | References | 178 |

Chapter 6: Conclusions and future work

| | | |
|-----|---------------------------------------|-----|
| 6.1 | CoMn for Fischer-Tropsch | 180 |
| 6.2 | CoMo for Alcohols production | 181 |
| 6.3 | Perovskites as catalysts and supports | 182 |

Chapter 1

Introduction

1.1 Aims of Study

The aim of this research project was to continue investigation into the development and testing of cobalt-based catalysts for the reaction of synthesis gas ('syngas').

The most common reaction involving syngas is the Fischer-Tropsch (FT) reaction, in which the syngas is converted into hydrocarbons of varying chain length by being passed over a metal catalyst. Different metals are active for FT at varying pressures and temperatures; Fe-based catalysts, for example, are active at pressures of between 7-30 bar, whereas Co or Ni

catalysts can operate at much lower pressures. They are, however, more susceptible to changes in temperature.

Despite the broad range of applicable metals, pressures and temperatures, a common theme throughout most of the catalysts is that of product distribution. Reactions synthesising hydrocarbons from syngas will not generally produce hydrocarbons of a single chain length; a mixture of products of broadly similar chain length will be observed. The distribution is generally assumed to be similar to that found in polymerisation reactions, where the probability of chain growth propagation and termination determines the average length of the chains produced.

Separation of the product mixture that results from these reactions is highly resource-intensive, and so catalysts capable of displaying high selectivity to a specific product (or at least a suitably narrow distribution of products) are greatly sought after. At the time of writing, the only product that can be produced with 100 % selectivity in FT reactions is CH₄, typically over Co or Ni catalysts at high temperatures.

However, methane has little value; it is in fact worth less than the syngas used to produce it. Alkenes of lower chain lengths (C₂ – C₄) are used as petrochemical feedstocks, and can be used to produce diesel. Alkanes are also useful; ethane and propane can be polymerised into plastics, and C₃ – C₄ alkanes are sold as fuels.

Medium-chain length hydrocarbon mixes can be added to petroleum to increase engine performance in cars, and long-chain hydrocarbon waxes can be cracked into more valuable products. However, the market for these products is considerably smaller and of less value than the short chain products.

The aim of this project, therefore, is synthesis of short-chain alkenes from synthesis gas. Work will also be conducted on the synthesis of short-chain primary alcohols from synthesis gas. The catalysts produced and developed continue on from the work of Hutchings *et. al.*¹⁻⁴ on CoMnO_x catalysts for FT synthesis and CoMoC catalysts for alcohols synthesis.

1.2 Heterogeneous Catalysis

Heterogeneous catalysis refers to the catalysing of reactions in which the phase of the reactants is different to that of the catalyst. Such catalysts have been known since the early 1800s, when such articles as the Döbereiner lamp (1823), which used platinum to catalyse hydrogen to produce a flame, became available. Whilst the Döbereiner lamp was rapidly ousted by the invention of the Lucifer match in 1827, several catalytic processes have seen continued industrial use for over a century now. For example, the Contact process patented in 1831 by Peregrine Phillips⁵ described a method of producing sulphuric acid from sulphur dioxide and oxygen using a vanadium oxide (V_2O_5) catalyst, and to this day is used to produce the concentrated sulphuric acid needed for industrial processes such as fertilizer creation.

Another well-known example of this is the Haber-Bosch process, which allows for the production of ammonia vital to the world's fertiliser production. Haber initially discovered the process in 1908 by feeding N_2 and H_2 over an osmium catalyst at high pressure. The German company Badische Anilin- und Soda-Fabrik (BASF) bought the patent and charged a team lead by Carl Bosch to scale up Haber's tabletop experiment to an industrial scale process. The catalyst they discovered, an iron based catalyst generated from magnetite exposed to high-temperature hydrogen, is still used to this day, and is responsible for the majority of ammonia production worldwide (131,000,000 tonnes in 2010⁶).

The importance of catalytic processes such as this cannot be overstated; the aforementioned Haber-Bosch process is believed to be responsible for indirectly providing food for one third

of the world's population via the fertilizers it produces. Catalytic processes are involved in almost every conceivable area of life, from food (Ni catalysts for margarine production) and fine chemicals (Friedel-Crafts) to fuel synthesis and refining.

Of particular note with respect to this project is the production of hydrocarbons via the Fischer-Tropsch synthesis. The importance of this procedure has waxed and waned since its discovery in the early 1900s; periods of interest frequently coincide with periods of oil scarcity or high oil prices. For example, the Fischer-Tropsch synthesis was vital to Germany during the Second World War as it allowed the country to use its relative abundance of coal to help offset its lack of reliable petroleum source. The coal would be converted into a syngas mixture, which was then in turn catalysed to form a liquid mixture of hydrocarbons and oxygenated hydrocarbons. Interest in the process then declined with the discovery of the Arabian oilfields in the 1950s, before renewing with the advent of the 1973 OPEC oil crisis.

Recently there has been an upturn in interest in Fischer-Tropsch synthesis as companies and governments seek ways to circumvent the current rising oil prices caused by dwindling oil reserves. There is also interest relating to the ability of Fischer-Tropsch to produce low-sulphur diesel fuels.

1.3 The Fischer-Tropsch Synthesis

In the most basic of terms, Fischer-Tropsch synthesis is a collection of processes which allow for the production of hydrocarbons from a mixture of carbon monoxide and hydrogen generally known as syngas. (Short for synthesis gas).

The origin of the process is now over a century old; in 1902 methane was synthesised from syngas by Sabatier and Senderens⁷. They achieved this at atmospheric pressure using both cobalt and nickel based catalysts at a range of temperatures between 200 and 300 °C. The

German company BASF followed up on this in 1913 with patents for the synthesis of oxygenates from syngas, but it was not until a decade later that the process as it is understood today came into being. Franz Fischer and Hans Tropsch, working for the Kaiser-Wilhelm-Institut for chemistry, showed that a liquid mix of oxygenated hydrocarbons could be produced at high pressures and temperatures (>100 bar and >400 °C respectively) over iron-based catalysts doped with alkaline species^{8,9}. The high pressures employed made this exact reaction difficult to apply industrially, but it was also shown that production of non-oxygenate hydrocarbons was possible at lower pressures. These catalysts were unsuitable due to rapid deactivation, which remains a problem with iron-based catalysts to this day. However, Fischer and Tropsch showed that the catalysts could be improved by the addition of zinc oxide to the iron oxides, which began a concerted effort to uncover catalysts which would be viable for low-pressure hydrocarbon synthesis on an industrial scale. It was this early research that identified what are generally regarded as the four main Fischer-Tropsch active metals; cobalt, iron, nickel and ruthenium. It also identified that higher pressures are generally unsuitable for the synthesis of hydrocarbons.

From an industrial standpoint, ruthenium was eliminated due to its scarcity; worldwide stockpiles would be insufficient to sustain industrial processes indefinitely. Nickel was also viewed unfavourably as an industrial catalyst due to its tendency towards the methanation reaction (i.e. the production of methane, an unfavourable product), as well as its rapid deactivation. Iron, the source of the original Fischer-Tropsch discovery, was not without its problems; low pressures were deemed desirable for hydrocarbon production, so the main thrust of testing was conducted at atmospheric pressures. Whilst this was suitable for cobalt and nickel, iron was later shown to operate more efficiently at higher pressures, typically in the range of 10-30 bar. Whilst this would not prove to eliminate it as a useable industrial catalyst, it would serve to delay their development as such until after the end of the Second World War. Under the atmospheric conditions employed iron suffered from poor yields and rapid deactivation, and so research in this early period was generally focussed on cobalt, which could operate at atmospheric pressures and generally possessed a longer catalyst lifetime and better activity than iron under such conditions.

The first large scale application of cobalt catalysts came in 1934 when Ruhrchemie AG were granted a plant licence for Fischer-Tropsch synthesis using a cobalt-thorium oxide-magnesium oxide-keiselguhr catalyst. It is believed that the plant was first developed as a means of utilising the excess coke present in the Ruhr region, and was used to produce chemicals primarily, and fuel secondarily during the war. Nine plants were constructed in Germany under this licence, with a further 9 built in other countries such as Japan, France and Manchuria. These plants served as a useful testing ground for the development of new catalysts, particularly those involving iron, before the end of the Second World War. At this time, several of the German plants had been destroyed and the remaining plants were closed down, mostly due to a waning of interest in the process brought about by a rise in the price of the coal needed to manufacture the syngas.

Several German scientists who had worked on the project were obtained for American test facilities in Missouri under Operation Paperclip after the Second World War. Test facilities based on the Ruhrchemie reports were set up in 1946 to try and allay fears of an upcoming petroleum shortage, and two German companies began using fixed bed reactors to produce waxes. Later in the 1940s two American companies developed fluidised bed reactors which were used by the Kellogg company. Both the American and German endeavours used iron-based catalysts and syngas derived from coal, and the reactor types that they developed are still in commercial use today. The interest in the Fischer-Tropsch process was short-lived, however, thanks to the discovery of large oil deposits in the Middle East. This depressed the price of petroleum products to the point where the firms could not compete, and all US plants were closed.

Whilst the interest in Fischer-Tropsch had died down in Europe and the US, research continued in other areas, particularly in South Africa, a country rich in coal but lacking in oil reserves. In 1952 a plant was commissioned by the South African Coal, Oil and Gas Corporation (SASOL) to use Fischer-Tropsch to generate diesel fuel from coal, a process referred to as coal-to-liquid (CTL). This plant utilises iron-based catalysts in both fixed and fluidised bed reactors to produce a wide range of products, including most of South Africa's diesel. Production of hydrocarbons began in 1955 and continues to this day. Examples of the SASOL reactors are shown below in **Figure 1.1**.

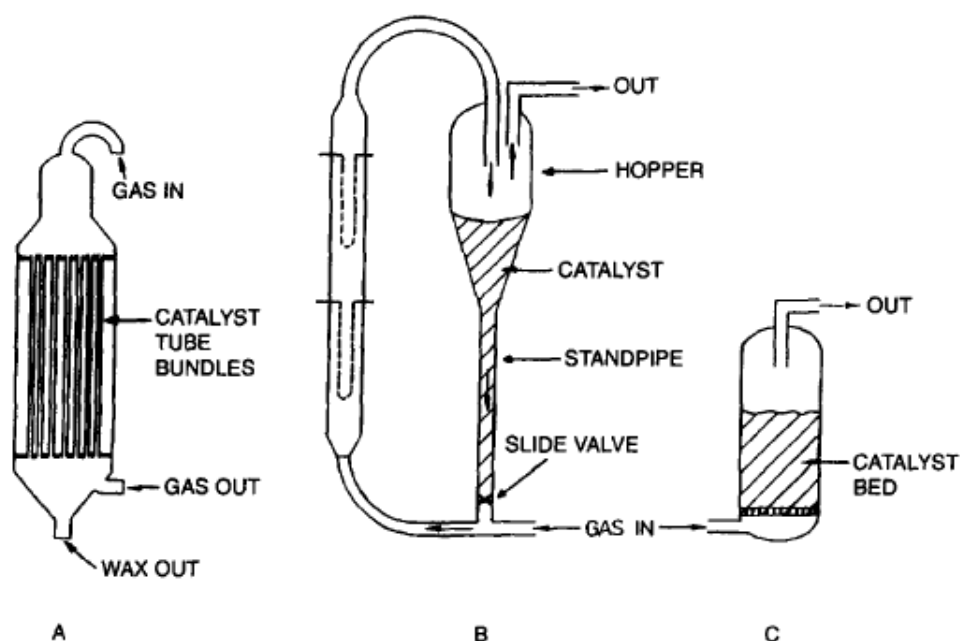


Figure 1.1 Examples of SASOL FT reactors¹⁰

A: Multi-tube ARGE Fixed Bed; B: Circulating fluidised synthol; C: Fixed fluidised or slurry

During the OPEC oil crisis in the early 1970s, the sudden rise in oil prices and general feeling of insecurity about oil supplies led to a significant boost in Fischer-Tropsch research. It was in this period that attention was given to cobalt as a potential catalyst once again; in the previous decades iron had taken precedence. This precedence was based on the location of the research, mainly; it primarily took place in Germany and South Africa, both of whom had an abundance of coal, but little oil. Syngas from coal, produced by coal gasification, has a CO:H₂ ratio of 1. At this level, iron can easily operate. Cobalt, however, is optimal when the CO:H₂ ratio is nearer to 2.

As a wider range of countries began to invest in the research, other sources of syngas were utilised. Syngas from methane, for example, has a CO:H₂ ratio of 3 if steam reforming is used, or 2 if CO₂ reforming is used. The USA was the foremost researcher of Fischer-Tropsch during this time, but interest once again waned once the Crisis was resolved.

In modern times, interest in Fischer-Tropsch is once again on an upswing due to the rising oil prices and increasing pressure for companies and governments to find greener routes for chemical production.

1.4 Products of Fischer-Tropsch

An issue that often complicates the use of Fischer-Tropsch synthesis for the production of chemicals and fuels is that of product distribution. Fischer-Tropsch catalysts will only be able to make C₁ products with 100 % selectivity due to the nature of the chain growth. At any given moment for a species on the surface of the metal there will be a chance for it to either continue reaction, thus extending the chain, or terminate, forming the product. This chance is referred to as the chain growth probability and ensures that any product formation beyond C₁ is some form of probability distribution over a range of products.

Various theoretical models have been created to attempt to explain the product distribution¹¹.¹². These models are generally based on the following assumptions:

- a) Chain growth occurs via a polymerisation process, increasing in single carbon increments
- b) The probability of chain propagation, and of chain termination, is independent of the current length of the hydrocarbon chain.

Anderson¹³ used these assumptions to derive an analytical function for determining the probability of chain growth based on the polymerisation distribution function developed by Schulz and Flory. The Anderson-Schulz-Flory (ASF) equation is shown below.

$$W_n/n = (1 - \alpha)^2 \alpha^{n-1}$$

Where n is the carbon number, W_n is the weight fraction of a product with carbon number n , and α is the chain growth probability.

α can be defined by the following equation:

$$\alpha = r_p / (r_p + r_t)$$

Where r_p and r_t are the rate of chain propagation and the rate of chain termination respectively. These rates are determined by a number of factors, such as reaction conditions, catalyst type, and even the CO:H₂ ratio in the syngas feed.

By taking the \log_{10} of both sides of the ASF equation, it can be rewritten as

$$\text{Log}(W_n/n) = n\log\alpha + \log(1-\alpha)^2/\alpha$$

This follows the equation of a straight line, $y = mx + c$. This allows for experimental data to be plotted graphically as a means of obtaining α for the system used. A plot of $\log(W_n/n)$ against n is known as an Anderson Schulz Flory plot, and will give a linear graph with a gradient of $\log\alpha$.

The predicted product distributions for different α values are shown below in **Figure 1.2**

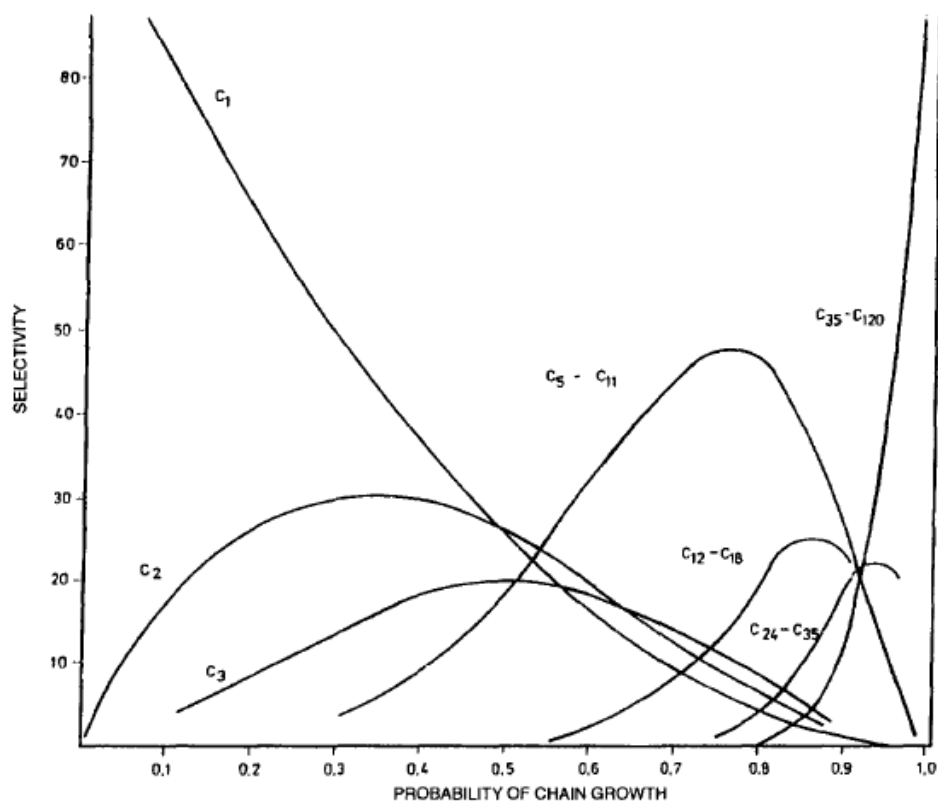


Fig. 3. Calculated hydrocarbon selectivity (C atom basis).

Figure 1.2 Predicted product distributions for different α values¹⁰

Experimental data using ASF distributions usually report that there are deviations from modelled behaviour. C_1 yields are commonly higher than would be anticipated, and C_2 yields are frequently lower. Other products may deviate as well, according to a number of different factors. The product distribution is most likely affected by a number of secondary reactions, such as hydrogenation and hydrogenolysis, or reinsertion of terminated products¹⁴⁻¹⁶. Several other attempts have been made to explain the discrepancies of the model, but thus far no model has proven up to the task of explaining all of them.

The fact that the system can be shown to (and indeed induced to) deviate from the ASF distribution allows for the possibility of improvement of the catalyst systems. For example, the presence of manganese in cobalt catalysts is reported to increase selectivity towards C_3 products¹⁷. Rather than simply changing α , the presence of manganese seems to promote a side reaction which favours C_3 products.

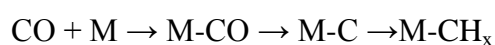
Most research into Fischer-Tropsch catalysts is aimed at distorting the ASF distribution, trying to narrow the product range to develop more selective systems. This is of particular importance if the target is a single compound (as in the fine chemicals industry) as opposed to a spread of products (as in synthetic diesel manufacture.)

There is also a large amount of research into the discernment of the mechanism of the Fischer-Tropsch reaction, as a means of achieving greater understanding of ways to optimise the catalysts.

1.5 Mechanisms of Fischer-Tropsch

In the most basic terms, Fischer-Tropsch synthesis is a complex reaction which forms hydrocarbons and oxygenates from carbon monoxide and hydrogen, and it appears to do so via a chain growth mechanism. However, elucidating the mechanism for the Fischer-Tropsch synthesis reaction is a problem that has existed as long as the reaction itself, and is a problem that remains unresolved to this day. Significant amounts of effort have been expended upon investigating the precise mechanism by which the chain lengthening process of carbon monoxide hydrogenation proceeds.

When the reaction was first discovered by Fischer and Tropsch⁹, they, after much deliberation, suggested a carbide-based mechanism¹⁸. Under this suggested system, the CO would adsorb on the surface before undergoing rapid dissociation, leaving a metal carbide. This carbide would then be hydrogenated to form a methylene group (=CH₂) which would act as the monomer in a polymeric process. A large body of evidence was accrued, particularly in the 1980s, which lent credence to the idea of methylene polymerisation for the formation of linear hydrocarbons¹⁹⁻²¹. A simple schematic of the reaction could be viewed as:



At this point polymerisation would occur with other groups formed in the same manner, although the exact nature of this polymerisation step is still up for debate. Research continues to this day on this potential mechanism, with experiments designed to determine the nature of the $-\text{CH}_x$ groups, and the manner in which they form C-C bonds^{22, 23} or insert themselves into the metal-alkyl bond²⁴. There is strong experimental evidence for both C-C coupling and metal-alkyl insertion, although it should be noted that the reactions under which these experiments occur are frequently different from the reaction conditions of Fischer-Tropsch synthesis. A schematic of the reaction mechanism for the carbide method is shown below in **Figure 1.3**.

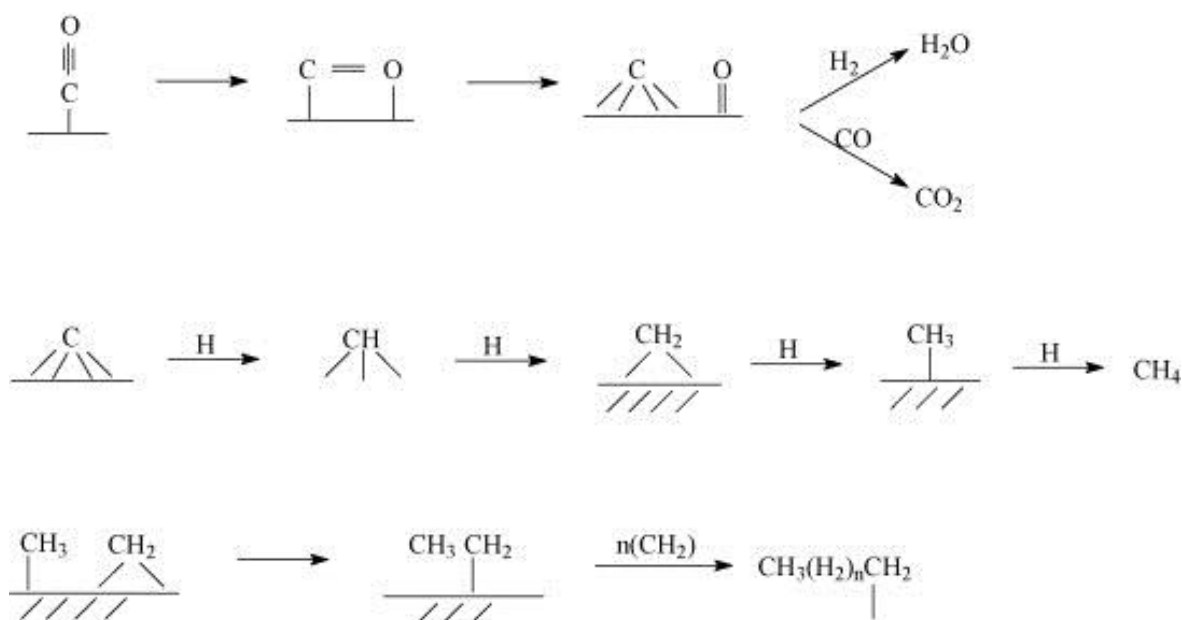


Figure 1.3 The carbide mechanism²⁵

There are, however, several flaws with the carbide mechanism. It is incapable of explaining the formation of oxygenate species, the production of which is a highly important area of Fischer-Tropsch style reactions. Another flaw is the unidirectionality that the polymerisation reaction should exhibit if the carbide mechanism were correct. That is to say; the methylene groups should be able to attack any other methylene group in an extant chain, or any metal-alkyl bond in the same chain, should that be the mechanism. This in turn should lead to a greater yield of branched products, which are generally regarded as very low in Fischer-Tropsch, and rarer the longer the chain length of the hydrocarbon.

Experiments using labelled ^{14}CO to form a carbide layer on an iron catalyst had also challenged the mechanism by showing that the carbide hydrogenation was not responsible for more than 10% of the methane formed under their reaction conditions²⁶. Also working against the supposition of carbide being a reaction intermediate was the fact that cobalt carbide, the carbide of a Fischer-Tropsch active material, is not even a catalyst, let alone an intermediate, in this reaction.

Other experiments involving ^{14}CO carbided iron led to the development of an alternative method by Emmett²⁷ and Storch²⁸. In this method, the CO molecules were not assumed to immediately dissociate upon adsorption to the metal surface, but could instead react with molecular hydrogen to give an intermediate species with the general formula of $\text{C}_x\text{H}_y\text{O}_z$. The exact stoichiometry of this species is still debated to this day²⁵. In this mechanism the CO adsorbs associatively on the metal surface before reacting with hydrogen to form a hydroxycarbene, $\text{M}=\text{CHOH}$. This intermediate would then undergo a condensation with a similar species nearby to create a C-C bond. This mechanism can either terminate by hydrogenation to form an alcohol, or further dehydration and hydrogenation to form alkenes or alkanes. Unless an oxygenated product is formed, the CO bond must still be broken at some point, but since it is not assumed to take place immediately after adsorption this mechanism is sometimes referred to as 'late bond splitting'.

A major advantage that this reaction mechanism has over the carbide mechanism is its ability to account for the formation of oxygenates. As with the carbide mechanism, there is a fair amount of evidence to support the mechanism^{29, 30}, and in particular it seems to be relevant to systems using manganese as a promoter³¹.

Variations on the theme have also been suggested by Voevodskii³² and Ekstroom³³, who combined elements of both the carbide mechanism and the hydroxycarbene mechanism. Voevodskii proposed that the hydroxycarbene be hydrogenated to form the methylene monomer from the carbide mechanism, which would then react with CO to form a new hydroxycarbene. This would then be hydrogenated, and so on and so forth until chain termination.

Ekstrom proposed that the methylene monomer would be formed by the hydrogenation of the hydroxycarbene, but that this would then undergo polymerisation with other methylene groups formed in the same manner.

The third commonly accepted mechanism for the chain growth of hydrocarbons in the Fischer-Tropsch reaction is the CO insertion mechanism. In this reaction the CO inserts itself into the metal hydride or metal alkyl bond before hydrogenation to form hydrocarbons. This was first demonstrated by Heck³⁴ before being expanded upon by Pichler and Schulz ten years later³⁵. The reaction mechanism shown below in **Figure 1.4** is often named after them.

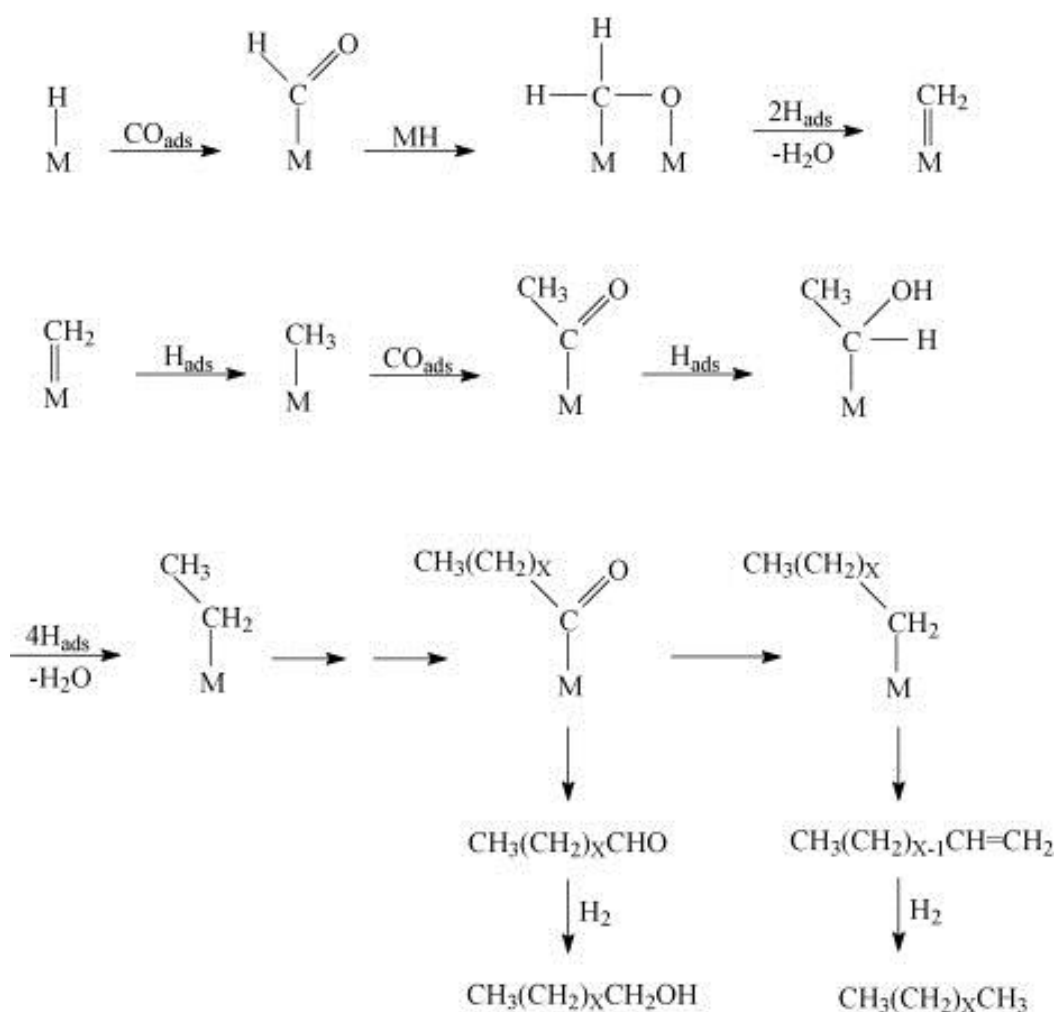


Figure 1.4 The CO insertion mechanism²⁵

The CO insertion mechanism has fairly widespread support, and is an excellent model for explaining several particulars of the Fischer-Tropsch reaction.

There are, in addition to this, several other proposed mechanisms for the chain growth step of Fischer-Tropsch, such as the two displayed below, proposed by Deluzarche³⁶ (**Figure 1.5**) and Sapienza³⁷ (**Figure 1.6**)

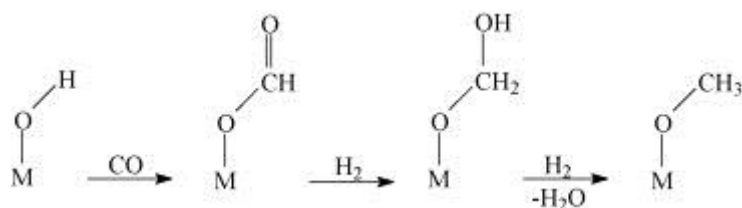


Figure 1.5 Proposed mechanism

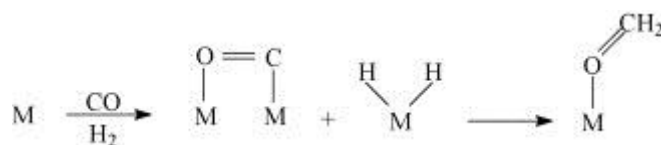


Figure 1.6 Proposed mechanism

Despite all of these possibilities, it has proven extremely difficult to ascertain what the actual mechanism is for any given system. It is possible that the mechanism is in fact a combination of several of these processes, plus others. It also seems to be the case that what may be an accurate representation of the mechanism for one system may not be the same for another. The carbide mechanism, for example, can be shown to be active over iron catalysts to an extent, but is not active for cobalt catalysts. The hydroxycarbene mechanism appears to occur on Ru catalysts with MnO promoters, but not on Ru catalysts without³¹.

1.6 Catalytically active metals for Fischer-Tropsch

Most Group VIII metals display at least some activity towards CO hydrogenation³⁸ due to their facility with the chemisorption of CO, widely regarded as the first step in the FT synthesis process. However, that in itself does not guarantee that the material will be FT-active; the key is determination of whether they allow for the production of the desired products. Iron, nickel, cobalt, iridium, ruthenium, rhodium, palladium and platinum³⁹⁻⁴⁴ can all be seen to display activity, but only four of these are considered 'useful' as Fischer-Tropsch catalysts; Iron, nickel, cobalt and ruthenium. Rhodium, palladium and platinum are active towards CO hydrogenation, but produce primarily oxygenated products as opposed to the hydrocarbons which are the products of FT. Other materials such as osmium are also active towards oxygenate formation.

Of the four 'main' FT active materials, ruthenium displays very high selectivity towards the formation of valuable products such as paraffin waxes, but ruthenium is scarce. It is unsuitable for industrial uses due to its high cost and extremely limited supply.

Nickel is extremely efficient at the absorption of CO; however, it does so dissociatively to form a Ni-C compound which will hydrogenate to form methane even at room temperature⁴⁰. This facility towards methanation leads to general disfavour as a FT catalyst, as methane is a cheap, and thus unwanted, product.

Iron catalysts are both cheap and active towards the production of hydrocarbons, but at the same time tends to require higher temperatures and pressures to be fully effective. Even under these conditions it generally deactivates rapidly, forming a mixture of carbide phases which shorten the catalyst's lifetime.

Cobalt, whilst more expensive than iron, is generally preferred as an industrial catalyst due to higher activity, gentler reaction conditions, and longer catalyst lifetime. Cobalt catalysts are generally reported to have good selectivities towards linear hydrocarbons, making them eminently suitable as catalysts for FT synthesis

1.6.1 Cobalt for Fischer-Tropsch

Cobalt as a Fischer Tropsch material has a history dating back to the early 20th century, but it has not been continuously researched in the intervening times. Much like the interest in Fischer-Tropsch itself, the interest in cobalt catalysts waxes and wanes based on global conditions. In times where oil prices are low, the need for alternative sources of fuel and petrochemicals is suppressed, and thus demand for any Fischer Tropsch catalyst is limited. Cobalt research suffers in these times. However, there are also additional factors to consider; cobalt catalysts function best with a CO:H₂ ratio of roughly 2, and this ratio is frequently determined by the source of the syngas. Several major Fischer-Tropsch utilizers, such as the Ruhr region during WWII and South Africa in the present day, obtain most of their syngas stocks from the gasification of their significant coal reserves. However, the gasification of coal leads to syngas with a Co:H₂ ratio of around 1, a ratio at which iron catalysts can happily function, but at which the effectiveness of cobalt is lessened.

Thus, even in periods of global conditions where a search for alternatives to oil creates favourable conditions for FT research, research into cobalt may be sidelined due to this. For example, whilst commercial processes in Germany in the late 1920s used both iron and cobalt catalysts, after this most FT applications focus around work in South Africa utilising iron catalysts.

It was not until the 1970s, with the advent of the OPEC oil crisis, that research into cobalt as an FT catalyst began to re-emerge. Cobalt was found to be more effective for Gas-to-Liquid applications, where the source of syngas was instead methane. They also gained popularity over iron catalysts due to their higher selectivity to long-chain hydrocarbons ($\alpha(\text{Co}) = 0.7-0.8$; $\alpha(\text{Fe}) = 0.5-0.6$)¹⁰ and lower reaction pressure and temperatures.

Optimisation of cobalt based systems is extensive and ongoing. It has been shown that the activity towards Fischer Tropsch displayed by cobalt catalysts is generally a function of the number of metal sites present in the catalyst. Whilst this does not appear to hold true of

catalysts with cobalt particle sizes smaller than 7-8nm, outside of this range it is taken as proof that the dispersion of the cobalt metal is crucial to its usefulness as a catalyst^{45, 46}. It is also taken as a strong implication that the ease of reducing of the cobalt to the metallic state is highly important.

Achieving the desired high dispersion is usually managed by supporting the cobalt on a support material such as silica, alumina, or titania. There is also literature geared towards supporting the cobalt on metal oxides which are not active for Fischer-Tropsch, but have a promoting effect upon cobalt. Examples of this would be vanadium, chromium⁴⁷, and manganese oxides⁴⁸.

The addition of manganese to the catalysts will be of particular interest during this study, as it is an area of work in which this group has prior experience. Based on the initial discovery that adding manganese oxide to iron catalysts⁴⁹ promoted the formation of C₂-C₄ light olefins, work was initiated into investigating the effect that manganese presence has on cobalt catalysts. Much of the early work centred on supporting the cobalt on the manganese oxide, or, in the case of this group, creating a mixed metal oxide of the two components. More recently efforts have been made to determine its use as a promoter in low loadings. The effects of adding manganese appear to be highly beneficial, with most cases reporting a drop in C₁ selectivity and an increase in C₃ selectivity. The exact reason for this promotion is not entirely clear, as most studies are more interested in improving preparation methods as opposed to investigation of the effect, but it is generally thought that the presence of MnO affects the reducibility of the cobalt species.

The use of carbon as a support is a fairly recent development, and was undertaken in an attempt to avoid the metal-support interactions that frequently arise when cobalt is supported on metal oxides such as manganese oxide or titania. Whilst the initial efforts in this regard appear to have been attempts to find an unreactive support, carbon supports have recently come into fashion with the advent of carbon nanotubes, carbon ribbons, carbon spheres and graphene. It has also been demonstrated that cobalt species supported on carbon will undergo

a reduction in an inert atmosphere, leading to interesting implications as to the reducibility of the catalysts.

1.7 Fischer-Tropsch for higher alcohols synthesis

Industrial production of higher alcohols from syngas is currently based around four ‘styles’ of catalyst. The first is modifications of the ZnO/Cr₂O₃ catalysts used for the production of methanol. These modifications usually take the form of addition of alkali and alkaline earth species to the catalyst to push its selectivity towards higher alcohols, and also changes in reaction conditions to help achieve this. Metals such as copper, cobalt, iron and nickel may also be added to these systems to increase alcohols production.

Rhodium based catalysts are an interesting area of study for the production of C₂₊ oxygenates, but unfortunately the high price and limited supply mean that investigation into this area is mostly academic rather than commercial.

The IFP catalysts (Institut Francais du Petrole) are based on oxides of copper and cobalt mounted on a variety of different materials such as aluminium, chromium and zinc.

Molybdenum sulphide catalysts alone are actually producers of hydrocarbons, but in the presence of alkali materials and at higher pressure, their selectivities shift strongly towards alcohols. Elements such as cobalt and nickel are frequently added to shift the selectivities away from methanol in favour of higher alcohols. These catalysts are considered industrially promising due to their high sulphur tolerance and coke resistance⁵⁰. It is on this area that our research will focus. The initial catalyst from which work was attempted was an alkali

modified MoS₂ catalyst with supported cobalt. However, the sulphide catalyst requires cofeeding of H₂S into the syngas flow or else the catalyst will deactivate⁵¹. The presence of sulphur in the gas stream is problematic, as the sulphur can be incorporated into the products by these catalysts.

To attempt to move away from these catalysts, this study will be investigating the possibility of making a CoMo-C mixed metal catalyst supported on carbon. Work by a previous student on the project seemed to prove the concept feasible.

1.8 References

1. M. Vanderriet, G. J. Hutchings and R. G. Copperthwaite, *Journal of the Chemical Society-Chemical Communications*, 1986, 798-799.
2. G. J. Hutchings, M. Vanderriet and R. Hunter, *Journal of the Chemical Society-Faraday Transactions I*, 1989, **85**, 2875-2890.
3. M. Vanderriet, R. G. Copperthwaite and G. J. Hutchings, *Journal of the Chemical Society-Faraday Transactions I*, 1987, **83**, 2963-2972.
4. M. Vanderriet, D. Copperthwaite, R. Hunter and G. J. Hutchings, *Journal of the Chemical Society-Chemical Communications*, 1988, 512-513.
5. *British Pat.*, 6096, 1881.
6. L. Apodaca, *Mineral commodity summaries*, 2011.
7. P. Sabatier and J. B. Senderens, *Comptes Rendus Hebdomadaires Des Seances De L Academie Des Sciences*, 1902, **134**, 514-516.
8. *German Pat.*, 411216, 1922.
9. F. Fischer and H. Tropsch, *Berichte Der Deutschen Chemischen Gesellschaft*, 1923, **56**, 2428-2443.
10. M. E. Dry, *Applied Catalysis a-General*, 1996, **138**, 319-344.

11. G. Henrici-Olive and S. Olive, *Angewandte Chemie-International Edition in English*, 1976, **15**, 136-141.
12. C. N. Satterfield and G. A. Huff, *Journal of Catalysis*, 1982, **73**, 187-197.
13. R. B. Anderson, in "Catalysts for Fischer-Tropsch Synthesis", vol 4, Van Nostrand Reinhold, New York 1956
14. S. Novak, R. J. Madon and H. Suhl, *Journal of Catalysis*, 1982, **77**, 141-151.
15. E. W. Kuipers, C. Scheper, J. H. Wilson, I. H. Vinkenburch and H. Oosterbeek, *Journal of Catalysis*, 1996, **158**, 288-300.
16. E. W. Kuipers, I. H. Vinkenburch and H. Oosterbeek, *Journal of Catalysis*, 1995, **152**, 137-146.
17. S. L. Gonzalez-Cortes, S. M. A. Rodulfo-Baechler, A. Oliveros, J. Orozco, B. Fontal, A. J. Mora and G. Delgado, *Reaction Kinetics and Catalysis Letters*, 2002, **75**, 3-12.
18. F. Fischer and H. Tropsch, *Berichte Der Deutschen Chemischen Gesellschaft*, 1926, **59**, 830-831.
19. R. C. Brady and R. Pettit, *Journal of the American Chemical Society*, 1980, **102**, 6181-6182.
20. R. C. Brady and R. Pettit, *Journal of the American Chemical Society*, 1981, **103**, 1287-1289.
21. A. T. Bell, *Catalysis Reviews-Science and Engineering*, 1981, **23**, 203-232.
22. J. Cheng, P. Hu, P. Ellis, S. French, G. Kelly and C. M. Lok, *Journal of Catalysis*, 2008, **257**, 221-228.
23. J. Cheng, X. Q. Gong, P. Hu, C. M. Lok, P. Ellis and S. French, *Journal of Catalysis*, 2008, **254**, 285-295.
24. P. Biloen and W. M. H. Sachtler, *Advances in Catalysis*, 1981, **30**, 165-216.
25. B. H. Davis, *Catalysis Today*, 2009, **141**, 25-33.

26. J. T. Kummer, T. W. Dewitt and P. H. Emmett, *Journal of the American Chemical Society*, 1948, **70**, 3632-3643.
27. H. H. Podgurski, J. T. Kummer, T. W. Dewitt and P. H. Emmett, *Journal of the American Chemical Society*, 1950, **72**, 5382-5388.
28. R. B. Anderson, R. A. Friedel and H. H. Storch, *Journal of Chemical Physics*, 1951, **19**, 313-319.
29. M. A. Vannice, *Journal of Catalysis*, 1975, **37**, 462-473.
30. W. K. Hall, R. J. Kokes and P. H. Emmett, *Journal of the American Chemical Society*, 1960, **82**, 1027-1037.
31. H. Trevino, T. Hyeon and W. M. H. Sachtler, *Journal of Catalysis*, 1997, **170**, 236-243.
32. V. V. Voevodskii in: M. Van der Riet, "Carbon monoxide hydrogenation with transition metal oxide supported cobalt and iron catalysts", PhD Thesis, University of Witwatersrand, 1988
33. A. Ekstrom, J. A Lapszwewicz, *J Phys. Chem.*, 1987, **91**, 4514
34. R. F. Heck and D. S. Breslow, *Journal of the American Chemical Society*, 1961, **83**, 4023-&.
35. H. Pichler and H. Schulz, *Chemie Ingenieur Technik*, 1970, **42**, 1162-&.
36. A. Deluzarche, R. Kieffer and A. Muth, *Tetrahedron Letters*, 1977, 3357-3360.
37. R.S. Sapienza, M.J. Sansone, L.D. Spaulding, J.F. Lynch, in: M. Tsutsui (Ed.), *Fundamental Research in Homogeneous Catalysis*, vol. 3, Plenum Press, 1979, p. 179.
38. S. A. Hedrick, S. S. C. Chuang, A. Pant and A. G. Dastidar, *Catalysis Today*, 2000, **55**, 247-257.
39. E. Bonnefille, J. M. M. Millet, J. P. Candy, J. Thivolle-Cazat, R. Bellabarba, R. Tooze and J. M. Basset, *Catalysis Letters*, 2012, **142**, 984-990.

40. J. A. Rabo, A. P. Risch and M. L. Poutsma, *Journal of Catalysis*, 1978, **53**, 295-311.
41. N. Tsubaki, S. L. Sun and K. Fujimoto, *Journal of Catalysis*, 2001, **199**, 236-246.
42. S. S. C. Chuang and S. I. Pien, *Journal of Catalysis*, 1992, **138**, 536-546.
43. X. H. Mo, J. Gao, N. Umnajkaseam and J. G. Goodwin, *Journal of Catalysis*, 2009, **267**, 167-176.
44. N. Kumar, M. L. Smith and J. J. Spivey, *Journal of Catalysis*, 2012, **289**, 218-226.
45. J. S. Girardon, E. Quinet, A. Griboval-Constant, P. A. Chernavskii, L. Gengembre and A. Y. Khodakov, *Journal of Catalysis*, 2007, **248**, 143-157.
46. R. Gheitanchi, A. A. Khodadadi, M. Taghizadeh and Y. Mortazavi, *Reaction Kinetics and Catalysis Letters*, 2006, **88**, 225-232.
47. R. Rao, A. Dandekar, R. T. K. Baker and M. A. Vannice, *Journal of Catalysis*, 1997, **171**, 406-419.
48. E. Tronconi, C. Cristiani, N. Ferlazzo, P. Forzatti, P. L. Villa and I. Pasquon, *Applied Catalysis*, 1987, **32**, 285-292.
49. J. Barrault and C. Renard, *Applied Catalysis*, 1985, **14**, 133-143.
50. J. M. Christensen, P. A. Jensen, N. C. Schiodt and A. D. Jensen, *Chemcatchem*, 2010, **2**, 523-526.
51. J. M. Christensen, P. M. Mortensen, R. Trane, P. A. Jensen and A. D. Jensen, *Applied Catalysis a-General*, 2009, **366**, 29-43.

Chapter 2

Experimental

2.1 Catalyst Preparation

The catalyst preparation step is frequently of great importance in the manufacture of catalysts, as different methods can be used to affect a wide range of catalyst characteristics such as surface area, metal dispersion, and morphology of active sites. When such alterations in method can produce such pronounced differences, it is important to have preparation methods which, above all, produce reliably reproducible catalysts.

There are several commonly used techniques which allow for such reproducibility, such as impregnation, sol immobilisation, and coprecipitation. As long as the relevant variables (such as pH, temperature, ageing, etc.) are controlled, these methods tend to produce consistent catalysts.

Several different methods of catalyst preparation have been used throughout this study. In some cases combinations of preparation methods have been used, such as sol-gel for preparation of a perovskite support followed by impregnation or coprecipitation of active metals to form a catalyst. Where this has occurred, it will be noted in the relevant experimental section.

2.1.1 Fischer-Tropsch Catalyst Preparation

Whilst the exact details of the preparation of each catalyst may vary, they can be broadly subdivided into major groups; Impregnation and Coprecipitation.

2.1.1.1 Impregnation

Impregnation is perhaps the simplest method available for production of catalysts, and as such it is highly useful on an industrial scale. There are two common forms of impregnation: Wet Impregnation and Incipient Wetness Impregnation.

The common theme between the both of them is that a salt solution of the desired metals will be made up to the required concentrations, and subsequently this solution will be added to a support material, typically a porous material. The solvent will then be removed, theoretically leaving metal salts evenly dispersed throughout the pores and/or on the surface of the support material^[1]. The drying method can be one of a wide variety of techniques, as long as the solvent is removed without also removing the metal salts.

In the wet impregnation technique, the volume of solvent used to make the solution of metal salts is greater than the total pore volume of the support. The vast majority of the catalysts

created for this study were prepared using wet impregnation. Throughout this thesis, whenever the terms ‘impregnation’ or IMP are used, it is referring to wet impregnation.

Incipient wetness impregnation differs from wet impregnation in that the volume of metal salt solutions used will be equal to or less than the total pore volume of the support material. The lower relative amount of solvent compared to wet impregnation allows for faster drying times, and theoretically deposits the material primarily in the pores, whereas wet impregnation is equally likely to deposit metals on exterior surfaces. This can make incipient wetness a better choice for support materials such as mesoporous silica, where the internal interconnected pore system can be important. However, depending on solvents and metal salts used it may not be possible to obtain as high metal loadings with incipient wetness impregnation as with wet impregnation.

Throughout this thesis, whenever the terms ‘incipient wetness’ or ‘IW’ are used, they are referring to Incipient Wetness Impregnation.

i) Preparation of CoMnC catalysts by Impregnation

The catalysts were prepared according to the following general method. Calculated amounts of cobalt nitrate $\text{Co}(\text{NO}_3)_2 \cdot 6\text{H}_2\text{O}$ (Aldrich 99.99 %) and $\text{Mn}(\text{NO}_3)_2 \cdot 4\text{H}_2\text{O}$ (Aldrich 99.999 %) were each separately added to absolute ethanol (Fischer) and stirred to dissolve. These solutions were then simultaneously added to a predetermined amount of High Surface Area Activated Carbon (Norit A SUPRA EUR 94011-8) to give the desired loadings and catalyst metal ratios.

This slurry was stirred in a crucible for 3 h prior to being covered and then dried in the crucible overnight (16 h) at 110 °C. This dry powder was designated as the catalyst precursor.

The precursor was then heat treated in a tube furnace at 400 °C for 4 h under flowing He (30 ml/min) with a ramp rate of 5 °C/min. Samples were allowed to cool to room temperature before being removed from the furnace. This dry powder is referred to as the catalyst, even though further treatments are performed *in-situ* after this point.

2.1.1.2 Coprecipitation

Coprecipitation is a technique in which mixtures of two or more metals are forced out of solution simultaneously, creating a catalyst with a highly even, homogenous dispersion of metals throughout the resultant material.

One of the major issues of coprecipitation is the large waste of reagents which occurs during the process. The problem arises because of the method of precipitation. Generally speaking, a chemical reagent will be used; ammonia was the precipitant of choice throughout all coprecipitations performed in this thesis, based on the findings of the previous student on the project. The addition of the ammonia raises the pH of the metal salt solution; the salts, being less soluble at higher pH levels, are forced to precipitate out of the solution. However, generally speaking the solubility of the metal salts in the solution will not be reduced to zero, and thus a quantity of the reagents will still remain trapped in solution, leading to material waste.

Another factor in coprecipitation reactions for catalyst formation is that they require a far higher degree of control than the various impregnation techniques to achieve reproducibility. Even small variations in parameters such as the pH, flow rate of solutions, and whether the metal solutions are added to a precipitant or vice versa, can all have a significant impact on the final catalyst. Should the necessary level of control be achieved, however, the methods prove to be highly reproducible.

There are two methods of coprecipitation used throughout this thesis; firstly, the simultaneous addition of both metal salt solutions and ammonia at constant flow rates to cause precipitation at a constant pH.

The second method involves the addition of the precipitating agent to the metal salt solution at a constant flow, or vice versa. This causes precipitation at a varying pH.

For the production of Fischer-Tropsch catalysts, only the former method was used, as detailed below.

i) Preparation of CoMnOx catalysts by coprecipitation at constant pH

The catalysts were prepared according to the following method. 29.09 g of cobalt nitrate $\text{Co}(\text{NO}_3)_2 \cdot 6\text{H}_2\text{O}$ (Aldrich 99.99 %) and 25.1 g of $\text{Mn}(\text{NO}_3)_2 \cdot 4\text{H}_2\text{O}$ (Aldrich 99.999 %) were each added to 100 ml of distilled water to create 1 M solutions. A 5.6 M solution of ammonia was prepared by dissolving 21.69 ml of NH_3 into 200 ml of water. The two nitrate solutions were mixed to form a 200 ml combined solution. Both solutions were preheated in a water bath to 70 °C.

100 ml of distilled water was placed in a round bottomed flask and placed in a water bath at 70 °C. This amount of water was needed to ensure coverage of the pH probe used to monitor the reaction.

The two solutions (NH_3 and metal salts) were both added at an individual flow rate of 5ml/min with stirring, for a total flow rate of 10 ml/min. This caused a black solid to precipitate out. This reaction was continued for *ca.* 45 mins, which allowed for all the reactants to be mixed, with an additional 5 mins of stirring. The solid was then filtered under vacuum in a preheated funnel, and then washed with 500 ml of preheated distilled water. The washed solid was dried in an oven (16 h in air at 110 °C). This black solid was designated as the catalyst precursor.

The dried sample was then heat treated in a tube furnace at 800 °C for 24 h under He (30 ml/min) with a ramp rate of 5 °C/min. Samples were allowed to cool to room temperature before being removed from the furnace. The black solid this produced was designated as the final catalyst.

2.1.2 Alcohols Catalyst Preparation

As with the Fischer-Tropsch catalysts, the alcohols catalysts can be divided into broad subgroups; Impregnation, Coprecipitation and Deposition Precipitation.

2.1.2.1 Impregnation

The alcohols catalysts said to be prepared by impregnation utilize a wet impregnation technique, the general nature of which is mentioned in section 2.1.1.1. The method for their production is outlined below.

i) Preparation of CoMoC catalysts by Impregnation

Ammonium Molybdate Tetrahydrate $(\text{NH}_4)_6\text{Mo}_7\text{O}_{24}\cdot 4\text{H}_2\text{O}$ (Aldrich, 99.99 %) was dissolved in absolute ethanol (100 ml) with stirring. At the same time, Cobalt Acetate $\text{Co}(\text{CH}_3\text{CO}_2)_2$ (Aldrich, 99.99 %) was also dissolved in an equal amount of absolute ethanol.

Once dissolved, both solutions were simultaneously added to Coconut Shell Activated Carbon (6.4 g, Norit G90) and stirred for 3 h at room temperature. This suspension was then dried on a rotary evaporator in a water bath at 50 °C and a rotation speed of 200 rpm.

The resultant catalyst precursor was dried in an oven overnight at 110 °C, before being heat treated for 5 h at 500 °C under flowing He (30 ml/min) at a ramp rate of 5 °C/min. The sample was allowed to cool to room temperature to produce the final catalyst.

2.1.2.2 Coprecipitation

The alcohol catalysts prepared by coprecipitation follow a slightly different method to that outlined in section 2.1.1.2, in that acetic acid was used as a precipitant, and that the precursor solutions are added to the precipitant rather than being mixed simultaneously. The method for the production of these catalysts by coprecipitation is outlined below.

i) Preparation of Co-MoS₂ catalysts by coprecipitation

A solution of (NH₄)₂MoS₄ was prepared by dissolving 15 g of ammonium molybdate tetrahydrate (NH₄)₆Mo₇O₂₄·4H₂O (Aldrich, 99.99 %) into 106 ml of (NH₄)₂S/H₂O (20 % solution in H₂O, Sigma Aldrich) with stirring at 70 °C for 1 h.

A solution of the cobalt metal salt was prepared by dissolving 10.5 g of cobalt acetate Co(CH₃CO₂)₂ (Aldrich, 99.99 %) in 200 ml of distilled water.

These two solutions were then added drop-wise simultaneously into a well-stirred solution of aqueous acetic acid solution (30 % solution) which had been preheated to 50 °C. The solution was vigorously stirred for 1 h. The resultant black product, designated the catalyst precursor, was filtered under suction in a preheated funnel before being left to dry in static air at ambient temperature overnight (16 h).

The catalyst precursor was heat treated for 1h in flowing nitrogen (30 ml/min) at 500 °C with a 5 °C/min ramp rate. The grey-black product was allowed to cool to room temperature before being mixed with potassium carbonate K₂CO₃, montmorillonite clay and sterotex® lubricant to give weight ratio of 66/10/20/4 (10 % K₂CO₃) unless otherwise noted. This mixed material was referred to as the final catalyst.

2.1.2.3 Deposition Precipitation

Deposition precipitation is related to coprecipitation; in both methods two or more metals will be simultaneously precipitated from a solution. The main difference is that in deposition precipitation a support material is added before the precipitation step. This causes the precipitating metals to bind to the support, allowing the homogeneity of coprecipitated catalyst metal distribution to be applied to a support system. The method used for synthesis of catalysts via deposition precipitation is outlined below.

i) Preparation of CoMoC catalyst by Deposition Precipitation

Ammonium Molybdate Tetrahydrate $(\text{NH}_4)_6\text{Mo}_7\text{O}_{24}\cdot 4\text{H}_2\text{O}$ (Aldrich, 99.99 %) was dissolved in distilled water with stirring to make a 1 M solution. At the same time, Cobalt Acetate, $\text{Co}(\text{CH}_3\text{CO}_2)_2$ (Aldrich, 99.99 %) was also dissolved in an equal amount of distilled water to make a 1 M solution. Once dissolved, both solutions were simultaneously added to Coconut Shell Activated Carbon (6.4 g, Norit G90). This mixture was stirred and preheated in a water bath to 80 °C.

A calculated amount of ammonium hydroxide NH_4OH was dissolved in distilled water to make a 5.6 M solution. This solution was preheated in a water bath to 80 °C.

The ammonium hydroxide solution was added to the metal salt and carbon mixture with a flow rate of 10 ml/min, causing the pH of the mixture to change over time from 4.35 to 8. The mixture was stirred vigorously throughout the addition of the ammonium hydroxide, and for an additional 5 mins thereafter, at which point the resultant black precipitate was filtered under suction in a preheated funnel before being washed with distilled water preheated to 80 °C. The product was collected and dried overnight (16 h) at 110 °C. This black material was designated as the catalyst precursor.

The catalyst precursor was heat treated under flowing He (30 ml/min) for 5 h at a temperature of 500 °C, with a ramp rate of 5 °C/min. The black product was allowed to cool to room temperature in flowing He before being collected and designated as the final catalyst.

2.1.2.4 Addition of metal promoters to catalysts

For some experiments it was necessary to add Cu metal as a promotor for the Co-MoS₂ catalysts. This was achieved as described in the method below.

i) Addition of copper metal to Co-MoS₂ by Impregnation

The pore volume of the catalyst precursor was determined via the gradual addition of distilled water to a weighed quantity of the material until a dry mull was formed. It was observed that this required 1.8 cm³ of distilled water for 5 g of precursor. This is as per the Incipient Wetness Impregnation method.

Solutions containing the required amount of copper were created using copper (II) nitrate hydrate, Cu(NO₃)₂·H₂O (Sigma Aldrich, 99.999%) as a precursor. These solutions were then applied to the catalyst, creating a mull. This mull was dried at 110 °C for 16 h before being heat treated at 400 °C for 4h under flowing He (30 ml/min) with a ramp rate of 5 °C/min. The samples were allowed to cool to room temperature before being mixed with additives as per section 2.1.2.2 to produce the final catalyst.

2.1.3 Perovskite preparation

i) Preparation of mixed metal oxides

Preparation of the mixed metal oxides was performed using a sol-gel technique sometimes referred to as the 'citrate route'^[2].

A calculated quantity of V₂O₅ (Aldrich, ≥98%) was placed in a suspension of water (50ml) and then reduced by addition of two drops of hydrazine hydrate solution, NH₂NH₂·H₂O (Aldrich, 25% wt in H₂O). After two minutes of stirring, a black slurry resulted, believed to be V₂O₃ based on colouration. To this slurry was added calculated amounts of the appropriate

metal nitrates; $\text{La}(\text{NO}_3)_3 \cdot 6\text{H}_2\text{O}$ (Sigma Aldrich, 99.999 %); $\text{Sr}(\text{NO}_3)_2$ (Sigma Aldrich ACS, ≥ 98 %); $\text{Ca}(\text{NO}_3)_2 \cdot 4\text{H}_2\text{O}$ (Sigma Aldrich, ≥ 99 %); and $\text{Ba}(\text{NO}_3)_2$ (Aldrich, 99.999 %), and an amount of citric acid (Anhydrous, Acros, 99.0 %) equal to the combined number of moles of metal dissolved. After stirring with heating, (70 °C for 30 mins) the solution turned deep blue, possibly due to V_2O_4 formation. This solution was dried slowly at 100 °C in a water bath until a dry powder remained.

This powder was heated to 900 °C under flowing air for 2 h and allowed to cool to room temperature to give a yellow powder. This powder was then in turn heated to 900 °C in 10 % H_2/Ar for 6 h before being allowed to cool to room temperature. This resulted in a black powder.

ii) Addition of precious metals on to mixed metal oxides

Calculated amounts of PdCl_2 and HAuCl_4 were added to water to make an aqueous solution of the desired concentration. To this was added an amount of 1 %wt PVA solution. The amount added was calculated so that $(\text{PVA}/(\text{Au}+\text{Pd})) (\text{wt.}/\text{wt.}) = 1.2$). To this an amount of 0.1 M NaBH_4 solution was added. The amount was calculated so that $(\text{NaBH}_4/(\text{Au}+\text{Pd})) (\text{mol.}/\text{mol.}) = 5$). This formed a dark brown sol, which was stirred for 30 min.

The colloid generated was immobilised by addition of the mixed metal oxide support in quantities calculated to give the desired metal loading. This suspension was then stirred for 1 h before being filtered under suction and washed with warm water. The resultant material was then dried overnight at 120 °C to give the finished catalyst.

2.2 Product Analysis

Gaseous products produced in these reactions were analyzed by online gas chromatography. Liquid products were collected at the end of the reactions and analysed by off-line gas chromatography.

2.2.1 Gas Chromatography

Chromatography (from the Greek for ‘Colour writing’) is an umbrella term used to describe a range of laboratory techniques used for the separation of mixtures of chemicals. The chemical mixture will be present in a mobile phase, which for this process is an inert carrier gas. The chemicals are heated to vapourisation prior to injection into a chromatographic column, which contains a stationary phase. Different chemicals will have a different affinity for this stationary phase, and repeated absorption/desorption events will cause the mixture of chemicals to become separated into discrete components, allowing for accurate analysis of the species present.

2.2.1.1 Anatomy of a Gas Chromatograph (GC)

Whilst the overall system used for a GC may be highly complex, all GCs can generally be thought of as consisting of the following components:

- i) Carrier Gas, ii) Injector Port, iii) Columns, iv) Column Oven, v) Detectors, and vi) Data Recording

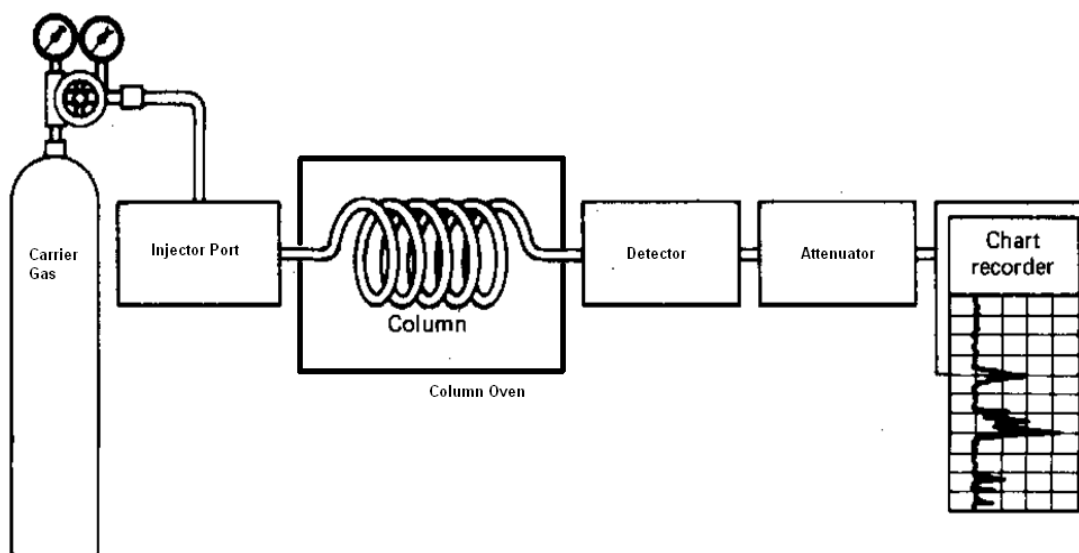


Figure 2.1: Diagram of a Gas Chromatograph system

i) Carrier Gas

The carrier gas is an inert mobile phase used to force the mixture through the column, thereby causing the partitioning of the individual components from the mixture. For all analysis performed by online gas chromatography throughout this thesis, the carrier gas is argon. For all offline gas chromatography the carrier gas is helium. The choice of carrier gas used can often be dependent on the differing natures of the columns used in the gas chromatograph.

ii) Injector Port

This is the point at which the mobile phase, consisting of sample and carrier gas, is inserted into the column. This stage is heated to cause the vapourisation of any components of the mixture which were not already in gaseous phase.

iii) Columns

There are two types of column commonly used in gas chromatography, which are packed columns and capillary columns.

- Capillary columns are thin tubes made of fused silica, the interior of which is coated with the stationary phase.
- Packed columns have wider bores, and are filled with finely-divided inert support material (typically silicone based) which has been coated with the stationary phase.

The choice of stationary material affects the separation of the mixture; this separation depends specifically on the absorption/desorption rate of each component with respect to the stationary phase.

iv) Column Oven

The column oven is used to keep the columns at a stable temperature, preventing the condensation of products in the column, and also ensuring that all chemicals in the mixture are not subject to temperature fluctuations during elution which may affect their retention time.

v) Detectors

There are two types of detector used throughout this thesis; Thermal Conductivity Detectors (TCD) and Flame Ionisation Detectors (FID). Each of these detectors is sensitive to different manners of chemicals, making the combination of both techniques preferable.

a. Thermal Conductivity Detector (TCD)

TCD detects chemicals by sensing a change in thermal conductivity between a reference flow of carrier gas and the column effluent. Under normal conditions, the column effluent is the same as the carrier gas, and as such no change in thermal conductivity is noted between the two detectors. However, when a chemical is present in the detector cell, the thermal conductivity will change relative to the reference cell. Generally speaking, almost all analytes will have a lower thermal conductivity than the carrier gas. This results in an increase in resistance which can be detected by a Wheatstone bridge circuit; this change will register as a difference in voltage, which is recorded.

Since TCD is capable of detecting any molecule with a thermal conductivity different to the carrier gas, it is sometimes referred to as the universal detector. It is useful in conjunction with the more sensitive FID technique, as it can detect non-flammable species which the FID would be unable to register. TCD is also a non-destructive technique.

b. Flame Ionisation Detector (FID)

FID uses a small hydrogen-air flame to pyrolyse chemicals in the column effluent, resulting in ions being formed. These ions are attracted to a collector plate, where their impact generates a current which is measured by an ammeter. The magnitude of this current is proportional to the amount and type of ions striking it, which can help for identification of species.

There are several drawbacks to FID, however. It is a destructive technique, so when used in conjunction with other chromatography detectors it will of necessity be last to be applied. Also, it is only sensitive to such compounds that can be pyrolysed in a hydrogen-air flame. This means that while it is excellent for hydrocarbons, it is less sensitive to compounds already containing oxygen (such as alcohols), and completely insensitive to compounds which cannot be ionised by the flame (H_2O , CO , CO_2 , ect.)

vi) Data Collection

The exact nature of the data collection system varies from GC to GC, but generally computer based systems provide excellent analysis of the data, plotting the received signals into chromatograms with adjustable scales of response factors.

2.3 Catalyst Testing

Testing of Fischer-Tropsch catalysts for the synthesis of alkenes from syngas was carried out in a 6-bed laboratory reactor. This allowed the testing of larger batches of different catalysts under identical conditions.

0.5 g of powdered catalyst was packed undiluted between quartz wool plugs in the ¼ ” steel reactor tubes. The catalysts were pre-reduced in-situ at 400 °C for 16 h under a pure H_2 flow (5 ml/min). The samples were cooled to room temperature before the syngas introduction ($\text{CO}/\text{H}_2 = 1:1$, flow rate= 5 ml/min GHSV = 600 h^{-1}). Pressure in the reactors was increased

to 6 bar by use of Back Pressure Regulators. The temperature was increased to 240 °C at 1 °C/min before being allowed to stabilize for 20 min.

Time on line studies were carried out for 90 h with gas sampling at 6 h intervals.

Testing of alcohols catalysts was performed in a specialised high-pressure alcohols reactor.

4.8 g of catalyst was mixed with 5.2 g of SiC (200-400 mesh) and loaded into the alcohols reactor on a quartz wool bed. The catalyst was then pre-reduced for 10 h at 350 °C under flowing H₂ (Flow 40 ml/min, ramp rate 1 °C/min) before being allowed to cool to room temperature. The reactor would then be pressurised with syngas (1:1 Co:H₂) to a pressure of 75 bar using a back pressure regulator. Syngas flow was varied based on experiment, as was the the temperature.

Time on line studies were carried out in the gas phase for 60 h, with sampling occurring every hour. At the end of the run the liquids would be collected and analysed by GC.

2.4 Catalyst Characterisation

2.4.1 Brunauer, Emmett and Teller (BET) method surface area measurements^[3]

Surface area of catalysts is known to be important in catalyst activity for many systems, and as such the ability to determine the surface area of a material with accuracy is of great relevance. The BET equation is an extension of the Langmuir model for monolayer molecular adsorption, and with a series of assumptions it can be used to estimate the surface area. These assumptions are that a) gas molecules adsorb on a solid in layers indefinitely; b) there is no interaction layer between each adsorption layer; and c) the Langmuir theory can be applied to each layer.

Thus, we arrive at the equation

$$\frac{1}{v[(P_0/P) - 1]} = \frac{c - 1}{v_m c} \left(\frac{P}{P_0} \right) + \frac{1}{v_m c} \quad (1)$$

Where P and P_0 are the equilibration and saturation pressure, v is the volume of adsorbed gas, and v_m is the volume of gas required to form a monolayer. C is the BET constant.

By using experimental results of absorption of nitrogen to plot a graph of $P / v(P_0 - p)$ against P / P_0 , a straight line with gradient equal to $(c - 1) / (v_m c)$, and an intercept of $1 / (v_m c)$. This allows for calculation of the volume required to form a monolayer.

Once v_m is known, the surface area can be calculated by the equation

$$A_s = (v_m / 22414) N_A \sigma$$

Where N_A is the Avogadro number and σ is the cross sectional area of one nitrogen molecule.

Measurement of surface areas were performed using Micromeritics ASAP2000 (Gemini), which took measurements using physisorption of nitrogen at the temperature of liquid nitrogen. Before measurement, each sample was degassed for 1 h at 110 °C under nitrogen. By measuring the pressure drop of nitrogen throughout the experiment it was possible to calculate the surface areas using the above method.

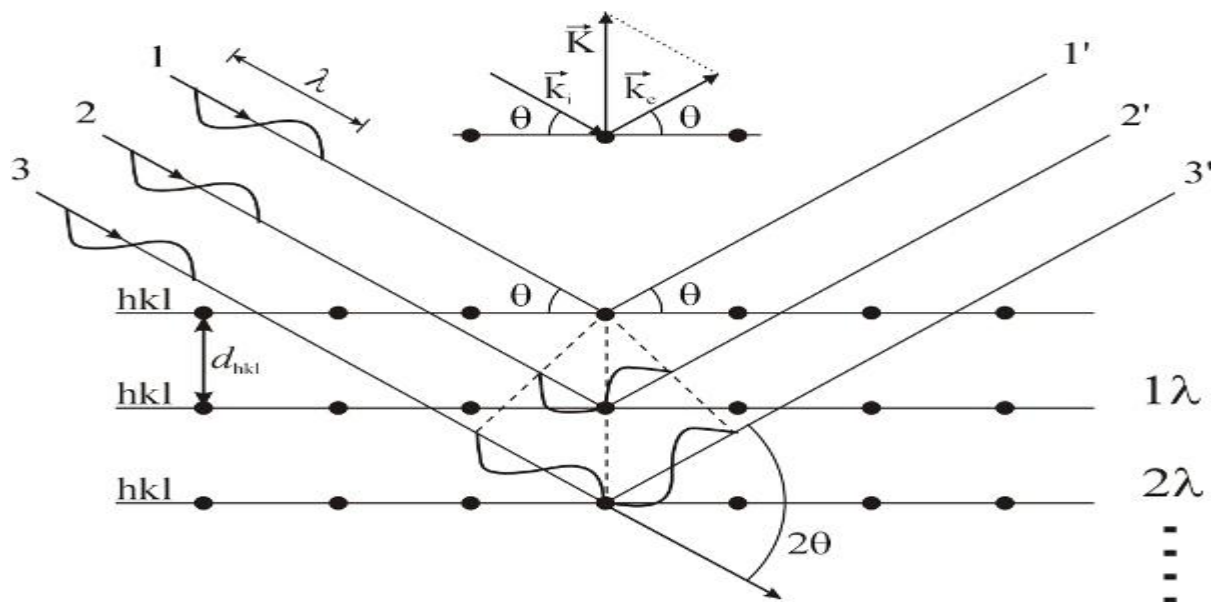
2.4.2 X-Ray Diffraction (XRD)

X-Ray diffraction is a non-destructive crystallographic technique capable of determining the lattice spacing of atoms in a crystalline compound. This data can be used to identify the compounds present, and their crystal structure.

XRD works due to the elastic scattering of the X-rays when they strike the atoms of the target compound. The radiation will be scattered in all directions, and in most directions the radiation will be cancelled out by destructive interference. However, in certain directions the interference will instead be constructive, generating a measureable signal. The positions which lead to constructive interference are given by Bragg's law of Diffraction:

$$2d \sin \theta = n\lambda$$

where d is the interplanar spacing, θ is the diffraction angle, n is an integer, and λ is the wavelength of the incident radiation.



In XRD an X-ray source and a monochromator are used to ensure that λ is known, and θ can be determined by the angle of the beam and the detector at the time of measurement. With these two parameters known, it is possible to calculate d , and thereby identify the crystal structures present. It can also calculate the dimensions of the elementary cell, and the relative quantities of different phases present

XRD is only viable for crystalline materials, as a regular spacing of atoms is needed. In amorphous materials, all diffracted radiation is cancelled out by destructive interference.

Powder XRD was used throughout this study to identify the compounds present in the catalysts. A diffractometer with a Cu K α source operated at 40 keV and 40 mA was used to obtain the data. Phase identification was performed using the X'Pert High Score data base of spectral patterns.

2.4.3 Scanning Electron Microscopy (SEM)

SEM is a surface sensitive technique which utilizes a beam of high-energy electrons to image the surface of a material. This technique generally takes place in ultra-high vacuum due to the absorption of electrons by air. The high-energy electrons used cause secondary electron emission as electrons are ejected from the material due to inelastic scattering. Because of their low energy, these emitted electrons will originate from within nanometers of the surface, hence the designation as a surface sensitive technique.

The emitted electrons are collected and amplified before being fired at a scintillator, which in turn emits flashes of light into a photomultiplier. The amplified signal generated by the photomultiplier is displayed as an intensity distribution pattern. The intensity of the signal is based on the number of electrons detected; surfaces not directly facing the electron beam will produce less electrons, and thus a weaker signal. In this manner the SEM can be used to generate a 3D appearance. It is possible to achieve resolutions of 0.5 nm using the detection of secondary electrons.

Another application of SEM is the detection of backscattered electrons; those which are reflected back at the detector due to elastic scattering. These electrons are of much higher energy than those detected from inelastic scattering, and thus a different detector within the machine must be used.

The detection of backscattered electrons is useful for identifying the elements present on the surface of the material; since heavier atoms backscatter electrons more strongly than lighter elements, this shows up as relatively higher intensity on the display. This can help to distinguish areas of differing chemical composition on the sample.

The analysis for both of these applications was performed using a Zeiss Evo-40 series Scanning Electron Microscope.

2.4.4 Energy Dispersive X-Ray Spectroscopy (EDX)

EDX is an analytical technique used for the elemental analysis of a sample. It works on the fundamental principle that each element has a unique elemental structure and thus unique electron energy levels.

To generate a signal, a beam of high-energy electrons (10-25 keV) strikes the surface of the sample. The electrons in the beam can cause an inner shell electron of the sample to become excited, thereby causing ejection, and leaving an electron hole. An electron from a higher energy level will then fill this hole, and the energy difference between the two energy levels will be emitted in the form of an X-ray.

To analyse elemental composition, the EDX detector measures both the energy and the number of emitted X-rays. Since the energy of the X-rays is fairly unique to each element, it is now known which atoms are present. As the number of X-rays emitted is assumed to be proportional to the relative amount of the emitting atoms, knowing the number of X-rays at each energy value provides an accurate assessment of elemental composition.

The detector works in three steps; firstly the X-ray generates a charge in a semiconductor via ionisation of atoms. This charge is then converted into a voltage, which is then registered for measurement.

The equipment used for EDX analysis in this thesis was a Zeiss Evo-40 series SEM in conjunction with an INCA-sight EDX detector.

2.4.5 Thermogravimetric Analysis (TGA)

TGA is a technique which monitors the change in weight relative to temperature in a sample. For this to be effective, three parameters need to be measured with extreme precision; the mass, the temperature, and the temperature change.

In TGA a sample is heated to temperatures whereupon some components of the sample will decompose into, or react to form, a different material, causing a change in mass. If the original composition of the material is known, TGA can be precise enough that the species lost or gained during heating can be determined by the percentage weight change that they induce.

TGA analysis is often combined in analysis with the differential thermal analysis (DTA) of a sample, which shows endothermic and exothermic changes. This can allow for greater interpretation of mass-change events, and can also be used to detect events which do not result in a change of mass, such as melting or crystallisation

The equipment used for TGA in this thesis was Labsys TGA-DTA 1600.

2.5 References

1. Twigg, M.V., *Catalysis Handbook*. 2nd ed. 1996: Manson Publishing. 608.
2. Baythoun, M.S.G. and F.R. Sale, *Production of strontium-substituted lanthanum manganite perovskite powder by the amorphous citrate process*. *Journal of Materials Science*, 1982. **17**(9) 2757-2769.
3. Brunauer, S., P.H. Emmett, and E. Teller, *Adsorption of gases in multimolecular layers*. *Journal of the American Chemical Society*, 1938. **60** 309-319.

Chapter 3

Effects of preparation on Co-Mn Fischer-Tropsch catalysts

3.1 Introduction

The work in this section is a continuation of the work of a previous student on the project, who showed that the final conversion and selectivities of the catalysts were heavily dependent upon a wide range of variables in the preparation steps.

The aim of this section of work is the selective production of light alkanes and alkenes ($C_2 - C_4$), particularly the alkenes which have high value as petrochemical feedstocks. The main problem that arises from such an undertaking is that whilst the Fischer-Tropsch reaction is capable of making such products, it is uncommon for it to do so with any great selectivity. This relates to the chain growth mechanism; as defined by the Anderson – Schulz - Flory equation described in **chapter 1**, the process will always produce a range of products. It is

possible to produce methane, the simplest product, with 100% selectivity, but the probability distribution pattern means that it is not possible to produce any higher carbon number product with the same selectivity.

The aim, therefore, of Fischer-Tropsch catalyst design is to attempt to narrow the range of products produced. This can be affected by a large number of factors; aside from the effects of preparation variations mentioned above, feedgas composition, presence of promoters, type of catalyst, and the temperature and pressure of the reactor can all have an effect.

In terms of catalyst composition, the presence of manganese has long been known to enhance C₂-C₄ selectivity¹⁻³.

3.2 Catalyst Preparation

With only one exception, all catalysts tested in this section of the study were prepared via the wet impregnation technique, which is explained in greater detail in Chapter 2.

Following this preparation, all catalysts (unless otherwise noted) were loaded into ¼” steel reactor tubes and reduced in the reactor at 400 °C for 16 h under flowing H₂ with a flow rate of 5 ml/min and a heating ramp rate of 5 °C/min.

Unless otherwise noted, these catalysts were tested using syngas with a CO:H₂ ratio of 1:1 at a flow rate of 5 ml/min (GHSV = 600 h⁻¹). Pressure was increased to 6 bar using Back Pressure Regulators, and temperature was increased to 240 °C with a ramp rate of 1 °C/min.

Reactions were conducted over 72 h, with online gas sampling every 6 h. All data displayed is gas phase data, as minimal liquids were recovered in all cases. Gas phase carbon mass balances (CMBs) were 100±10 % unless otherwise noted.

3.3 Preparation Method Variations

In the initial series of experiments, it was undertaken to investigate to what extent the preparation methods could influence the activity of the catalyst. In most cases the catalysts tested were of a narrow range of compositions,

3.3.1 Variations in Heat Treatment Temperature

In this section catalysts were prepared according to the wet impregnation technique set out in **Chapter 2**, save that the heat treatment temperature of the preparation was varied between 400 °C and 800 °C in 100 °C steps. The aim was to investigate if differing temperatures could result in the formation of different metal species within the catalyst, leading to changed and perhaps improved catalyst performance.

3.3.1.1 Results

The changes of conversion and selectivity with respect to heat treatment temperature are displayed below in **Table 3.1** and **Figure 3.1**.

Table 3.1. Conversion and selectivity data for catalysts prepared with different heat treatment temperatures

| HT Temperature | 400 | 500 | 600 | 700 | 800 |
|----------------------------------|-------|------|-------|-------|-------|
| CO Conversion | 66.42 | 52.4 | 52.29 | 48.08 | 26.5 |
| Product selectivities (%) | | | | | |
| CH ₄ | 3.04 | 3.2 | 3.92 | 2.49 | 1.79 |
| C ₂ H ₄ | 0.87 | 0.9 | 0.36 | 1.25 | 1.88 |
| C ₂ H ₆ | 6.37 | 6.5 | 4.85 | 3.69 | 4.17 |
| C ₃ H ₆ | 20.28 | 22.9 | 21.53 | 22.37 | 22.24 |
| C ₃ H ₈ | 6.83 | 7.8 | 8.58 | 4.6 | 5.39 |
| C ₄ H ₈ | 18.09 | 19.3 | 18.09 | 20.34 | 19.28 |
| C ₄ H ₁₀ | 2.85 | 3.4 | 5.44 | 4.15 | 4.83 |
| C ₅ + | 26.36 | 26.1 | 29.65 | 33.87 | 35.49 |
| CO ₂ | 15.33 | 9.9 | 7.58 | 7.24 | 4.92 |

Catalyst test condition: Co:H₂ = 1:1, Temp. = 240 °C, Flow rate = 5 ml/min. Mass = 0.5 g GHSV = 600 h⁻¹

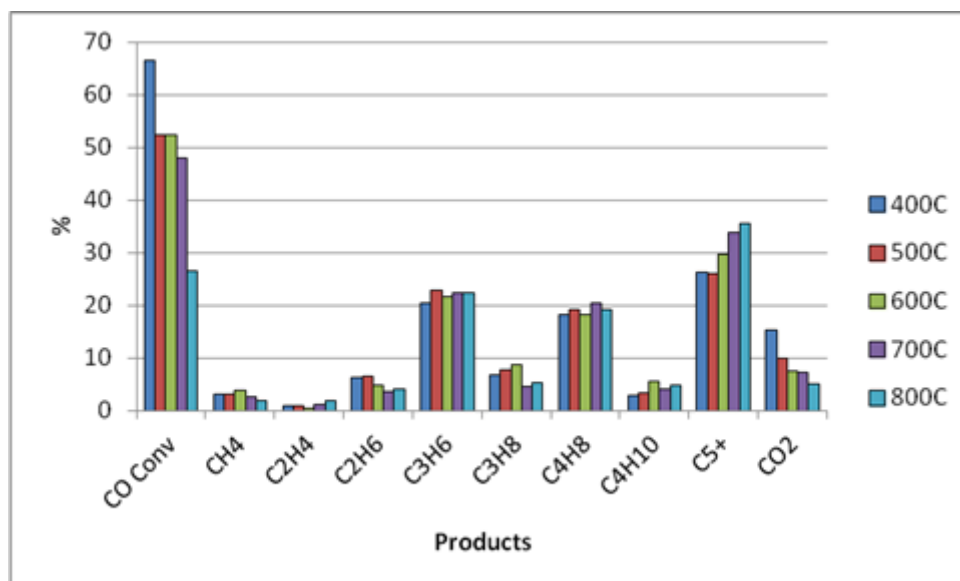


Figure 3.1. Bar chart for comparison of catalysts prepared with different heat treatment temperatures

Examination of these results shows a defined trend of decreasing CO conversion with increasing heat treatment temperature. The products of the reaction are predominantly C₂-C₄, which is in agreement with literature stating that manganese promotes light olefin production¹⁻³. An increase in C₅+ products was also observed with increasing HT temperature, and a decrease in CO₂ selectivity can be discerned. No directly corresponding literature study on this was found; Heat treatment temperature studies have been performed for other catalysts^{4, 5}, but not carbon supported CoMn. Higher temperatures are usually avoided due to the tendency of Co to bond with the supporting metal oxide, which is not an issue for these catalysts.

The most notable drop in CO conversion appears between 700 and 800 °C, implying that a major change in catalyst behaviour is caused by some structural or compositional change which occurs during heating between these temperatures.

Unfortunately the data for these catalysts combined all selectivity results above C₄ into one category, C₅+. Whilst an Anderson-Shulz-Flory plot can still be plotted with the remaining data, only two points would be considered valid by the exclusions mentioned earlier, and thus the linear trend could not be considered reliable.

Another set of experiments was therefore conducted, with the catalysts being prepared with heat treatment temperatures varying between 700 and 800 °C in 25 °C increments. The results for these experiments are shown below in **Table 3.2** and **Figure 3.2**.

Table 3.2. Conversion and selectivity data for catalysts prepared with different heat treatment temperatures

| HT Temperature (°C) | 700 | 725 | 750 | 800 |
|----------------------------------|------|-------|-------|-------|
| CO Conversion | 37.7 | 7.7 | 9.8 | 3.63 |
| Product selectivities (%) | | | | |
| CH ₄ | 15.2 | 13.45 | 12.05 | 12 |
| C ₂ H ₄ | 0.7 | 2.94 | 1.4 | 2.0 |
| C ₂ H ₆ | 6.6 | 3.46 | 3.64 | 4.17 |
| C ₃ H ₆ | 21.0 | 20.7 | 21.2 | 20.75 |
| C ₃ H ₈ | 5.6 | 3.46 | 4.4 | 4.48 |
| C ₄ H ₈ | 14.3 | 13.1 | 13.35 | 12.5 |
| C ₄ H ₁₀ | 3.6 | 2.95 | 3.75 | 3.6 |
| C ₅ + | 30.2 | 37.1 | 35.8 | 35.1 |
| CO ₂ | 2.9 | 1.8 | 2.3 | 1.1 |

Catalyst test condition: Co:H₂ = 1:1, Temp. = 240 °C, Flow rate = 5 ml/min. Mass = 0.5 g GHSV = 600 h⁻¹

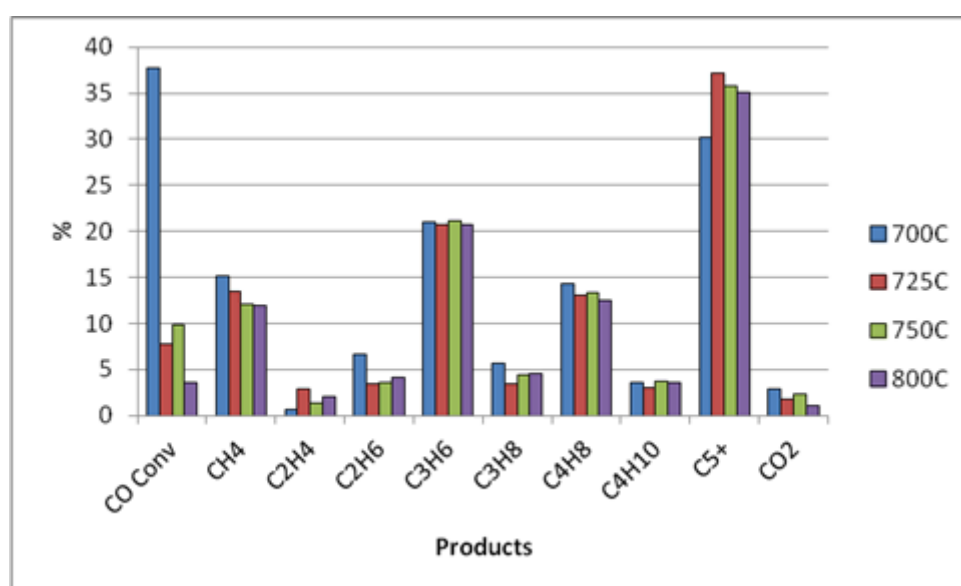


Figure 3.2. Bar chart for comparison of catalysts prepared with different heat treatment temperatures

As can clearly be seen, there is a highly significant loss of CO conversion between the heat treatment temperatures of 700 and 725 °C, although the product selectivities have remained broadly similar. Also of note is the difference between the results for 700 and 800 °C in this series of experiments compared to those in the previous set of experiments. In particular, CO conversions have dropped and CH₄ selectivity has increased markedly. This is believed to be due to a combination of two factors; the vessel in which these were prepared (shown to be significant in **Section 3.3.4**) and a recalibration of the reactor which happened in the interim period.

An Anderson-Schulz-Flory (ASF) plot for this data is shown below in **Figure 3.3**, with the accompanying α values displayed in **Table 3.3**.

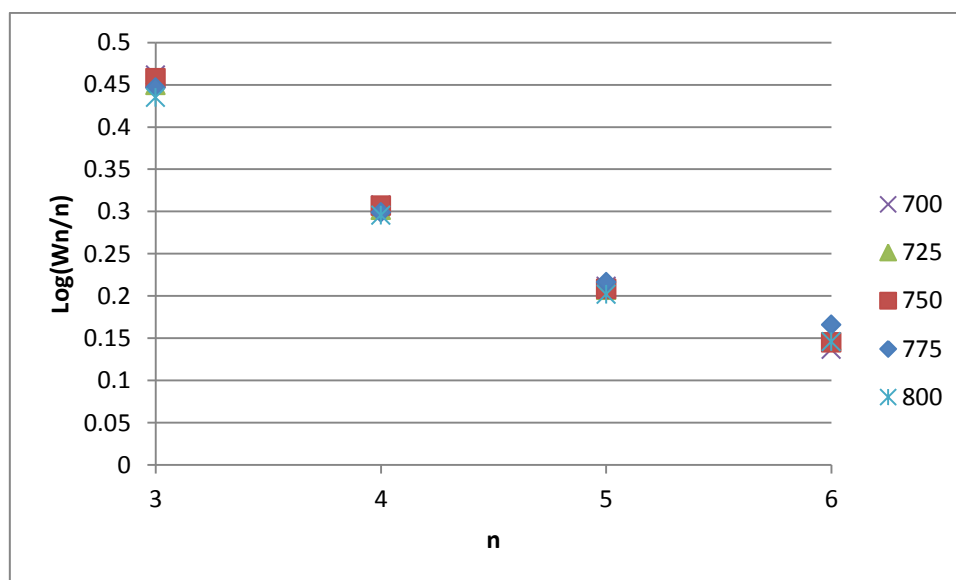


Figure 3.3 ASF plot for catalysts heat treated at temperatures between 700 and 800 °C

Table 3.3 Calculated values of α for catalysts heat treated at temperatures between 700 and 800 °C

| Catalyst | 700 | 725 | 750 | 775 | 800 |
|----------|---------|---------|---------|---------|---------|
| Gradient | -0.1071 | -0.1002 | -0.1036 | -0.0925 | -0.0961 |
| α | 0.781 | 0.794 | 0.788 | 0.808 | 0.801 |

Whilst the numbers are not completely identical, there is no clear trend in the α values with increasing HT temperatures. Also of note is that there is no major shift between ‘700’ and the higher temperatures, despite the large drop in the CO conversion at ‘725’ and higher. This

has interesting implications; it suggests that the factor that is contributing to the loss of CO conversion has little to no effect on the product selectivity. This could be of great potential use; should a catalyst be synthesised with desirable selectivities, these results imply that it is possible to increase the CO conversion of these catalysts without affecting these selectivities.

3.3.1.2 Characterisation

A series of characterisation techniques were utilised to try and ascertain the source of this massive loss of CO conversion. The results are displayed below in **Table 3.4** and **Figures 3.4** to **3.6**.

Surface area measurements of the catalysts after heat treatment were obtained using the BET method as described in **Section 2.4.1**. The results of this are shown below in **Table 3.4**.

Table 3.4 BET surface area measurements of catalysts after heat treatment.

| Catalyst Heat Treatment | Surface area (m²/g) |
|--------------------------------|---------------------------------------|
| Temperature (°C) | After Heat Treatment |
| 400 | 448 |
| 500 | 433 |
| 600 | 469 |
| 700 | 438 |
| 800 | 178 |

The BET results show a large loss in surface area between 700 and 800 °C heat treatment temperatures, which coincides perfectly with the results showing a large loss of CO conversion within the same temperature range.

Since it is believed that the carbon support is the cause of the high surface areas of the catalyst, it seems plausible to assume that collapse of the carbon support is a likely cause of the loss of surface area. To test this, thermo gravimetric analysis was performed on a sample of the catalyst precursor under an inert atmosphere (N_2) to see if the temperature at which the collapse occurs could be pinpointed.

The results of this analysis are displayed below in **Figure 3.4** and **Figure 3.5**.

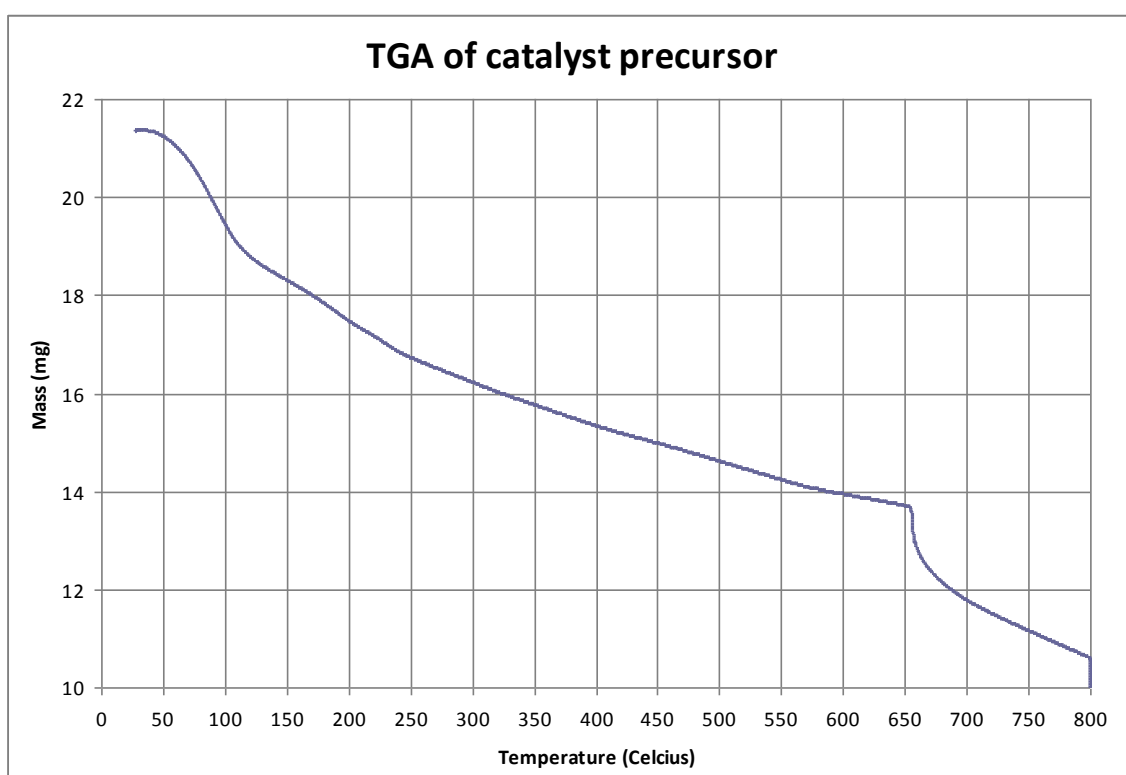


Figure 3.4. Graph showing mass loss of catalyst precursor with respect to temperature

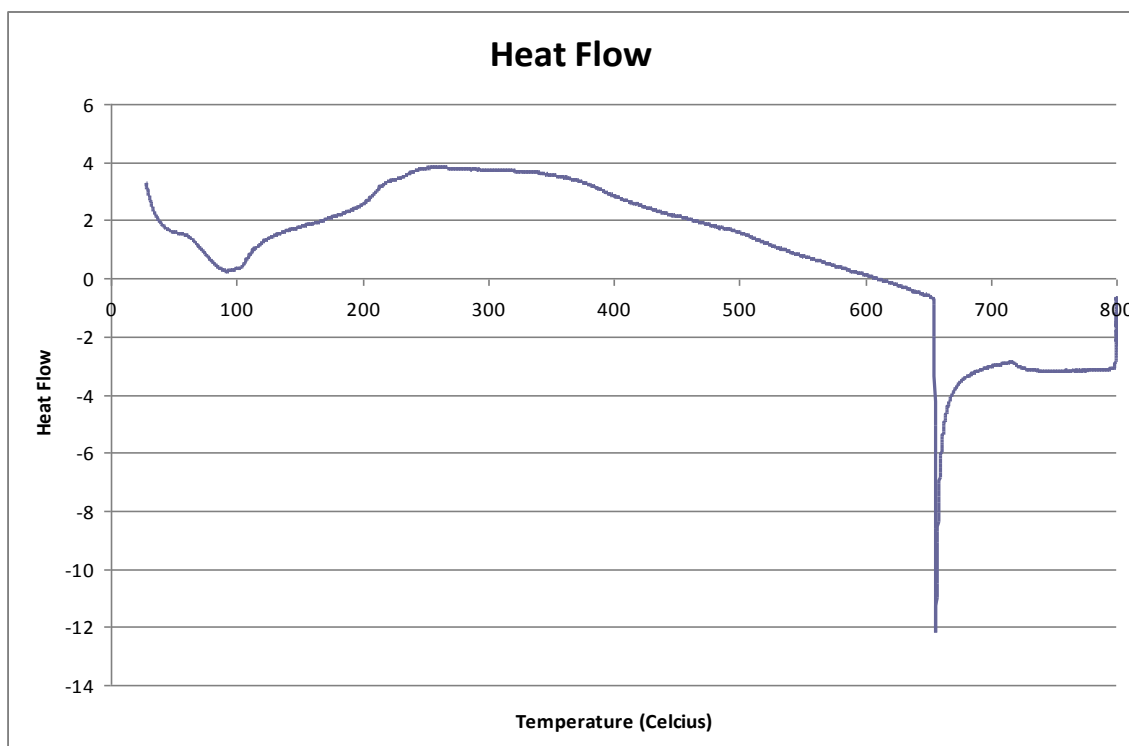


Figure 3.5 Graph showing change in heat flow with respect to temperature

Whilst these TGA results show a clear and sudden drop in catalyst mass, the temperature at which this happens (665 °C) is below the range at which the CO conversion drop occurs. Two explanations are considered plausible at this point: firstly, that the inert gas used (N₂) in the TGA experiments differs from that used in the heat treatments (He). If the N₂ were to contain impurities, this may cause the reaction at a lower temperature.

Secondly, it is possible that the loss of catalyst mass is not the exact cause of the loss in CO conversion, but may be a precursor to it. An example of this would be if the collapse of the carbon support allowed the dispersed metal particles to come into closer proximity, perhaps leading to sintering and loss of metal surface area. This would be ascertainable by measurement of the metal surface areas across this range, but unfortunately this capability was not available during the time of this study.

SEM was utilised to ascertain if any significant changes in the bulk structure or dispersion of the catalyst could be detected visually, but the results are not included here as all heat

treatment temperatures resulted in highly similar images. There were no discernible differences between the catalysts.

Another possible cause of the loss of surface area and activity would be the formation of a different metal species, which may be less active. To determine if this was the case, XRD traces were obtained for all heat treatment temperatures. A combined graphic of these results is displayed below in **Figure 3.6** and **Figure 3.7**.

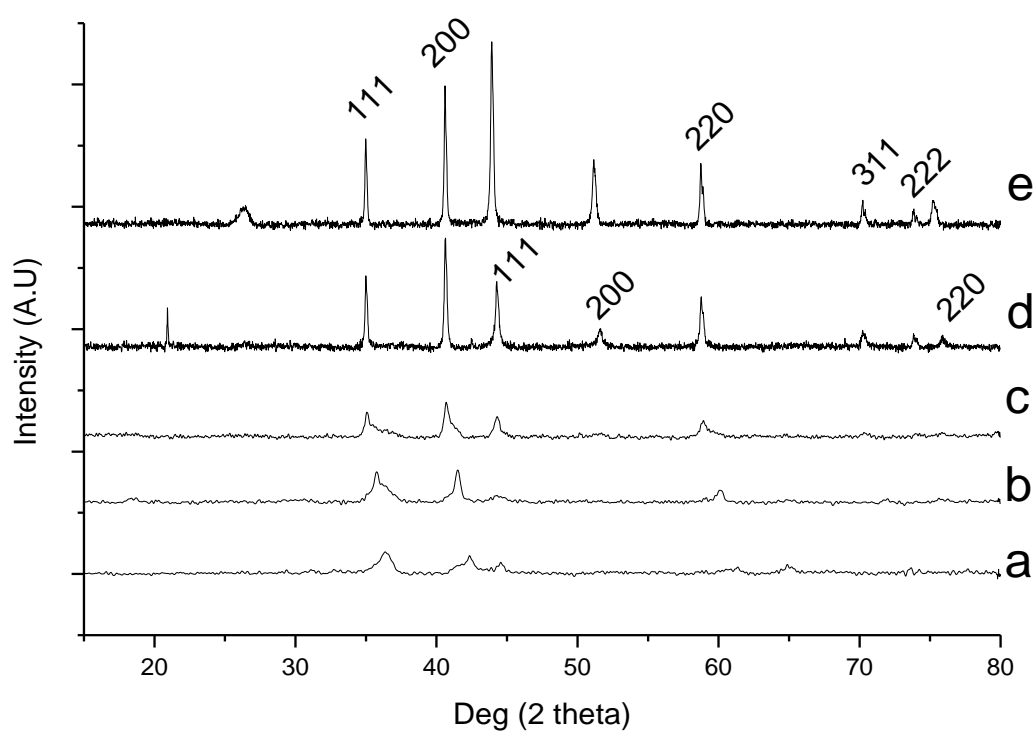


Figure 3.6. XRD traces from catalysts prepared at different heat treatment temperatures, with hkl notation

HT Temperatures: a: 400; b: 500; c: 600; d: 700; e: 800

The species present are consistent with patterns for MnO and Co metal. The hkl planes for MnO are labelled in (e). The hkl planes for Co metal are labelled in (d). The additional phase which appears in ‘800’ appears to be the Mn₃O₄ (101) plane. It is not present in any of the other temperatures, and may be linked to the drop in CO conversion. As can be seen, there is no significant change in composition of the catalysts between heat treatment temperatures of

400 and 800 °C, although the peaks become much clearer and well defined at 700 °C and 800 °C, indicating either an increase in crystallinity or particle size. The relative intensity of the Co metal peaks also seems to increase.

This differs significantly from literature on cobalt manganese catalysts, wherein both species will be present in higher oxidation states, or as mixed metal oxides^{4, 6}. However, it does link to discoveries by Coville et. al⁷. who showed that supported cobalt on carbon can undergo reduction during heat treatment in an inert atmosphere. However, Coville suggested that this occurred at 480 °C, whereas here it is observed at 400 °C.

Interestingly, it is believed that the cobalt-manganese species that take part in the reaction are cobalt metal on MnO^{6, 8, 9}. Usually a reduction step is needed to reach this point, but with these catalysts it seems to have been formed after heat treatment alone.

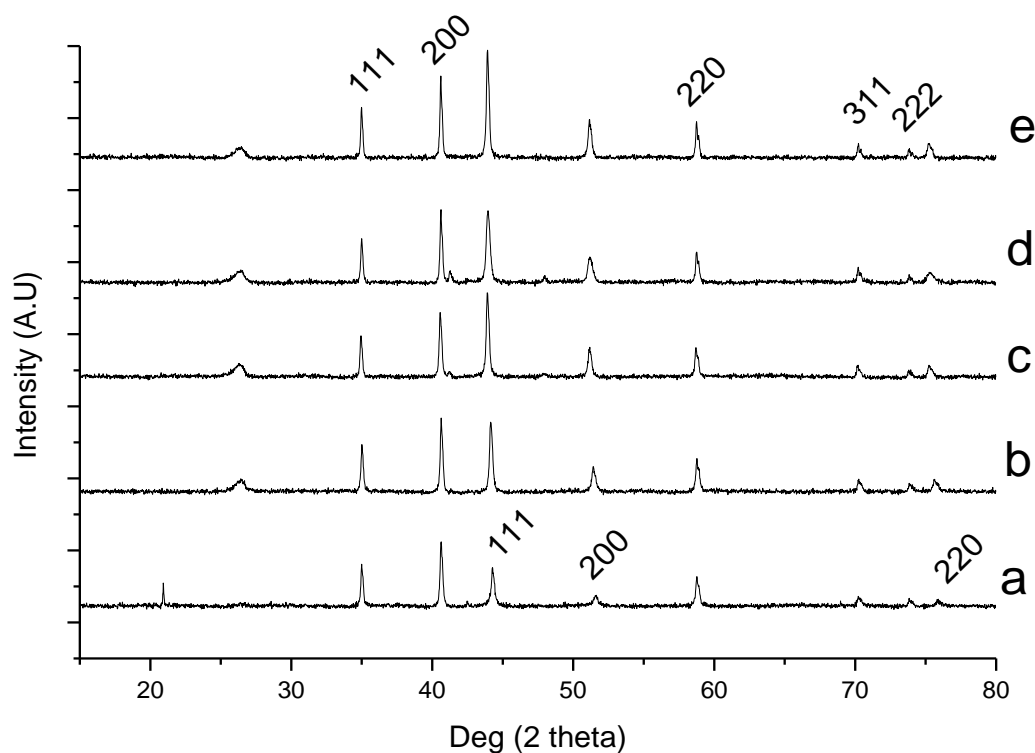


Figure 3.7 XRD traces of catalysts heat treated between 700 and 800 °C.

a: 700; b: 725; c: 750; d: 775; e: 800

The phases present once again appear to be MnO and cobalt metal. The hkl planes of MnO are noted on (e). The hkl planes of Co metal are noted on (a). The relative intensity of the cobalt metal peaks once again appears to increase with increasing HT temperature. These traces strongly imply that the drop in conversion seen with increasing HT temperature is not caused by any change in the metal species present in the catalyst, although it should be noted that the Mn_3O_4 (111) plane only appears above 700 °C, in the HT temperature range which the CO conversion drop occurs.

Given that there are no significant structural changes, this would imply that the loss of CO conversion is an effect caused by the sudden and large drop in surface area brought about by the increased heat treatment temperatures. It is possible that the collapse of the support allowed for sintering of the metal particles, lowering dispersion and increasing particle size. Both of these factors are known to affect FT performance in cobalt catalysts.¹⁰⁻¹² It is also possible that the formation of the Mn_3O_4 phase is significant.

3.3.2. Mechanical mixing of catalyst and support

The previous set of experiments provided evidence that the catalysts lose surface area and CO conversion at above 700 °C. It was also noted that as the temperature increased, the selectivities for CH_4 and CO_2 both decreased. Since the catalyst does not appear to undergo a compositional or structural change at this point except for the formation of small amounts of Mn_3O_4 , it is thought that the carbon support has undergone some transition causing loss of surface area to the catalyst as a whole. This transition likely takes the form of decomposition of the support. It was therefore suggested that if the catalyst material (CoMnO_x) was to be prepared separately at these higher heat treatment temperatures and then subsequently mixed with the carbon support a catalyst might be procured with both the desired selectivities and high surface areas.

In this section all catalysts were prepared utilising the coprecipitation method described in **Section 2.1.1.2**, save that the heat treatment step was conducted at 800 °C. Once this catalyst material had been obtained, 0.8 g of the mixed metal oxide was added to 1.2 g of activated

carbon. The two components were then mixed via stirring with an amount of solvent added. In the initial tests 5 ml of the solvents water, methanol, ethanol, propanol and butanol were used. An additional run was also conducted with no carbon added; only the mixed metal oxide prepared by coprecipitation was used. All catalysts were re-dried for 16 h at 110 °C after this mixing step.

A second series of experiments followed using 1.5 ml of the solvents butanol, octanol and decanol. The higher chain length alcohols were used due to results observed in the initial tests. The lower amount of solvent was used to create a mull rather than a slurry whilst mixing. All catalysts were re-dried for 16 h at 110 °C after this mixing step.

A third set of experiments was conducted in a similar fashion to the second, save that the catalysts were subjected to a secondary heat treatment after the mixing step. This heat treatment step was conducted at 400 °C for 4 h under flowing He (30 ml/min, ramp rate 1 °C/min). This temperature was chosen because previous experiments had shown that there was no surface area loss at this lower temperature.

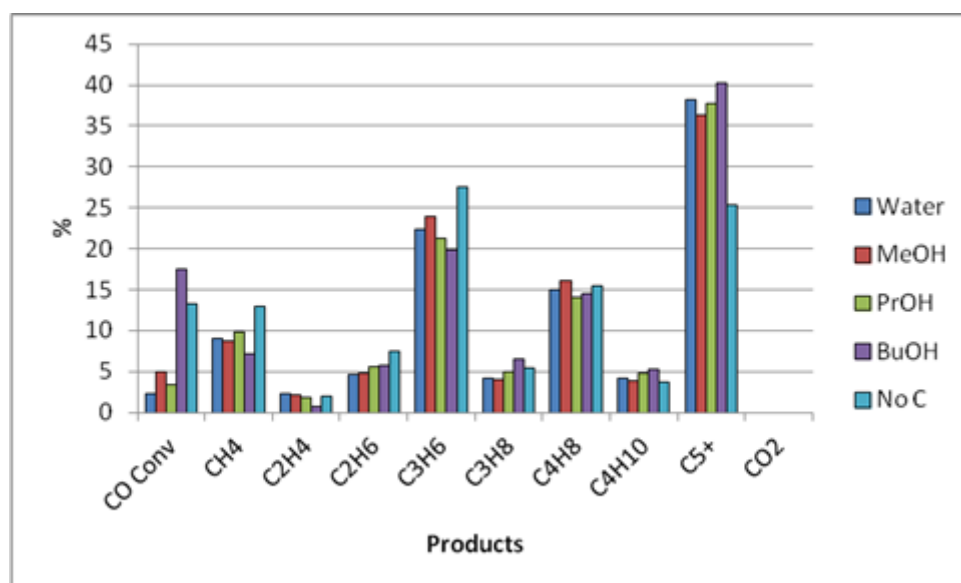
3.3.2.1 Results

The results for this series of experiments are displayed below in **Tables 3.5 to 3.10** and **Figures 3.8 to 3.13**.

Table 3.5 Conversion and selectivity data for physically mixed catalysts

| Mixing agent | Water | MeOH | PrOH | BuOH | No Carbon |
|------------------------------------|-------|------|------|------|-----------|
| CO Conversion | 2.34 | 5 | 3.38 | 17.5 | 13.2 |
| Product selectivities (%) | | | | | |
| CH₄ | 9.1 | 8.8 | 9.8 | 7.2 | 12.9 |
| C₂H₄ | 2.3 | 2.1 | 1.9 | 0.7 | 2 |
| C₂H₆ | 4.7 | 4.8 | 5.6 | 5.7 | 7.5 |
| C₃H₆ | 22.3 | 23.9 | 21.3 | 19.9 | 27.6 |
| C₃H₈ | 4.2 | 4 | 4.9 | 6.5 | 5.4 |
| C₄H₈ | 15 | 16.1 | 14 | 14.5 | 15.5 |
| C₄H₁₀ | 4.1 | 3.8 | 4.8 | 5.3 | 3.7 |
| C₅+ | 38.2 | 36.3 | 37.7 | 40.2 | 25.4 |
| CO₂ | 0 | 0 | 0 | 0 | 0 |

Catalyst test condition: Co:H₂ = 1:1, Temp. = 240 °C, Flow rate = 5 ml/min. Mass = 0.5 g GHSV = 600 h⁻¹

**Figure 3.8** Graph displaying differences in conversion and selectivity for physically mixed catalysts

With the exception of the catalyst using butanol as a mixing agent, the conversions were universally low. Even the relatively high CO conversion of the butanol-mull catalyst is low when compared to those catalysts prepared by impregnation, which frequently display CO conversions of over 50 or 60 %. It was, however, noted that the CO₂ selectivity was

particularly low; its partial pressures in the gas stream were so low that the detector was often unable to resolve any amount of CO₂.

ASF plots and calculated α values for these catalysts are displayed below in **Figure 3.9** and **Table 3.6**.

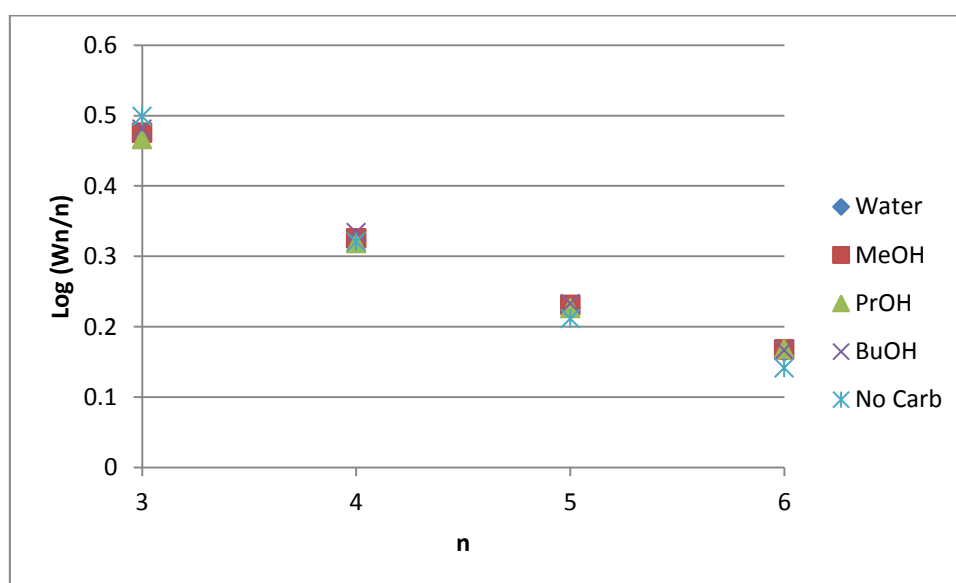


Figure 3.9 ASF plot for mechanically mixed catalysts

Table 3.6 Calculated α values for mechanically mixed catalysts

| Catalyst | Water | MeOH | PrOH | BuOH | No Carb |
|----------|--------|---------|---------|---------|---------|
| Gradient | -0.103 | -0.1019 | -0.0985 | -0.1043 | -0.118 |
| α | 0.789 | 0.791 | 0.797 | 0.787 | 0.762 |

As can be seen, there is no significant change in α brought about by changing the mixing agent. There does appear to be a small difference in catalysts with carbon present, and the catalyst without. These α values are all lower than the catalyst from the previous set of experiments, in which the catalysts was supported upon carbon before HT at 800 °C ($\alpha = 0.801$).

Since the low CO₂ selectivity was deemed desirable and the higher conversion of the catalyst mixed with butanol thought to be promising, another set of experiments was conducted using higher chain

length alcohols; hexanol, octanol and decanol. In these experiments only 1.5 ml of the mixing agent was used, as 5 ml was creating a wet slurry rather than the desired dry mull. The results for this series of experiments are displayed below in **Table 3.7** and **Figure 3.10**.

Table 3.7 Conversion and selectivity data for mechanically mixed catalysts

| Mixing Agent | Hexanol | Octanol | Decanol |
|------------------------------------|---------|---------|---------|
| CO Conversion | 7.76 | 11.7 | 10.79 |
| Product selectivities (%) | | | |
| CH₄ | 18 | 23 | 25 |
| C₂H₄ | 1.3 | 0.8 | 0.8 |
| C₂H₆ | 4 | 4 | 3 |
| C₃H₆ | 18 | 13.2 | 9 |
| C₃H₈ | 3 | 3.4 | 3 |
| C₄H₈ | 13 | 10.1 | 9 |
| C₄H₁₀ | 3 | 3.9 | 3 |
| C₅+ | 39.9 | 38.8 | 45.5 |
| CO₂ | 1.2 | 0.95 | 0.77 |

Catalyst test condition: Co:H₂ = 1:1, Temp. = 240 °C, Flow rate = 5 ml/min. Mass = 0.5 g GHSV = 600 h⁻¹

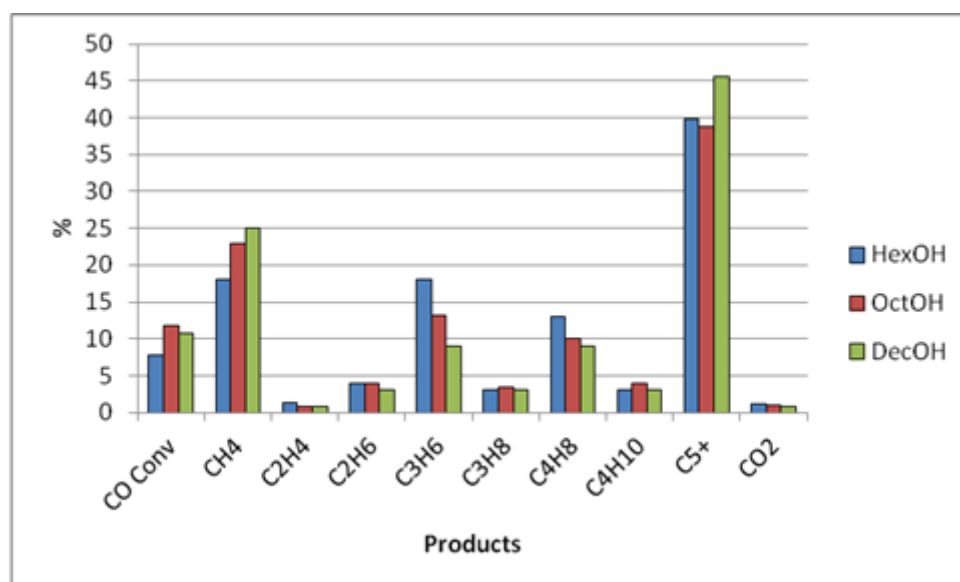


Figure 3.10 Graph displaying trends in conversion and selectivity for mechanically mixed catalysts

These catalysts, although displaying slightly higher conversion than many of the previous series, were still not active enough to be classed as ‘productive’ catalysts. There was also an undesirable trend with increasing mixing agent chain length; an increase in CH₄ selectivity with decreasing selectivities to alkenes.

ASF plots for these catalysts, along with calculated α values, are displayed below in **Figure 3.11** and **Table 3.8**.

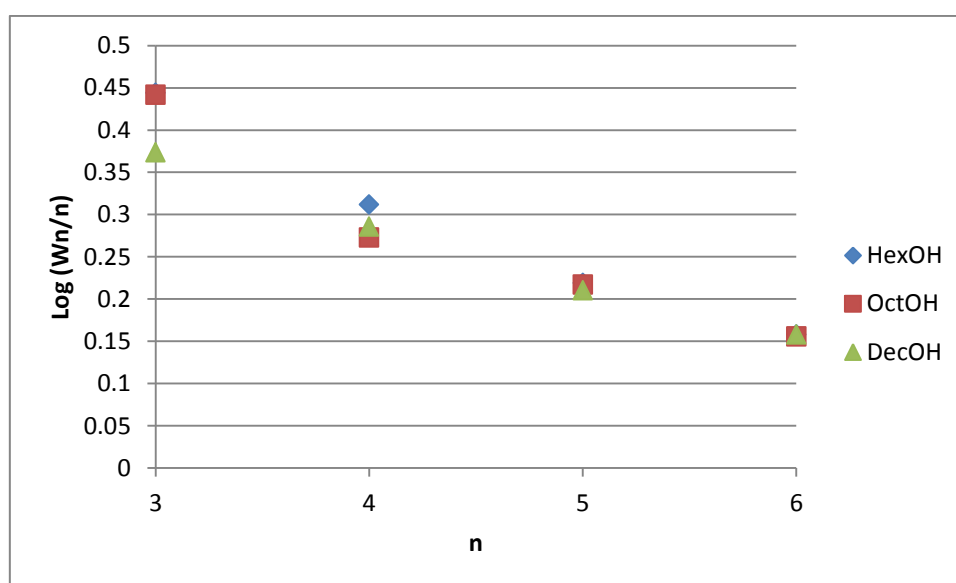


Figure 3.11 ASF plots for mechanically mixed catalysts

Table 3.8 Calculated α values for mechanically mixed catalysts

| Catalyst | HexOH | OctOH | DecOH |
|----------|---------|---------|---------|
| Gradient | -0.0951 | -0.0913 | -0.0721 |
| α | 0.803 | 0.810 | 0.847 |

The differences in α appear to be more significant in these cases than they were with the original selection of mixing agents. However, in this case we have only increased the value from the value of the supported catalyst ($\alpha = 0.801$), which pushes the product distribution away from the C₂-C₄ range desired towards higher chain alcohols.

A final series of experiments on this theme was conducted, in which the catalyst was mixed as before, but was then subjected to a second, gentler heat treatment for 4 h at 400 °C under flowing He (5 ml/min, ramp rate 1 °C/min). The theory behind this was that the catalyst was not binding to the support under the previous conditions, whereas this secondary heat treatment might induce some catalyst-support interaction. The results of this set of experiments are displayed below in **Table 3.9** and **Figure 3.12**.

Table 3.9 Conversion and selectivity data for reheated mechanically mixed catalysts

| Mixing Agent | Hexanol | Octanol | Decanol |
|------------------------------------|---------|---------|---------|
| CO Conversion | 35.74 | 35.88 | 19.3 |
| Product selectivities (%) | | | |
| CH₄ | 11.73 | 11.2 | 11.4 |
| C₂H₄ | 0.84 | 0.89 | 0.7 |
| C₂H₆ | 6.2 | 5.59 | 6.1 |
| C₃H₆ | 21.9 | 21.03 | 20 |
| C₃H₈ | 4.9 | 4.86 | 5.7 |
| C₄H₈ | 14.7 | 14.33 | 13.5 |
| C₄H₁₀ | 4.3 | 4.11 | 5.2 |
| C₅+ | 35.5 | 34.4 | 34.9 |
| CO₂ | 3.16 | 3.33 | 2.5 |

Catalyst test condition: Co:H₂ =1:1, Temp. = 240 °C, Flow rate = 5 ml/min. Mass =0.5 g GHSV = 600 h⁻¹

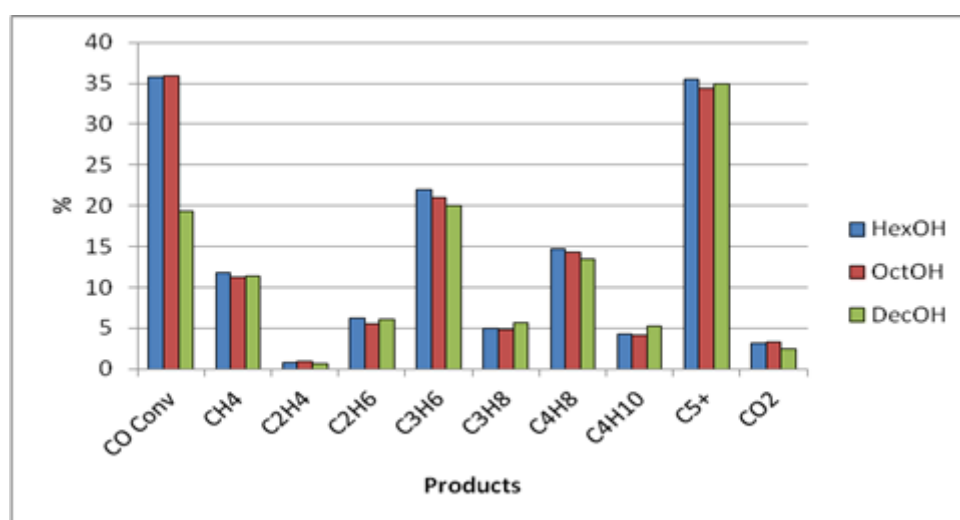


Figure 3.12 Graph displaying differences in conversion and selectivity for reheated mechanically mixed catalysts

These catalysts display a marked increase in CO conversion compared to those which did not undergo a secondary heat treatment. The conversion, however, is still low compared to catalysts of the same metal-carbon ratios prepared by impregnation. Also, the negative trends noted in the previous set of experiments have mostly been eliminated; the selectivities are mostly stable.

ASF plots of these reheated catalysts, plus the accompanying α values, are given below in **Figure 3.13** and **Table 3.10**.

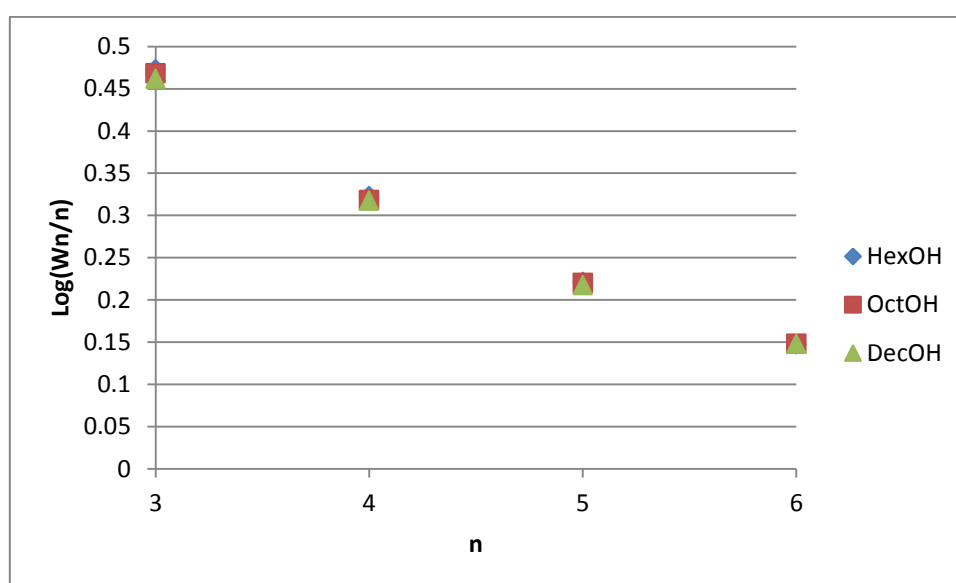


Figure 3.13 ASF plot for mechanically mixed and reheated catalysts

Table 3.10 Calculated α values for mechanically mixed and reheated catalysts

| Catalyst | HexOH | OctOH | DecOH |
|----------------------------|---------|---------|---------|
| Gradient | -0.1078 | -0.1081 | -0.1041 |
| α | 0.780 | 0.780 | 0.787 |

The α values here reflect the increased stability of the reheated catalysts. The variations in the product distribution were small, and this is reflected in the values. The shift between the two sets of catalysts is quite large; 0.06 for the DecOH mixing agent, triple the largest shift seen up to this point. This would imply that the catalyst is undergoing a significant change. A possibility is that due to the higher boiling points of the solvents, the drying step was not

vigorous enough to remove all of the liquid. However, the reheating at 400 °C is significantly higher than the boiling points of the solvents used, and may have resulted in successfully driving off the liquids. This may account for the increased stability across the selectivities.

Overall the results of these three sets of experiments have not been promising, displaying low conversion and higher selectivity to C₅₊ products than would be liked. It is quite probably that in most cases, the mechanical mixing had no beneficial effect, serving only to dilute the oxide material with inactive carbon. The reheating step in the final experiments may have served to promote some support-metal interactions, but it still displays far lower CO conversion than supported catalysts from earlier experiments.

3.3.2.2 Characterisation

XRD traces were obtained for all of the initial catalysts. These are displayed below in **Figure 3.14**.

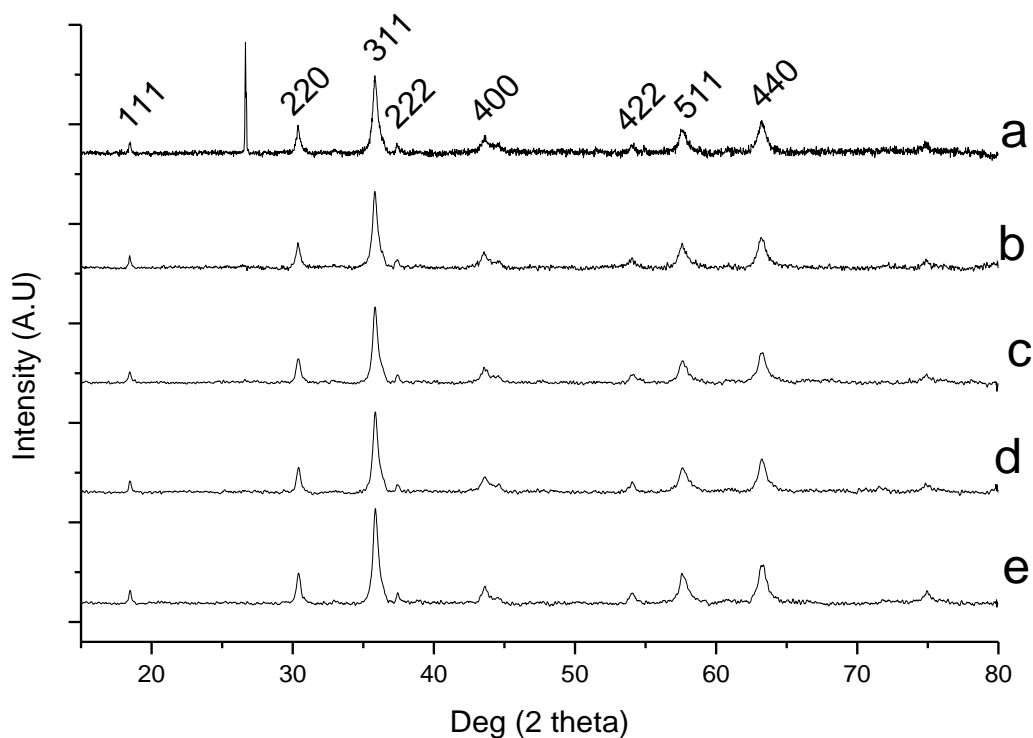


Figure 3.14 XRD traces for mechanically mixed catalysts with hkl notation

As can be seen, the displayed is that of the cobalt-manganese spinel, MnCo_2O_4 . The additional peak seen in trace (a) is consistent with graphitic carbon. It is interesting to note that trace (e) is identical to the others, despite not having undergone the mechanical mixing stage. This indicates that the presence of mechanically mixed carbon has made no difference to the metal species formed in the catalysts. The phases present are consistent with those reported in literature for CoMnO_x catalysts^{6,13}.

Also relevant is a comparison with the catalyst from the previous section, which was supported on carbon before heat treatment at $800\text{ }^\circ\text{C}$. This is displayed below in **Figure 3.15**.

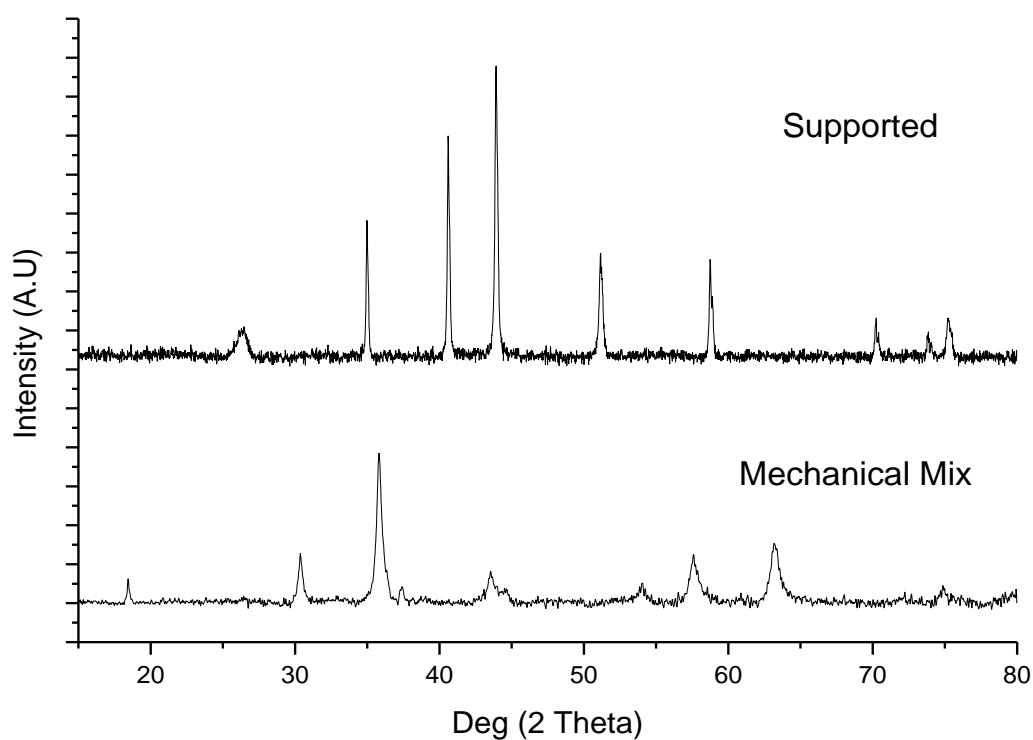


Figure 3.15 XRD trace comparison of catalysts heat treated at 800 °C

As can be seen, the materials are different, with the mechanically mixed catalyst having formed a spinel and the supported equivalent having formed Co metal supported on MnO. The catalyst undergoing heat treatment when supported on carbon appears to be in a more reduced form than the one having undergone mechanical mixing. This implies that when supported on carbon, the catalysts are somehow reduced by heat treatment in an inert atmosphere. This assertion has been noted before in the literature by Coville^{7, 14}. This effect will be noted several times throughout this study, and will be referred to as **autoreduction**.

Surface area measurements for these catalysts were measured using the BET method. These results are displayed below in **Table 3.11**.

Table 3.11 Surface area measurements of mechanically mixed catalysts

| Mixing agent | Surface Area (m ² /g) |
|--------------|----------------------------------|
| Water | 499 |
| Methanol | 314 |
| Ethanol | 378 |
| Propanol | 352 |
| Butanol | 575 |
| No Carbon | 12 |

There is no logical trend in these results, as although the highest CO conversion was recorded by the catalyst with the highest surface area, the lowest CO conversion was recorded by the catalyst with the second highest surface area. Given the assumption that the presence of the carbon has done nothing more than dilute the active phase, these surface area measurements likely represent a weighted average between the very low surface area of the metal oxides (~12 m²/g) and the very high surface area of the activated carbon (~1700 m²/g).

XRD traces of a mechanically mixed catalyst and its reheated equivalent were also obtained to see what effects the reheating step had upon the catalyst. These traces are displayed below in **Figure 3.16**.

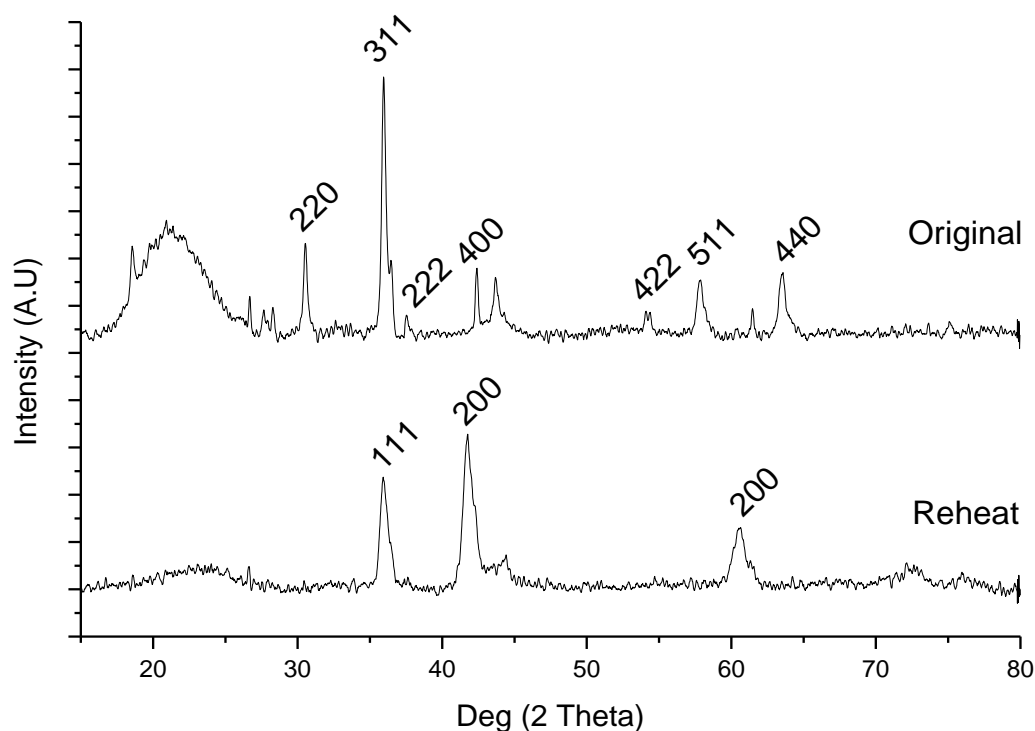


Figure 3.16 XRD trace comparison between mechanically mixed and reheated catalyst.

The mechanically mixed material has a trace consistent with the spinel MnCo₂O₄. The reheated version of this, however, displays a trace consistent with CoO, with a small amount of Co metal. It appears that upon reheating in contact with carbon, the cobalt has undergone the autoreduction mentioned previously. It seems interesting that this effect occurs without actually directly supporting the materials, and would seem to go some way to explaining the shift in conversion and selectivities between the mixed and reheated catalysts. It is unclear why there are no Mn-related peaks in the reheated material, although it is possible that the peaks labelled CoO are in fact a combination of CoO and MnO. These materials are very close in terms of XRD pattern, and distinguishing them from lower angle peaks in particular can be difficult.

3.3.3 Variations in heat treatment duration

Having shown that the temperature of heat treatment could have significant bearing on the final activity of the catalyst, it was decided to further investigate the heat treatment step by conducting experiments into the effects of the duration of the heat treatment step.

The catalysts prepared for these experiments were created using the method outlined in **Section 2.1.1.1**, save that the duration of the heat treatment step was varied for each catalyst. The durations used were 4, 8, 12, 16, and 20 hours, although due to a furnace malfunction the catalyst heat treated for 8 h did not produce a viable catalyst.

3.3.3.1 Results

The results for this series of experiments are displayed below in **Table 3.12** and **Figure 3.17**.

Table 3.12 Conversion and selectivity data for catalysts prepared with different heat treatment durations

| HT Duration (h) | 4 | 12 | 16 | 20 |
|----------------------------------|------|-------|-------|-------|
| CO Conversion | 53.3 | 48.27 | 46.44 | 45.42 |
| Product selectivities (%) | | | | |
| CH ₄ | 1.3 | 1.46 | 1.42 | 1.17 |
| C ₂ H ₄ | 0.5 | 0.53 | 0.71 | 1.09 |
| C ₂ H ₆ | 5.4 | 5.46 | 4.64 | 4.28 |
| C ₃ H ₆ | 19.6 | 19.9 | 20.8 | 22.06 |
| C ₃ H ₈ | 7.3 | 7.08 | 6.55 | 6.07 |
| C ₄ H ₈ | 19 | 19.2 | 18.45 | 19 |
| C ₄ H ₁₀ | 4.8 | 4.6 | 5.39 | 5.46 |
| C ₅ + | 31.7 | 31.39 | 31.97 | 37.08 |
| CO ₂ | 10.5 | 10.36 | 10.06 | 3.79 |

Catalyst test condition: Co:H₂ =1:1, Temp. = 240 °C, Flow rate = 5 ml/min. Mass =0.5 g GHSV = 600 h⁻¹

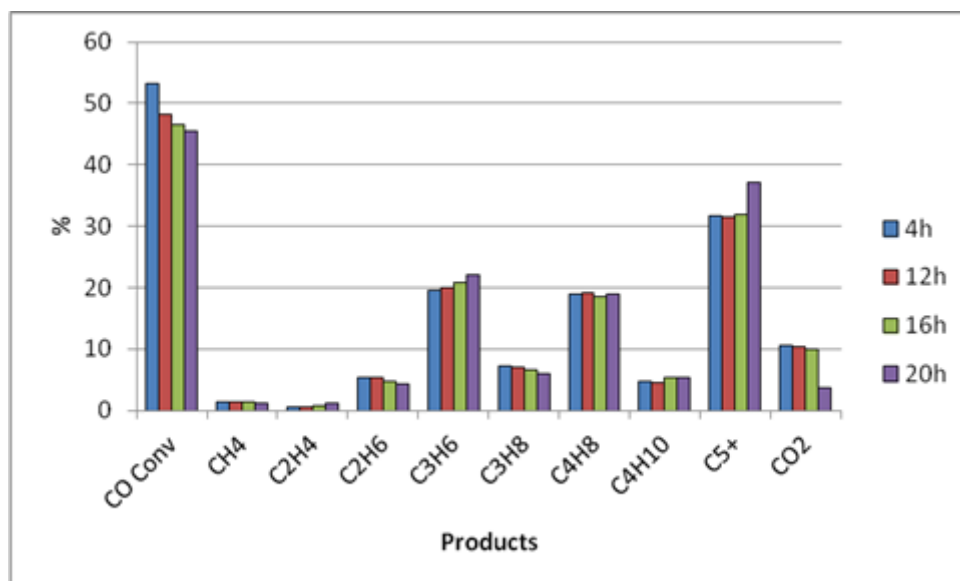


Figure 3.17 Graph displaying trends in conversion and selectivity for catalysts prepared with different heat treatment times

The catalysts show a decrease in CO conversion with an increase in duration of heat treatment. The selectivities of the catalysts remain broadly unchanged, although the catalyst heat treated for 20 h displays markedly lower CO₂ selectivity and increased selectivity to C₅₊ products. Whilst the reduced CO₂ is desirable, as is the slight increase in C₃H₆ selectivity, it was deemed that the increase in C₅₊ selectivity and decrease in CO conversion outweighed these benefits.

The standard preparation outlined in **Section 2.1.1.1** was based on these results, and those of **Section 3.3.1**, leading to the lower heat treatment temperatures and durations used throughout this thesis.

Unfortunately, as these results were obtained at a point where C₅₊ data was defined as the single category 'C₅₊', it is not possible to plot an ASF distribution for this data.

3.3.3.2 Characterisation

The catalysts tested in this section were subjected to BET and XRD analysis in an attempt to uncover the source of the trends in CO conversion and selectivity. The results of these techniques are displayed below in **Figure 3.18** and **Table 3.13**.

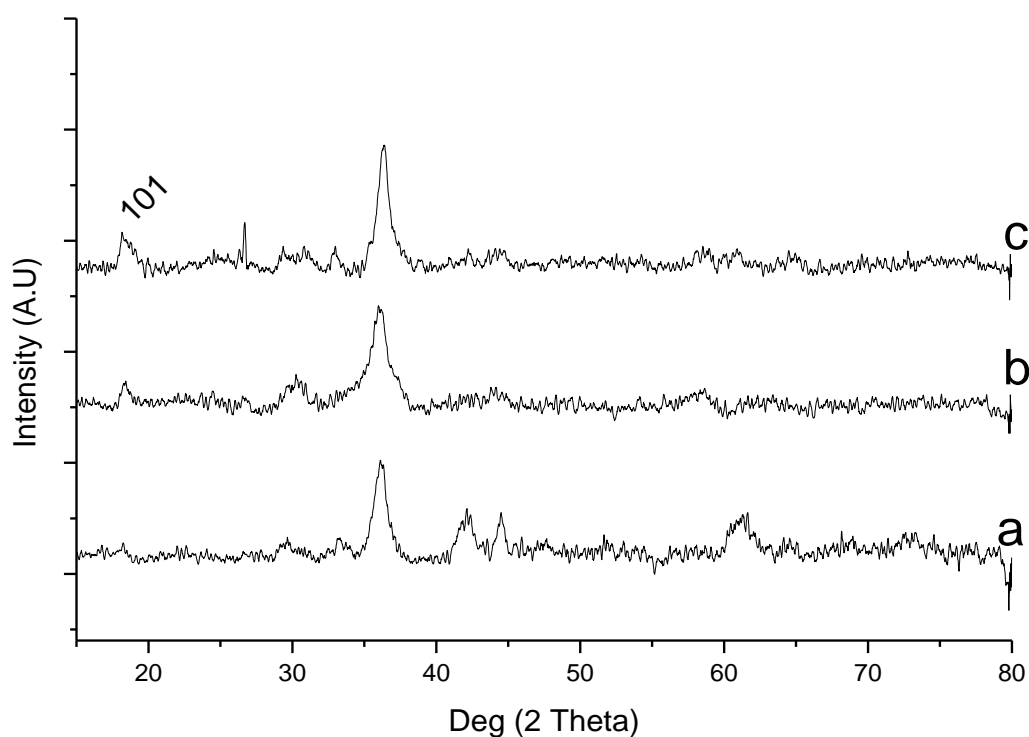


Figure 3.18 Graphic displaying overlaying XRD patterns of catalysts prepared using different heat treatment durations

The catalysts display low crystallinity, resulting in broader peaks. This makes it difficult to identify the species present. The peaks that can be discerned seem to indicate the presence of MnO and Mn₃O₄ in the case of (b) and (c), although (a) seems to contain Co metal peaks and no Mn₃O₄.

Table 3.13 Surface area measurements of catalysts prepared with varying heat treatment durations

| Heat Treatment time (h) | Surface area (m ² /g) |
|----------------------------|----------------------------------|
| | After Heat Treatment |
| 4 | 449 |
| 12 | 431 |
| 16 | 417 |
| 20 | 355 |

There is a definite trend of decreasing surface area with increasing heat treatment duration. This corresponds with the decreasing CO conversion observed with increasing heat treatment duration, leading to the conclusion that for these catalysts, higher surface area will result in higher CO conversion.

3.3.4 Variations of drying step

With the previous series of experiments having shown that the final performance of the catalyst to be sensitive to conditions in the preparation steps, it was decided that experiments should be conducted on all of the separate steps.

The drying step had previously been shown to influence the final catalyst; in earlier work it had been noted that a catalyst which had been prepared in a beaker had lower CO conversion than an equivalent catalyst which had been prepared in a ceramic bowl. More effort was therefore applied to investigating the effects of these variables.

A series of experiments were performed wherein the catalysts were dried in differing vessels; a beaker, a bowl, and a Petri dish, as shown below in **Figure 3.19**.



Figure 3.19 Drying vessels

Two sets of experiments were conducted; one where the drying steps were performed with the vessels uncovered, and a second where the vessels were covered with a large watch glass. Excluding the variation in drying vessel, the catalysts were prepared according to the method set out in **Section 2.1.1.1**.

3.3.4.1 Results

The first set of experiments carried out in this series was testing catalysts dried in an uncovered vessel. The results for these experiments are shown below in **Table 3.14** and **Figure 3.20**.

Table 3.14 Conversion and selectivity data for catalysts dried in an uncovered vessel

| Drying Vessel | Beaker | Bowl | Petri Dish |
|----------------------------------|--------|-------|------------|
| CO Conversion | 43.13 | 62.25 | 49.03 |
| Product selectivities (%) | | | |
| CH ₄ | 15.87 | 17.42 | 16.79 |
| C ₂ H ₄ | 0.64 | 0.41 | 0.59 |
| C ₂ H ₆ | 8.02 | 8.71 | 7.34 |
| C ₃ H ₆ | 19.8 | 20.47 | 20.7 |
| C ₃ H ₈ | 6.62 | 6.57 | 6.3 |
| C ₄ H ₈ | 13.13 | 13.93 | 12.95 |
| C ₄ H ₁₀ | 3.25 | 1.8 | 2.66 |
| C ₅ + | 29.74 | 26.4 | 26 |
| CO ₂ | 2.94 | 4.29 | 4 |

Catalyst test condition: Co:H₂ = 1:1, Temp. = 240 °C, Flow rate = 5 ml/min. Mass = 0.5 g GHSV = 600 h⁻¹

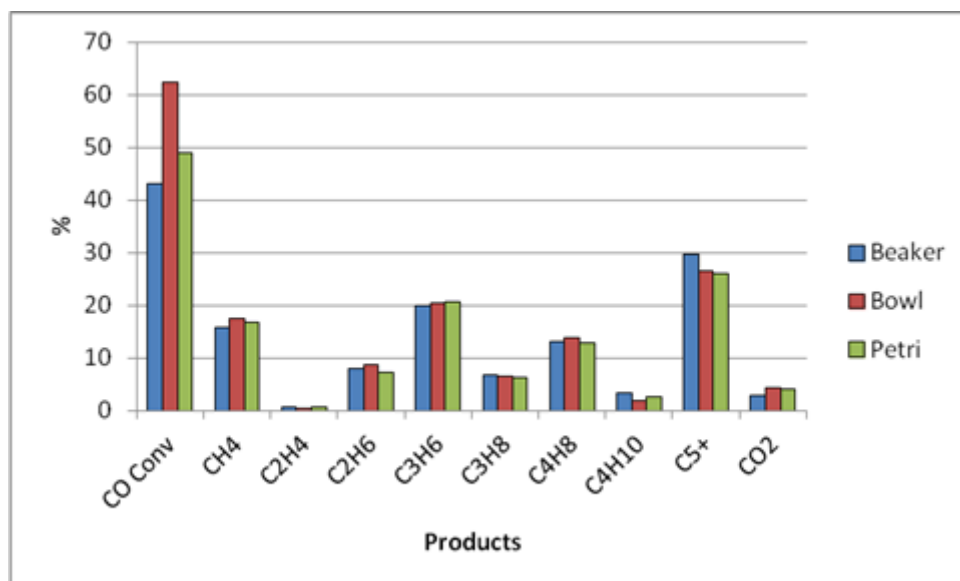


Figure 3.20 Graph showing differences in conversion and selectivity for catalysts dried in an uncovered vessel

The selectivity of the catalysts prepared in this manner seems to be largely unaffected by the drying vessel. The CO conversion, however, shows a difference of nearly 20 % between the beaker-dried and bowl-dried samples.

Whilst this was initially believed to be a matter of rate of catalyst drying, this does not bear close scrutiny; were this the case, it would be expected that the higher surface area – to – volume ratio of the Petri dish would produce the most active catalyst.

It could be the case that the surface area-to-volume ratio is still playing a part, as in the case of the beaker and the petri dish, the surface area will stay constant with decreasing volume due to the flat sides of the vessel. In the case of the bowl, however, the surface area will decrease with decreasing liquid volume due to the curved sides. It is also possible that the material of the vessel has contributed; the vessel which produced the most active catalyst was dried in a ceramic vessel as opposed to glass.

ASF plots and the corresponding α values are displayed below in **Figure 3.21** and **Table 3.15**

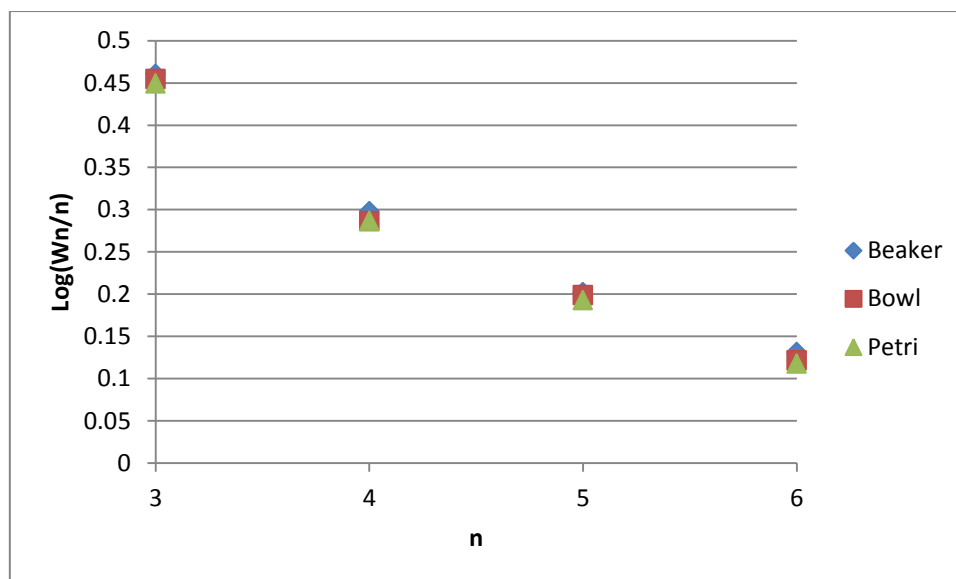


Figure 3.21 ASF plots of catalysts dried in different uncovered vessels

Table 3.15 Calculated α values for catalysts dried in different uncovered vessels

| Catalyst | Beaker | Bowl | Petri |
|----------|---------|---------|---------|
| Gradient | -0.1083 | -0.1087 | -0.1089 |
| α | 0.779 | 0.779 | 0.778 |

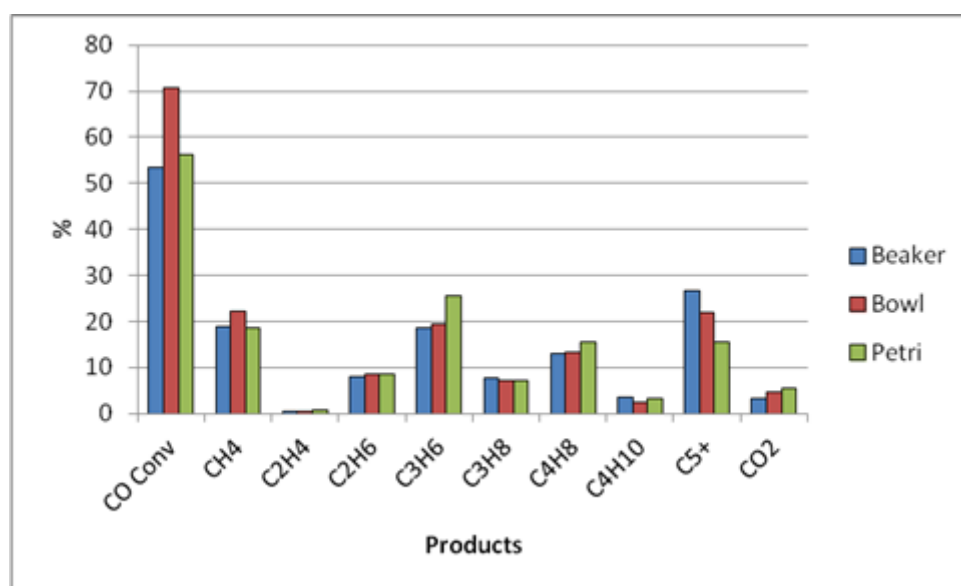
Despite the significant differences in conversion, the α values are incredibly similar. This lends itself to the earlier conclusion that CO conversion and α do not seem to be affected by the same factors.

The next series of experiments was testing catalysts dried in vessels covered by a watch glass. The results for this series of experiments are displayed below in **Table 3.16** and **Figure 3.22**.

Table 3.16 Conversion and selectivity data for catalysts dried in a covered vessel

| Mixing Agent | Beaker | Bowl | Petri Dish |
|----------------------------------|--------|-------|------------|
| CO Conversion | 53.44 | 70.6 | 56.25 |
| Product selectivities (%) | | | |
| CH ₄ | 18.78 | 22.23 | 18.5 |
| C ₂ H ₄ | 0.56 | 0.46 | 0.7 |
| C ₂ H ₆ | 7.88 | 8.66 | 8.43 |
| C ₃ H ₆ | 18.58 | 19.38 | 25.47 |
| C ₃ H ₈ | 7.68 | 7.1 | 7.1 |
| C ₄ H ₈ | 13.06 | 13.2 | 15.4 |
| C ₄ H ₁₀ | 3.42 | 2.41 | 3.18 |
| C ₅ + | 26.78 | 21.98 | 15.62 |
| CO ₂ | 3.26 | 4.58 | 5.6 |

Catalyst test condition: Co:H₂ = 1:1, Temp. = 240 °C, Flow rate = 5 ml/min. Mass = 0.5 g GHSV = 600 h⁻¹

**Figure 3.22** Graph displaying trends in conversion and selectivity for catalysts dried in covered vessels

The catalysts dried in covered vessels display a similar trend to the uncovered vessels with respect to CO conversion, although the covered vessel catalysts display uniformly higher conversion than their uncovered counterparts. There are also more pronounced differences in selectivities, but the greatly increased conversion was deemed to be more relevant than the

smaller changes in C_3H_6 and C_{5+} selectivities, leading to all future catalysts being prepared in covered bowls.

ASF plots and the α values calculated from them are displayed below in **Figure 3.23** and **Table 3.17**.

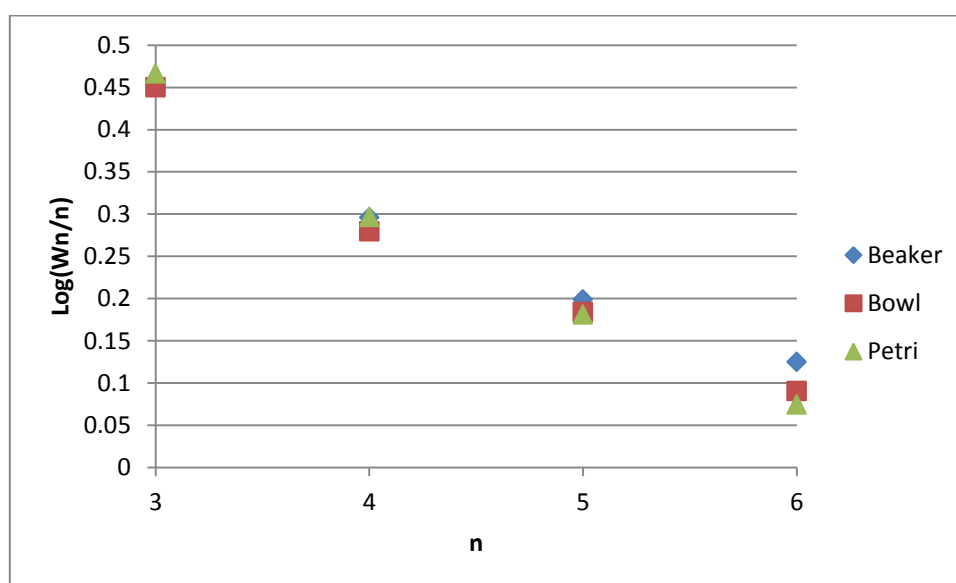


Figure 3.23 ASF plots for catalysts dried in different covered vessels

Table 3.17 Calculated α values for catalysts dried in different covered vessels

| Catalyst | Beaker | Bowl | Petri |
|----------|--------|---------|--------|
| Gradient | -0.109 | -0.1175 | -0.129 |
| α | 0.778 | 0.763 | 0.743 |

The α values for the covered catalysts display a greater variance than those dried in uncovered vessels. The covered petri dish in particular possesses a low value, which is reflected in its higher selectivity to C_3 products. This lowered α value does not appear to have increased C_1 product production as much as one might have expected. This implies that the production of C_1 species is not governed entirely by chain growth probability.

A final series of experiments relating the drying step was performed, in which the catalyst precursors were dried at ambient temperature, rather than at 110 °C as is standard. These experiments were divided into two pairs; the first consisting of a covered and an uncovered bowl as drying vessels, and the second consisting of an uncovered bowl dried with and without stirring. Where used, stirring was conducted at 200 rpm using a magnetic stirrer.

The catalysts were prepared as described in **Section 2.1.1.1**, save that the drying step was conducted as outlined above. The results for these experiments are displayed below in **Table 3.18**, **Figure 3.24** and **Figure 3.25**.

Table 3.18 Conversion and selectivity data for catalysts dried at ambient temperature

| | Covered | Uncovered | | Stirred | Unstirred |
|------------------------------------|---------|-----------|--|---------|-----------|
| CO Conversion | 16.5 | 19.8 | | 18.1 | 19.8 |
| Product selectivities (%) | | | | | |
| CH₄ | 18.8 | 19.9 | | 14.2 | 19.9 |
| C₂H₄ | 0.2 | 0.8 | | 0.5 | 0.8 |
| C₂H₆ | 3.6 | 5.2 | | 4.9 | 5.2 |
| C₃H₆ | 9.9 | 10.7 | | 8.7 | 10.7 |
| C₃H₈ | 6.1 | 6.1 | | 7.3 | 6.1 |
| C₄H₈ | 9.8 | 9.8 | | 9.1 | 9.8 |
| C₄H₁₀ | 4.5 | 4.9 | | 6.8 | 4.9 |
| C₅+ | 45.5 | 40.9 | | 47.8 | 40.9 |
| CO₂ | 1 | 1.7 | | 0.7 | 1.7 |

Catalyst test condition: Co:H₂ = 1:1, Temp. = 240 °C, Flow rate = 5 ml/min. Mass = 0.5 g GHSV = 600 h⁻¹

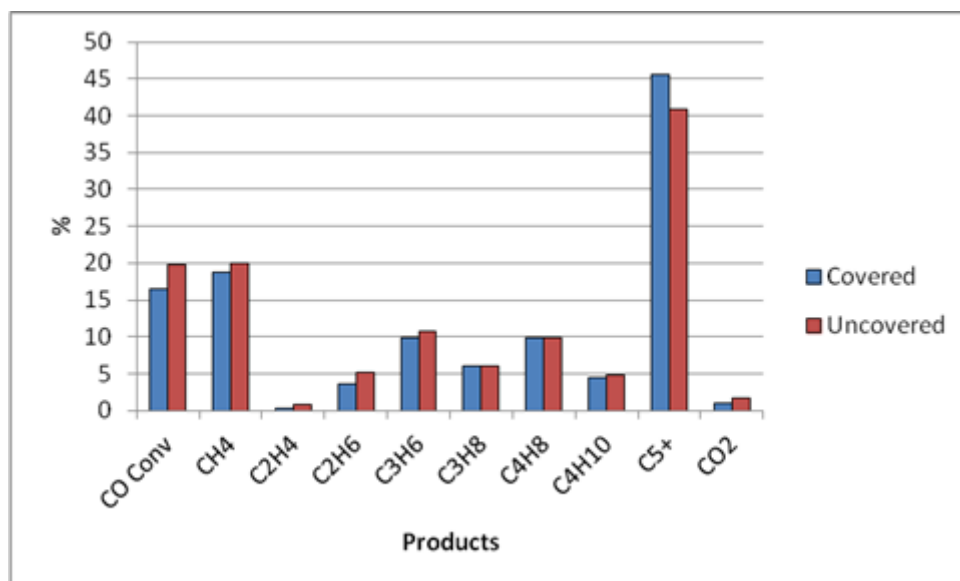


Figure 3.24 Graph displaying conversion and selectivity for catalysts dried at ambient temperature in a bowl

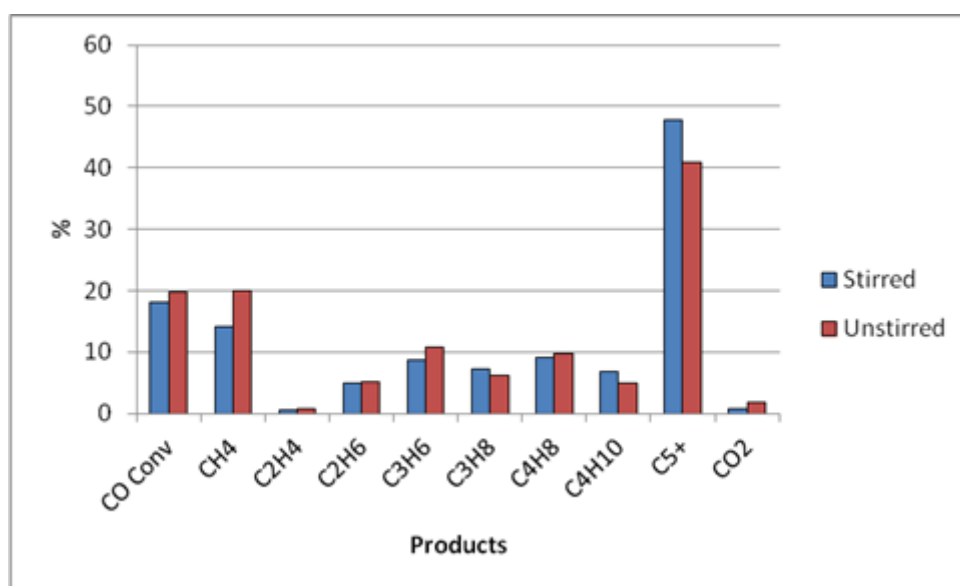


Figure 3.25 Graph displaying conversion and selectivity for catalysts dried at ambient temperature with and without stirring in an uncovered bowl

The uncovered, unstirred catalyst dried at ambient temperature possessed the highest conversion, but it did not prove to be an effective catalyst compared to those prepared by drying at 110 °C. Also of note was the increased selectivity towards an undesirable product, C₅+. Because of these factors it was deemed ineffective to dry these catalysts at ambient temperatures.

A further series of experiments was to be conducted, in which the catalysts would be rapidly dried at higher temperatures. However, it was found that at these higher temperatures the activated carbon support undergoes combustion in air. TGA analysis implied that this occurred at 200 °C, but was observed in catalyst preparation at temperatures as low as 140 °C. Since facilities for drying in an inert atmosphere were not readily available, this line of inquiry was not pursued further.

3.3.4.2 Characterisation

XRD analysis was performed on the all the catalysts prepared in this series of experiments. The results of this are displayed below in **Figure 3.26** and **Figure 3.27**.

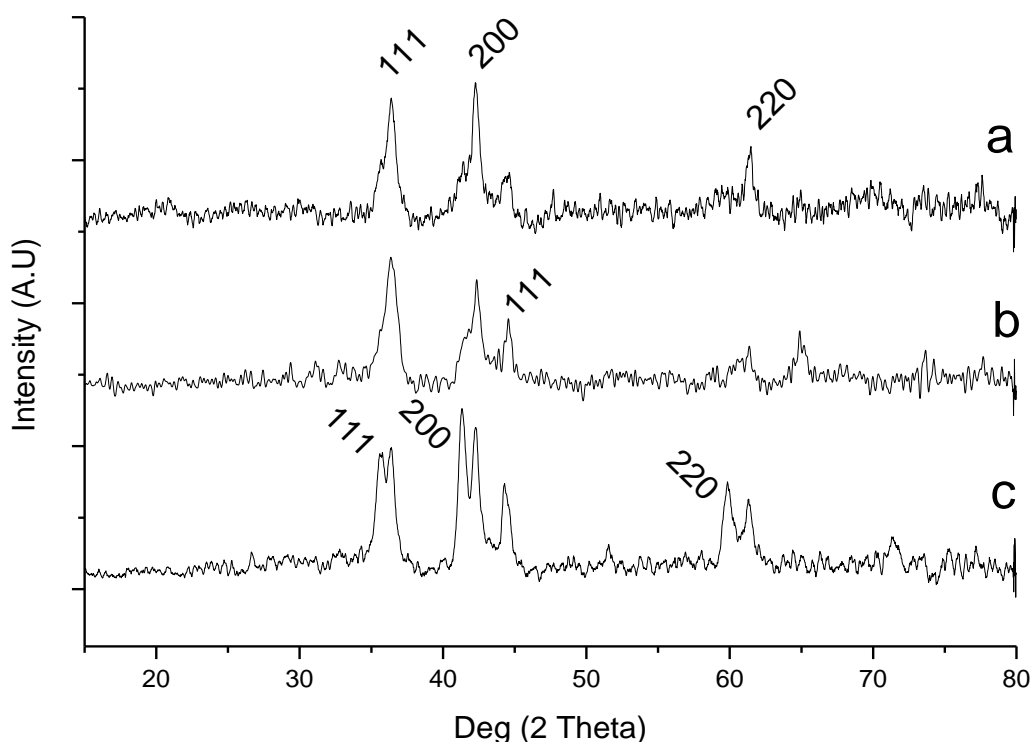


Figure 3.26 XRD traces of catalysts dried in an uncovered vessel

a: Beaker; b: Bowl; c: Petri

The catalysts display patterns consistent with MnO, CoO and Co metal. The catalyst dried in a petri dish displays the most clear mixture of MnO and CoO, with Co metal also present.

The hkl planes of CoO are marked on (a). The hkl planes of Co metal are marked on (b). The hkl planes of MnO are marked on (c).

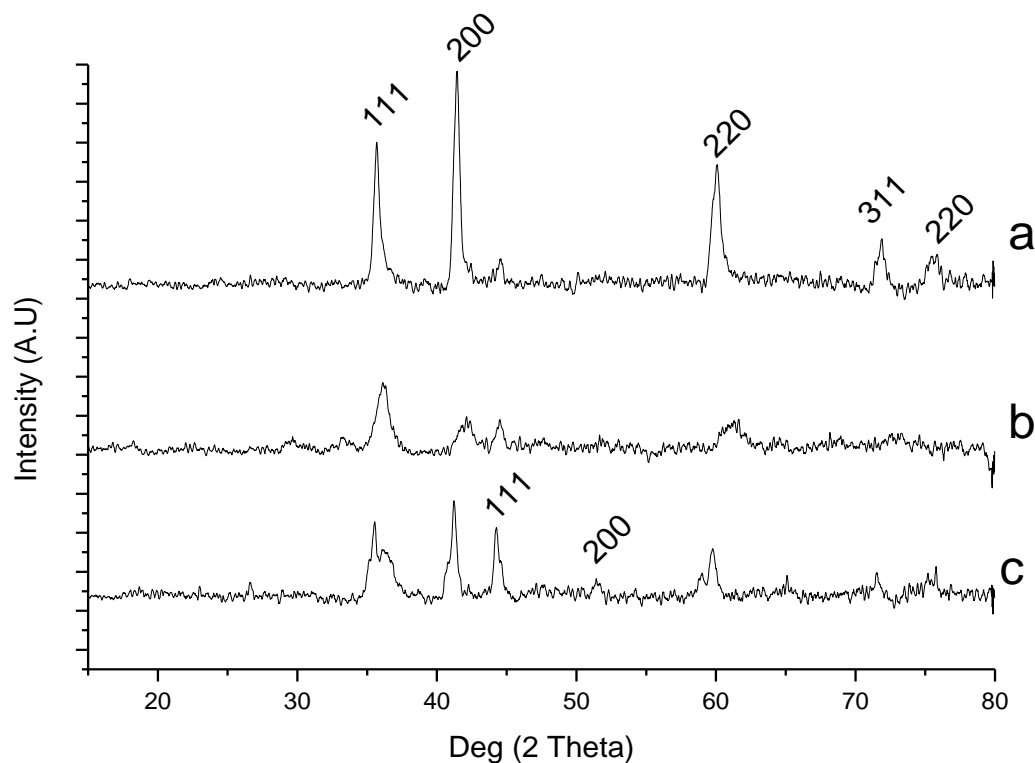


Figure 3.27 XRD pattern of catalysts prepared in covered vessels with hkl notation
 a: Beaker; b: Bowl; c: Petri

These XRD patterns consistently show the presence of MnO and Co. The hkl planes of MnO are marked on (a). The hkl planes of Co are marked on (c). (c) also seems to display some peak splitting, possibly indicative of the presence of both CoO and MnO. This behaviour was also noted in the XRD traces of the catalysts dried in uncovered vessels.

3.3.5 Variations of reduction step

With both drying and heat treatment steps having been investigated, the next logical step was an investigation of the reduction step of the reaction. The first series of reactions investigated the effect of changing the duration of the reduction step.

3.3.5.1 Duration of reduction

Two sets of experiments were performed in this section; firstly, a set of catalysts was prepared according to the method described in **Section 2.1.1.1**, giving catalysts with ratios of Co/Mn/C of 20/20/60. A second batch of catalysts was created using the same method, save that the relative quantities of Co and Mn precursors were altered to give a final catalyst with a composition of Co/Mn/C = 30/10/60.

The results for these experiments are displayed below in **Tables 3.19** and **3.20**, as well as **Figures 3.28** and **3.29**.

3.3.5.1.1 Co/Mn/C = 20/20/60

Table 3.19 Conversion and selectivity data for catalysts reduced for different durations

| Red. Duration | 16 h | 4 h | 0.5 h |
|----------------------------------|-------|------|-------|
| CO Conversion | 70.6 | 66.3 | 57.9 |
| Product selectivities (%) | | | |
| CH ₄ | 22.23 | 18.6 | 19.2 |
| C ₂ H ₄ | 0.46 | 0.2 | 0.5 |
| C ₂ H ₆ | 8.66 | 9.9 | 7.8 |
| C ₃ H ₆ | 19.38 | 18.6 | 19.8 |
| C ₃ H ₈ | 7.1 | 10.8 | 5.9 |
| C ₄ H ₈ | 13.2 | 12.8 | 14.4 |
| C ₄ H ₁₀ | 2.41 | 1.9 | 2.3 |
| C ₅ + | 21.98 | 22.1 | 25.8 |
| CO ₂ | 4.58 | 5.1 | 4.1 |

Catalyst test condition: Co:H₂ = 1:1, Temp. = 240 °C, Flow rate = 5 ml/min. Mass = 0.5 g GHSV = 600 h⁻¹

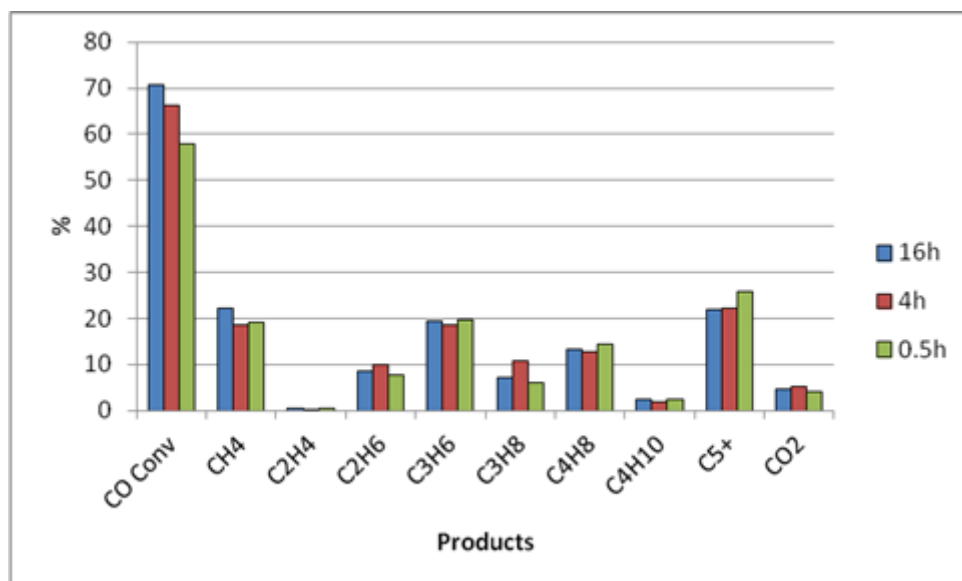


Figure 3.28 Graph displaying the trends in conversion and selectivity for catalysts reduced for different durations

Whilst the CO conversion seems to decrease with decreasing reduction times, the selectivities appear to be broadly stable across this range of durations, with the 0.5 h reduction catalyst possessing slightly higher C₅+ being the only deviance readily evident.

ASF plots and the accompanying α values are given below in **Figure 3.29** and **Table 3.20**.

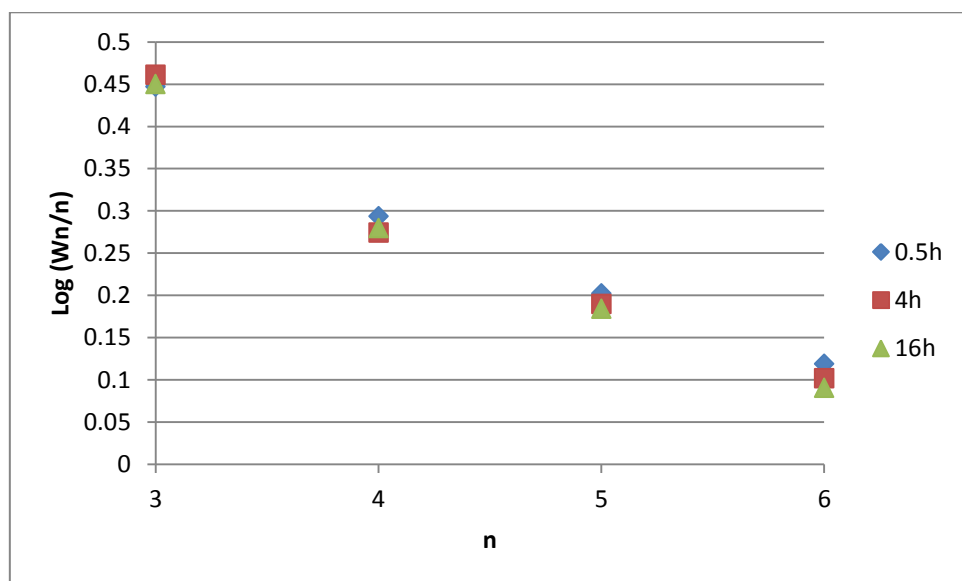


Figure 3.29 ASF plot for Co:Mn = 1:1 catalysts having undergone different reduction durations

Table 3.20 Calculated α values for Co:Mn = 1:1 catalysts having undergone different reduction durations

| Catalyst | 0.5 h | 4 h | 16 h |
|----------|---------|---------|---------|
| Gradient | -0.1076 | -0.1162 | -0.1175 |
| α | 0.781 | 0.765 | 0.763 |

These plots confirm the stability of the selectivities across this range of reduction temperatures, although the C₅₊ selectivity increase for the 0.5 h reduction time has produced a slightly higher α value. There is no trend linking these values with the changes in CO conversion.

3.3.5.1.2 Co/Mn/C = 30/10/60

The reduction time experiments were repeated, this time utilising a catalyst with a higher Co:Mn ratio. The results of these experiments are displayed below in **Table 3.21** and **Table 3.22**, as well as **Figure 3.30** and **Figure 3.31**.

Table 3.21 Conversion and selectivity data for catalysts reduced for different durations

| Red. Duration | 16 h | 4 h | 0.5 h |
|----------------------------------|------|------|-------|
| CO Conversion | 83.3 | 78.4 | 82.9 |
| Product selectivities (%) | | | |
| CH ₄ | 22.2 | 24.6 | 25.9 |
| C ₂ H ₄ | 0.1 | 0.1 | 0.1 |
| C ₂ H ₆ | 9.5 | 10.9 | 11.1 |
| C ₃ H ₆ | 13.6 | 7 | 9.6 |
| C ₃ H ₈ | 12.1 | 17.7 | 18 |
| C ₄ H ₈ | 9.1 | 8.1 | 9.5 |
| C ₄ H ₁₀ | 2 | 2.5 | 2.4 |
| C ₅₊ | 24.8 | 21.4 | 15.1 |
| CO ₂ | 6.6 | 7.8 | 8.4 |

Catalyst test condition: Co:H₂ = 1:1, Temp. = 240 °C, Flow rate = 5 ml/min. Mass = 0.5 g GHSV = 600 h⁻¹

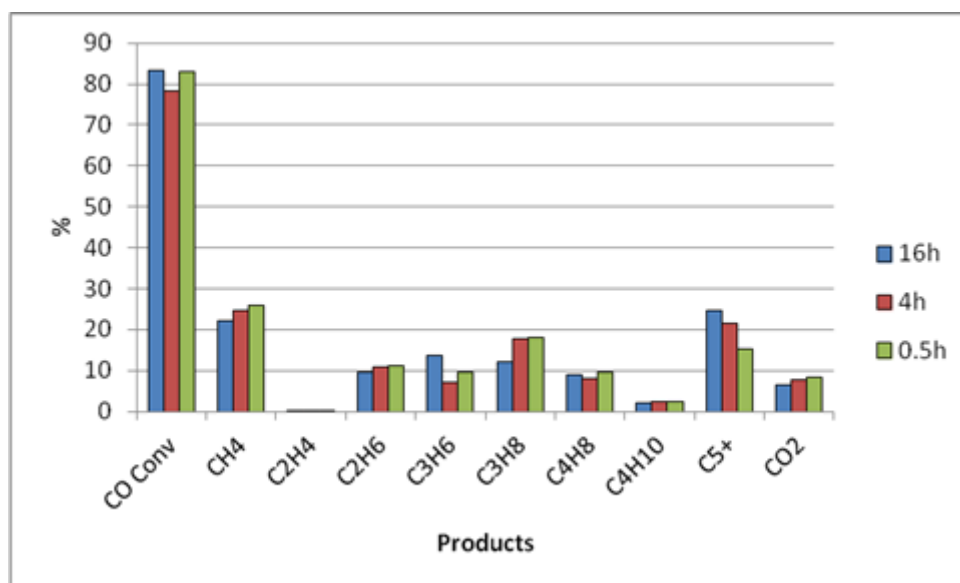


Figure 3.30 Graph displaying the trends in conversion and selectivity for catalysts reduced for different durations

The CO conversion of the higher Co:Mn ratio catalysts seems to have been broadly unaffected by the change in reduction time duration, although the selectivity patterns display far more noticeable trends, with significant decreases in C₅₊ selectivity and increases in lower C-number products with decreasing reduction duration.

One explanation for this is that the shortened reduction times are not sufficient to fully reduce all of the cobalt species. This would explain why there is more of an effect with higher cobalt loading.

ASF plots and the relevant α values are displayed below in **Figure 3.31** and **Table 3.22**.

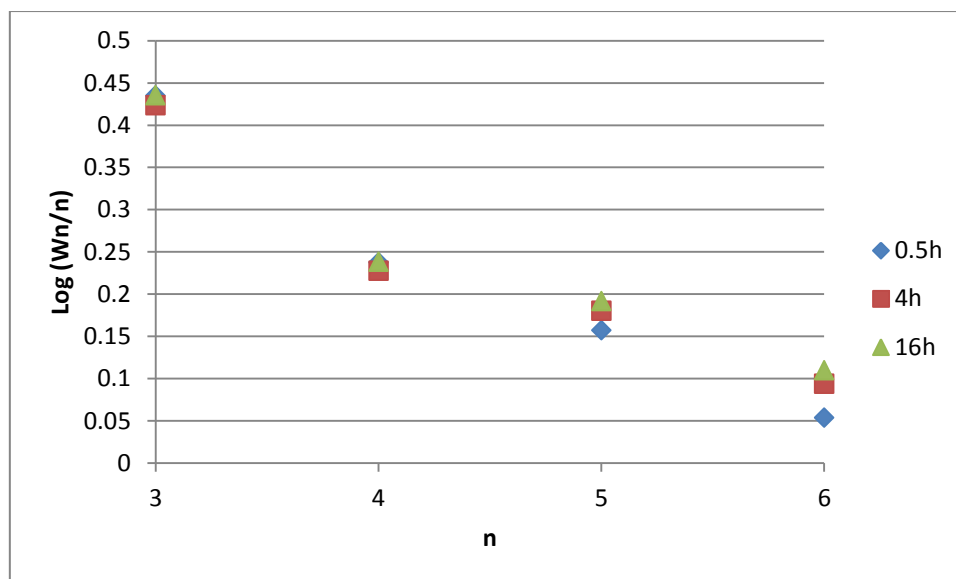


Figure 3.31 ASF plot for Co:Mn = 3:1 catalysts reduced for different durations

Table 3.22 Calculated α values for Co:Mn = 3:1 catalysts reduced for different durations

| Catalyst | 0.5 h | 4 h | 16 h |
|----------|---------|---------|---------|
| Gradient | -0.1223 | -0.1037 | -0.1023 |
| α | 0.755 | 0.788 | 0.790 |

There appears to be a trend here of decreasing α values with decreasing reduction times. This is not the same as the catalysts with Co:Mn = 1:1. This would imply that the reduction of the cobalt primarily is important, a fact reflected in the practice of adding promoters such as Ru to aid cobalt reduction^{15, 16}. However, the effect may be slightly convoluted by the previously noticed autoreduction effect; in most of our catalysts the cobalt already appears to be in a highly reduced state after heat treatment.

However, this hinges on the assumption that the higher Co:Mn ratio catalyst also undergoes this autoreduction effect.

3.3.5.1.3 Characterisation

The catalyst with a higher Co:Mn ratio was analysed by XRD to see if it too had undergone the autoreduction effect. This is displayed below in **Figure 3.32**. Additionally, and *in-situ* XRD of the heat treatment and reduction steps of the Co:Mn =1:1 catalyst was performed, to

see if the point of autoreduction could be determined, and what effect the reduction step has on the catalyst. The results of this are displayed below in **Figure 3.33** and **Figure 3.34**.

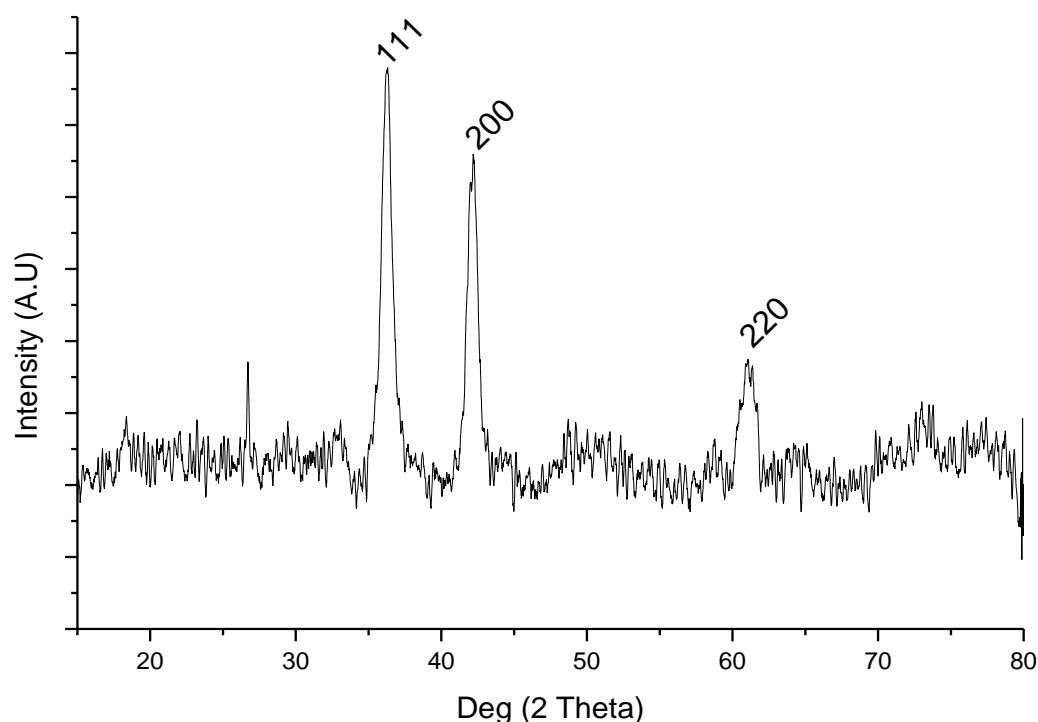


Figure 3.32 XRD trace of catalyst with Co:Mn = 3:1

Whilst this trace appears similar to MnO at first glance, closer inspection of the d-spacings indicates that this is in fact a form of CoO. This would seem to be significant, as it implies that the autoreduction is affected by the amount of various metals present. This partially ties in with the literature: Coville reported that this autoreduction phenomenon occurred at 480 °C for Co supported on carbon nanotubes, yet we have observed it at a lower temperature than this. This would suggest that the presence of manganese acts to promote this autoreduction effect, as catalysts with a 1:1 Co:Mn ratio have been observed to form cobalt metal under inert atmospheres at 400 °C, whereas cobalt alone needs 480 °C. This is somewhat hinted at in the literature; as manganese has been shown to enhance cobalt reducibility¹⁷ it would seem likely that it would also enhance the autoreduction effect. The temperature needed to promote autoreduction in Co:Mn = 3:1 catalysts is unknown; it would have been useful to be able to

perform higher temperature in-situ work on these catalysts, but access to the required equipment was limited. Additionally, as will be shown below, the in-situ programming did not seem able to overcome the problem of fluorescence from cobalt species, which may have complicated detection of emergent cobalt metal species. An alternative would have been to heat treat a higher cobalt ratio catalyst at 500 °C and run a normal XRD trace. This would not have determined the temperature of autoreduction precisely, but would have shown that it occurred between 400 and 500 °C.

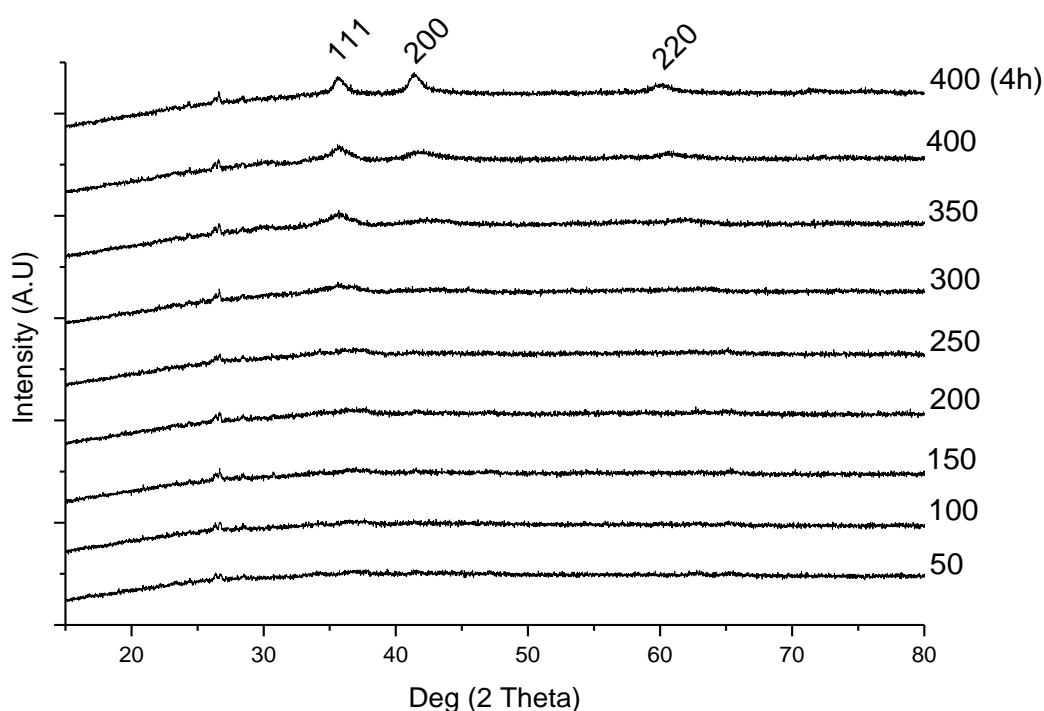
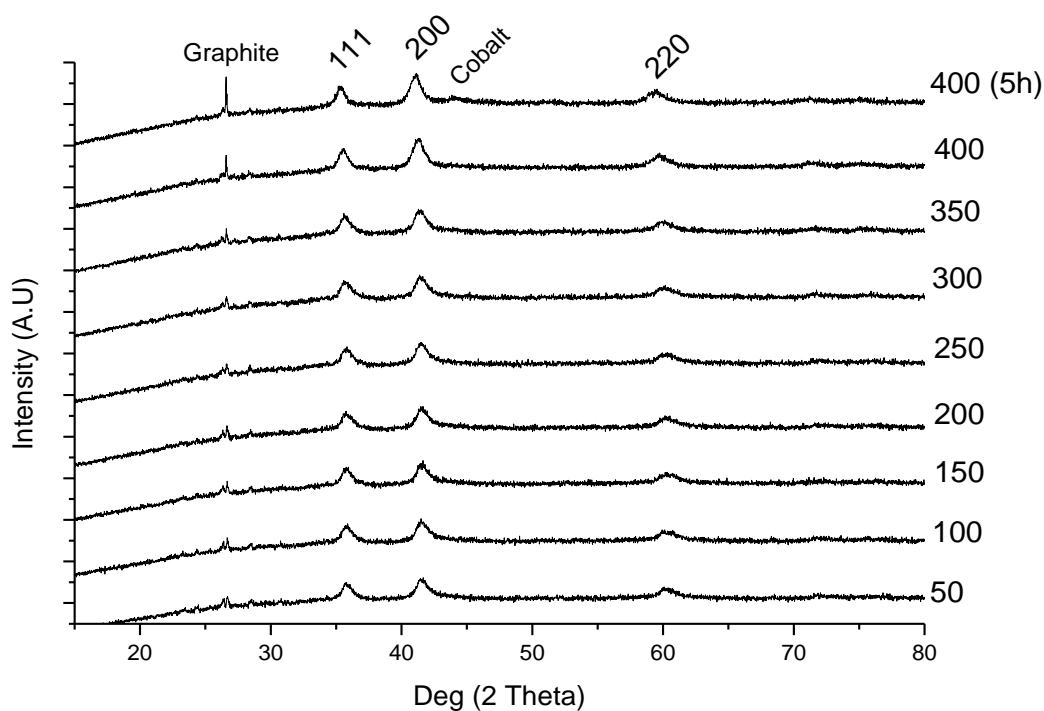


Figure 3.33 In-situ XRD traces of CoMn/C undergoing a heat treatment in He

Unfortunately the in situ XRD programming, unlike the regular XRD programming, was not designed to deal with cobalt fluorescence, resulting in high backgrounds and poor peak resolution. Indeed, it was not possible to distinguish any cobalt species in these traces. The emergence of the MnO phase from the amorphous precursor material can be seen to start occurring at 300 °C, with the peak intensities rising with increasing temperature. The small peak at $\sim 26^\circ$ (2θ) is carbon.



3.34 in situ XRD traces of the reduction of 1:1 Co:Mn catalyst

Throughout the whole range of reduction temperatures, the only observable changes are a distinct sharpening of the carbon peak and a slight increase in the definition of the MnO peaks. In the final trace there appears to be a hint of the emergence of the (111) phase of cobalt metal, but it is difficult to say with any certainty. What is notable, however, is that the reduction step has not changed the catalyst in any significant manner, as far as can be discerned. This would seem to imply that the autoreduction phenomenon observed for this catalyst before negates the need for a reduction step.

3.3.5.2 Reduced and unreduced catalysts

Given that the catalysts in the previous set of experiments were largely unaffected by the durations of the reduction step, along with the implications of the results of the in situ XRD, an experiment was conducted to see if the reduction step was necessary. The catalysts for this

were prepared according to the method set out in **Section 2.1.1.1** and tested according to the conditions described in **Section 3.2**, save that one catalyst underwent a normal 16 h reduction, and the second underwent no reduction whatsoever. The results of this experiment are displayed below in **Table 3.23** and **Figure 3.35**.

Table 3.23 Conversion and selectivity data for reduced and unreduced catalysts

| | Reduced | Unreduced |
|------------------------------------|---------|-----------|
| CO Conversion | 66.3 | 28.3 |
| Product selectivities (%) | | |
| CH₄ | 18.8 | 20.9 |
| C₂H₄ | 0.5 | 0.6 |
| C₂H₆ | 7.7 | 6.5 |
| C₃H₆ | 20.8 | 15.6 |
| C₃H₈ | 7.4 | 5.1 |
| C₄H₈ | 12.5 | 12.8 |
| C₄H₁₀ | 2 | 3.6 |
| C₅⁺ | 25.9 | 33.1 |
| CO₂ | 4.4 | 1.9 |

Catalyst test condition: Co:H₂ = 1:1, Temp. = 240 °C, Flow rate = 5 ml/min. Mass = 0.5 g GHSV = 600 h⁻¹

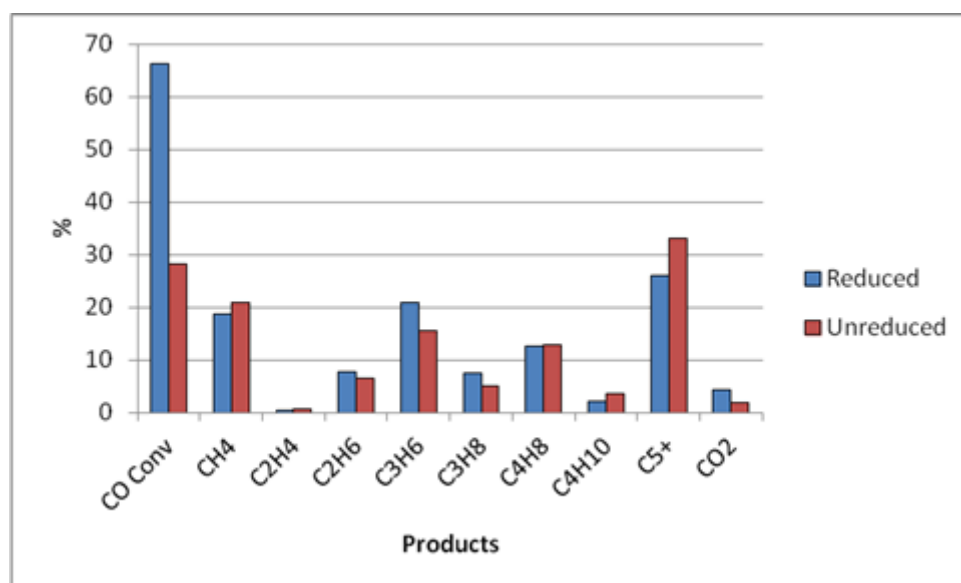


Figure 3.35 Graph displaying the trends in conversion and selectivity for reduced and unreduced catalysts

There is a clear and significant difference between the reduced and the unreduced catalyst in terms of both CO conversion and selectivities. This is at odds with *in-situ* XRD performed previously, which implied that the reduction step was not necessary.

ASF plots and the resultant α values are displayed below in **Figure 3.36** and **Table 3.24**.

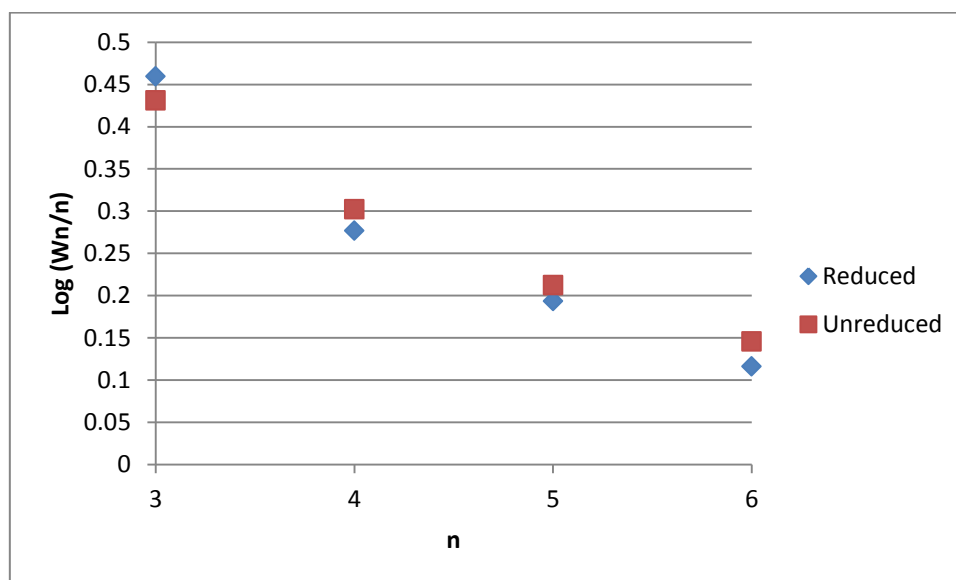


Figure 3.36 ASF plots for reduced and unreduced versions of a catalyst

Table 3.24 Calculated α values for reduced and unreduced versions of a catalyst

| Catalyst | Reduced | Unreduced |
|----------|---------|-----------|
| Gradient | -0.1113 | -0.0945 |
| α | 0.774 | 0.804 |

There is a significant difference between the two versions of the catalyst, although it is not clear why this should be so given previous results.

3.3.5.3 In-Situ heat treatment

The data from the previous section appeared to contradict the data observed from *in situ* XRD of the catalysts; experimental data showed that the lack of a reduction step had significant

impact upon the catalyst performance. It was noted that there was a slight difference in catalyst exposure; in the XRD, the catalyst was reduced immediately after being heat treated, whereas under normal catalyst preparation techniques the catalyst will be removed from its inert He atmosphere and exposed to air before being loaded into the reactor tubes to undergo reduction. It was suggested that during this step the catalyst undergoes mild passivation in air, which would go some way to explaining why even a very short reduction step was fully effective, but removing the reduction step entirely was not. To test this, the catalyst precursor was heat treated *in situ* in the reactors in much the same manner as it would normally be reduced. The temperatures and times of this heat treatment were identical to those described in **Section 2.1.1**. The catalysts were not then reduced as per the normal procedure, although the testing regime was otherwise the same.

The results of this experiment are displayed below in **Table 3.25** and **Figure 3.37**.

Table 3.25 Conversion and selectivity data for catalysts having undergone an *in situ* heat treatment and no reduction

| | Co : Mn :C ratio | | |
|------------------------------------|-------------------------|-----------------|-----------------|
| | 30:10:60 | 20:20:60 | 10:30:60 |
| CO Conversion | 74.48 | 47.6 | 16.98 |
| Product selectivities (%) | | | |
| CH₄ | 35.31 | 28.36 | 26.88 |
| C₂H₄ | 0.09 | 0.33 | 0.28 |
| C₂H₆ | 10.07 | 6.82 | 4.38 |
| C₃H₆ | 7.08 | 14.22 | 6.99 |
| C₃H₈ | 13.08 | 5.5 | 4.94 |
| C₄H₈ | 8.11 | 12.51 | 7.16 |
| C₄H₁₀ | 2.24 | 2.34 | 5 |
| C₅+ | 14.22 | 25.58 | 42.02 |
| CO₂ | 9.79 | 4.33 | 2.35 |

Catalyst test condition: Co:H₂ =1:1, Temp. = 240 °C, Flow rate = 5 ml/min. Mass =0.5 g GHSV = 600 h⁻¹

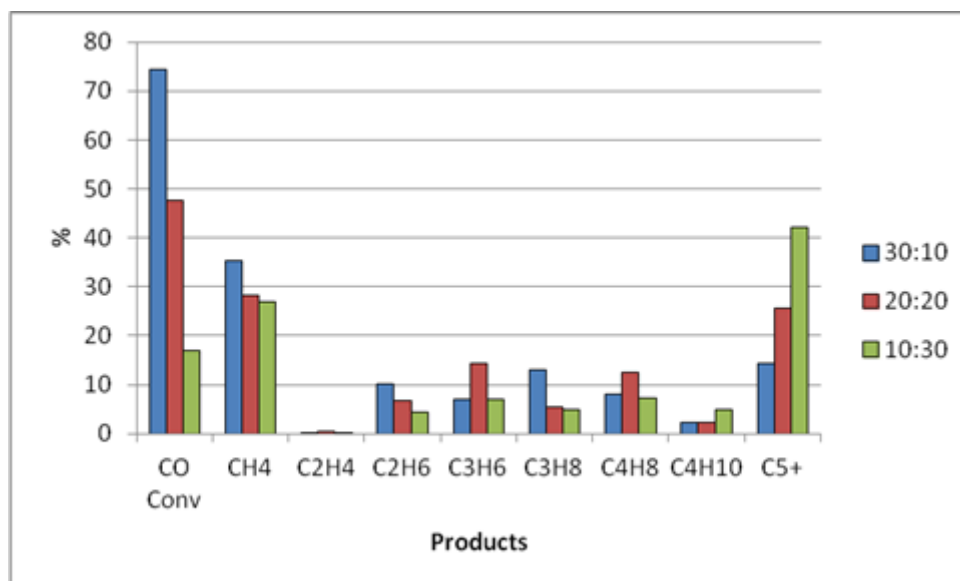


Figure 3.37 Graph displaying the trends in conversion and selectivity for catalysts having undergone an in situ heat treatment but no reduction. Key depicts Co:Mn ratio.

As can be seen from the results, these catalysts are an improvement over the previously tested unreduced catalysts, but are marginally worse than catalysts which have undergone an in situ reduction. They possess slightly lower conversions, and their selectivities are higher for methane. The catalyst Co:Mn:C 30:10:60 actually displays lower than expected C₅+ selectivity, continuing the trend seen with the earlier experiments in the lowering of the reduction time.

ASF plots for these catalysts, and the α values they yield, are displayed below in **Figure 3.38** and **Table 3.27**.

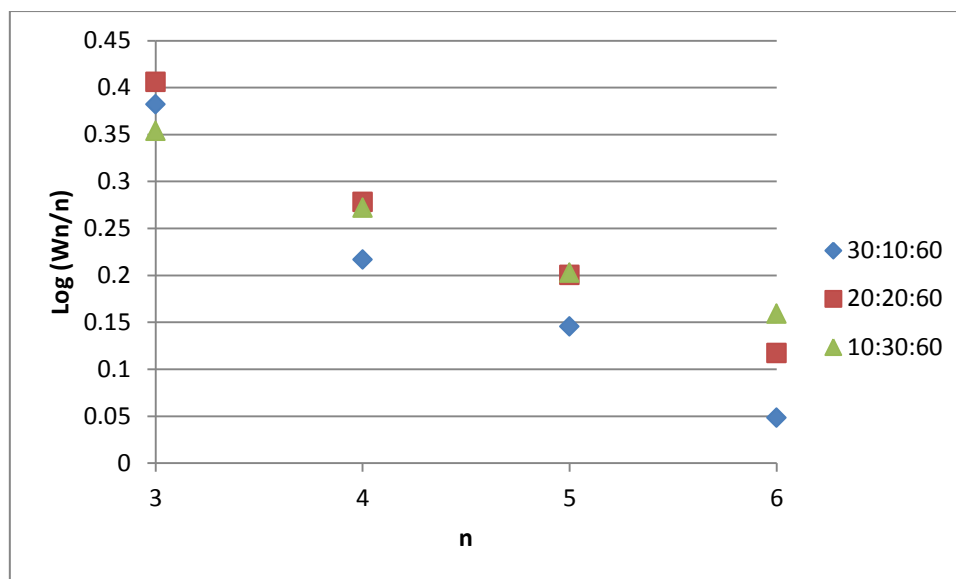


Figure 3.38 ASF plots for catalysts having undergone an in situ heat treatment but no reduction

Table 3.27 Calculations of α for catalysts having undergone an in situ heat treatment but no reduction

| Catalyst | 30:10:60 | 20:20:60 | 10:30:60 |
|----------|----------|----------|----------|
| Gradient | -0.1073 | -0.0945 | -0.0654 |
| α | 0.781 | 0.804 | 0.860 |

There are clearly significant differences in the selectivity patterns of these catalysts. What is slightly unusual is the direction that the trend runs; Mirzaei et. al⁶ showed that in CoMnO_x catalysts, the increasing amount of Mn lead to an increase in selectivity to lower C number products. In terms of α , this would be represented as a decrease. However, we see an increase. This is likely related to the no-reduction method we are using here; experiments performed later in this study showed that increasing Mn fraction does decrease α under normal conditions.

In this case, it could be that it is reduced manganese species present in the catalyst are responsible for lowering α . Normally this issue would not arise, since the catalyst would undergo a reduction step before use. For these specific experiments it would seem that the autoreduction effect, whilst effective on cobalt species, is perhaps less effective at the reduction of Mn species. However, heat treating manganese nitrate alone on carbon yields Mn_3O_4 and MnO , whereas heating equal amounts of cobalt and manganese nitrate on a

carbon support yields MnO and Co metal. This would seem to imply that the presence of the reduced cobalt species in turn aids the reduction of the manganese. This potentially symbiotic relationship would be interesting to investigate in future. Thermogravimetric analysis would provide a simple method of determining the exact temperature of autoreduction.

3.4 Variation of catalyst composition

The variations in the various factors involved in drying, heat treating and reducing the catalyst have been shown to contribute significantly to the final activity of the catalysts. The other major area of catalyst preparation to investigate is thus the catalyst composition. Whilst the intention is to retain the bimetallic system of cobalt and manganese, the ratios of these components to each other and the ratio of the metal components to the support material still allows for a wide range of variations to be investigated.

3.4.1 Variation of metal-support ratio

The initial experiments in varying the catalyst composition centred on the total metal-support ratio. The catalysts prepared in this section broadly follow the experimental procedure set out in **Section 2.1.1.1**, with variations in the amounts of the precursors used to affect the desired changes to the metal-support ratio. Each catalyst retained a 1:1 ratio of cobalt to manganese in the final catalyst. All catalysts were tested using the regime outlined in **Section 3.2**. The results of these experiments are displayed below in **Table 3.28** and **Figure 3.39**.

Table 3.28 Conversion and selectivity data for catalysts with varying metal-support ratios

| Metal % | 20 | 40 | 60 |
|------------------------------------|-------|-------|-------|
| CO Conversion | 40.03 | 42.1 | 47.23 |
| Product selectivities (%) | | | |
| CH₄ | 15 | 13.3 | 10.2 |
| C₂H₄ | 3.5 | 2 | 0.78 |
| C₂H₆ | 6.2 | 5.4 | 5.33 |
| C₃H₆ | 23.5 | 24.5 | 21.49 |
| C₃H₈ | 5.2 | 4.1 | 5.04 |
| C₄H₈ | 16.8 | 16.16 | 14.12 |
| C₄H₁₀ | 5.3 | 4 | 4.06 |
| C₅+ | 21 | 22 | 23.64 |
| CO₂ | 5.3 | 4.3 | 15.34 |

Catalyst test condition: Co:H₂ = 1:1, Temp. = 240 °C, Flow rate = 5 ml/min. Mass = 0.5 g GHSV = 600 h⁻¹

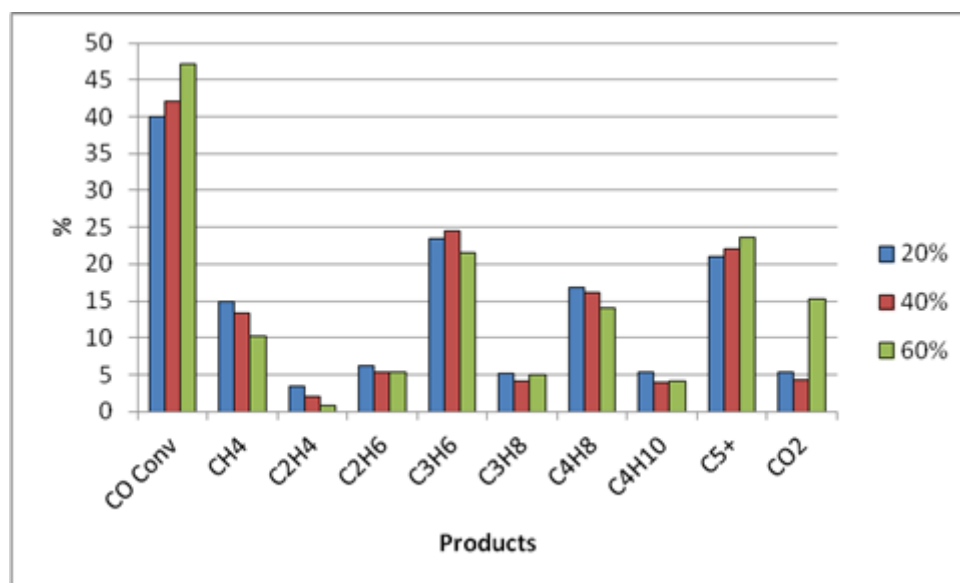


Figure 3.39 Graph displaying the trends in conversion and selectivity for catalysts with varying metal-support ratios. Key denotes catalyst metal %; remainder is activated carbon support

Whilst the CO conversion increases with increasing metal coverage, it was noted that CO₂ selectivity was greatly increased at the highest tested metal loading. C₅+ selectivity was also

noted to have increased with increasing metal loading, although the selectivity to CH_4 decreased. It was decided that a 40 % metal loading would be used as the standard loading; despite slightly lowered CO conversion, the higher selectivity to propene combined with lower selectivities to C_{5+} and CO_2 made this the more applicable catalyst.

ASF plots are not available for these experiments, as the data for carbon numbers above 4 has been collated into one category.

3.4.1.1 Characterisation

XRD traces were obtained for all catalysts, and BET surface areas of the materials were measured. Both sets of measurements were taken after the heat treatment step of the catalyst preparation. The results of these are displayed below in **Figure 3.40** and **Table 3.29**.

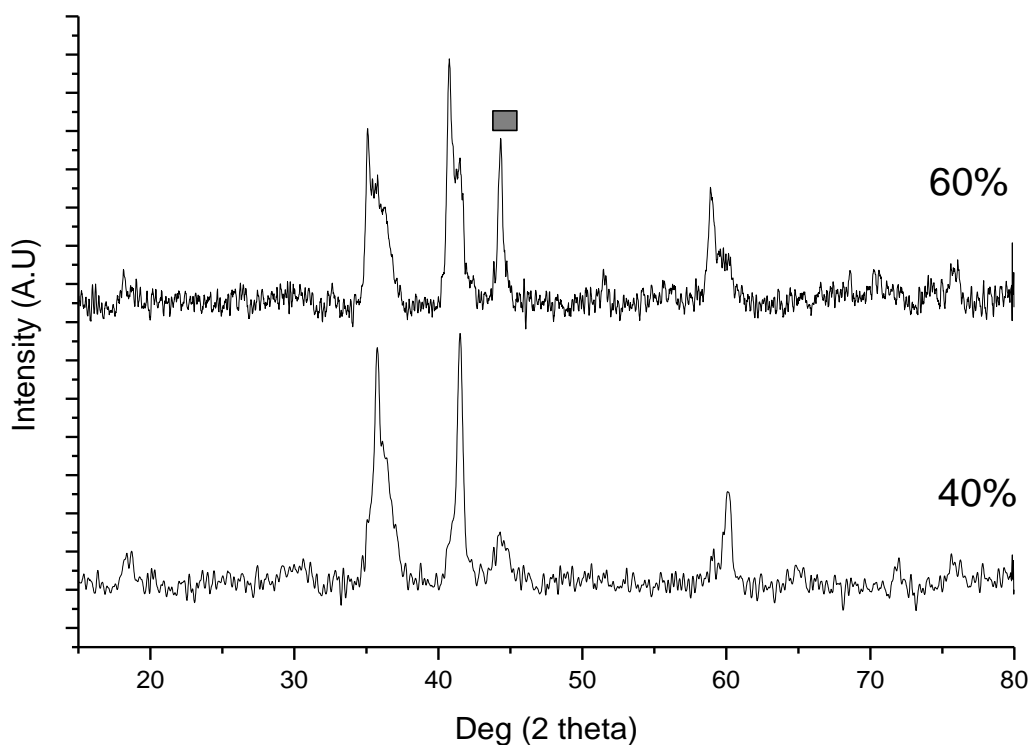


Figure 3.40 XRD traces of catalysts with different metal loadings onto an activated carbon support.

These XRD traces show a higher amount of cobalt metal phases in the catalyst with the higher metal loading. The other phases present are MnO and, in the higher loading, CoO. It is possible that in the highest metal loading not enough carbon is available to reduce all of the cobalt oxide. This is somewhat borne out by SEM images of certain catalysts, shown below in **Figures 3.41** and **3.42**. It should be noted that the catalysts displayed in the images are NOT the catalysts tested in this section. They were synthesised separately for the purpose of examination via SEM, and serve to illustrate the difference in metal coverage.

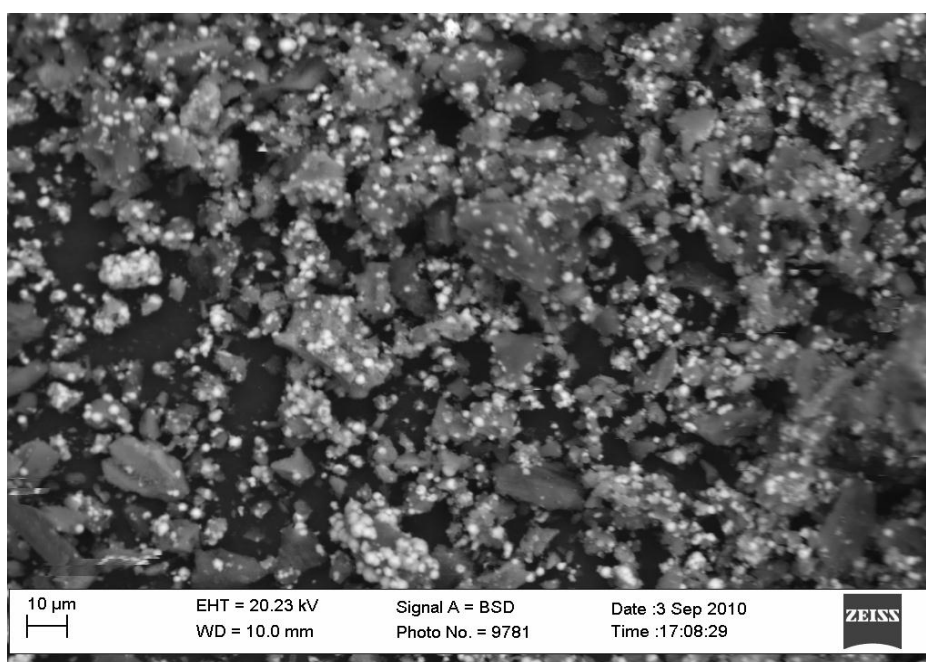


Figure 3.41 SEM image of a catalyst with 40 % metal loading on an activated carbon support.

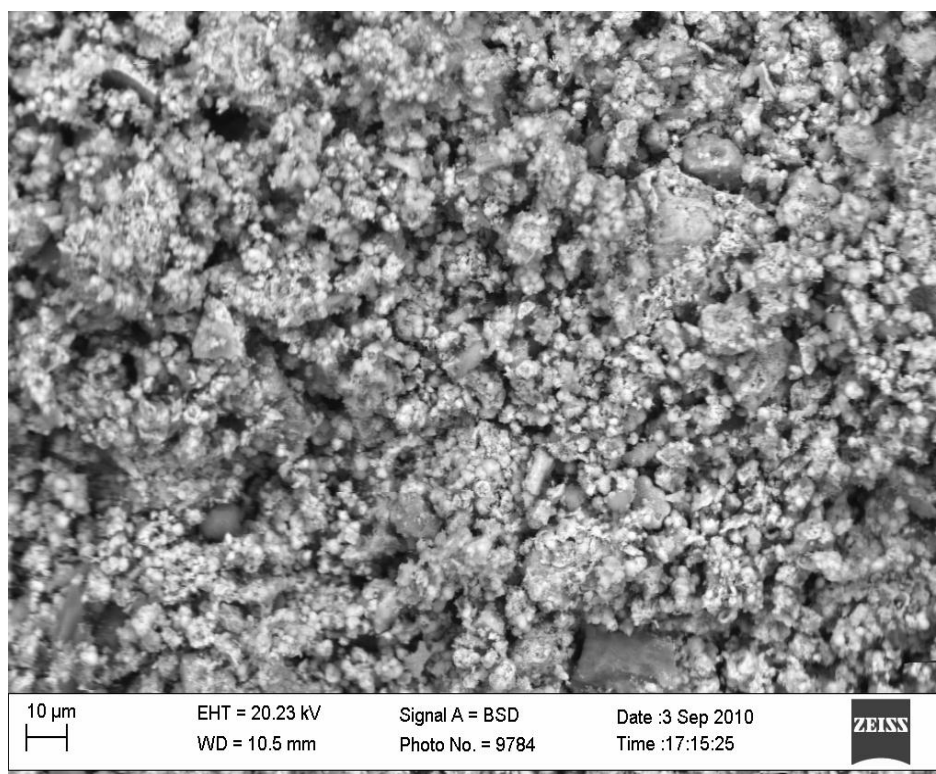


Figure 3.42 SEM image of a catalyst with 75 % metal loading on an activated carbon support

Both of these SEM images were taken using identical settings. With the lighter areas representing metals, it is readily evident that the higher loading has covered almost all of the carbon present.

Table 3.29 Surface areas of catalysts after heat treatment

| Metal Loading (%) | Surface area (m ² /g) |
|-------------------|----------------------------------|
| | After Heat Treatment |
| 20 | 411 |
| 40 | 433 |
| 60 | 471 |
| 75* | 23 |

Given the evidence of the SEM images, it is perhaps somewhat counterintuitive that the surface areas increase with increasing metal loadings, however, it could be that at 60 % loading the metal has not completely covered the surface, allowing the extremely high surface area of activated carbon ($\sim 1700 \text{ m}^2/\text{g}$) to influence the readings.

3.4.2 Variation of cobalt-manganese ratio

The next series of experiments involved a series of systematic adjustments to the ratio between cobalt and manganese, whilst keeping the overall metal-to-carbon support ratio at 40-60. The catalysts were prepared using the method outlined in **Section 2.1.1.1**, but with adjustments made to the relative amounts of metal precursors used to ensure the correct metal ratios were attained. All catalysts were tested using the regime outlined in **Section 3.2**.

The results of this series of experiments are displayed below in **Table 3.30**, as well as **Figures 3.43** and **3.44**. The results are organised by % cobalt. Since the total metal amount of the catalyst is 40 %, the difference between this and the % cobalt can be taken to be % manganese.

Table 3.30 Conversion and selectivity data for catalysts with varying cobalt-manganese ratios

| Cobalt % | 0 | 5 | 10 | 15 | 20 | 25 | 30 | 35 | 40 |
|------------------------------------|-------|-------|-------|------|------|------|------|------|------|
| CO Conversion | 0.62 | 0.84 | 35.8 | 66.2 | 71.1 | 88.9 | 83.1 | 88.5 | 12.4 |
| Product selectivities (%) | | | | | | | | | |
| CH₄ | 2.3 | 6.1 | 11.5 | 14.3 | 20 | 21.7 | 22.2 | 27.7 | 29.5 |
| C₂H₄ | 0.05 | 2.05 | 0.85 | 0.33 | 0.2 | 0.1 | 0.1 | 0 | 0.4 |
| C₂H₆ | 0.66 | 1.28 | 7.75 | 9.4 | 10.8 | 10.8 | 9.5 | 11 | 5 |
| C₃H₆ | 1.22 | 10.11 | 26.08 | 21.9 | 17.1 | 9.9 | 13.6 | 12.4 | 8.5 |
| C₃H₈ | 1.36 | 3.16 | 5.5 | 8.6 | 14.5 | 16.8 | 12.1 | 9.3 | 4.7 |
| C₄H₈ | 7.1 | 6.1 | 13.9 | 15.8 | 8.6 | 7.2 | 9.1 | 5.4 | 8.1 |
| C₄H₁₀ | 0.41 | 2.67 | 3.89 | 1.83 | 2.1 | 2.8 | 2 | 3.5 | 4.7 |
| C₅+ | 87.11 | 63.3 | 28.05 | 27.1 | 21 | 23.2 | 24.8 | 21 | 37.6 |
| CO₂ | 0 | 5.06 | 2.28 | 5.12 | 5.2 | 7.5 | 6.6 | 9.8 | 1.5 |

Catalyst test condition: Co:H₂ = 1:1, Temp. = 240 °C, Flow rate = 5 ml/min. Mass = 0.5 g GHSV = 600 h⁻¹

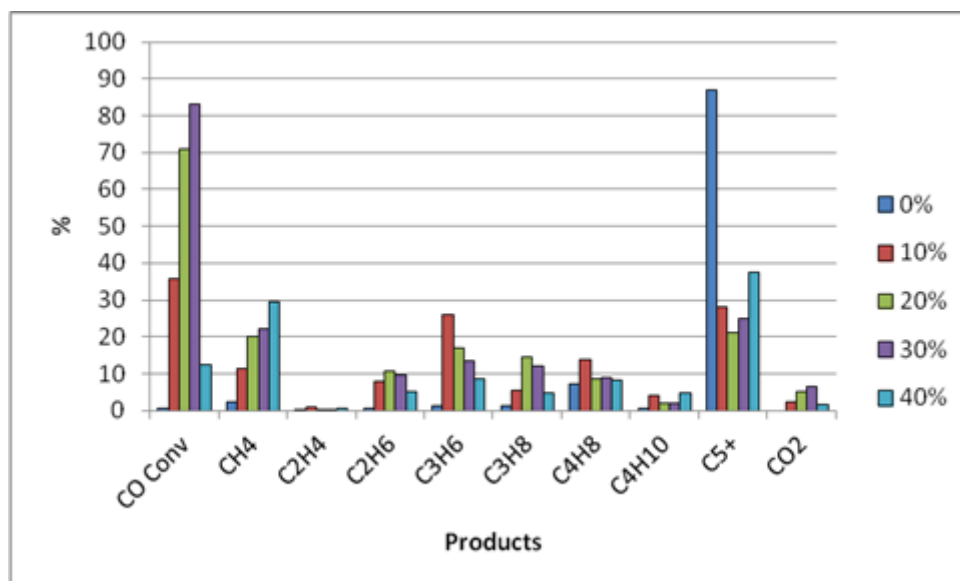


Figure 3.43 Graph displaying differences in conversion and selectivity between a selection of catalysts with different cobalt-manganese ratios.

Manganese alone is highly ineffective at hydrogenation of CO; this is in agreement with literature. Cobalt alone is also not highly effective for FT. Cobalt is a FT active metal, and as such a higher reactivity might have been expected.

There are several clear trends to be observed from these results. As long as there is manganese present, an increasing amount of cobalt leads to increases in CO conversion, as well as CH₄ selectivity. There appears to be a negative trend to the propene selectivity, which falls with increasing cobalt loading. This is likely linked with the ability of Mn to promote C₃ products. CO₂ selectivity remains generally low (<10 %), and appears to follow an almost identical trend to CO conversion.

If the extreme compositions are ignored, and greater focus paid to the intermediate values, a slightly different picture appears, as displayed below.

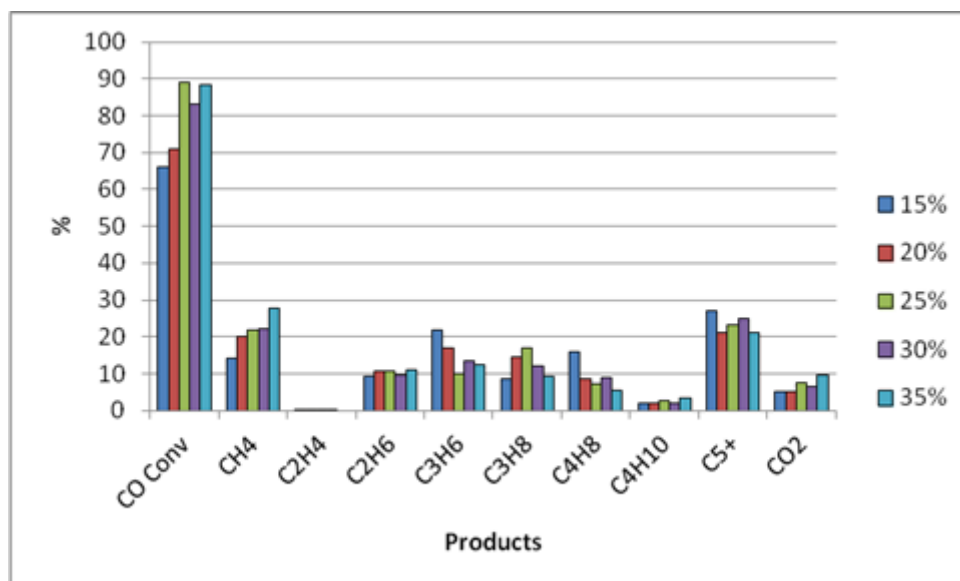


Figure 3.44 Graph displaying differences in conversion and selectivity between a selection of catalysts with different cobalt-manganese ratios.

In this graph we can see that there is a broad range of compositions leading to very high CO conversion. CO₂ selectivity still appears to follow a very similar trend to CO conversion. CH₄ selectivity still rises with increasing cobalt loading. The selectivities of the C₃ products seem to be interrelated; a fall in one corresponds to a rise in the other, with the total C₃ selectivity throughout the range of 10-30 % cobalt remaining around 25-30 % in all cases. The other selectivities appear stable, but overall it appears a great deal of control over conversion and selectivity can be exercised by manipulation of the cobalt-manganese ratio.

ASF plots of newly tested catalysts, and the α values calculated from them, are displayed below in **Figure 3.45** and **Table 3.31**.

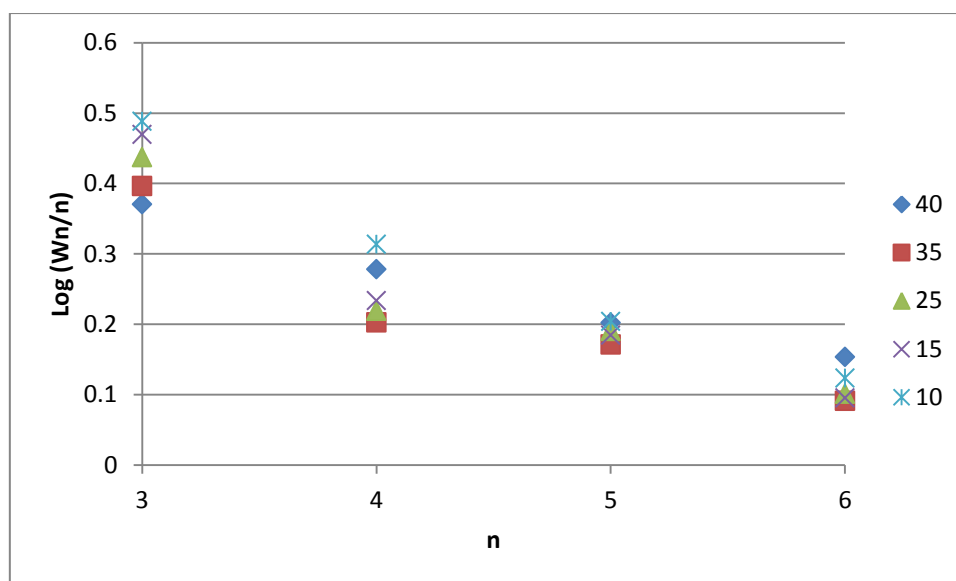


Figure 3.45 ASF plot of newly tested Co:Mn ratio catalysts
Key denotes % Co

Table 3.31 Calculated α values for catalysts with a range of Co:Mn ratios

| Cobalt % | 40 | 35 | 30 | 25 | 20 | 15 | 10 |
|----------|---------|---------|---------|---------|---------|---------|---------|
| Gradient | -0.0727 | -0.0948 | -0.1023 | -0.1036 | -0.1175 | -0.1171 | -0.1203 |
| α | 0.846 | 0.804 | 0.79 | 0.788 | 0.766 | 0.764 | 0.758 |

There is a definite trend displayed by these ASF plots and calculated α values; as Mn content increases, α decreases. This is in agreement with findings in the literature⁶, and is represented graphically in **Figure 3.46** below. Also, close examination of the ASF plots reveals that several of the catalysts deviate from an ideal plot; it is difficult to determine if this is C_3 overproduction or C_4 underproduction. Slight deviations of this nature have been seen in previous plots, and it is well known that C_1 and C_2 products do not obey the Schulz-Florey distribution. Together this implies that the mechanism for FT synthesis is not as simple as to be described by polymeric chain growth alone.

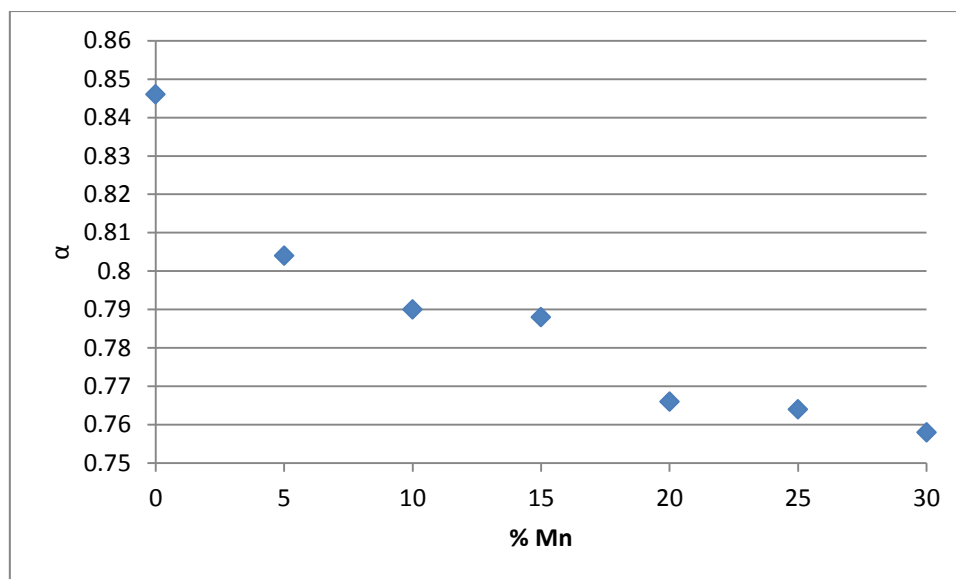


Figure 3.46 Plot of α against manganese content

3.4.2.2 Characterisation

XRD traces were obtained for all of the catalysts tested in this section. Due to the large number of traces and broad range of compositions displayed, the XRDs have been divided for convenience. Fortunately, the XRDs are able to be grouped into three distinct sections; high manganese, roughly equal, and high cobalt. These sets of XRDs are displayed below in **Figures 3.47, 3.48, and 3.49.**

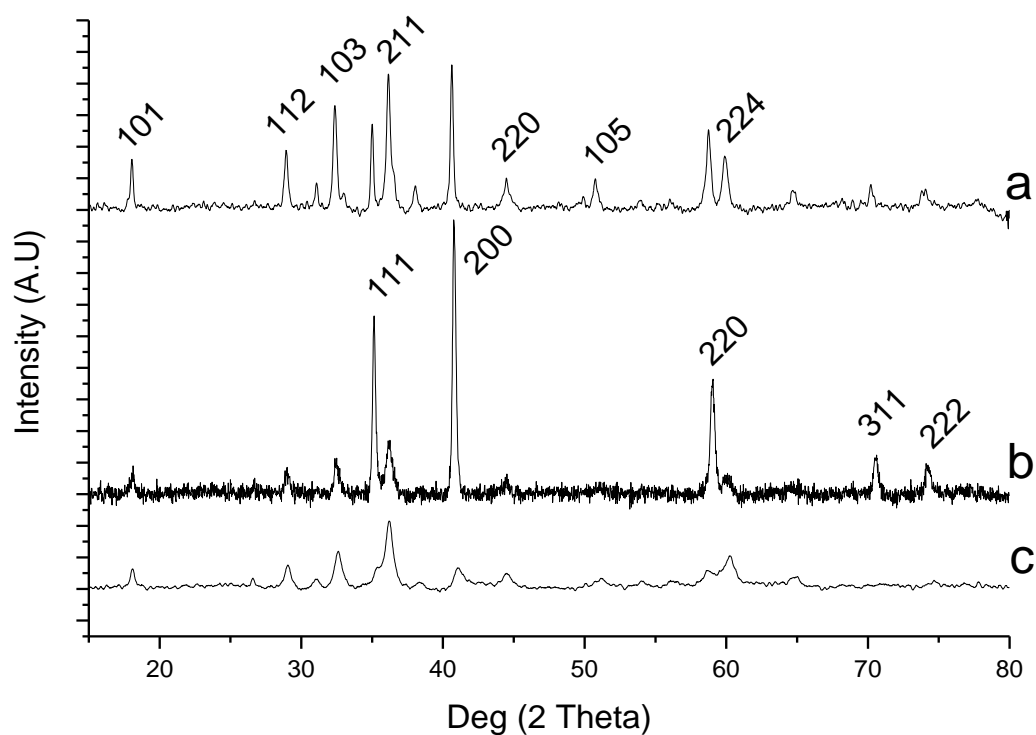


Figure 3.47 XRD traces of high manganese catalysts with hkl notation

Co %: a: 0 %; b: 5 %; c: 10 %

All three of these catalysts display a mixture of Mn_3O_4 and MnO . The planes of Mn_3O_4 are labelled on trace (a). The planes of MnO are labelled on trace (b). No cobalt peaks are seen, most likely due to its low concentration. The higher oxidation states of the manganese displayed here seems to imply that manganese does not undergo this autoreduction at 400 °C with the same ease as cobalt.

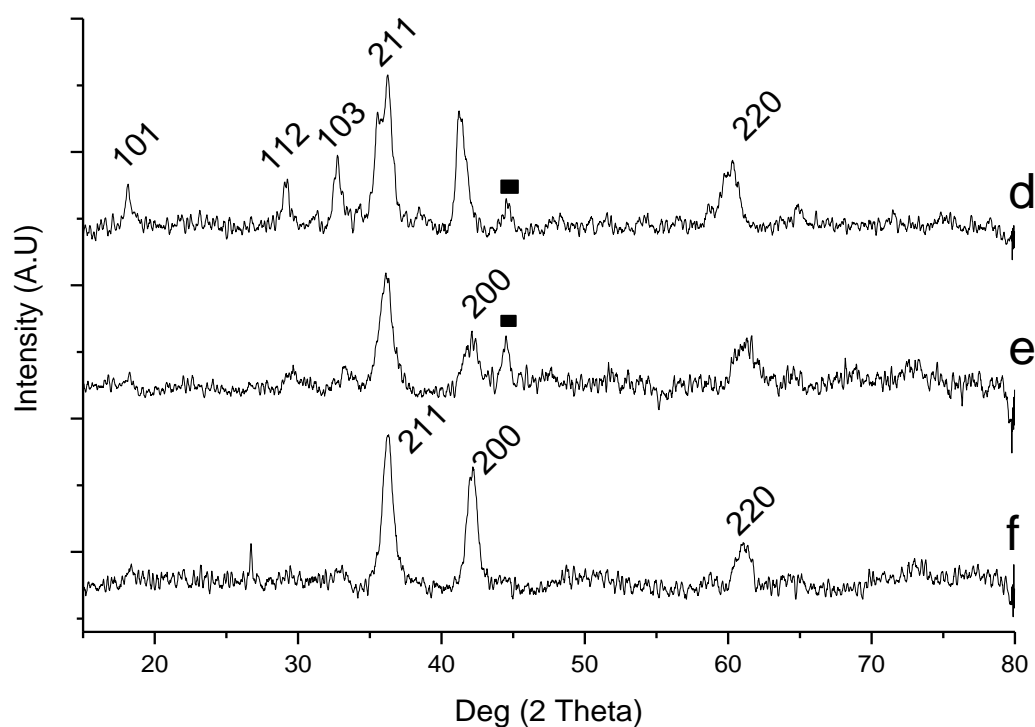


Figure 3.48 XRD traces of catalysts with roughly equal Co and Mn. hkl notation included
Co %: d: 15%; e: 20%; f: 25%

These catalysts display a mixture of phases. (d) contains Mn_3O_4 , as well as what appears to be CoO , and at least one peak for Co metal. The hkl notations for Mn_3O_4 are marked on (d). This seems to be a transitional point for the autoreduction phenomenon: The fully reduced Co metal is present, but the Mn species are not fully reduced.

(e) contains MnO and Co metal, fully displaying the autoreduction trend earlier noted. The planes for MnO are marked on this trace.

(f) contains only CoO , with a small Co metal peak. The planes of CoO are marked on this trace. Working on the earlier notion that the presence of manganese lowers the autoreduction temperature, it would seem to be at this point that the manganese concentration is low enough to push the autoreduction temperature above the $400\text{ }^\circ\text{C}$ point used for the heat treatments of these catalysts.

It is worth noting that in (e) and (f) it is likely that both traces contain peaks for both MnO and CoO. However, at the angles of the major peaks, these two species are often $\sim 1^\circ$ apart, and therefore can be difficult to resolve without the higher angle peaks.

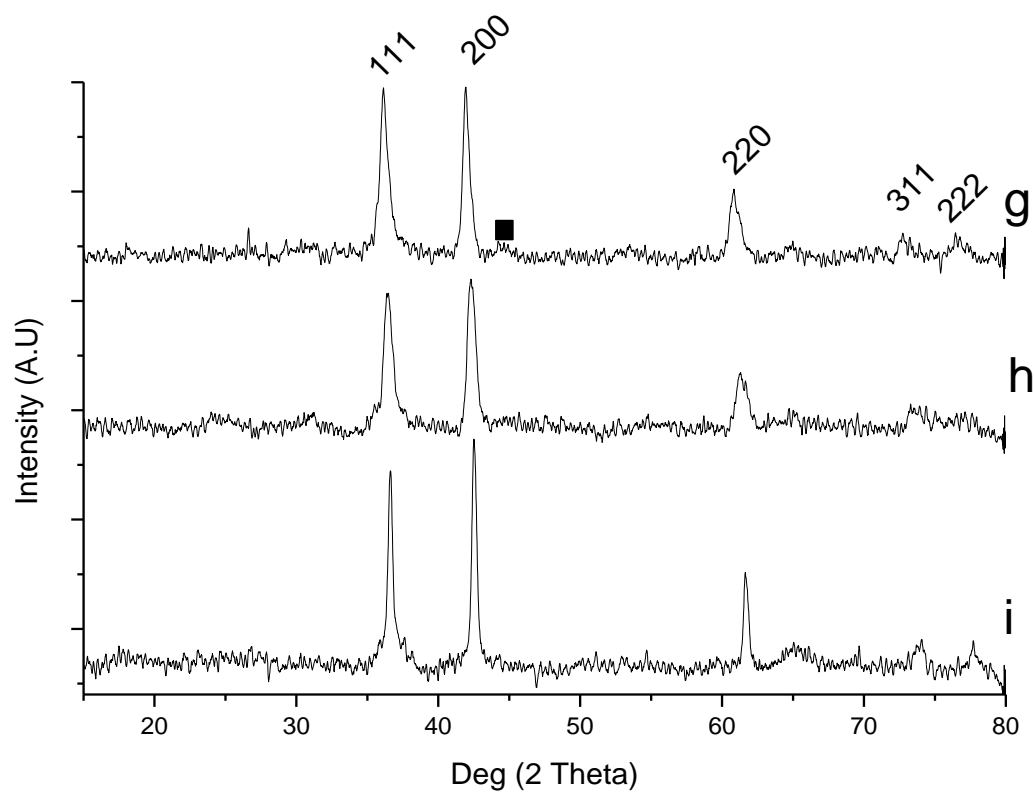


Figure 3.49 XRD traces of high cobalt catalysts with hkl notation

Co %: g: 30 %; h: 35 %; i: 40 %

All of the catalysts with higher cobalt loadings appear to be pure CoO phases. This supports the assumption that manganese presence aids the autoreduction of cobalt on carbon.

3.5 Conclusions

From the work presented in this chapter it can be concluded that the preparation of these catalysts is dependent upon a large number of factors. In the initial precursor production step, it has been shown that the performance of the final catalyst is affected by the vessel in which the material is dried. This is likely to be an issue of drying rate, although it may also be linked to the material that the drying vessel is made of.

The heat treatment step of the catalyst is also significant. Heat treatments of longer duration and higher temperature are shown to be detrimental to the activity of the catalyst. This can be linked to a decrease in surface area in both cases. It is also possible that the higher temperatures and longer heating period are allowing the metal particles to sinter, lowering the overall metal surface area.

Attempts to adhere the oxide material to a carbon support after heat treatment of the oxides proved ineffective. Evidence suggests that the material does not adhere to the carbon support.

The reduction step was shown to be of only minor importance; the cobalt on carbon catalysts undergo autoreduction in an inert atmosphere, meaning that the catalysts are almost entirely reduced after heat treatment. Only a brief reduction was found to be needed. It is presumed that this is to remove the passivation layer formed in contact with air. The temperature at which the autoreduction effect occurs was found to be affected by the presence of Mn in the catalyst. There also seems to be a synergistic effect, in that the manganese species alone did not undergo autoreduction, but would be reduced if cobalt was present.

Variations in the catalyst composition showed that cobalt and manganese individually are ineffective for FT, but perform extremely well in concert. Increasing cobalt tended to lead to increased CO conversion and CH₄ production, although this trend only applied as long as some Mn was present.

3.6 References

1. S. Colley, R. G. Copperthwaite, G. J. Hutchings and M. Vanderriet, *Industrial & Engineering Chemistry Research*, 1988, **27**, 1339-1344.
2. M. J. Keyser, R. C. Everson and R. L. Espinoza, *Applied Catalysis a-General*, 1998, **171**, 99-107.
3. H. Atashi, F. Siami, A. A. Mirzaei and M. Sarkari, *Journal of Industrial and Engineering Chemistry*, 2010, **16**, 952-961.
4. M. Feyzi, M. M. Khodaei and J. Shahmoradi, *Fuel Processing Technology*, 2012, **93**, 90-98.
5. M. Feyzi, M. Irandoust and A. A. Mirzaei, *Fuel Processing Technology*, 2011, **92**, 1136-1143.
6. A. A. Mirzaei, M. Faizi and R. Habibpour, *Applied Catalysis a-General*, 2006, **306**, 98-107.
7. H. F. Xiong, M. Moyo, M. K. Rayner, L. L. Jewell, D. G. Billing and N. J. Coville, *Chemcatchem*, 2010, **2**, 514-518.
8. F. Morales, E. de Smit, F. M. F. de Groot, T. Visser and B. M. Weckhuysen, *Journal of Catalysis*, 2007, **246**, 91-99.
9. F. Morales, F. M. F. de Groot, P. Glatzel, E. Kleimenov, H. Bluhm, M. Havecker, A. Knop-Gericke and B. M. Weckhuysen, *Journal of Physical Chemistry B*, 2004, **108**, 16201-16207.
10. G. L. Bezemer, J. H. Bitter, H. Kuipers, H. Oosterbeek, J. E. Holewijn, X. D. Xu, F. Kapteijn, A. J. van Dillen and K. P. de Jong, *Journal of the American Chemical Society*, 2006, **128**, 3956-3964.
11. E. Iglesia, *Applied Catalysis a-General*, 1997, **161**, 59-78.
12. S. Rane, O. Borg, E. Rytter and A. Holmen, *Applied Catalysis a-General*, 2012, **437**, 10-17.
13. M. Zakeri, A. Samimi, M. Khorram, H. Atashi and A. Mirzaei, *Powder Technology*, 2010, **200**, 164-170.
14. H. F. Xiong, M. A. M. Motchelaho, M. Moyo, L. L. Jewell and N. J. Coville, *Journal of Catalysis*, 2011, **278**, 26-40.
15. T. K. Das, G. Jacobs and B. H. Davis, *Catalysis Letters*, 2005, **101**, 187-190.

16. H. Karaca, O. V. Safonova, S. Chambrey, P. Fongarland, P. Roussel, A. Griboval-Constant, M. Lacroix and A. Y. Khodakov, *Journal of Catalysis*, 2011, **277**, 14-26.
17. M. Moyo, M. A. M. Motchelaho, H. F. Xiong, L. L. Jewell and N. J. Coville, *Applied Catalysis a-General*, 2012, **413**, 223-229.

Chapter 4

Cobalt-molybdenum catalysts for the production of alcohols from syngas

4.1 Introduction

The work in this chapter is based on unpublished work by a previous project student, whose results implied that a mixed metal catalyst of cobalt and molybdenum supported on activated carbon was active for the production of C₂-C₄ oxygenates from syngas via a Fischer-Tropsch style reaction.

The previous student's work was initially based on the DOW alkali-doped Co-MoS₂ catalysts used industrially^{1, 2}. These catalysts are effective for the production of alcohols, but require the continuous co-feeding of H₂S into the syngas stream. If this does not occur, the catalyst will slowly deactivate³. The deliberate inclusion of sulphur into the reaction mixture is awkward, and can result in the incorporation of sulphur groups into products. This can in turn lead to sulphur oxygenate products such as thiols to be formed, which are highly toxic.

The idea behind the previous research was to follow on from the success of mounting cobalt-manganese onto activated carbon for the production of alkenes from syngas. If the alcohol catalyst were to be mounted on carbon, they could benefit from the high surface areas of the support, hopefully increasing cobalt dispersion to make a more active catalyst.

It should be noted that this study focusses on the impregnation of both cobalt and molybdenum onto carbon, but does not aim to use molybdenum carbides⁴⁻⁶. This is a valid area of research, however, and several groups are looking into it as a way of moving away from the difficult sulphide catalysts^{7,8}.

The aims of this study are to continue the work of the previous student into finding a valid alcohol catalyst via the supporting of cobalt and molybdenum oxides onto a high surface area activated carbon support.

4.2 Preparation details

There are two significant classes of cobalt-molybdenum catalysts created and used throughout this chapter. The cobalt molybdenum sulphide catalysts from the original DOW patents^{9,10} (Co-MoS₂) were prepared using the coprecipitation method outlined in the original patent, which is described in **Section 2.1.2.2**. For these catalysts it was also necessary to add 0.2 % wt Cu as a promoter; this was done by impregnation as described in **Section 2.1.2.4**.

The other group of catalysts are cobalt and molybdenum on an activated carbon support. These were prepared in one of two manners; wet impregnation or deposition precipitation, described in **Section 2.1.2.1** and **Section 2.1.2.3** respectively.

Following these preparations, all catalysts were tested in a similar manner. The catalysts would be mixed with SiC as a dilution agent. The purpose of this is to allow some space between the active materials of the catalyst: Since the Fischer-Tropsch reaction is exothermic, this helps to prevent hotspots forming. 4.8 g of the catalyst would be mixed with 5.2 g of SiC and placed in the steel tube of a custom built reactor.

In some cases the catalyst will have a number of mixing agents added to it. This is the case for all of the sulphide catalysts, and the exact quantities are noted in **Section 2.1.2.2**. Where

noted, some of the non-sulphide catalysts also undergo the addition of mixing agents; in these cases, quantities identical to those for sulphide catalysts are used.

Once loaded into the reactor, the catalysts undergo an *in-situ* reduction step for 10 h under flowing H₂ gas. (Final temperature: 350 °C; heating ramp rate: 1 °C/min; H₂ flow rate: 40 ml/min). Following this, the catalysts are allowed to cool to room temperature before being pressurised to 75 bar with syngas (CO:H₂ ratio 1:1) using a back pressure regulator.

For the non-sulphide catalysts, the flow rate would then be set to 140.6 ml/min to give a GHSV of 1875 h⁻¹ unless otherwise noted. Some experiments used different flow rates; where this occurs it will be duly noted and the GHSV values adjusted accordingly.

For the sulphide catalysts, the flow was set to 100 ml/min to give a GHSV of 1225 h⁻¹.

The temperature of the reactor was set to 250 °C for non-sulphide catalysts, and 305 °C for sulphide catalysts. Both catalyst groups utilised a 1 °C/min ramp rate. Gaseous products were analysed by an online GC, and liquid products were trapped out and analysed offline in a separate GC. The results are then combined to give total conversion and selectivities.

4.3 Cobalt-molybdenum on activated carbon support

The aim of this body of work was to reproduce and extrapolate from the work of a previous student, who had shown that it was possible to support these metals on carbon and produce similar conversions and selectivities to the DOW Co-MoS₂ catalyst. Whilst effective, the DOW catalyst is difficult to work with due to the presence of sulphur; in long-term industrial reactions it is necessary to introduce sulphur into the gas stream to replace that which is lost from the catalyst during the reactions. This leached sulphur must then be cleaned from the product stream, leading to additional cost and complication. The possibility, therefore, that sulphur was not necessary either as an integral part of the catalyst or as an element of the feedstock composition was considered extremely significant. If verified, it could potentially allow for greener alcohol synthesis catalysts.

The aim was, therefore, to use the notes of the previous student to reproduce their catalysts, and then use these results as a base catalyst which could then be experimented with and improved upon.

4.3.1 Reproduction of CoMo/C produced by deposition precipitation

It was initially attempted to reproduce the catalysts using the deposition precipitation method outlined in **Section 2.1.2.3**. Two batches of the catalyst were made using this method and tested separately using the methods and conditions outlined in **Section 4.2**. The results of these experiments are displayed below in **Table 4.1** and **Figure 4.1**.

Table 4.1 Conversion and selectivity data for CoMo/C catalysts prepared by DP

| Catalyst | A | B |
|------------------------------------|------|-------|
| CO Conv | 3.09 | 2.79 |
| Product selectivities (%) | | |
| CO₂ | 0 | 0 |
| CH₄ | 3.21 | 3.38 |
| C₂-C₆ | 1.56 | 0.83 |
| MeOH | 84.3 | 84.03 |
| EtOH | 10.1 | 10.5 |
| PrOH | 0.5 | 0.72 |
| 1-BuOH | 0.1 | 0 |
| C>4OH | 0 | 0 |
| Total Alc | 95 | 95.25 |
| CMB (%) | 78 | 81 |

Reaction conditions: Temp; 250 °C, Flow rate 140.6 ml/min, pressure 75 bar

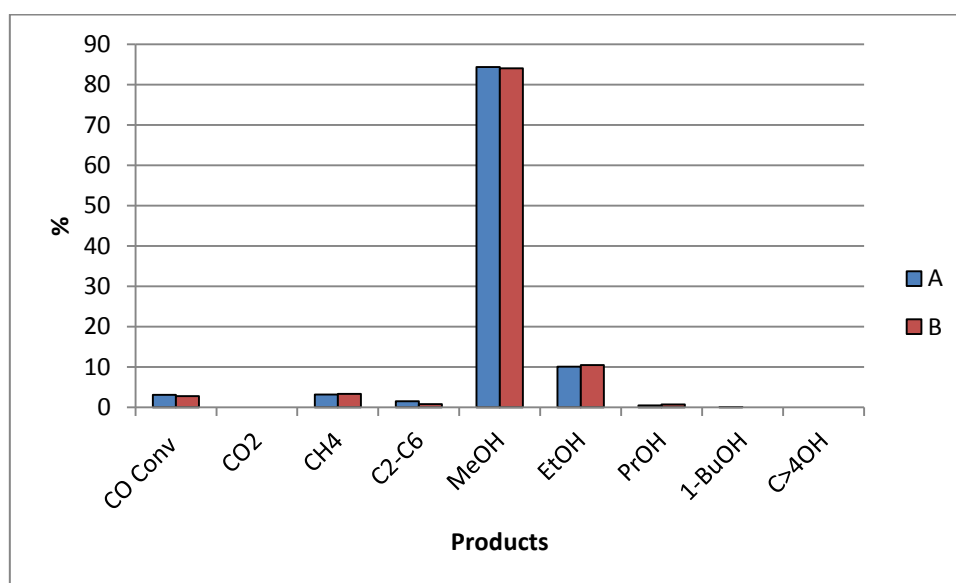


Figure 4.1 Bar chart displaying conversion and selectivity data for catalysts produced via DP

The conversion and selectivity data indicates that these two catalysts are reproducible. It also acts as proof of concept in that these CoMo/C catalysts demonstrate the requisite ability to produce alcohols from syngas under these conditions.

Conversion of carbon monoxide is low, however, and the predominant product is methanol, which is undesirable in this reaction. The CO₂ and CH₄ selectivities were low, and overall alcohols production was high.

4.3.2 Reproduction of CoMo/C produced by impregnation

It was subsequently attempted to create viable catalysts using the impregnation method as outlined in **Section 2.1.2.1**. Two batches of the catalyst were made using this method and tested separately using the methods and conditions outlined in **Section 4.2**. The results of these experiments are displayed below in **Table 4.2** and **Figure 4.2**.

Table 4.2 Conversion and selectivity data for catalysts prepared by IMP

| Catalyst | A | B |
|----------------------------------|------|------|
| CO Conv | 6.79 | 7.11 |
| Product Selectivities (%) | | |
| CO ₂ | 5.5 | 5.2 |
| CH ₄ | 25.6 | 28.8 |
| C ₂ -C ₆ | 4.1 | 3.9 |
| MeOH | 52.8 | 48.8 |
| EtOH | 8.56 | 9.95 |
| PrOH | 2.1 | 2.3 |
| 1-BuOH | 0.74 | 0.55 |
| C _{>4} OH | 0 | 0 |
| Total Alc | 64.2 | 61.6 |
| CMB (%) | 85 | 84 |

Reaction conditions: Temp; 250 °C, Flow rate 140.6 ml/min, pressure 75 bar

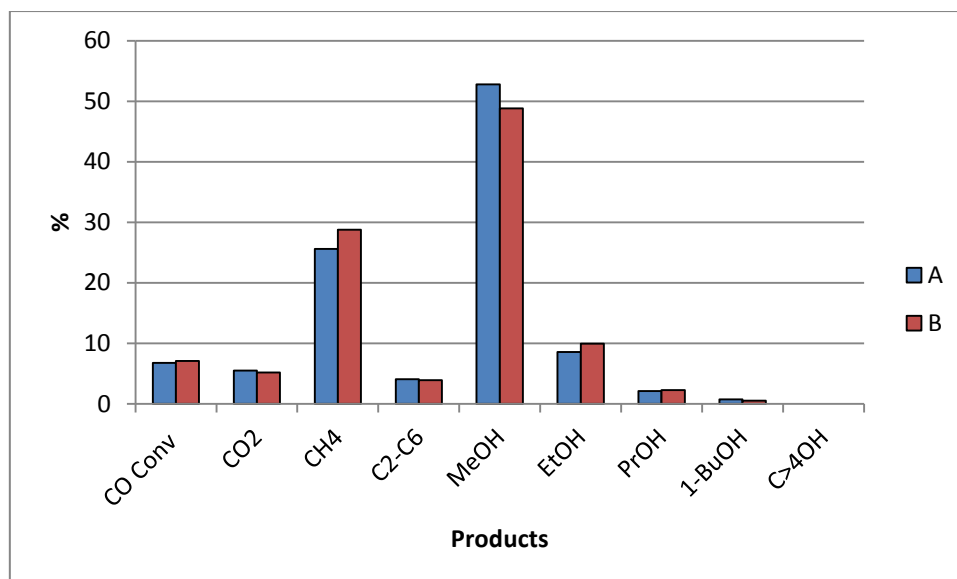


Figure 4.2 Bar chart displaying conversion and selectivity data for catalysts produced via IMP

As was seen with the catalysts prepared by DP, the catalysts are reproducible.

The conversion of carbon monoxide with these catalysts is slightly higher than was observed with the catalysts prepared by DP. The predominant product is still methanol, although in terms of alcohols-only product distribution there was an increase in the amount of ethanol, propanol and butanol present. There was a significant increase in the selectivity towards methane production, and CO₂ selectivity has also risen.

Whilst there was an increase in the production of undesirable products, the higher conversion and increased production of C₂₊ alcohols was considered promising. Unless otherwise stated, all CoMo/C catalysts synthesised after this juncture were prepared via impregnation.

4.3.2 (i) Characterisation

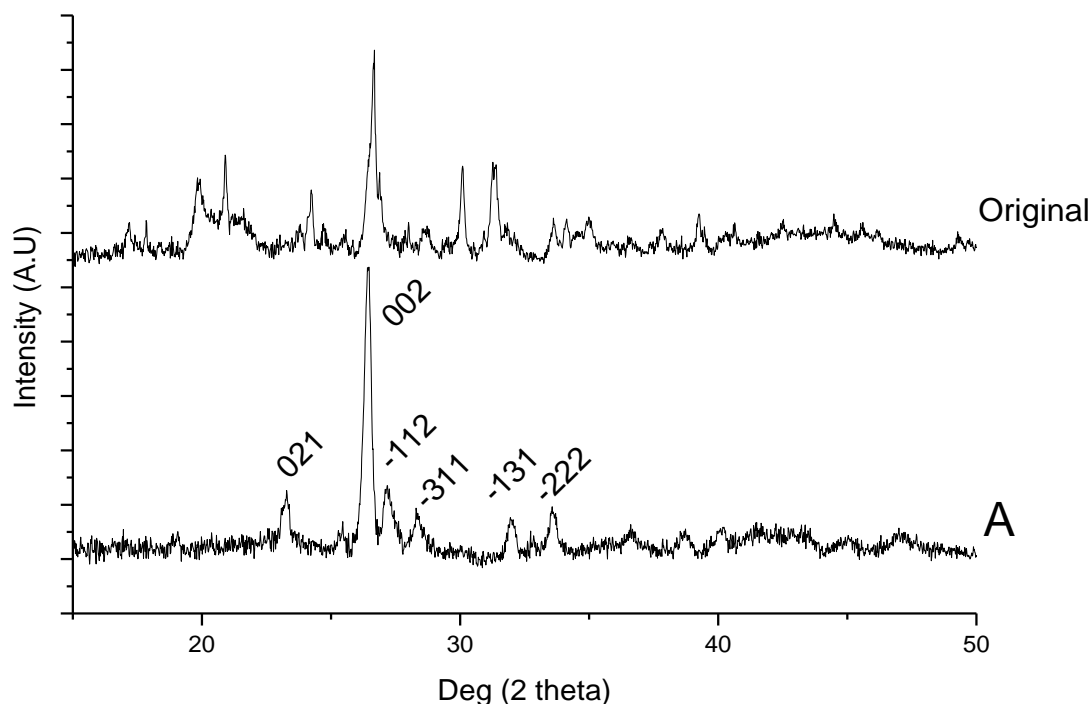


Figure 4.3 XRD traces of CoMo-C catalysts produced by impregnation with hkl notation

The primary phase present in both cases appears to be the mixed metal oxide CoMoO_4 , although the original also contains a small amount of MoO_3 . Given that both catalysts have the same predominant phase, it does not seem like catalyst composition was the cause of the large discrepancy in catalyst activity between the two.

4.3.2.1 Addition of mixing agents

Inquiries into the method of catalyst preparation method used in previous catalysts lead to the observation that the original CoMo/C catalysts were based very closely upon the DOW patent catalysts, the basic aim having been to substitute out the sulphur for a more benign compound. With this in mind it was resolved to test the catalysts with the same addition of mixing agents that would normally be applied to the sulphide catalysts; that is to say, mixing the catalyst with K_2CO_3 , montmorillonite clay, and Sterotex[®] lubricant in the ratio 66/10/20/4 (10 % K_2CO_3). The catalysts chosen to be mixed in this manner were prepared by impregnation as outlined in **Section 2.1.2.1**. This mixture was treated as the final catalyst; 4.8

g of this mixture was added to 5.2 g SiC and the reaction was otherwise carried out according to the method outlined in **Section 4.2**.

The results for these experiments are displayed below in **Table 4.3** and **Figure 4.4**.

Table 4.3 Conversion and selectivity data for catalysts prepared by IMP with mixing agents

| Catalyst | A | B |
|------------------------------------|------|------|
| CO Conv | 3.21 | 2.99 |
| Product selectivities (%) | | |
| CO₂ | 8.2 | 6.1 |
| CH₄ | 40.5 | 39.4 |
| C₂-C₆ | 15.5 | 14.4 |
| MeOH | 32.8 | 39.9 |
| EtOH | 2.5 | 3.5 |
| PrOH | 0 | 0 |
| 1-BuOH | 0 | 0 |
| C>4OH | 0 | 0 |
| Total Alc | 35.3 | 43.4 |
| CMB | 75 | 77 |

Reaction conditions: Temp; 250 °C, Flow rate 140.6 ml/min, pressure 75 bar

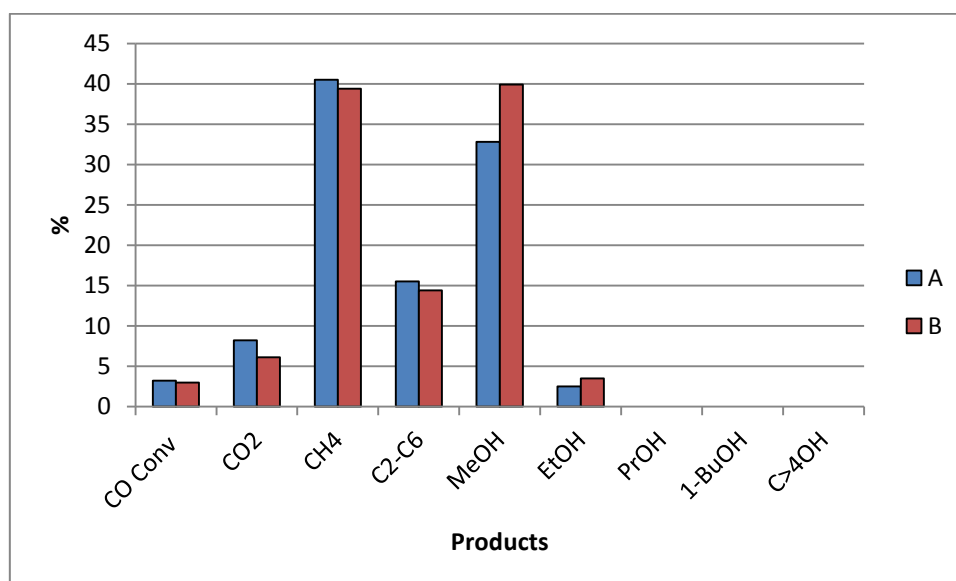


Figure 4.4 Bar chart displaying conversion and selectivity for catalysts prepared by IMP with additional mixing agents.

These catalysts appear to be highly reproducible. However, the addition of mixing agents appears to have had a detrimental effect on the performance of the catalysts. CO conversion remains low; it is slightly reduced from the catalysts tested without the presence of mixing agents. The selectivities have also changed, with a marked decrease in total alcohol production and elimination of the production of any alcohol product of greater than C₂ chain length. CH₄ and CO₂ production have also increased with the addition of the mixing agents, and the production of C₂-C₆ non-oxygenated hydrocarbons has increased significantly.

These experiments were not regarded as conclusively against the addition of mixing agents; it could just as easily be the case that errors in some other part of the preparation procedure were causing these errors. To help shed light on this, a precursor catalyst (i.e. one which had not undergone heat treatment) created prior to the beginning of this study was heat treated before being combined with the same mixing agents as used before. Ideally a comparative run would have been performed with a sample of the catalyst without mixing agents, but only a small amount of precursor was available; there was not enough to create a full 4.8g of catalyst needed for a standard run.

The results of this run, plus a comparison to the original results of the catalyst created from this precursor, are displayed below in **Table 4.4** and **Figure 4.5**.

Table 4.4 Conversion and selectivity data for previous catalyst with mixing agents

| Catalyst | A | B | Old +mix |
|--------------------------------|------|------|-------------|
| CO Conv | 3.21 | 2.99 | 1.1 |
| Product selectivity (%) | | | |
| CO ₂ | 8.2 | 6.1 | 8.2 |
| CH ₄ | 40.5 | 39.4 | 47.5 |
| C ₂ -C ₆ | 15.5 | 14.4 | 15.5 |
| MeOH | 32.8 | 39.9 | 27.2 |
| EtOH | 2.5 | 3.5 | 0 |
| PrOH | 0 | 0 | 0 |
| 1-BuOH | 0 | 0 | 0 |
| C>4OH | 0 | 0 | 0 |
| Total Alc | 35.3 | 43.4 | 27.2 |
| CMB | 75 | 77 | 69 |

Reaction conditions: Temp; 250 °C, Flow rate 140.6 ml/min, pressure 75 bar

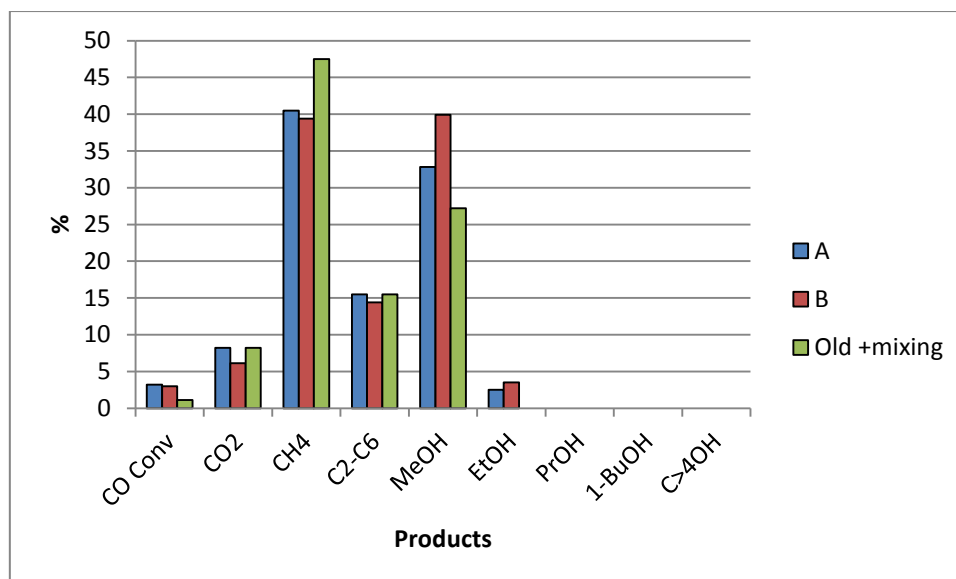


Figure 4.5 Bar chart displaying conversion and selectivity of previous catalyst with mixing agents, compared with two new catalysts with mixing agents

All results are from gas phase analysis, as no liquids were produced. The tendency towards production of non-oxygenate products seems to be more pronounced in this catalyst. In both cases so far the addition of the mixing agents does not appear to agree with literature, which is that the addition of alkali promoters such as K_2CO_3 promotes oxygenate formation by blocking sites which would adsorb CO dissociatively. The vast majority of the products in the catalyst tests involving mixing agents have been C_1 , implying that the chain growth propagation is being inhibited. However, it could be that these factors are in fact linked; oxygenate formation is promoted by inhibiting the dissociation of the C-O bond, but chain growth propagation proceeds by dissociation. It seems that the addition of the mixing agents to these catalysts is causing the product distribution to shift heavily towards C_1 products by prevention of dissociation.

What can also be concluded from the results here, though, is that the poor performance of the catalysts is not limited to just the freshly prepared ones; since even a previously proven precursor produced poor results, it can be inferred that there is either an error after the precursor creation (i.e. from the heat treatment onwards), or that the mixing agents are a significant inhibitor in this reaction with these catalysts.

4.3.2.1 (i) Characterisation

The XRD trace of the material is displayed below in **Figure 4.6**.

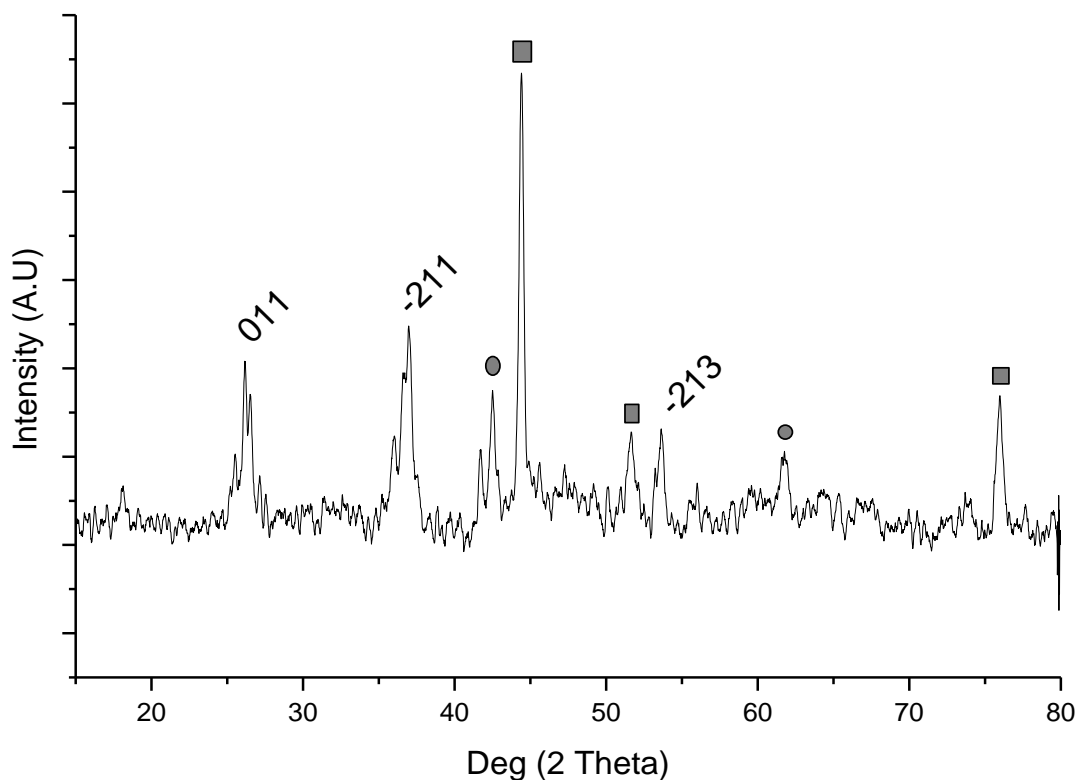


Figure 4.6 XRD trace of older catalyst, before addition of mixing agents, with hkl notation of MoO_2 . Other phases: \square : Co metal \circ : CoO

The phases present in this catalyst differ markedly from the phases seen in the original catalyst, possessing a mixture of MoO_2 , Co metal and CoO phases. The difference between the phases present is not assumed to have caused the large loss of activity, as previous runs with this catalyst performed previously had not been seen to display such low activity. It is assumed that the reduction step of catalyst preparation would change these structures prior to the reaction.

4.3.2.2 Amount of Activated Carbon support.

At this point a possible source of error was located; the scheme from which the catalysts were being prepared called for 4 g of activated carbon, but more recent calculations implied that

this should instead by 6.4 g. Previous work on a separate area of the project (CoMn/C catalysts for alkene production, see **Chapter 3**) had shown that at higher metal loadings the high surface area of the carbon support becomes entirely irrelevant as the metal appears to entirely cover the surface of the support. This in turn led to a significant drop in surface area, and a noticeable reduction in catalytic activity. Thus, a discrepancy of over 50% in the mass of the support for these catalysts could help to account for the significant reduction in activity of the newer catalysts. (It would not, however, account for the relative ineffectiveness of the previous catalyst in the presence of mixing agents.)

With this new information, it was decided to prepare a single batch of catalyst via the impregnation method outlined in **Section 2.1.2.1**, updated to account for the new amount of support material required. This batch of catalyst was split into two samples, one of which was combined with mixing agents, and one which was not. They were then tested according to the procedure outlined in **Section 4.2**. It was intended that this would provide two pieces of information: firstly, whether the extra support material was significant, and secondly, if the addition of mixing agents was significant. The results of these runs are displayed below in **Table 4.5** and **Figure 4.7**.

Table 4.5 Conversion and selectivity data for catalyst prepared by IMP, with and without mixing agents

| Catalyst | With | Without |
|------------------------------------|------|---------|
| | | |
| CO Conv | 3.24 | 12.2 |
| Product selectivity (%) | | |
| CO₂ | 11.1 | 2.35 |
| CH₄ | 50.3 | 19.28 |
| C₂-C₆ | 15.5 | 4.02 |
| MeOH | 22.2 | 28.25 |
| EtOH | 1.5 | 30.61 |
| PrOH | 0 | 12.15 |
| 1-BuOH | 0 | 3.04 |
| C>4OH | 0 | 0.32 |
| | | |
| Total Alc | 23.7 | 74.37 |
| CMB | 78.5 | 80.2 |

Reaction conditions: Temp; 250 °C, Flow rate 140.6 ml/min, pressure 75 bar

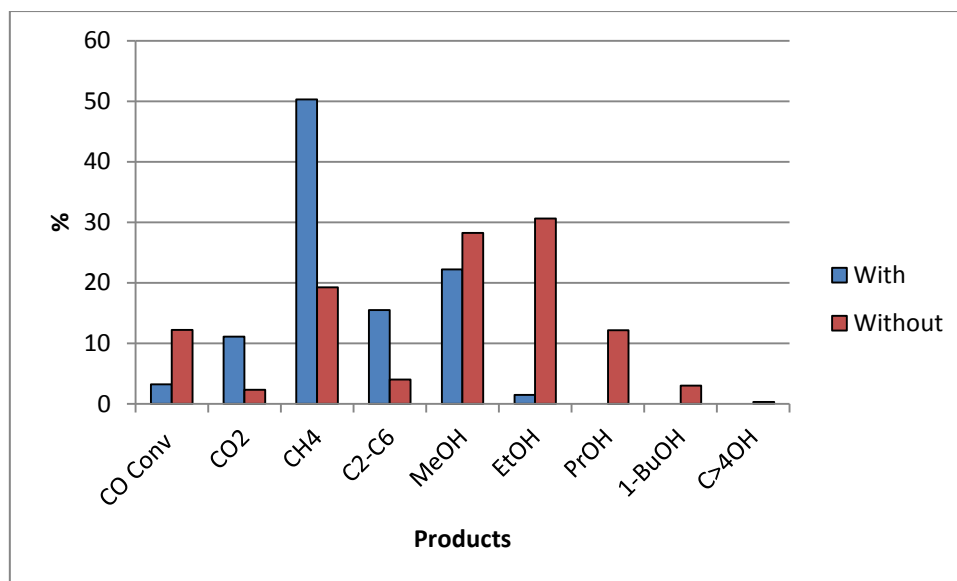


Figure 4.7 Bar chart displaying conversion and selectivity of catalyst prepared by adjusted IMP, with and without mixing agents

These results conclusively prove that for these catalysts, the mixing agents appear to inhibit catalytic activity. The results also seem to imply that the mixing agents are acting to inhibit chain growth in these catalysts, as well as formation of oxygenates. This differs from the literature regarding the sulphide catalysts upon which these were originally based; studies have shown that addition of potassium will promote oxygenate formation over linear hydrocarbons, although they agree that it inhibits catalytic activity overall.

However, as mentioned before, the factor causing promotion of oxygenates was believed to be the inhibition of CO dissociation. If chain growth is conducted through the dissociation of CO, as literature implies, then this inhibition would also cause the product distribution to tend towards C₁ products. This is in agreement with the results which are observed when mixing agents are added.

It seems that the relative ratios of mixing agents which have proven suitable for the DOW Co-MoS₂ catalysts are not suitable for the CoMo/C catalysts, where they appear to over-inhibit the dissociation of CO.

This new impregnation method without mixing agents did succeed in producing the catalyst with the highest CO conversion of any of the new catalysts. The evidence of enhanced CO conversion and an alcohols product distribution in which methanol was not the most favoured

product were both seen as positive steps. The suppression of CO₂ and linear hydrocarbons was also seen as promising.

3.2.2.2 (i) Characterisation

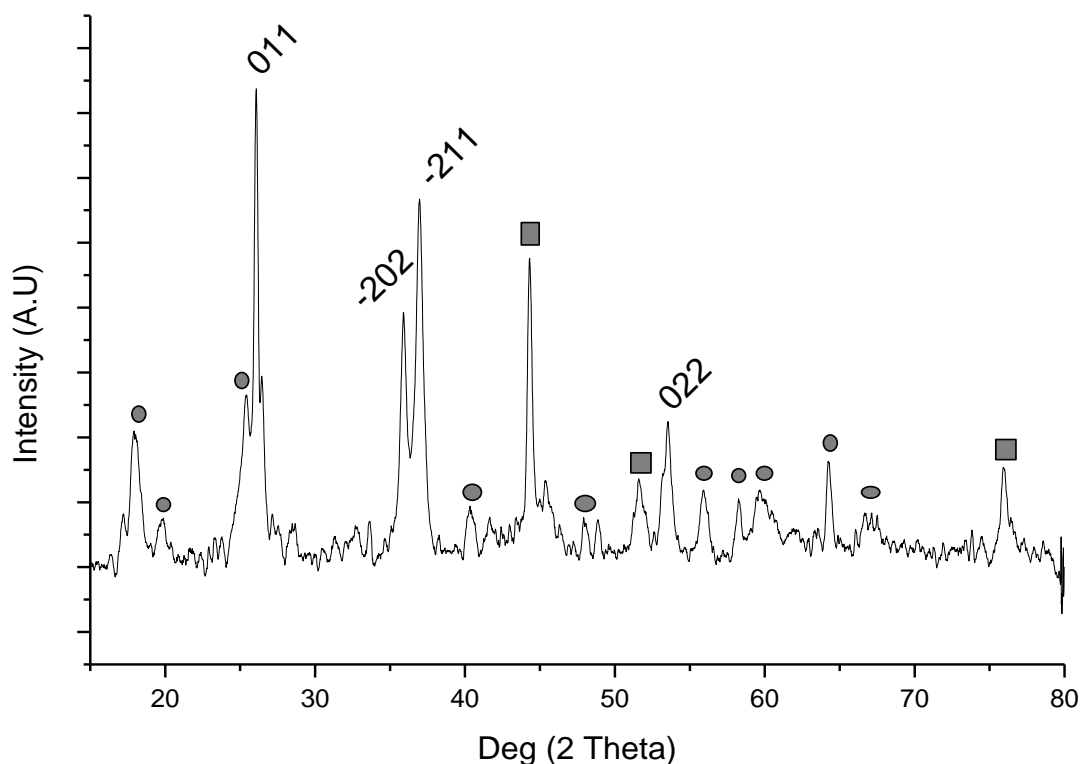


Figure 4.8 XRD trace of CoMo-C catalyst prepared by the modified IMP method, with hkl notation of MoO₂
Other phases: □: Co metal; ○: Co₂Mo₃O₈

Whilst MoO₂ and Co metal have been noted in previous catalysts, the mixed metal oxide phase Co₂Mo₃O₈ is thus far without precedent. The presence of this phase does not appear to have been detrimental to the catalyst performance; indeed, it represents the best catalyst thus far produced in this study.

4.3.2.3 Modification of heat treatment

At this point in the study it was decided to investigate other variables that could be contributing to the lack of activity in the freshly prepared catalysts. The results utilising a previously validated catalyst precursor implied that the issue might have been linked a step after the precursor preparation, such as heat treatment. However, the lower conversion may

also have been a result of the addition of mixing agents, which were subsequently shown to be detrimental to catalyst performance.

A sample of a catalyst precursor which had produced a viable catalyst prior to the initiation of this study was subjected to heat treatment, followed by testing. This decision was undertaken to ascertain which area of further investigation would be most useful. If the catalyst outperformed the catalysts synthesised thus far, it would show that the error lay in the precursor formation step. If, however, the catalyst did not outperform the current catalysts, it would show that the error lay in the heat treatment step, the reduction step, or the reaction conditions.

In the preparation method for this catalyst it was observed that a specific tubular furnace for the heat treatment of her catalysts; the different furnaces were known to have different cooling rates, and it was thought that this difference in cooling rates could affect the final catalysts. To test this, the catalyst precursor batch was split in two, with one portion being heat treated in the furnace specified by the preparation method (**Furnace A**), and the other being heat treated in a bench furnace known to have a much higher rate of cooling (**Furnace B**).

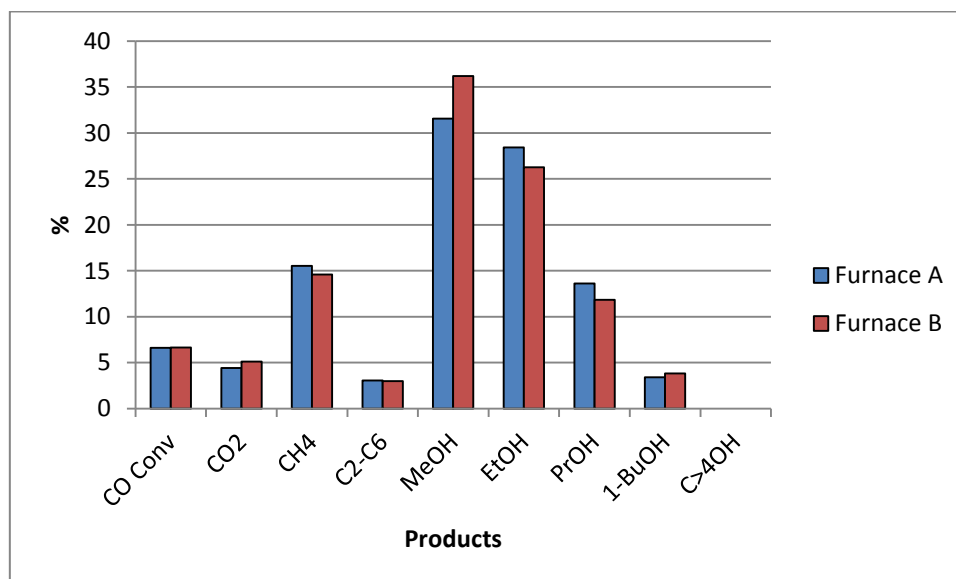
The results of these tests are displayed below in **Table 4.6** and **Figure 4.9**.

Table 4.6 Conversion and selectivity data for catalyst heat treated in different furnaces

Furnace A: specified by procedure; Furnace B: higher cooling rate

| Catalyst | Furnace A | Furnace B |
|------------------------------------|-----------|-----------|
| CO Conv | 6.59 | 6.63 |
| Product selectivities (%) | | |
| CO₂ | 4.4 | 5.1 |
| CH₄ | 15.53 | 14.6 |
| C₂-C₆ | 3.04 | 2.98 |
| MeOH | 31.54 | 36.17 |
| EtOH | 28.43 | 26.26 |
| PrOH | 13.59 | 11.84 |
| 1-BuOH | 3.41 | 3.82 |
| C>4OH | 0 | 0 |
| Total Alc | 76.97 | 78.09 |
| CMB | 78 | 74 |

Reaction conditions: Temp; 250 °C, Flow rate 140.6 ml/min, pressure 75 bar

**Figure 4.9** Bar chart comparing conversion and selectivity of catalysts heat treated in different furnaces

These results show that the furnace used for the heat treatment makes little to no difference to the final performance of the catalyst. Also, by the fact that previously shown to be effective did not outperform a more recently synthesised catalyst allows us to rule out the precursor preparation as the source of the error. It can therefore be assumed that the main source of error lies in the heat treatment, the reduction step, or the reaction conditions.

4.3.2.3 (i) Characterisation

An XRD trace of the material is shown below in **Figure 4.12**.

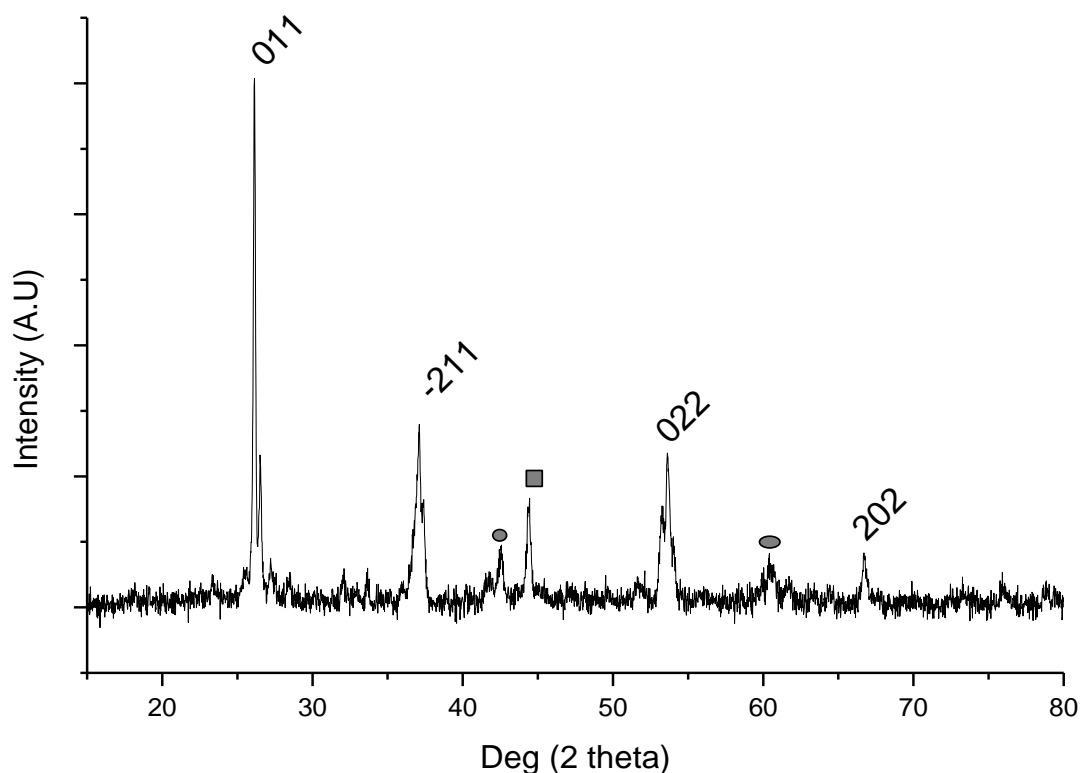


Figure 4.10 XRD trace of newly heat treated sample of previous catalyst with hkl of MoO_2

Other phases: □: Co metal; ○: CoO

This catalyst shows a similar pattern indicative of a mixture of MoO_2 , Co and CoO.

4.3.3 Modification of the reaction conditions

The next area of investigation was into the effect of alterations in the reaction conditions. It was decided to pursue this line of enquiry because the heat treatment regime and reduction conditions had remained essentially unchanged since the initial experiments based on the DOW Co- MoS_2 catalysts. Several conditions of the reactions, however, had been altered; the reaction temperature and GHSV being two such changes.

3.3.3.1 Modification of reaction temperature

The CoMo-C catalysts are run at a reaction temperature of 250 °C with a GHSV of 1875 h⁻¹. The DOW catalyst ran at a reaction temperature of 305 °C and a GHSV of 1225 h⁻¹. An initial test involving running one of the CoMo-C catalysts at these reaction conditions was unsuccessful; the gas stream analysis consisted predominantly of methane and CO₂, and the reaction was forced to be aborted after just 28 h due to a blockage caused by wax formation. The formation of these waxes was so extensive that once cooled it proved difficult to clean the reactor. It was necessary to reheat the reactor to over 200 °C to soften the waxes enough for the catalyst bed to be removed.

These observations imply that at higher temperatures the dissociation of CO to form non-oxygenated hydrocarbon products. Runaway chain propagation caused the formation of large amounts of wax.

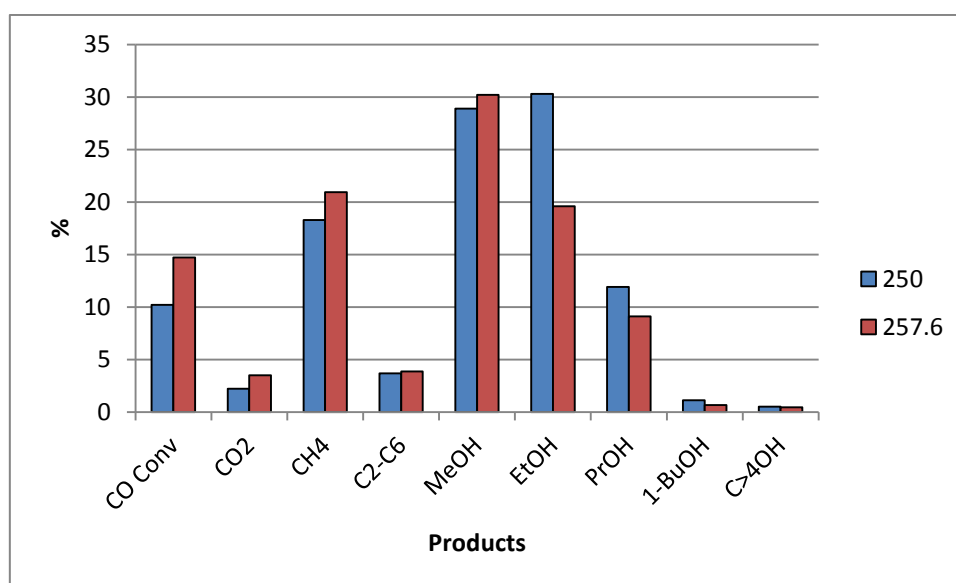
A potential, less extreme temperature discrepancy arose from the difference between the reactor temperature control readings, and the readings generated by the thermocouple located in the reactor tube itself. The thermocouple reading was generally found to be ~7.5 °C higher than the temperature reading on the reactor control unit under reaction conditions. A catalyst batch was synthesised and divided into two final catalysts after heat treatment; one to be tested with the thermocouple reading 250 °C and the second with the control unit reading 250 °C (Thermocouple: 257.6 °C)

The results of these experiments are shown below in **Table 4.7** and **Figure 4.11**.

Table 4.7 Conversion and selectivity data for different reactor temps

| Temperature (°C) | 250 | 257.6 |
|------------------------------------|-------|-------|
| CO Conv | 10.2 | 14.7 |
| Product selectivity (%) | | |
| CO₂ | 2.22 | 3.48 |
| CH₄ | 18.27 | 20.94 |
| C₂-C₆ | 3.66 | 3.87 |
| MeOH | 28.9 | 30.2 |
| EtOH | 30.3 | 19.6 |
| PrOH | 11.9 | 9.1 |
| 1-BuOH | 1.1 | 0.67 |
| C>4OH | 0.5 | 0.43 |
| Total Alc | 72.7 | 60 |
| CMB | 84 | 88 |

Reaction conditions: Temp: varies, Flow rate 140.6 ml/min, pressure 75 bar

**Figure 4.11** Bar chart displaying differences in conversion and selectivity for different reactor temperatures

As can be seen from these results, there was only a small difference in CO conversion caused by this difference in temperature. The selectivity pattern of the catalyst was affected more significantly, with a notable drop in ethanol production and an increase in C₁ products. There

was an overall loss in total alcohol production. After the reaction there was a slight wax build-up noted in the reactor tubes.

This is consistent with the observations made at much higher reaction temperatures.

3.3.3.2 Modification of gas flow

At this point it was undertaken to test the varying the GHSV of the reaction. Whilst the initial testing was done with full runs, it was soon realised that to test a substantial range of GHSVs would be too time consuming to perform in this manner. A decision was made to alter the GHSV parameters whilst the reaction was still online.

Due to the reactor setup requiring collection of all liquids for offline analysis post-reaction, any changes in liquid phase products caused by these changes in reaction conditions would not be distinguishable: the liquid results would be an agglomeration of all of the separate product streams from different GHSVs. Because of this, the liquid results were ignored in favour of simply analysing the TCD data, as it was determined that increasing the CO conversion of the catalysts was the highest priority.

The results of these reactions are displayed below in **Table 4.8**, **Figure 4.12** and **Figure 4.13**.

Table 4.8 Conversion and selectivity data for different GHSVs

| Flow rate (ml/min) | 140.6 | 120 |
|------------------------------------|--------------|------------|
| CO Conv | 10.2 | 11.2 |
| Product selectivity (%) | | |
| CO₂ | 2.22 | 3.81 |
| CH₄ | 18.27 | 19.64 |
| C₂-C₆ | 3.66 | 2.77 |
| MeOH | 28.9 | 32.2 |
| EtOH | 30.3 | 28.6 |
| PrOH | 11.9 | 10.61 |
| 1-BuOH | 1.1 | 0.47 |
| C>4OH | 0.5 | 0.3 |
| Total Alc | 72.7 | 72.18 |
| CMB | 84 | 82 |

Reaction conditions: Temp; 250 °C, Flow rate: Varies, pressure 75 bar

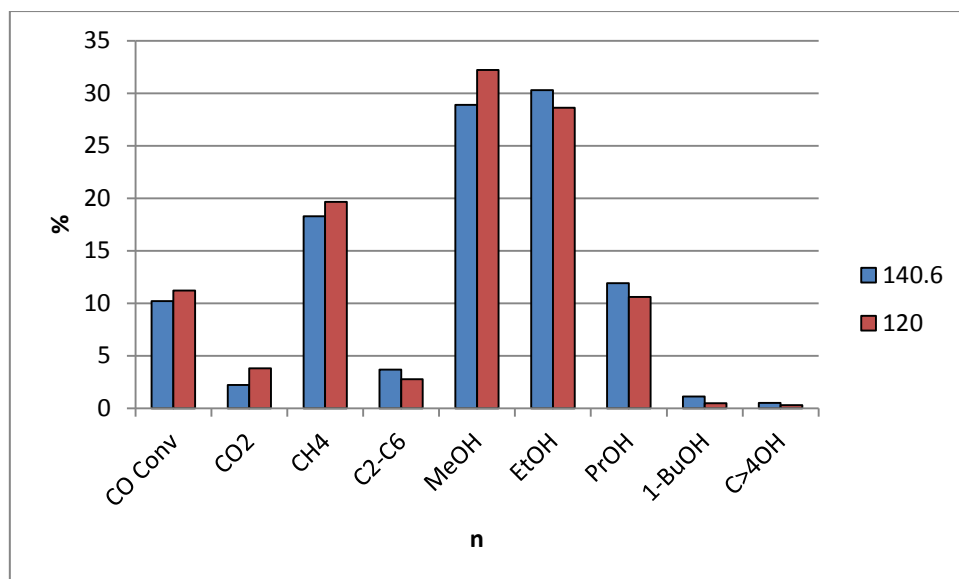


Figure 4.12 Bar chart displaying conversion and selectivity differences at different GHSVs

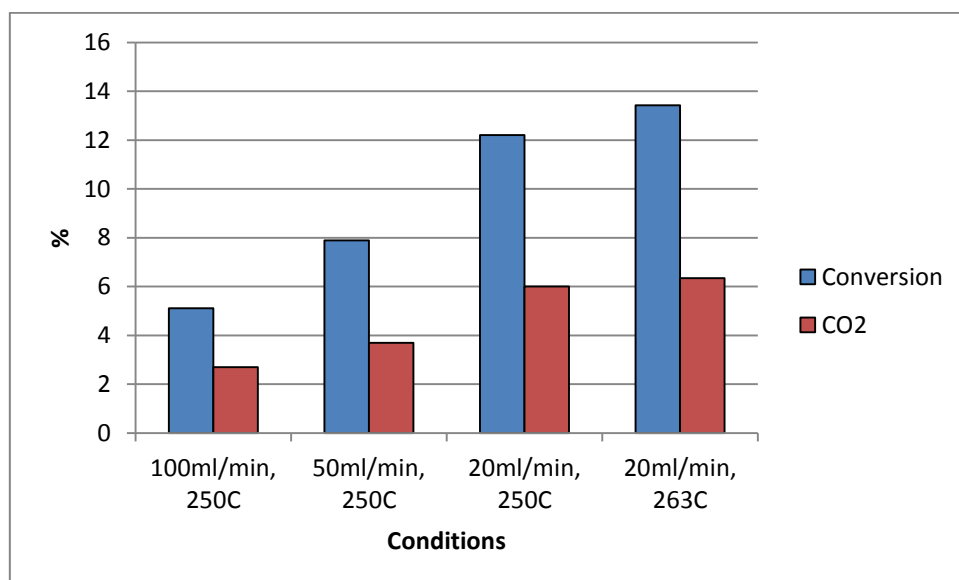


Figure 4.13 Bar chart displaying changes in CO conversion and CO₂ selectivity with decreasing GHSV

The initial two runs appear to produce counterintuitive results; lowering the flow rate, and thus the GHSV, should serve to increase the contact time that the species have with the catalyst. This would, in turn, be expected to increase the average chain length of the products observed. However, lowering the flow to 120 ml/min from 140.6 ml/min has led to an increase in the selectivity to C₁ products. It has also increased CO conversion marginally. This could be related to water gas shift activity; increasing amounts of CO₂ would imply that water is being converted to H₂, which could possibly be causing the drop in oxygenate products.

The second set of experiments show a similar trend, albeit on a more limited scale. The conversion and CO₂ selectivity both increase with decreasing flow rates, as was seen with the previous tests. Increasing temperature also increased both conversion and CO₂ production, again in line with previous results.

A different tack was taken at this point: it was possible that there was not a problem with the catalyst preparation or the reaction conditions. It was possible that the reactor itself was at fault, with some malfunction, blockage, or GC fault causing the discrepancy in the results.

With this in mind, it was undertaken to reproduce a different alcohols catalyst. Work had previously been done on impregnation of Cu onto DOW Co-MoS₂ catalysts with good results. The exact preparation details of this preparation method were readily available in literature, hopefully lessening the margin for misinterpretation. If this catalyst also proved unable to be reproduced, it could therefore be assumed that there a problem had arisen in the reactor setup. If the catalyst could be reproduced, this would instead imply that the problem of reproducing the CoMo-C catalysts was still unresolved.

4.4 Reproduction of Co-MoS₂ + 0.2 %wt Cu

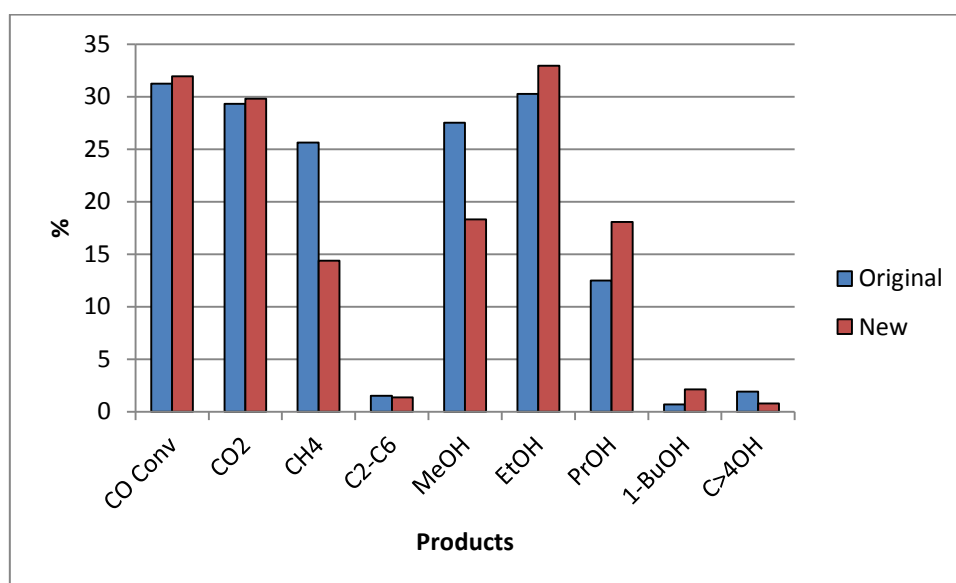
The catalyst was produced by coprecipitation, the method of which is outlined in **Section 2.1.2.2**. Following this, the catalyst was impregnated with a 0.2 %wt Cu loading according to the method outlined in **Section 2.1.2.4**.

The catalyst was tested according to the conditions listed in **Section 4.2** for the testing of sulphide catalysts. The results of the experiment, and the original data for comparison, are displayed below in **Table 4.9** and **Figure 4.14**.

Table 4.9 Conversion and selectivity data for Co-MoS₂ + 0.2 % wt Cu

| Catalyst | Original | New |
|------------------------------------|----------|-------|
| CO Conv | 31.23 | 31.95 |
| Product selectivity (%) | | |
| CO₂ | 29.3 | 29.8 |
| CH₄ | 25.63 | 14.38 |
| C₂-C₆ | 1.5 | 1.37 |
| MeOH | 27.52 | 18.3 |
| EtOH | 30.25 | 32.94 |
| PrOH | 12.5 | 18.05 |
| 1-BuOH | 0.7 | 2.11 |
| C>4OH | 1.9 | 0.77 |
| Total Alc | 72.87 | 72.17 |
| CMB | 72.68 | 67.12 |

Reaction conditions: Temp; 305 °C, Flow rate 100.2 ml/min, pressure 75 bar

**Figure 4.16** Bar chart displaying conversion and selectivity data for Co-MoS₂ + 0.2 % wt Cu

As can be seen, there is a high degree of reproducibility between the two catalysts, with the reproduction possessing marginally higher total alcohols and selectivity to ethanol. This strongly implies that there are no problems with the reactor.

At this point further production attempts of the CoMo-C catalysts in their current format were curtailed. A large amount of time had been expended with little significant progress made,

and it was decided to halt this line of inquiry until new information as to the cause of the errors could be identified.

4.5 Variations of catalyst composition

At this point it was decided to move away from incremental adjustments to a preparation method and focus instead on a more basic understanding of how the composition of the catalyst affected the CO conversion and selectivity of the catalysts.

From the XRD traces of the previous section, it was seen that a wide array of phases and combinations of phases could be obtained from repeated attempts at the same preparation method. The simplest system observed was the mixed metal oxide CoMoO_4 . This was observed for the first catalysts. Other catalysts had a mixture of phases and oxidation states, implying that the catalyst synthesis is affected by a large number of factors.

An attempt was made to rework the catalyst from basic principles. The original preparation method in the DOW literature uses coprecipitation to deposit cobalt onto MoS_2 . The heptamolybdate precursor is used to make ammonium molybdenum sulphide, which is then precipitated in acetic acid.

In the preparation methods used in this study impregnation is used instead to place molybdenum and cobalt onto a carbon support. The amounts used in the preparation method were taken directly from the original DOW preparation method, without adjustment. In an impregnation method all of the metal ions will remain in the system after drying, whereas in coprecipitation much of the material may still be retained in solution. It was noted that 15 g of the heptamolybdate precursor creates a massive excess of Mo compared to the amount of Co present in the calculations.

To examine the effect of this large excess of molybdenum, an initial test was run using a catalyst prepared via the method outlined in **Section 2.1.2.1**, save that only 7.5 g of the molybdate precursor were used in the impregnation.

The results of this experiment, and comparison to a previous run, are shown below in **Table 4.10** and **Figure 4.15**. Due to an error arising with the FID, no gas phase data could be collected for hydrocarbons.

Table 4.10 Conversion and selectivity data for catalyst with half Mo content

| Catalyst | Normal | 1/2Mo |
|------------------------------------|---------------|--------------|
| | | |
| CO Conv | 9.23 | 6.7 |
| Product selectivity (%) | | |
| CO₂ | 1.35 | 1.13 |
| CH₄ | - | - |
| C₂-C₆ | - | - |
| MeOH | 16.26 | 33.54 |
| EtOH | 35.22 | 38.01 |
| PrOH | 20.99 | 19.1 |
| 1-BuOH | 8.77 | 8.22 |
| C>4OH | 0 | 0 |
| | | |
| Total Alc | 81.24 | 98.87 |

Reaction conditions: Temp; 250 °C, Flow rate 140.2 ml/min, pressure 75 bar

Note that the total alcohols value will be skewed as to be higher than normal; usually the results are combined with the gas phase data to present the final results. In this case the liquid analysis represents almost the entirety of the data, and thus the liquid alcohols appear to dominate. As such, these results are comparable to each other, but should not be compared to other results in this chapter.

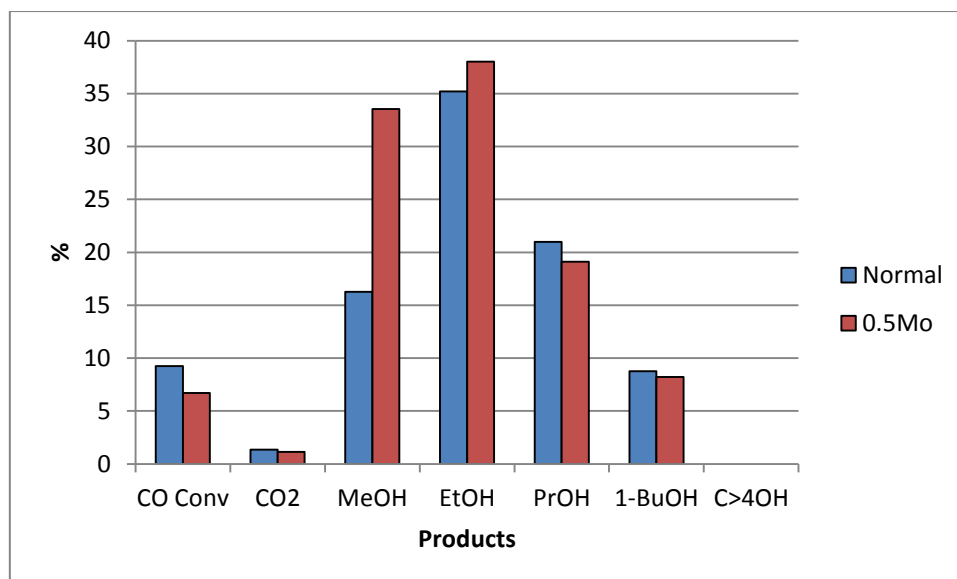


Figure 4.15 Bar chart showing conversion and selectivity data for catalysts with different amounts of Mo

The results did not seem to be promising initially, but of interest was the XRD trace obtained for this material, shown below in **Figure 4.16**.

4.5 (i) Characterisation

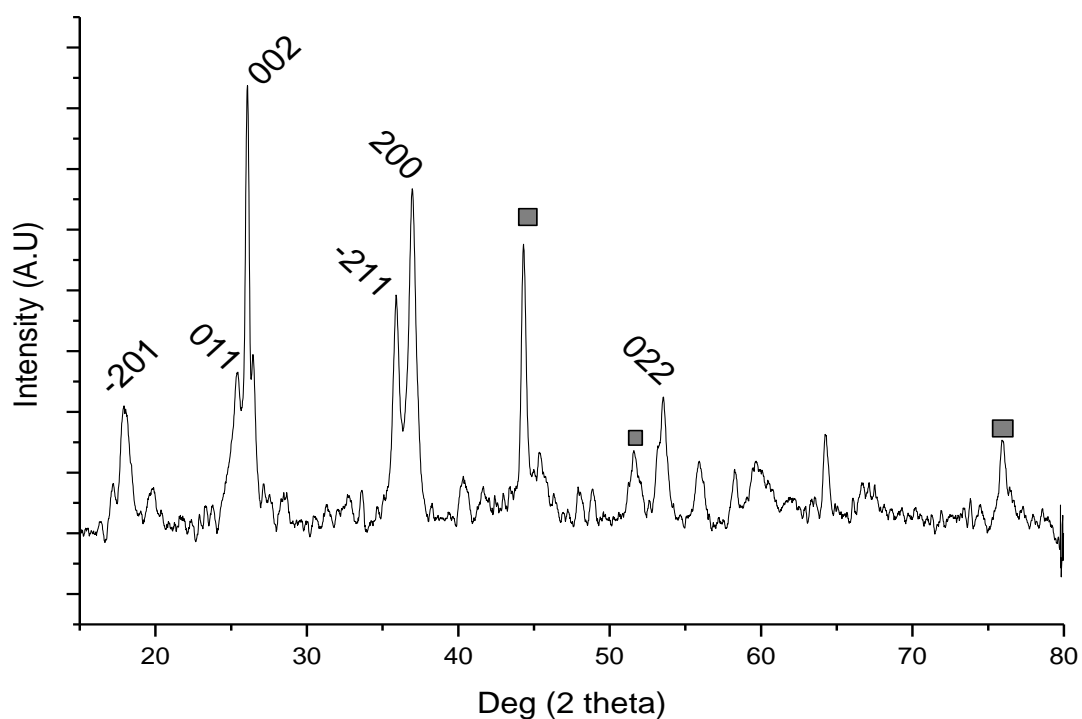


Figure 4.16 XRD trace of catalyst containing $\frac{1}{2}$ amount of molybdenum with hkl notation of MnO_2 and CoMoO_4 . \square : Co metal

This trace displays a mix of phases, mostly MnO₂ and Co metal, but also containing CoO and CoMoO₄.

Since lowering the amount of molybdenum had such a pronounced effect on the phases present, it was decided to undertake a series of experiments with a new preparation method in which the ratio between cobalt and molybdenum was altered whilst keeping the amount of metals relative to the catalyst support constant. The experiments were based on a series of experiments performed in **Chapter 3** where the cobalt-manganese ratio was altered in a similar manner.

A ratio of metals-to-support of 40-60 was chosen, identical to that used in the cobalt-manganese experiments mentioned. This required a large reduction in the amount of molybdenum precursor used: generally only around 2g was needed. The catalysts were prepared according to the preparation method outlined in **Section 2.1.2.1**, save that the amounts of the precursors were altered to produce the desired metal loadings.

The results of these experiments are shown below in **Table 4.11** and **Figure 4.17**.

Table 4.11 Conversion and selectivity data for catalysts with varying metal ratios

| Cobalt % | 40 | 35 | 30 | 25 | 20 | 10 | 5 | 0 |
|------------------------------------|-----------|-----------|-----------|-----------|-----------|-----------|----------|----------|
| CO Conv | 5.39 | 5.22 | 11.31 | 20.1 | 16.1 | 7.75 | 0 | 0 |
| Product selectivity (%) | | | | | | | | |
| CO₂ | 11.4 | 6.6 | 6.5 | 5.5 | 4.1 | 3.33 | 0 | 0 |
| CH₄ | 5.63 | 5.64 | 3.25 | 3.32 | 4.58 | 7.46 | 0 | 0 |
| C₂-C₆ | 2.27 | 1.19 | 0.1 | 0.87 | 2.22 | 4.73 | 0 | 0 |
| MeOH | 21.72 | 14.34 | 14.02 | 12.56 | 16.9 | 30.45 | 0 | 0 |
| EtOH | 39.62 | 46.89 | 48.68 | 50.21 | 46.3 | 38.55 | 0 | 0 |
| PrOH | 18.73 | 20.55 | 22.06 | 22.66 | 17.3 | 15.1 | 0 | 0 |
| 1-BuOH | 10.88 | 10.67 | 9.72 | 9.48 | 8.95 | 8.22 | 0 | 0 |
| Total Alc | 90.95 | 92.45 | 94.48 | 94.91 | 89.45 | 92.32 | 0 | 0 |

Reaction conditions: Temp: 250 °C, Flow rate 100.2 ml/min, pressure 75 bar

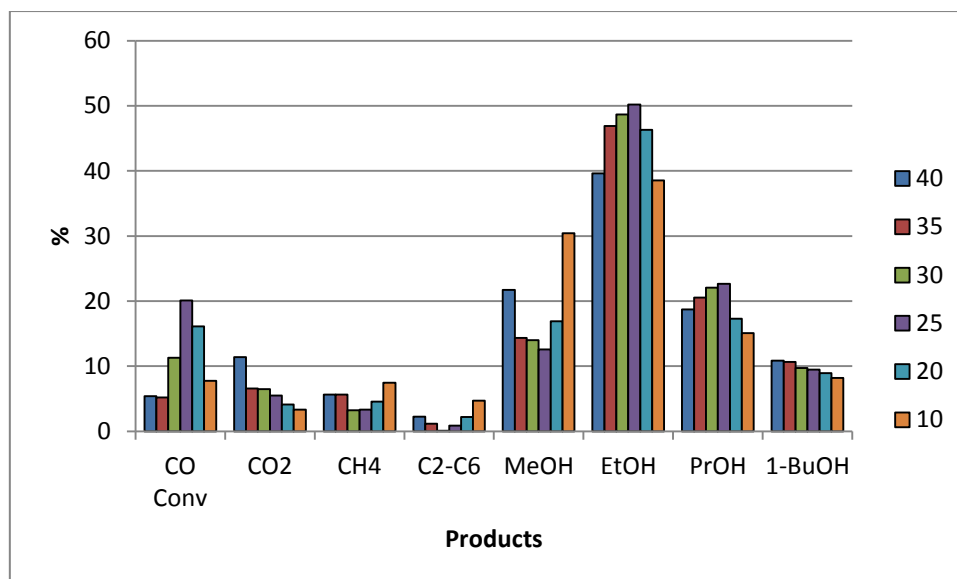


Figure 4.17 Bar chart displaying conversion and selectivity data for catalysts with varying metal ratios
Key denotes cobalt %

These catalysts represent a significant improvement over anything seen thus far in the study. Of particular note are the very high ethanol and propanol selectivities. Both of these are extremely desirable products, and the selectivities towards these two products for Co:Mo:C = 25:15:60 in particular represent a significant step. Also of note are the trends in CO₂, CH₄, linear hydrocarbons and methanol, all undesirable products. CO₂ selectivity decreases with increasing molybdenum content, and the other three products all reach a minimum at Co = 25 %. The CO conversion of these catalysts reaches 20 %, almost twice the previous best catalyst. The selectivities towards C₂-C₄ alcohols display a significant improvement.

4.5 (ii) Characterisation

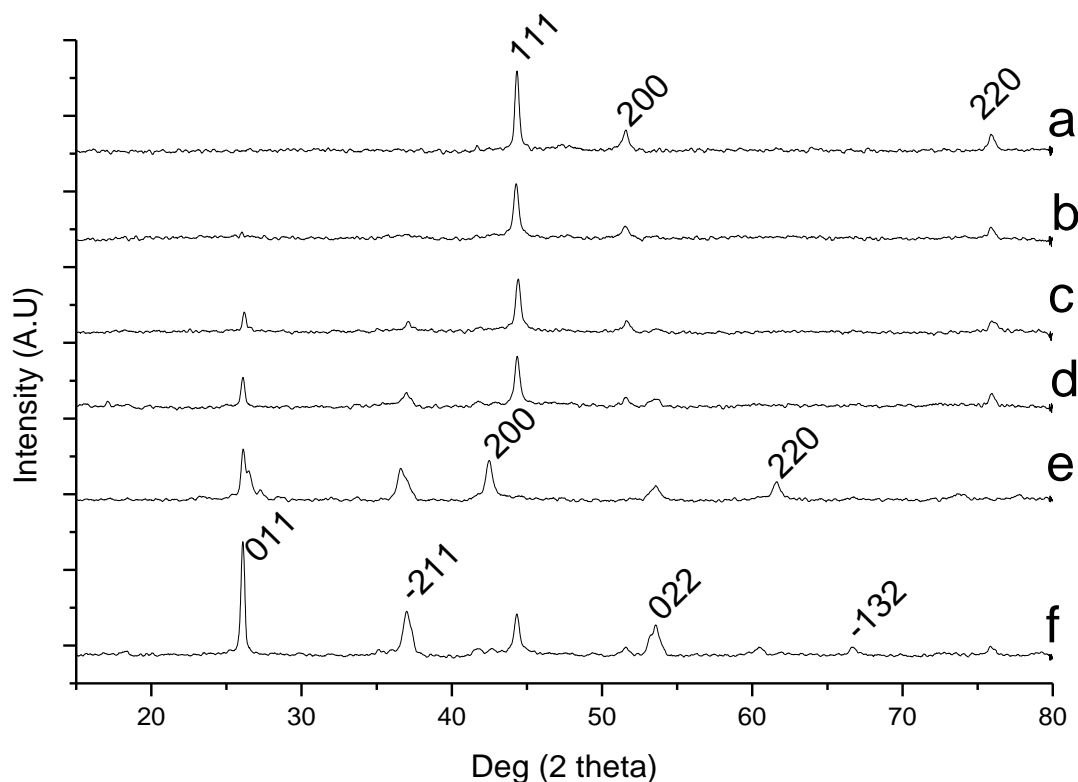


Figure 4.18 XRD traces of catalysts with varying metal ratios

Co%: a: 40; b: 35; c: 30; d: 25; e: 20; f: 10

The higher cobalt % catalysts show traces consistent with cobalt metal, the hkl notation of which is displayed on (a). The presence of the fully reduced metallic form would seem to agree with findings that the presence of carbon can cause the reduction of cobalt in an inert atmosphere¹¹. Trace (e) displays the presence of CoO, the only catalyst in the sequence to do so. It is not clear why this should be the case, but it is possible that at this ratio of metals a different set of precursors is formed, which leads to a different heat treatment profile. The hkl notation of CoO is marked on (e). As the Mo % increases the emergence of the MoO₂ phase becomes evident, the hkl notation of which is marked on (f). Since all of the catalysts seem to display fundamentally the same structures, it is not thought that a change in these is responsible for the conversion or selectivity patterns witnessed.

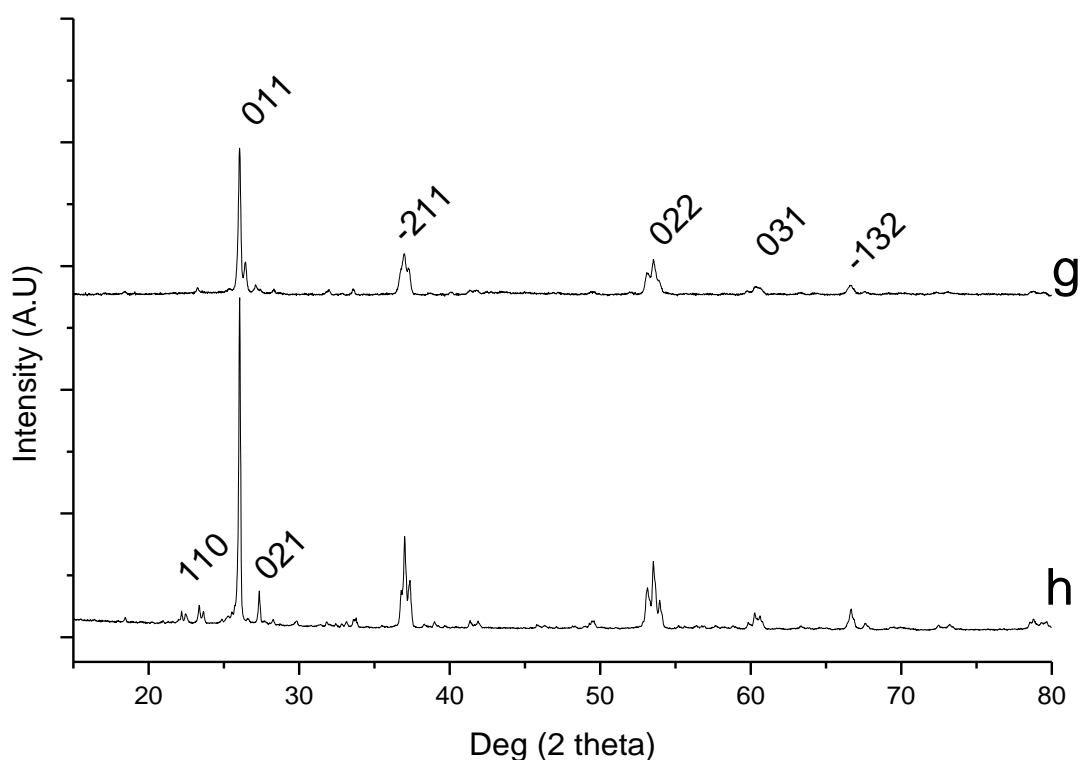


Figure 4.19 XRD traces of inactive high-Mo % catalysts, with hkl notations.

Co %: g: 5; h: 0

These traces display primarily MoO_2 phases, the hkl notation of which is marked on (g). The MoO_3 phase is also present in small amounts in (h), and as such the hkl notations are marked on that pattern. There is no evidence of cobalt species in either trace, which may be the cause of their inactivity. Whilst molybdenum oxides can be used to produce oxygenates, they usually do so at higher temperatures and pressures that are used here.

4.6 Conclusions and future work

The initial process of incremental adjustments to a catalyst proved inefficient and unsuccessful. Through these processes it was shown that the addition of potassium-based mixing agents in a similar ratio to the industrial catalysts upon which these were based causes a promotion of C_1 products and a loss of CO conversion. This is thought to be due to potassium ions blocking sites of CO dissociation, which is believed to be a key step in chain

propagation. It is possible that addition of potassium in smaller quantities could have the effect which is stated in literature; the promotion of oxygenate products.

The reactions were also shown to be affected by changes in temperature and flow rate, although not in the manner that was anticipated. It appears that competition between CO hydrogenation and the water gas shift reaction is a significant factor for this class of catalyst.

Once it was undertaken to gain a fuller understanding of the basic catalyst composition, progress was considerably more rapid. It was shown that mixtures of cobalt and molybdenum are more active for CO hydrogenation than either cobalt or molybdenum individually. Increasing molybdenum content of these catalysts was shown to promote CO hydrogenation, as well as increasing selectivity to C₂ and C₃ alcohols, both of which are desirable products. This trend did not continue indefinitely; conversion and favourable selectivities began to decline again once molybdenum made up 50 % or more of the metals mixture.

Of particular note was the catalyst with composition Co:Mo:C = 25:15:60, which displayed both the highest conversions and the greatest selectivity to C₂₊ alcohols. Future work into this area should be based upon using this catalyst as a reproducible starting point from which to make incremental improvements. Considerations should also be given to the addition of promoters such as potassium and copper. Despite the mixed results seen so far in this study, such promoters are an important part of catalyst design.

4.7 References

1. J. M. Christensen, P. A. Jensen and A. D. Jensen, *Industrial & Engineering Chemistry Research*, 2011, **50**, 7949-7963.
2. J. M. Christensen, P. A. Jensen, N. C. Schiodt and A. D. Jensen, *Chemcatchem*, 2010, **2**, 523-526.
3. J. M. Christensen, P. M. Mortensen, R. Trane, P. A. Jensen and A. D. Jensen, *Applied Catalysis a-General*, 2009, **366**, 29-43.
4. A. Griboval-Constant, J. M. Giraudon, G. Leclercq and L. Leclercq, *Applied Catalysis a-General*, 2004, **260**, 35-45.
5. J. L. Dubois, K. Sayama and H. Arakawa, *Chemistry Letters*, 1992, 5-8.
6. S. T. Oyama, *Catalysis Today*, 1992, **15**, 179-200.
7. J. M. Christensen, L. D. L. Duchstein, J. B. Wagner, P. A. Jensen, B. Temel and A. D. Jensen, *Industrial & Engineering Chemistry Research*, 2012, **51**, 4161-4172.
8. S. Zaman and K. J. Smith, *Catalysis Reviews-Science and Engineering*, 2012, **54**, 41-132.
9. R. R. Stevens, European patents, 1986, 0,172,431
10. N. E. Kinkade, European patents, 1985, 0,149,255 and 0,149,256
11. H. F. Xiong, M. Moyo, M. K. Rayner, L. L. Jewell, D. G. Billing and N. J. Coville, *Chemcatchem*, 2010, **2**, 514-518.

Chapter 5

Catalytic properties and support effects of perovskites

5.1 Introduction

Whilst in the literal sense the term perovskite only applies to the mineral CaTiO_3 discovered in 1893, the term has broadened in scope over the years to include any mixed metal oxide which possesses the same structure as calcium titanate. There are also in existence several examples of non-oxide perovskites, such as NaMgF_3 , but for the purposes of this study the term perovskite will refer to mixed metal oxides.

Perovskite oxides as a whole are a highly diverse series of materials, with a general formula of ABO_3 , where A is a cation of larger ionic radius than B, which is also a cation. There are a

very large number of possible combinations that fit this general formula; it is known that around 90% of the natural metallic elements in the periodic table are stable in a perovskite oxide form. In addition to this it is widely documented that it is possible to synthesise multicomponent perovskite oxides by partial substitution of either the A or the B cation. These substituted perovskites have a general formula of $A_{1-x}A'_xB_{1-x}B'_xO_3$. It has also been seen that metal ions can occupy unusual oxidation states in the crystal structure, such as is the case for La-Ba-Cu oxide, which contains a metallic $Cu^{2+} - Cu^{3+}$ mixed valence state¹.

The wide range of viable combinations allows perovskites to be used in a variety of different catalyst applications. The ease of substitution of additional metals into the basic perovskite structure is also desirable, as this can allow, in theory, for selective tailoring of the material properties of the perovskite. Specifically in this study, the interest was in tailoring the acid-base properties of the perovskites.

Studies have shown that in most cases for perovskites, the large, low-charge cations (*i.e.* the A cation in the general formula ABO_3) show a strong predominance for determination of surface basic properties²⁻⁴. The implication was, therefore, that substitution of a more basic A cation into a perovskite structure would allow for fine control of the basicity of the catalyst. This was corroborated in a paper by *Trikalitis et. al.* in which the substitution of lanthanum by strontium in the perovskite $LaVO_3$ caused an increase in basic character, as assessed using conversion of isopropyl alcohol (IPA) as a test reaction⁵.

The reaction of IPA is considered a suitable test reaction because it produces different products depending on the acid-base properties of the catalyst^{6, 7}. (It is worth noting that this was long thought to be the only factor in determining the product selectivities, but it has since been shown that the redox properties of a catalyst will also play a role⁸.)

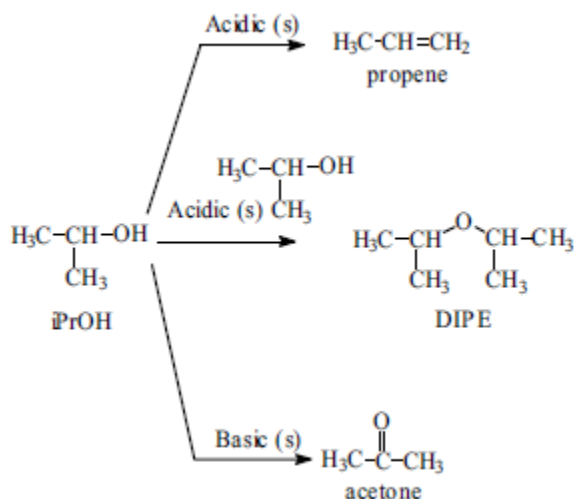


Figure 5.1 products of the IPA reaction⁷

The dehydration of IPA to form propene happens in the presence of both Lewis and Brønsted acid sites. In the presence of acid-base pair sites, or in some cases acid sites alone, diisopropyl ether is formed by intermolecular dehydration. In the presence of basic sites, acetone is formed by dehydrogenation⁹⁻¹¹. The comparison of product selectivities therefore allows for a rough assessment of the acid-base properties. Due to the additional factors involved product selectivities (redox properties, temperature of reaction, etc.) it is not possible to use the IPA reaction as a direct measurement of acidic and basic sites, but the testing of similar materials under similar conditions should give a good indication of the relative number of acidic and basic sites.

Just as the IPA reaction produces different products depending on the availability of acidic and basic sites, so do a large number of other reactions, which could lead to the possibility of a tuneable catalyst being of high commercial value. One such reaction is the oxidation of benzyl alcohol to benzaldehyde¹². Previous work has shown that it is possible for this reaction to proceed under relatively mild, solvent-free conditions¹³⁻¹⁵, using molecular oxygen via use of supported precious metal nanoparticles. The conditions of the reaction differ markedly from current industrial processes, where stoichiometric oxygen donors such as chromium trioxide are used^{16, 17}.

Many such reagents, particularly chromium compounds, have significant environmental risks associated with them, making greener techniques more attractive.

Under the conditions used by *Hutchings et. al.* the reaction of benzyl alcohol was found to proceed by two main routes: oxidation to form benzaldehyde, benzyl benzoate and benzoic acid, and disproportionation to form benzaldehyde, toluene and water¹⁸⁻²². Dehydration to form dibenzyl ether was also observed in some cases, but in low amounts. Using toluene production as a guide, it was found that the disproportionation reaction occurred more favourably when Au-Pd catalysts were supported on materials with greater acidic character, such as activated carbon and titania, as opposed to zinc oxide and magnesium oxide, which showed no activity for disproportionation, but lower overall benzaldehyde production¹⁸.

This raised an interesting link to the potential for tailoring the properties of the perovskites. It was decided to investigate if it would be possible to tune a perovskite such that it would not be active towards disproportionation, but retain the higher conversion of the more acidic supports. To this end, work began on the reproduction of the results of *Trikalitis et.al.* regarding the substitution of Sr into LaVO_3 ⁵, before continuing on to include a wider range of substituted metals.

5.2 Preparation details

All perovskites prepared in this study were created using the citrate method^{23, 24} followed by high temperature calcination and reduction. These perovskites were either tested as they were, or used as metal supports for precious metals. In the experiments where precious metals were supported onto these perovskites, the metal loadings were achieved via a sol-gel immobilization technique. All of these techniques are explained in greater detail in **Chapter 2**. (Citrate method: **Section 2.1.3, (i)**; Sol-gel immobilization: **Section 2.1.3 (ii)**)

Three different categories of reaction were carried out over the course of these experiments:

- i) The initial set of experiments, isopropyl alcohol test reactions involving combinations of lanthanum and strontium perovskites were conducted in a continuous flow reactor. The catalysts were loaded into quartz tubes and tested with a flow of vaporized isopropyl alcohol in helium (1.02 ml/min IPA in 40 ml/min He). The reactions were conducted at a series of temperatures between 200 °C and 400 °C. The products were tested via on-line GC.
- ii) The experiments into perovskites for benzyl alcohol oxidation were conducted in four identical sealed glass reactors under 2 bar pressure of O₂. Set amounts of catalyst and benzyl alcohol were placed in each reactor, which were then heated to 120 °C with stirring. At periodic times a reactor would be removed and quenched, with the liquid products then centrifuged and tested in an off-line GC.
- iii) The experiments into perovskites as catalysts for Fischer-Tropsch were carried out in an identical manner to the one outlined in **Chapter 3, Section 3.2**.

5.3 Isopropyl Alcohol Test Reaction

For these reactions a series of perovskites were synthesized, with LaVO₃ as the first perovskite, followed by incremental substitution of La for Sr in the preparation method until such a point as SrVO₃ was produced. The % substitutions chosen were 0, 10, 20, 40, 60, 80 and 100, reflecting the catalyst compositions used by Trikalitis and Pomonis⁵.

5.3.1 Results and discussion

5.3.1.1 Initial tests

Changes in the conversion and selectivity data for the different substitutions of Sr into LaVO_3 over a range of temperatures are displayed below in **Figures 5.2** and **5.3**.

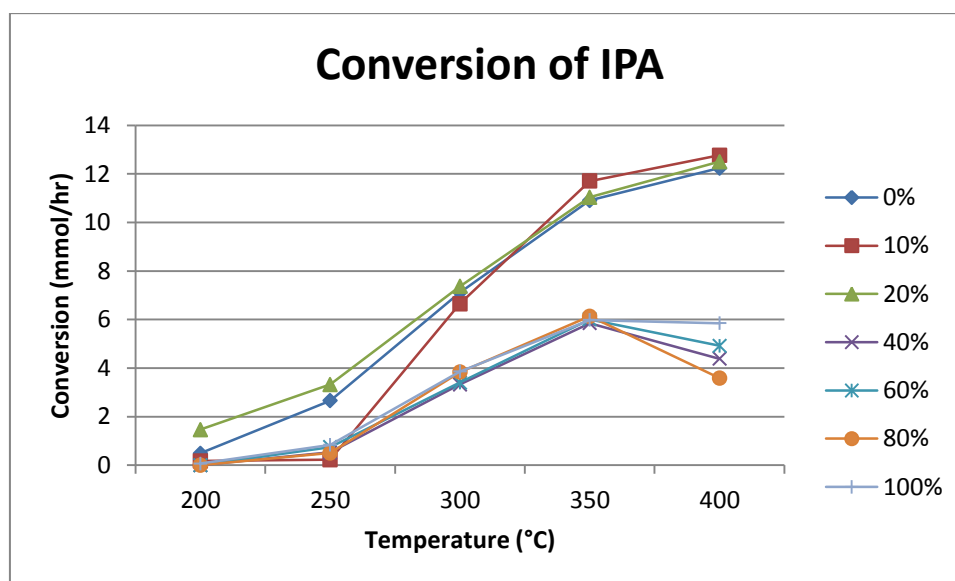


Figure 5.2 Line graph displaying conversion of IPA. Legend represents % of La substituted for Sr.

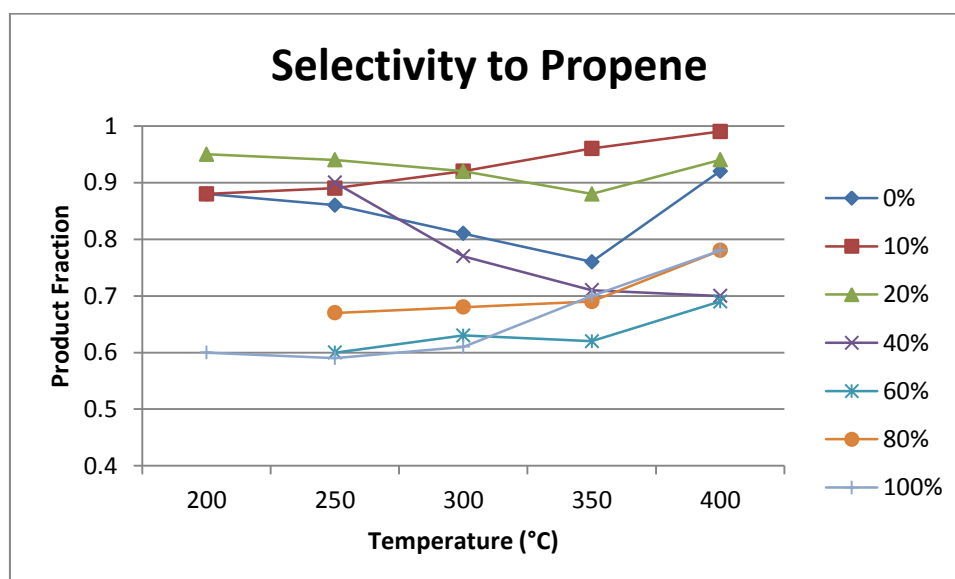


Figure 5.3 Line graph displaying selectivity to propene. Legend represents % of La substituted for Sr.

As acetone is the only other observed product, it can be inferred that the acetone selectivity, although not shown here, is (1- propene selectivity).

There are two trends readily apparent in the data, beyond the rate increase commonly displayed with increasing temperature. Firstly, it is extremely noticeable that whilst the conversion does change with Sr substitution, this does not appear to be a gradual effect. When the substitution is $\leq 20\%$, the conversion is in the range of 11-12 mmol/hr at 350 °C for all three catalysts in this range. However, at all higher substitutions only ~6 mmol/hr conversion is displayed at the same temperature. This is somewhat similar to what is displayed in the *Trikalitis et. al.* paper⁵ that this study was based upon, but there are differences to be noted. In the original paper, it was stated that the IPA conversion dropped rapidly with increasing substitution up to the point of 20 % substitution, after which point the conversion remained fairly stable. However, as can be seen from our results, the conversion appears to remain stable with catalysts of up to 20 % Sr substitution, before undergoing this rapid drop, and thereafter remaining stable. The selectivities, whilst generally slightly higher towards propene than those in the literature, display the same trends of increasing acetone production with increasing strontium substitution. A comparison between the activity and selectivity of the catalysts in the literature and those in this study is shown below in **Table 5.1**.

Table 5.1 activity and selectivity data for perovskite catalysts, and comparison with literature

| La _(1-x) Sr _x VO ₃ | R | | Selectivity | |
|---|------------------------------|-------|-------------|-------|
| | mol/g/s (x10 ⁻⁶) | | (Propene %) | |
| x | Literature | Study | Literature | Study |
| 0 | 0.85 | 0.74 | 71 | 86 |
| 0.2 | 0.4 | 0.92 | 81 | 92 |
| 0.4 | 0.35 | 0.14 | 70 | 75 |
| 0.6 | 0.35 | 0.2 | 65 | 67 |
| 0.8 | 0.35 | 0.14 | 63 | 60 |
| 1 | 0.3 | 0.21 | 59 | 59 |

The original paper offers little explanation as to why this change occurs, although in their calculations of activation energy they did show that E_{acetone} for $\text{La}_{0.6}\text{Sr}_{0.4}\text{O}_3$ was abnormally high compared to the others, being 163.9 kJ/mol for this reaction and generally ranging between 120-130 kJ/mol for the other substitutions. It is unclear why this is so, although it is worth noting that this level of substitution is the one at which split peaks begin to appear in the XRD patterns, and also, in the preparation methods it is the level of substitution at which explosive decomposition occurs during the calcination step. It appears that the catalyst undergoes significant changes at this point, with corresponding effects upon its catalytic behaviour.

The second trend is in selectivity, which broadly shows a decrease in propene selectivity with increasing substitution of La for Sr. Since in the IPA reaction the selectivity towards propene is generally regarded as a rough measure of acid sites in the catalyst, it can be said that the substitutions are decreasing the acidic character of the catalyst. This is in line with the expectations garnered from the original paper; with the addition of the more basic Sr^{2+} into the perovskite, the number of basic sites available for reaction increases. This confirms the supposition that the number of acid and base sites in the perovskites can be controlled, to an extent, and thus hopefully allows us to tune catalysts to produce desirable products in certain reactions.

5.3.1.1.1 Characterisation

The catalysts tested in this section were characterised by X-Ray Diffraction (XRD) and BET surface area analysis. Initial XRD traces for LaVO_3 and SrVO_3 are displayed below in **Figures 5.4** and **5.5**.

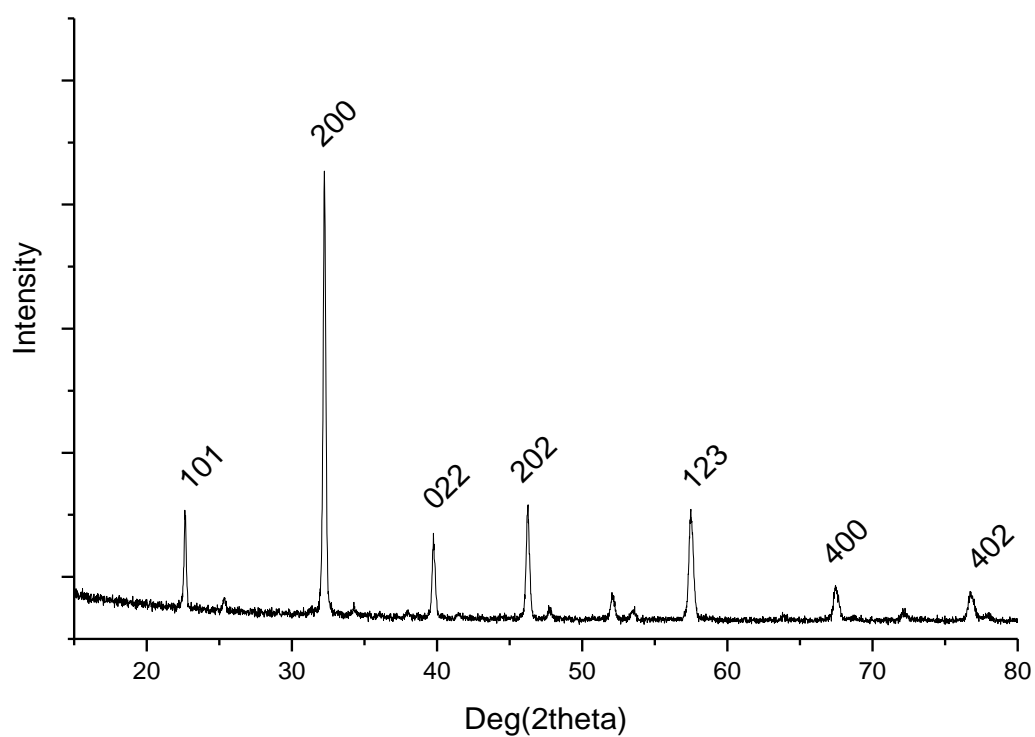


Figure 5.4 XRD trace of LaVO₃ perovskite catalyst displayed with hkl notations

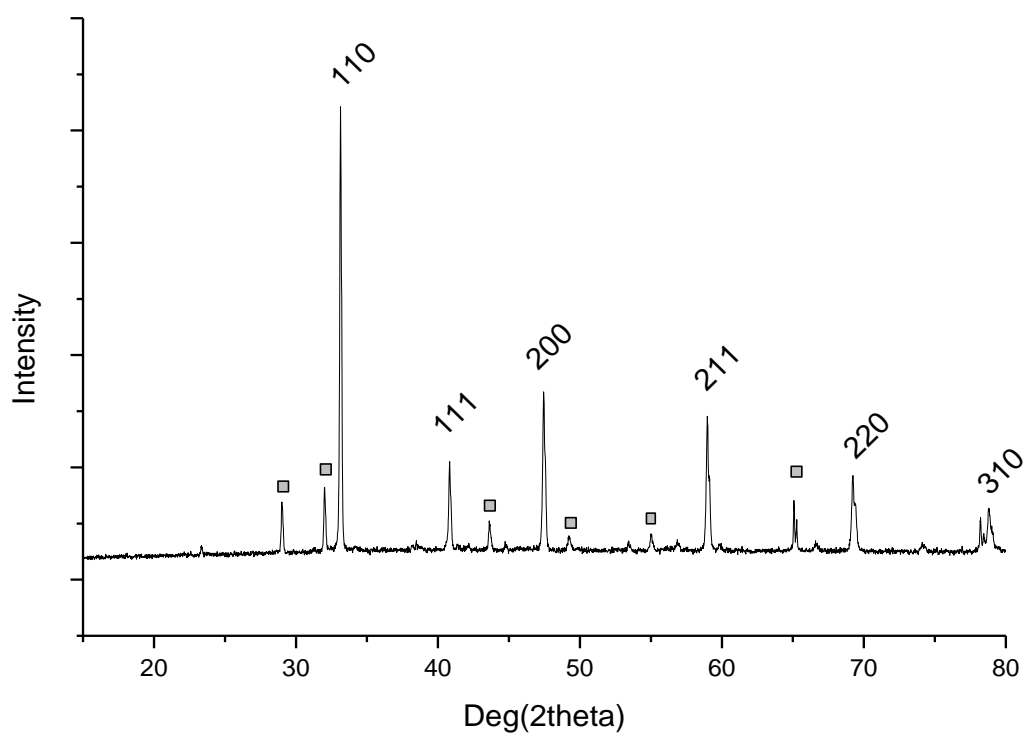


Figure 5.5 XRD trace of SrVO₃ perovskite catalyst displayed with hkl notations. □: Sr₃V₂O₈ phase

The traces displayed show that the two materials possess very similar structures, although not identical. The two materials are actually of different crystal systems; LaVO_3 is orthorhombic, whereas SrVO_3 is cubic. The SrVO_3 material can also be seen to display an additional phase, the orthovanadate $\text{Sr}_3\text{V}_2\text{O}_8$. This phase was noted in the initial literature, and later analysis showed it to be present as roughly 15 % of the material²⁵. The phase is present in the unreduced form of the material, along with the pyrovanadate phase $\text{Sr}_2\text{V}_2\text{O}_7$. It appears that in the reduction step, the pyrovanadate material is reduced to become the perovskite phase, but that the conditions employed do not cause significant reduction of the orthovanadate.

The oxidised phase of LaVO_3 is LaVO_4 , and this appears to undergo complete reduction to the perovskite phase, as no other phases are present in the final material.

Analysis of the XRD traces for these materials allows us to test the hypothesis that the substituted metal ions are undergoing incorporation into the material. If the strontium is indeed being incorporated into the LaVO_3 perovskite, a change in peak position would be expected as the material transitioned from one perovskite to another, an effect resulting from the differences in ionic radii between La^{3+} and Sr^{2+} . This does indeed appear to happen for some of the range of substitutions, however, when $0.4 \leq x \leq 0.6$ in $\text{La}_{(1-x)}\text{Sr}_x\text{VO}_3$ a splitting of major peaks can be observed. The shifting of peaks, and the peak splitting, are displayed below in **Figure 5.6** and **Figure 5.7**.

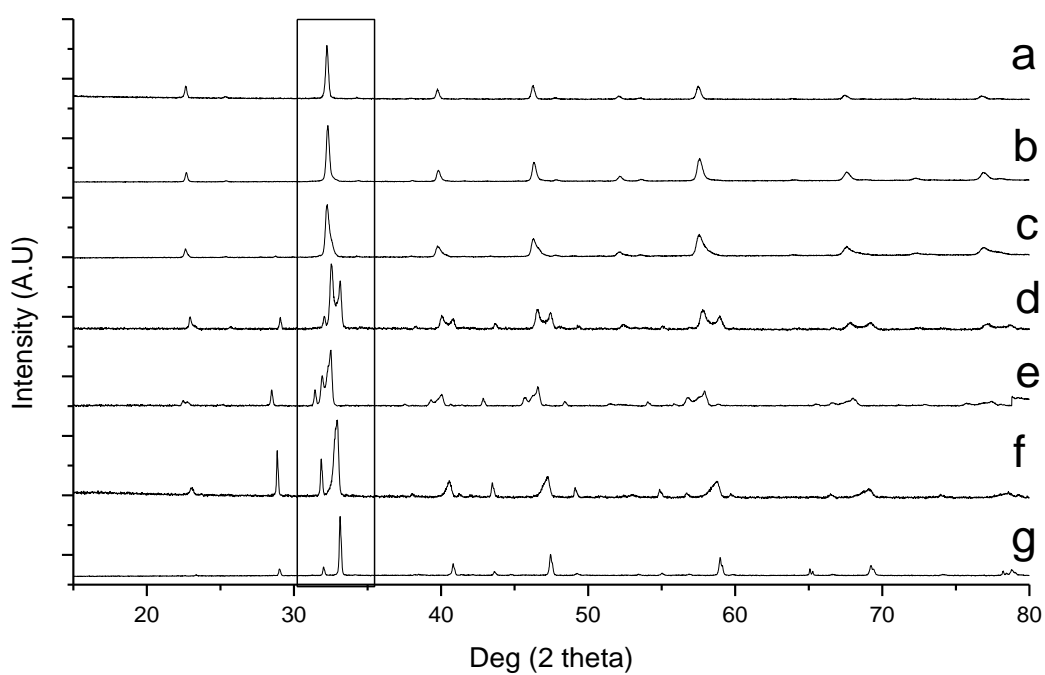


Figure 5.6 XRD traces of substituted perovskite material $\text{La}_{(1-x)}\text{Sr}_x\text{VO}_3$

X values: a: 0; b: 0.1; c: 0.2; d: 0.4; e:0.6; f: 0.8; g: 1

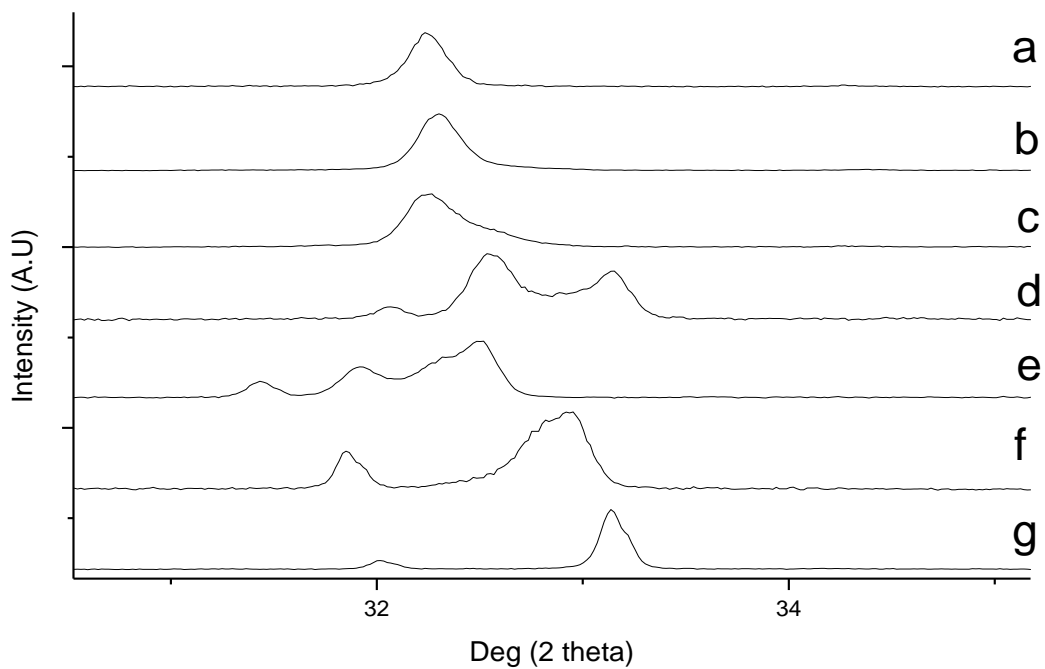


Figure 5.7 XRD traces of main peak in perovskite material $\text{La}_{(1-x)}\text{Sr}_x\text{VO}_3$

X values: a: 0; b: 0.1; c: 0.2; d: 0.4; e:0.6; f: 0.8; g: 1

For convenience, the d-spacings of the major peak for both LaVO_3 (200) and SrVO_3 (110) are shown below in **Table 5.2** and **Figure 5.8**.

Table 5.2 d-spacings of LaVO_3 (200) and SrVO_3 (110) with substitution

| Sr Fraction | d-spacing(Å) | |
|-------------|--------------|---------|
| | La | Sr |
| 0 | 2.77656 | - |
| 0.1 | 2.77047 | - |
| 0.2 | 2.78038 | - |
| 0.4 | 2.75254 | 2.70194 |
| 0.6 | 2.77385 | 2.72155 |
| 0.8 | - | 2.7169 |
| 0.9 | - | 2.7114 |
| 1 | - | 2.70405 |

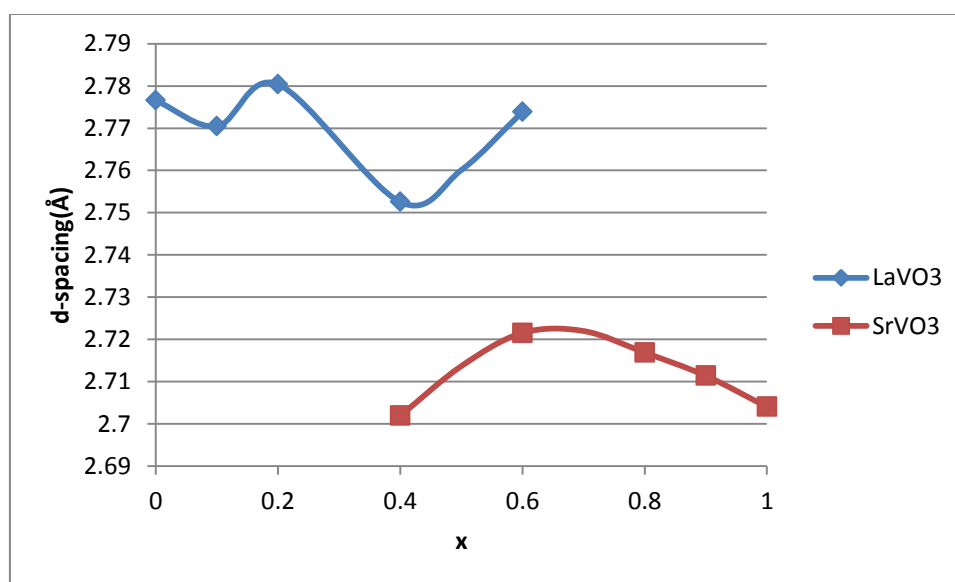


Figure 5.8 Graph displaying changes in d-spacing with substitution in $\text{La}_{(1-x)}\text{Sr}_x\text{VO}_3$. Peak measured is 200 phase in LaVO_3 and 110 phase in SrVO_3

Apart from the curious anomaly at $x = 0.2$, there is a clear trend of decreasing d-spacings with increasing strontium substitution. At $x = 0.4$ the peaks begin to split, but the d-spacings suggest that the substitution is still occurring at this point; it is the lowest peak value for the LaVO_3 (200) plane. Judging by the d-spacing data, the SrVO_3 peak appears to be unsubstituted, suggesting that the substitution of LaVO_3 with strontium has at this point reached a maximum, with the excess strontium forming its own pure phase.

At $x = 0.6$ the LaVO_3 (200) plane is indicative of the pure perovskite, and the SrVO_3 (110) plane is at its highest d-spacing. This suggests the inverse of the $x = 0.4$ substitution level; at this point the strontium perovskite has exceeded its maximum substitution of lanthanum, and the excess lanthanum has appeared as its own pure perovskite phase. Outside of these two values, the data indicates substitution proceeds as expected. From this it can be inferred that strontium substitution has a negative effect on the activity of the catalyst, but a positive effect on the acetone selectivity. This latter point is consistent with the aim of increasing the basic character

BET surface area measurements were also obtained for all the tested catalysts. Their surface areas are displayed below in **Table 5.3**.

Table 5.3 Table of surface areas of substituted perovskite $\text{La}_{(1-x)}\text{Sr}_x\text{VO}_3$

| x | Surface area (m^2/g) |
|-----|--|
| 0 | 1.5 |
| 0.1 | 1.5 |
| 0.2 | 1 |
| 0.4 | 1.5 |
| 0.6 | 2 |
| 0.8 | 1.5 |
| 0.9 | 1 |
| 1 | 2 |

As can clearly be seen, the surface areas of these materials are uniformly low. This is a common problem of perovskites, and is generally a product of sintering caused by the high temperatures needed to form the perovskite phase. Given the uniformly low surface areas, it is not assumed that they are a factor in the catalytic activity of these compounds.

5.3.1.2 Additional substitutions

The previous set of experiments showed a large and sudden decrease in IPA conversion between the 20 % and 40 % substitution catalysts. To investigate this effect, three further perovskites were synthesised; 25, 30 and 35 % substitution of La by Sr. These perovskites were then tested in the same manner as before, and the results compared to those from the previous set of experiments. The results of these experiments are shown below in **Figure 5.9**.

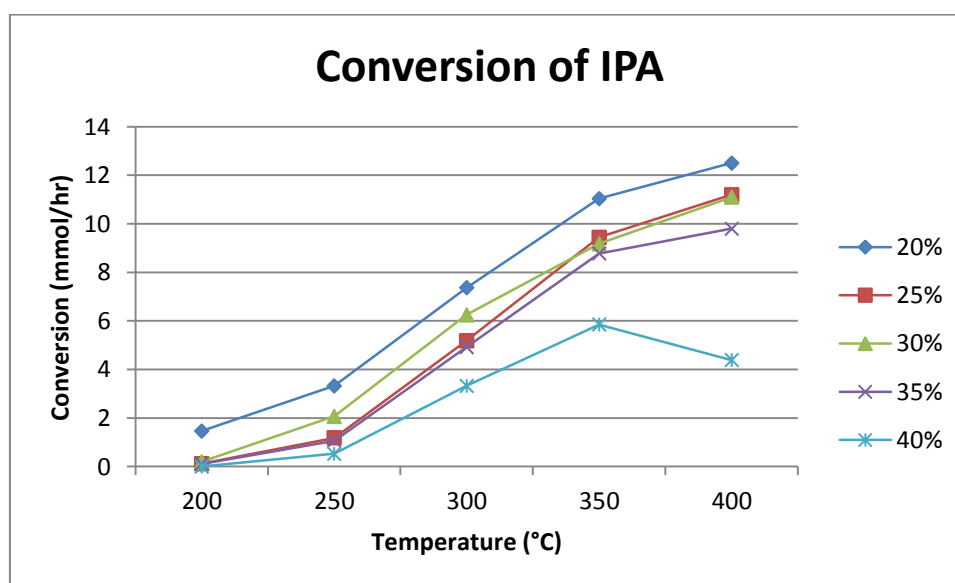


Figure 5.9 Line graph displaying conversion of IPA. Legend represents % of La substituted for Sr.

These results show that there is still a sharp decrease in conversion, although it has reduced the boundaries of this drop from 20-40 % to 35-40 %. Due to the time-consuming nature of producing the perovskites, it was decided not to investigate this decline in

conversion with any further alternative substitutions. Interestingly, as can be seen in the later XRD traces of these materials, they still display single, if broadened, peaks. The peak splitting observed at 40 % substitution appears to be very significant with regards to the activity of the catalyst in this reaction.

5.3.1.2.1 Characterisation

These materials, as with those in the previous section, were analysed by X-ray diffraction, and surface areas of the materials were measured by the BET method. The results of this are shown below in **Figure 5.10** and **Table 5.4**

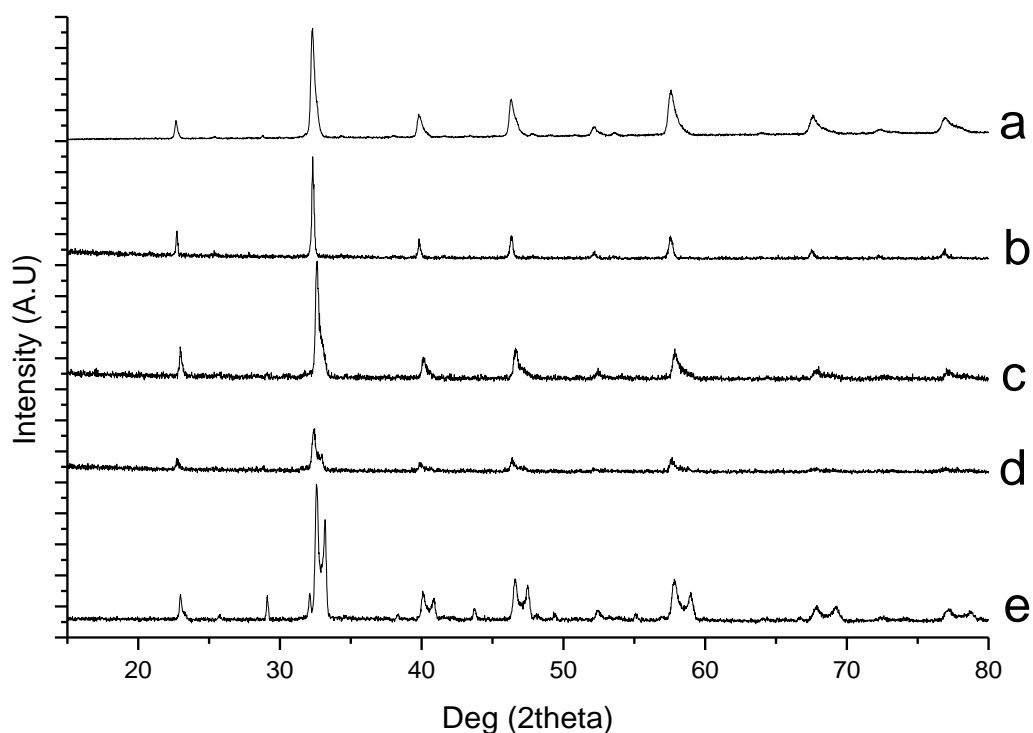


Figure 5.10 XRD traces of substituted perovskite material $\text{La}_{(1-x)}\text{Sr}_x\text{VO}_3$

X values: a: 0.2; b: 0.25; c: 0.3; d: 0.35; e: 0.4

These traces show the peak splitting event occurs at $x = 0.4$, with some small indication of peak separation beginning at $x = 0.35$. The low crystallinity of $x = 0.35$ makes distinguishing the separate peaks difficult. It is possible that the lowering of peak intensity is some precursor of the change that the catalyst undergoes at this substitution level, but this is empirically difficult to verify with XRD. What this does highlight is the suddenness of the change, a fact reflected in the catalyst test data earlier in this section.

The BET surface areas of the new materials are listed below in **Table 5.3**. As before, the materials are possessed of very low surface areas.

Table 5.4 Table of surface areas of substituted perovskite $\text{La}_{(1-x)}\text{Sr}_x\text{VO}_3$

| x | Surface area (m^2/g) |
|------|--|
| 0.2 | 1 |
| 0.25 | 1.5 |
| 0.3 | 1.5 |
| 0.35 | 1.5 |
| 0.4 | 1.5 |

5.3.1.3 Deactivation over time

The results in **Section 5.3.1.1** showed that at 400 °C, IPA conversion for many of the higher substitution catalysts (40 %+ substitution of La with Sr) was lower than that at 350 °C. This seemed to imply rapid deactivation of the catalysts, and so it was decided to gather time on-line data for these catalysts over an extended run. The results of these experiments are displayed below in **Figures 5.11, 5.12, and Table 5.5**.

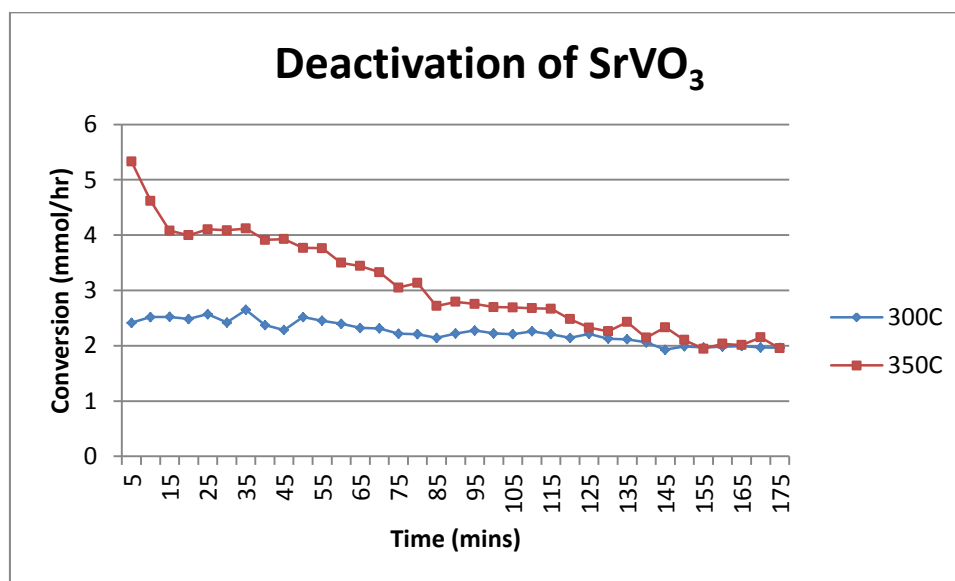


Figure 5.11 Line graph displaying deactivation of SrVO₃ over time. Deactivation displayed relative to IPA conversion rates.

All the tested catalysts displayed similar trends, and so the data has been tabulated below for easier comparison. Another trend noted in all catalysts tested in this manner was that the propene selectivity rose with time, particularly with the catalysts tested at the higher temperature.

| x | 300 °C | | | 350 °C | | |
|-----|---------|------|--------|---------|------|--------|
| | Initial | 3 h | % Loss | Initial | 3 h | % Loss |
| 0 | 5.66 | 5.65 | 0.21 | 9.13 | 5.08 | 44.40 |
| 0.2 | 5.45 | 5.40 | 0.98 | 8.90 | 4.09 | 54.01 |
| 0.4 | 2.54 | 2.10 | 17.28 | 6.93 | 0.51 | 92.71 |
| 0.6 | 2.55 | 1.96 | 23.44 | 6.86 | 1.74 | 74.61 |
| 0.8 | 2.46 | 1.73 | 29.73 | 8.39 | 3.06 | 63.55 |
| 1 | 2.53 | 1.96 | 22.63 | 5.32 | 1.94 | 63.50 |

Table 5.5 Table displaying conversion in mmol/hr of substituted catalysts La_(1-x)Sr_xVO₃ initially and after 3 h. Also showing % of IPA conversion lost over a 3 h period.

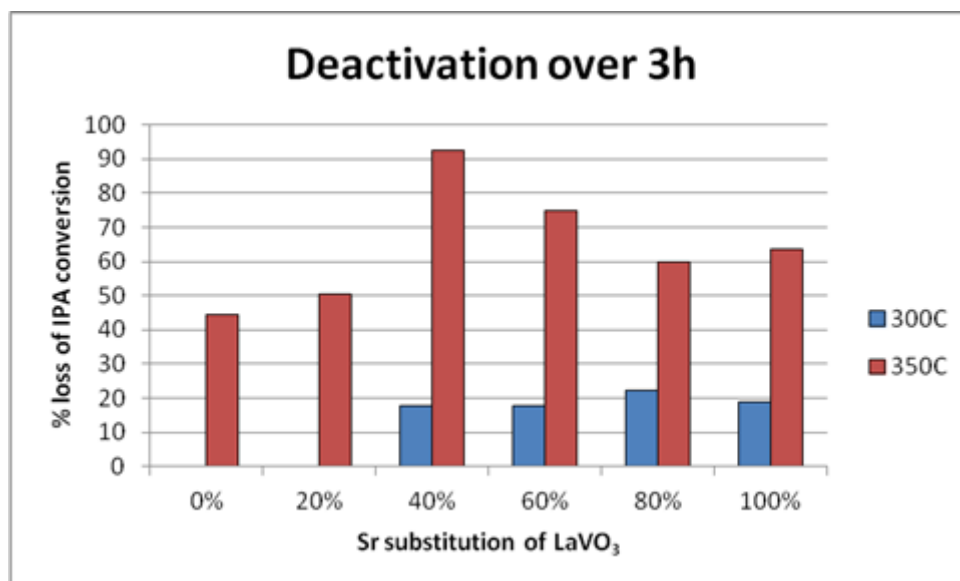


Figure 5.12 Bar chart displaying % decrease in activity of catalysts after 3h. Deactivation measured relative to IPA conversion

Close examination of this table shows that the deactivation is highly significant; in several cases the conversion after 3 h at the higher temperature has dropped below the level of conversion displayed by the catalysts tested at the lower temperatures.

The reason for this high degree of deactivation is unclear. It seems unlikely to be due to catalyst sintering as the high temperatures used in manufacturing the perovskites usually mean that they are thermally stable.

A possibility is water adsorption: the deactivation phenomenon is more pronounced on the catalysts possessing a more basic nature (i.e. higher degree of strontium substitution). Water molecules would have a higher affinity for the basic sites, possibly blocking these sites and causing the deactivation. However, the high temperatures used would usually be sufficient to expel adsorbed water.

Another possibility is that the perovskites are undergoing some manner of surface oxidation. Whilst perovskites are highly stable under a wide range of conditions, they are susceptible to oxidation. It is possible that an oxygen-containing molecule is being decomposed at the surface, oxidising the perovskite surface. Literature implies that the oxidised phases of these perovskites are not active for the transformation of IPA.

A final possibility is that the surface is building up a carbon layer due to decomposition of the starting material or products. This seemed to be the case; by examining the raw data it could be discerned that the carbon mass balances decrease as the reactions continued at the higher temperature. Analysing the individual FID responses of both acetone and propene, it appears that the propene signal in all cases descends more slowly than the acetone signal, which drops off very rapidly at 350 °C. This would imply that whatever is causing the deactivation occurs primarily on the basic sites of the catalyst, but that it is not solely restrained to these areas.

The evidence of the decreasing carbon mass balances would seem to imply that carbon is being laid down on the catalyst surfaces. The drop of in acetone production implies that this occurs primarily on the basic sites, which would also account for the rise in propene selectivity.

Despite this high degree of deactivation displayed, it was not considered to be detrimental to the overall aims of the project: the benzyl alcohol oxidation reaction takes place at 120 °C during this project, and Fischer-Tropsch synthesis is conducted at 240 °C. The deactivation of these materials in this manner seemed unlikely to be a factor at these lower temperatures.

Additionally, in the case of the benzyl alcohol oxidation the materials are primarily intended as supports, and thus deactivation of catalytic activity is not a concern.

5.3.1.4 Substitution of other GrpII metals

Since it had been demonstrated that substitution of La for Sr in the perovskites affected the conversion and selectivity, it was decided to try substitutions with other GrpII metals. Whilst the incorporation of Sr had lowered the IPA conversion in all cases, it had also increased the acetone production. This implies a change in the acid-base properties of the

catalyst, and with the possibility of tuning these characteristics being one of the prime aims of this study it was decided to investigate further.

Barium and calcium were chosen as the additional substitution metals, being one period either side of Sr. It was decided to attempt to use these materials instead of continuing with the gradual substitution of strontium into lanthanum vanadate because this would allow the elements used to be confined to a single group. This would hopefully reduce the number of variables affected by the substitution; substituting a group II metal in place of lanthanum in a perovskite structure would also affect the electronic state of the vanadium cation, changing it from 3+ in lanthanum vanadate to 4+ in strontium vanadate. With all group II metals the vanadium oxidation state should remain 4+, allowing us to eliminate it as a factor in the experiments.

The catalysts were prepared in an identical manner to those in the previous section, save the use of barium or calcium nitrate instead of lanthanum or strontium. The catalysts were tested in an identical manner to the catalysts in the previous section.

The results from these tests are displayed below in **Figures 5.13** and **5.14**.

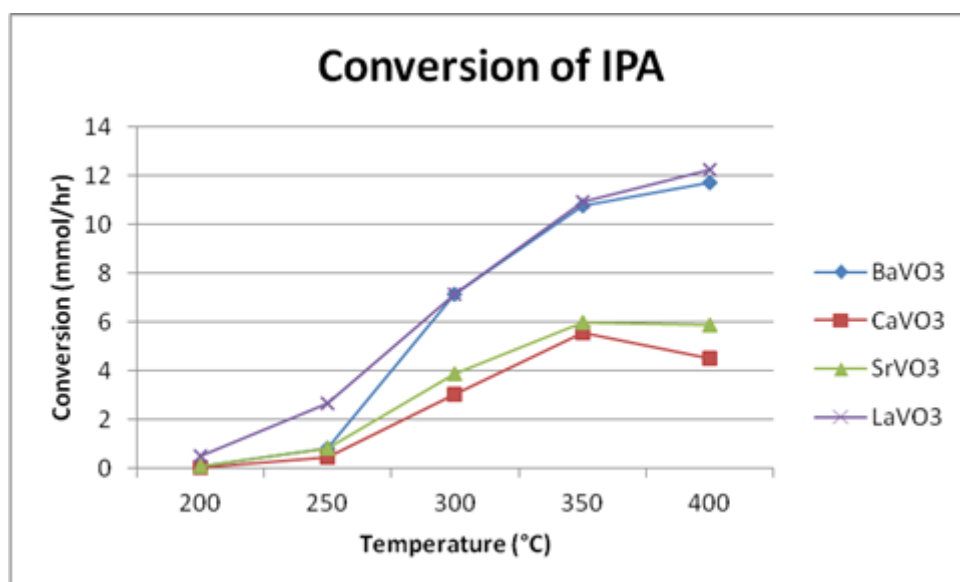


Figure 5.13 Line graph displaying conversion of IPA.

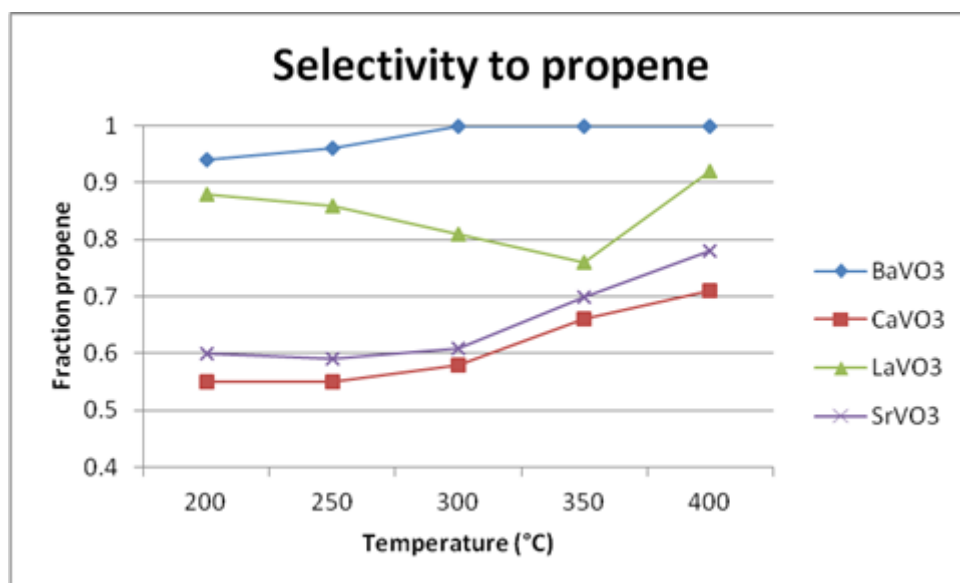


Figure 5.14 Line graph displaying selectivity of products towards propene.

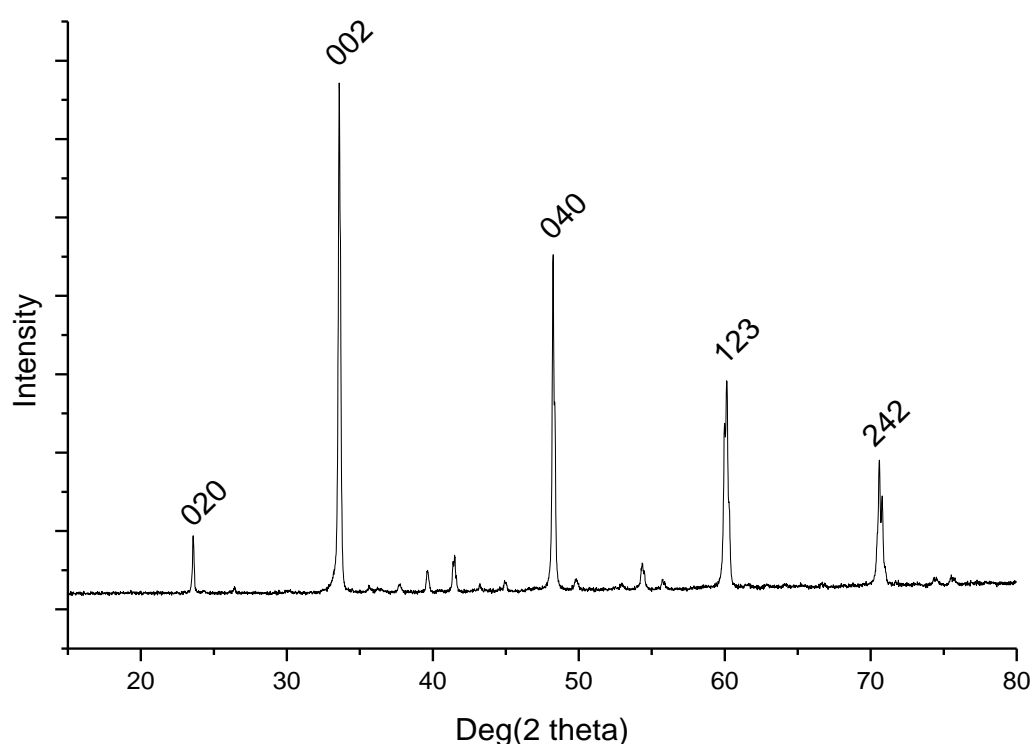
As can be seen from the above graphs, calcium vanadate and strontium vanadate have similar conversions and selectivities, and whilst lanthanum vanadate and barium vanadate have similar conversions, the barium catalyst displays even higher selectivity to propene than the lanthanum. This is indicative of more acidic sites, which is somewhat counterintuitive as Ba^{2+} is more basic than La^{3+} . A possible reason for this is described by the XRD traces in the next section.

5.3.1.4.1 Characterisation

The new perovskite materials were analysed by X-ray diffraction, and their surface areas were measured by the BET method. The results of this are displayed below in **Figure 5.15**, **Figure 5.16**, and **Table 5.6**.

Table 5.6 Surface area measurements for vanadate materials

| Vanadate | Surface area (m ² /g) |
|-----------|----------------------------------|
| Calcium | 3 |
| Strontium | 2 |
| Barium | 1.5 |
| Lanthanum | 1.5 |

**Figure 5.15** XRD trace of CaVO₃ perovskite catalyst material with hkl notation

This figure shows that the CaVO₃ perovskite has an identical general structure to LaVO₃, indicating that a pure perovskite phase is formed with this combination of metals under the preparation conditions utilised. CaVO₃, like LaVO₃, is orthorhombic, unlike SrVO₃ which was cubic. The extra phase present in the strontium substituted sample is not seen. The diffraction peaks show the same shifting as in previous samples: this is due to the

changes in ionic radii of the metals used. The larger ionic radius of Sr^{2+} with respect to Ca^{2+} (132 pm and 114 pm respectively²⁶) may be the reason for the additional phase displayed in the former; the cations may be too large to be easily accommodated in the crystal lattice, and so a different structure may result.

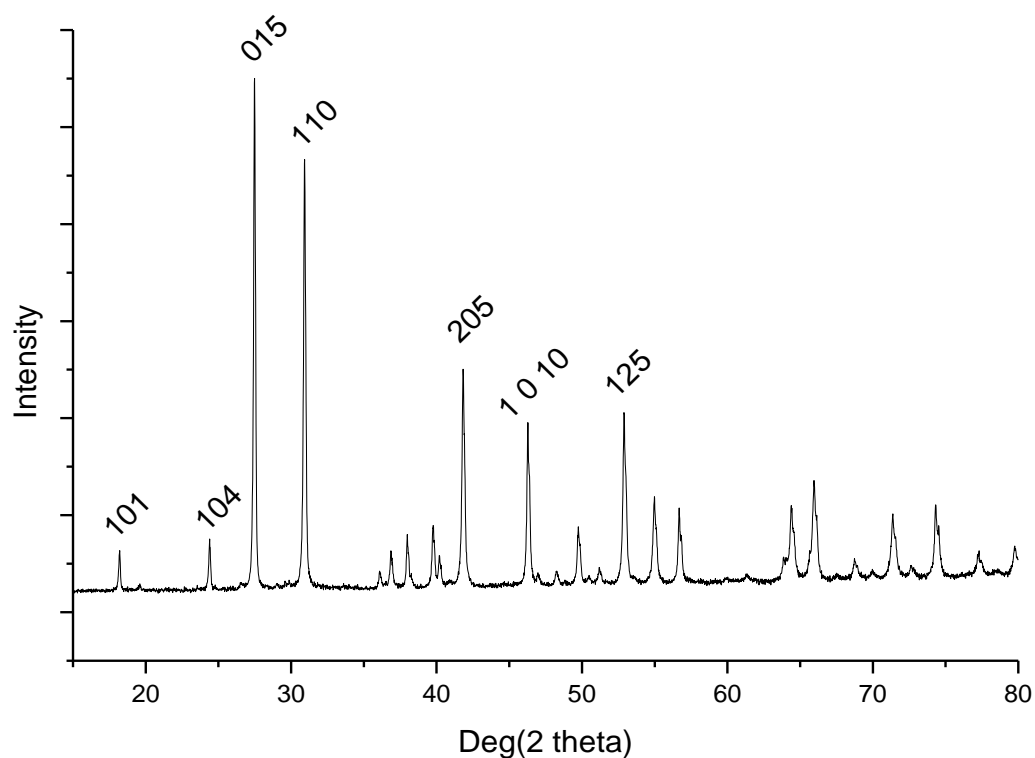


Figure 5.16 XRD trace of barium vanadate catalyst material with hkl notation

The barium substituted compound does not display a perovskite structure at all, with the trace displaying pure $\text{Ba}_3\text{V}_2\text{O}_8$. Ba^{2+} possesses an ionic radius higher than Sr^{2+} (149 pm compared to 132 pm²⁶), which seems to imply that increasing ionic radius of the intended A cation of the perovskite material increases the amount of the orthovanadate phase present.

Investigation into this shows that the ideal ABO_3 perovskite structure is cubic, and in such a structure the following relationship between the ionic radii would hold true:

$$r_A + r_O = \sqrt{2} (r_B + r_O)$$

However, this relationship is not obeyed for any of the materials created so far. Goldschmidt²⁷ showed that it was possible for perovskites to deviate from this and still possess a cubic structure, and introduced a tolerance factor to describe this. It is governed by the equation:

$$t = (r_A + r_O) / \sqrt{2} (r_B + r_O)$$

Ionic radii and calculations of the tolerance factor are shown below in **Table 5.7**

Table 5.7 Tolerance factor calculations for perovskites

| Perovskite | r_A (pm) | r_B (pm) | t |
|-------------------------|------------|------------|-------------|
| CaVO₃ | 114 | 72 | 0.86 |
| SrVO₃ | 132 | 72 | 0.92 |
| BaVO₃ | 149 | 72 | 0.98 |
| LaVO₃ | 117.2 | 78 | 0.84 |

Goldschmidt found that although for ideal perovskites t will equal unity, the cubic perovskite phase could be formed in the range $0.75 \leq t \leq 1.0$. These calculations help to explain in this case why the strontium vanadate perovskite possessed a cubic structure, but both calcium vanadate and lanthanum vanadate possessed orthorhombic. Based on the calculations, it seems reasonable to assume that had the barium vanadate perovskite phase been successfully formed, it would have possessed a cubic crystal structure since its t -value is even closer to unity. The orthorhombic distortion possessed by calcium vanadate and lanthanum vanadate is quite common in perovskites; Goldschmidt's relationship

predicts that a cubic structure can be formed, but it does not say at what temperature a material will do so. Several materials will form the cubic form only at higher temperatures, relaxing into a distorted form under ambient conditions. A good example of this is perovskite CaTiO_3 , which is in fact orthorhombic despite being the original perovskite material²⁸.

As well as not determining at what temperature the cubic phase is stable, the relationship also does not allow us to know at what temperature a perovskite phase, even a distorted one, would form. Literature on the subject shows that to prepare pure perovskite phases of strontium vanadate or barium vanadate requires higher temperatures than were used in this study. SrVO_3 ²⁹, for example, requires multiple reduction steps of at least 1000 °C, and BaVO_3 requires reductions at 1350 °C³⁰.

The failure to form the pure perovskite phase helps to shed some light on a slightly counterintuitive set of results seen previously; namely, the selectivity patterns of the grpII substituted materials (See **Figure 5.13**). It had been expected that as the grpII metals substituted into LaVO_3 became more basic (i.e. $\text{Ca} < \text{Sr} < \text{Ba}$ in terms of basicity), the resultant perovskite would display more basic character. The opposite was observed, however, with increasing selectivity to the ‘acid’ product as the grpII metal basicity increased. It now seems likely that this is due to the increasing presence of the orthovanadate phase; whilst in a perovskite structure the acid-base properties are primarily dictated by the A cation in the formula ABO_3 , the orthovanadate possesses a more open structure, exposing the more acidic V^{5+} to the reaction. Thus, although strontium is more basic than calcium, the strontium material also possessed more of the acidic orthovanadate, increasing the selectivity to propene. The trend continues to the barium material, which contains nothing but the orthovanadate phase, and displayed the highest selectivity to propene, exceeding even the lanthanum vanadate perovskite.

5.4 Benzyl alcohol oxidation

Previous studies have shown that in benzyl alcohol oxidation via supported precious metals, both the rate of conversion and the selectivity of products are influenced by the acid-base character of the support material¹⁸. Generally speaking, it has been shown that the more acidic supports have higher conversion and higher selectivity to an undesirable product, toluene. Conversely, precious metals on highly basic supports such as MgO display very high selectivity to benzaldehyde, the desired product, but have lower overall conversion.

Having demonstrated in the previous section that it is possible to adjust the number of acid and basic sites of a perovskite material via metal ion substitution, it was decided to investigate if it would be possible to tune the acid-base character of a perovskite support material such that the higher conversion could be retained whilst reducing or eliminating the toluene selectivity. The perovskite supports were made according to the method outlined in **Section 2.1.3 (i)**. These bare perovskite support materials were tested for catalytic activity to benzyl alcohol oxidation in sealed reactors under 2 bar O₂ pressure as outlined in **Section 5.2**. Precious metals were supported onto the perovskites using the method outlined in **Section 2.1.3 (ii)**. The catalysts were tested in sealed reactors under 2 bar O₂ pressure, as outlined in **Section 5.2**.

5.4.1 Results and discussion

5.4.1.1 AuPd loading on La/Sr perovskites

For the initial experiments in this section, a selection of La/Sr perovskites were selected as supports for a 1 % loading of AuPd. The perovskites chosen were LaVO₃ with Sr substitutions of 0 %, 20 %, 80 % and 100 %. These materials were first tested without precious metal loadings to examine their catalytic activity.

The results for the bare perovskite experiments are displayed below in **Figure 5.17**.

The results for the precious metal supported perovskites are displayed below in **Figures 5.18** and **5.19**.

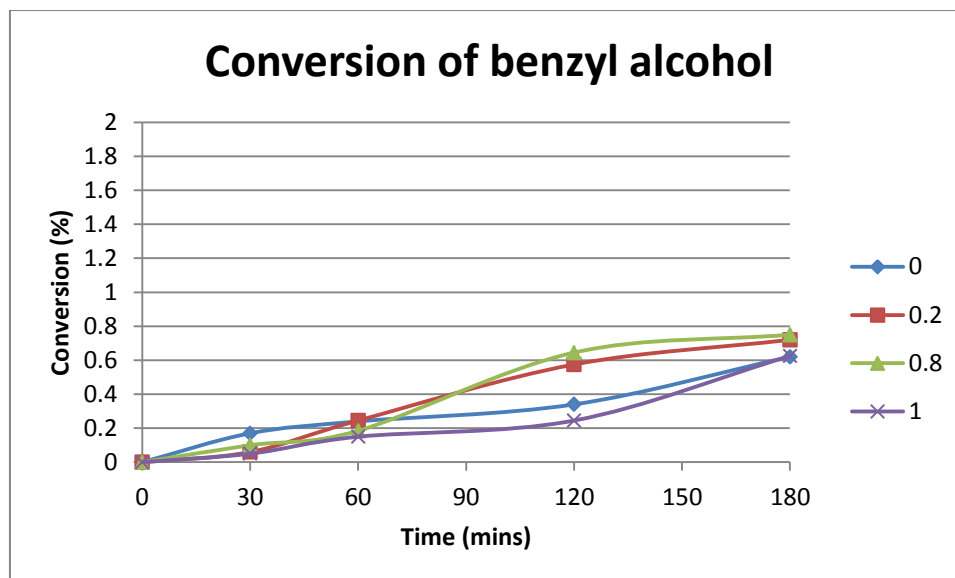


Figure 5.17 Chart displaying conversion of benzyl alcohol against time using bare perovskite materials $\text{La}_{(1-x)}\text{Sr}_x\text{VO}_3$. Legend denotes x

After 3 hrs of reaction, the bare perovskite materials have universally failed to convert even 1 % of the benzyl alcohol starting material. Whilst there is some catalytic activity, it is assumed that this is low enough that any results in future experiments can be attributed solely to the presence of precious metals.

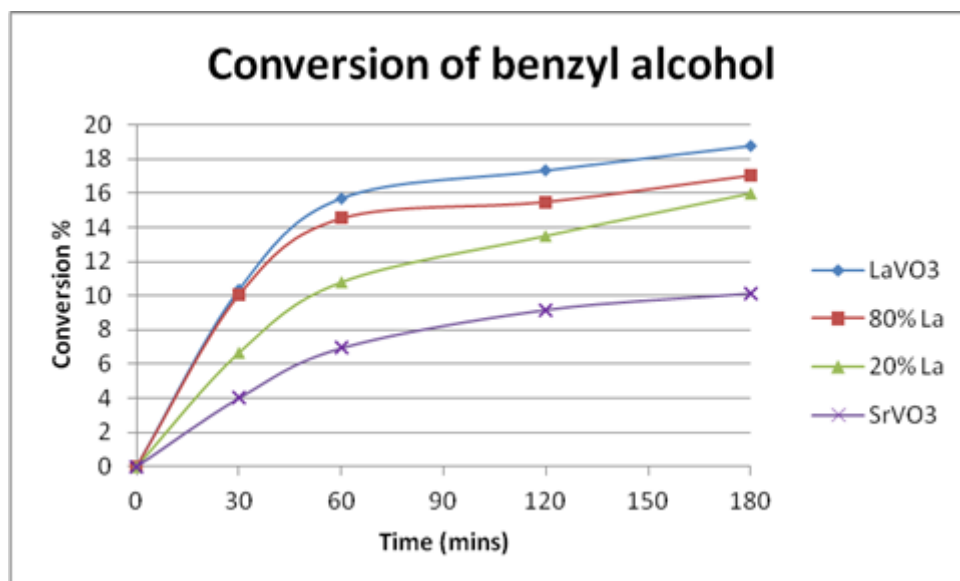


Figure 5.18 Line graph displaying conversion of benzyl alcohol over time on 1% AuPd/perovskite

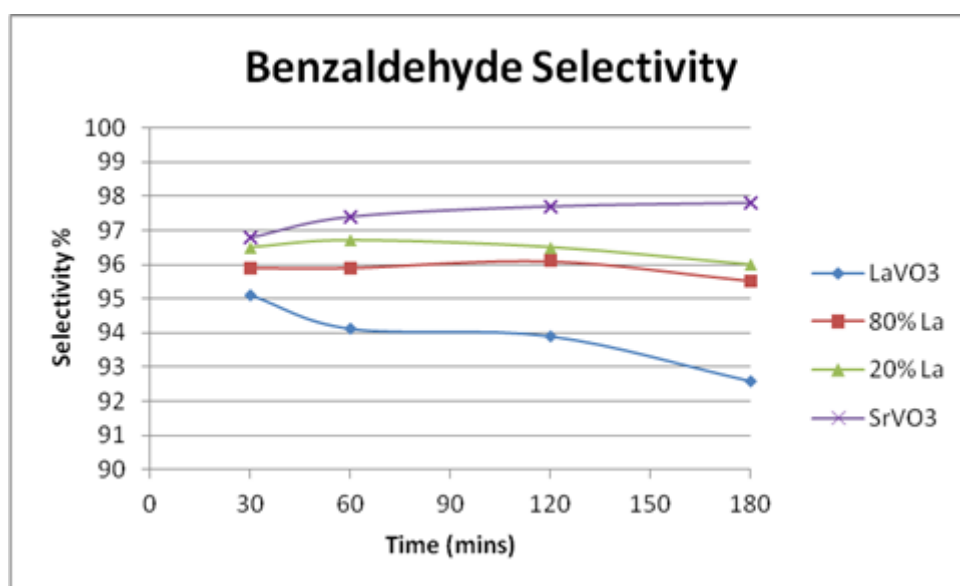


Figure 5.19 Line graph displaying product selectivity to benzaldehyde on 1 % AuPd/perovskite

These results are comparable with experiments conducted by Hutchings *et. al.*²², where catalysts of the same loading and preparation method were supported on titania. Their catalysts showed 25-27 % conversion with an 88-90 % selectivity to benzaldehyde after 3 h. Later experiments under slightly different conditions showed conversions of up to 60 % after 3 h for 1 % AuPd/TiO₂¹⁸. Our results display lowered conversion, but improved selectivity to benzaldehyde, This would be consistent with literature on the subject if the

perovskite supports were assumed to be more basic than titania. It is also possible that the extremely low surface areas of the perovskite supports relative to titania may be having an effect.

Two distinct trends are readily visible; as the level of Sr substitution increases, the selectivity to benzaldehyde also increases, but the conversion falls. Curiously, there is not the significant drop between 20 % and 80 % substitution displayed in the IPA test reactions. This is likely to do with the differences in the active species in the two reactions. In the IPA test reaction there are no supported precious metals, and so any activity by definition comes from the perovskite. Changes in the perovskite were shown to have a direct impact on the performance of the catalyst for the IPA reaction. In the benzyl alcohol reaction, however, the activity comes from the precious metals; these materials are active towards benzyl alcohol oxidation on practically any support. It has been shown that the support material does make a difference to the overall performance of the catalyst, so a change in performance was to be expected. However, the change seems more gradual than in was seen for these materials in the IPA test reaction, implying that the phase separation noted at 40 % substitution is less significant for this reaction; it is possible that the changes are linked to the change in acid-base sites rather than any sudden phase change.

However, the important result to be observed from these experiments was the confirmation that by adjusting the acid-base properties of the perovskite support via ion substitution, the conversion and selectivity pattern of precious metal catalysts for benzyl alcohol oxidation can be adjusted.

5.4.1.2 Variation of metal loading

Since it was planned to conduct experiments using different combinations of precious metals, it was decided to use Turn Over Number (TON) as a gauge of reactivity, as opposed to conversion. TON is a measure of conversion per mole of metals, and improves

accuracy when comparing the effects of different metals; i.e. a 1 %wt loading of Pd may seem more active than a commensurate loading of Au by conversion, but this may be due to the increased number of moles of Pd present; a factor of its lower molecular weight.

For the next set of experiments, therefore, a series of different precious metal loadings on the most active support were tested. The support chosen was LaVO_3 , and the loadings used were 1 %, 0.1 %, and 0.05 % AuPd by weight.

The results of these experiments are shown below in **Figure 5.20** and **5.21**

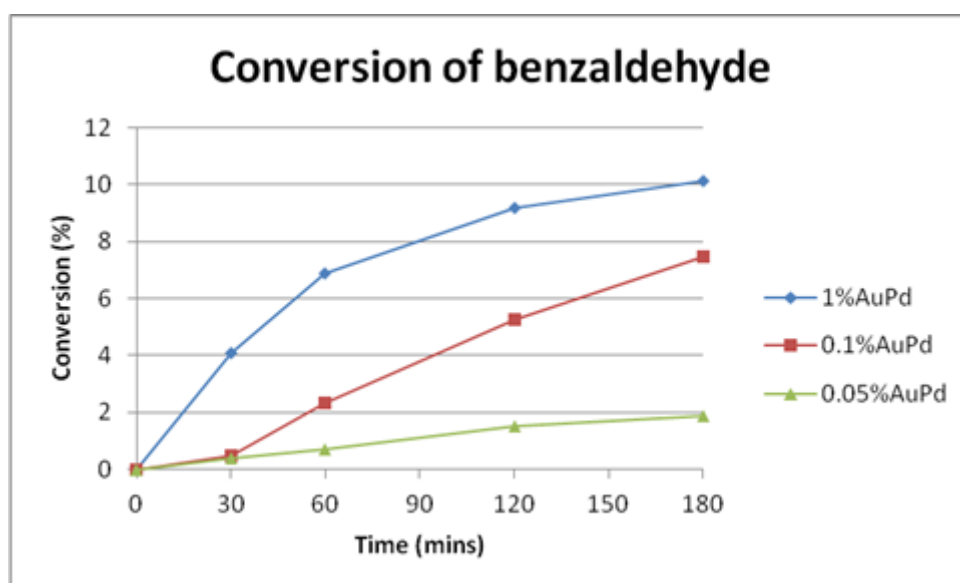


Figure 5.20 Line graph displaying conversion of benzyl alcohol over time

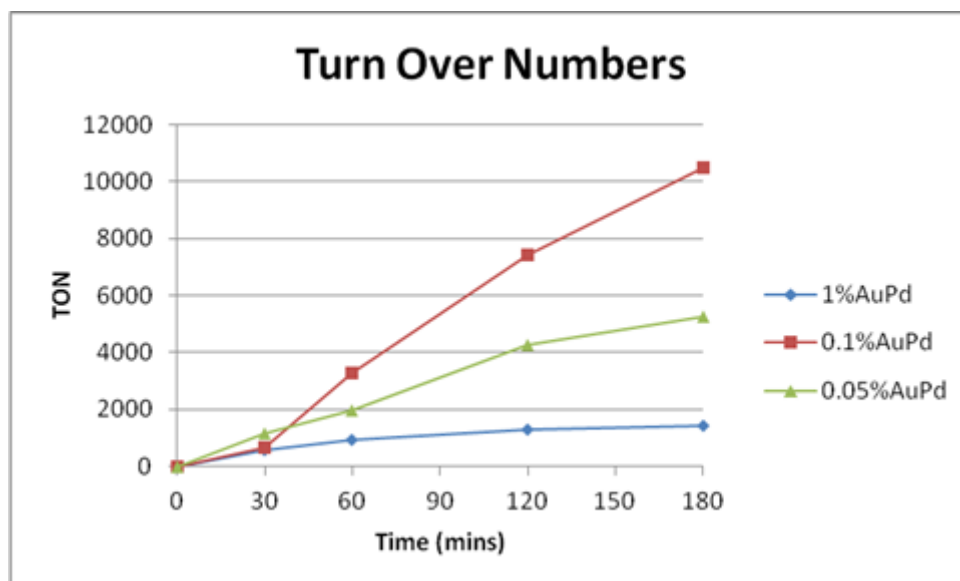


Figure 5.21 Line graph displaying TON of benzyl alcohol over time

As can clearly be seen, although the highest loading produces the highest overall conversion, it is the 0.1 % loading that produces the highest conversion per mole of metal. It is possible that this result is linked to the very low surface areas of the perovskite materials. It is possible that even at such a low loading as 1 % there is insufficient surface area of support material for the AuPd sol material to fully disperse. Were this the case, clumps of the AuPd material could form, lowering the surface area of the active material. An attempt was made to try and resolve this using SEM imaging, but at 1 % loading the precious metal particles were still too small to resolve. This is demonstrated in **Figure 5.22**, below.

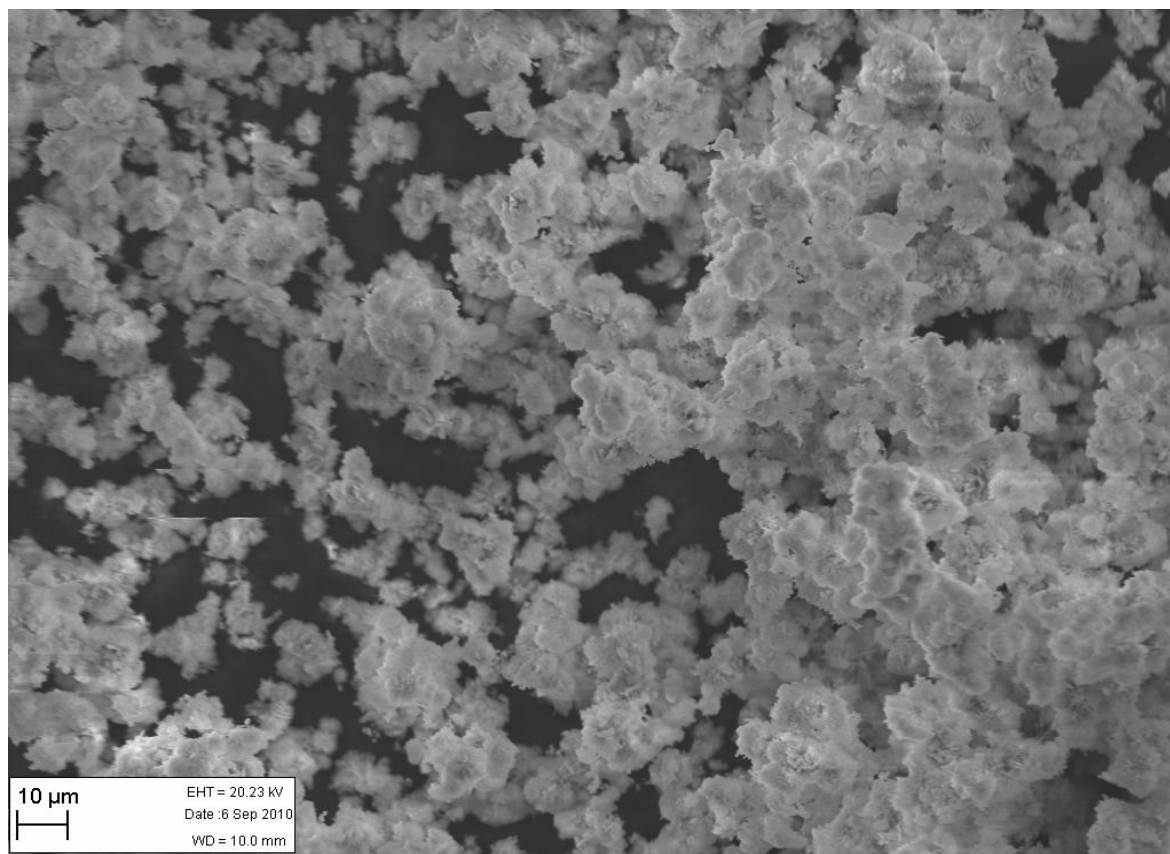


Figure 5.22 SEM image of 1 % AuPd/SrVO₃. Image using Backscatter detector (BSD) for enhanced metal contrast.

From this point on, all metal loadings are at the 0.1 % level due to the enhanced TONs displayed.

5.4.1.3 Substitution of GrpII metals

Following on from the work of the previous sections, LaVO₃, SrVO₃, CaVO₃ and BaVO₃ were prepared as support materials and tested without precious metals as a blank run and tested as described in 5.2. The results of these tests are displayed below in **Figure 5.23**.

These materials were then loaded with 0.1 % wt AuPd and tested as described in **Section 5.2**. One minor difference in method of testing was that instead of having four identical pots and quenching after periods of time, each pot was loaded with a different catalyst

and allowed to run for 3 h before quenching, allowing us to run more experiments simultaneously. This applied to the blank runs as well.

The results of these experiments are displayed below in **Table 5.8**, **Figure 5.24**, and **Figure 5.25**.

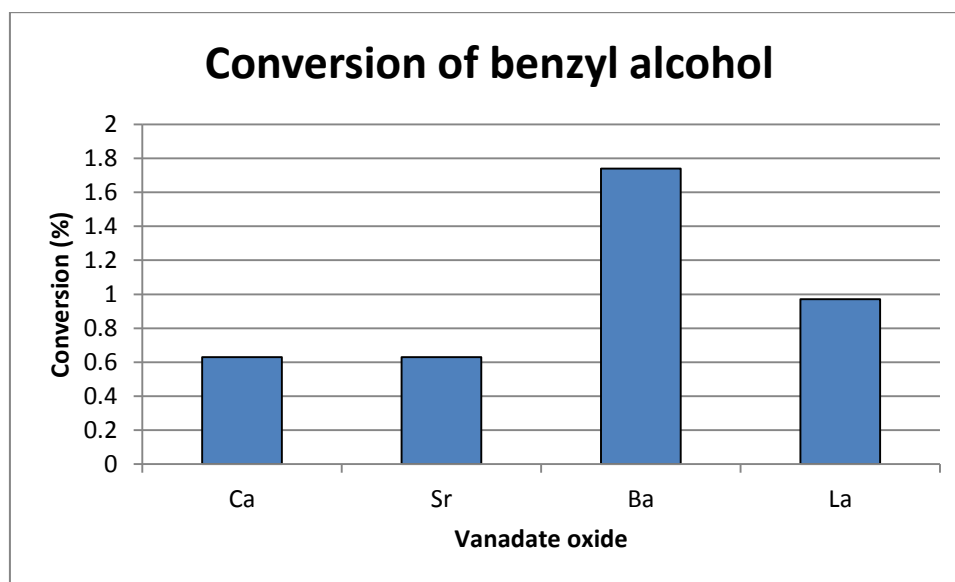


Figure 5.23 Bar chart displaying conversion of benzyl alcohol after 3 h for support materials without precious metals

In most cases the conversion after 3 h is extremely low, although it is notable that the barium vanadate is almost twice as active as the lanthanum vanadate. It is possible to assume, therefore, that the orthovanadate material present is somewhat active towards this reaction. This is not reflected in the strontium vanadate tests, however, which also contain some amount of the orthovanadate phase.

Whilst still low, the barium vanadate conversion is high enough that it should be taken into account in tests with precious metal loadings.

| Catalyst | Conversion | Selec. Benzaldehyde | Selec. Toluene | TON |
|-----------------------------|------------|---------------------|----------------|-------|
| 0.1 %PdAu/CaVO ₃ | 1.42 | 98.2 | 1.68 | 2000 |
| 0.1 %PdAu/SrVO ₃ | 2.68 | 96.8 | 2.36 | 3780 |
| 0.1 %PdAu/BaVO ₃ | 9.68 | 95.3 | 3.73 | 13578 |
| 0.1 %PdAu/LaVO ₃ | 7.98 | 96.1 | 3.1 | 11220 |

Table 5.8 Conversion, selectivity and TON data for benzyl alcohol oxidation after 3h

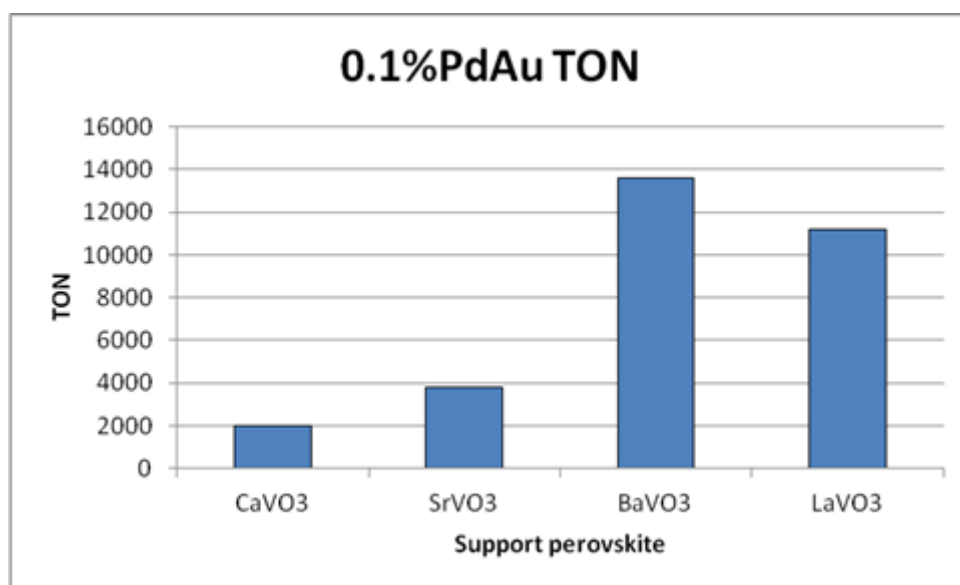


Figure 5.24 Bar graph displaying TON of benzyl alcohol after 3 h

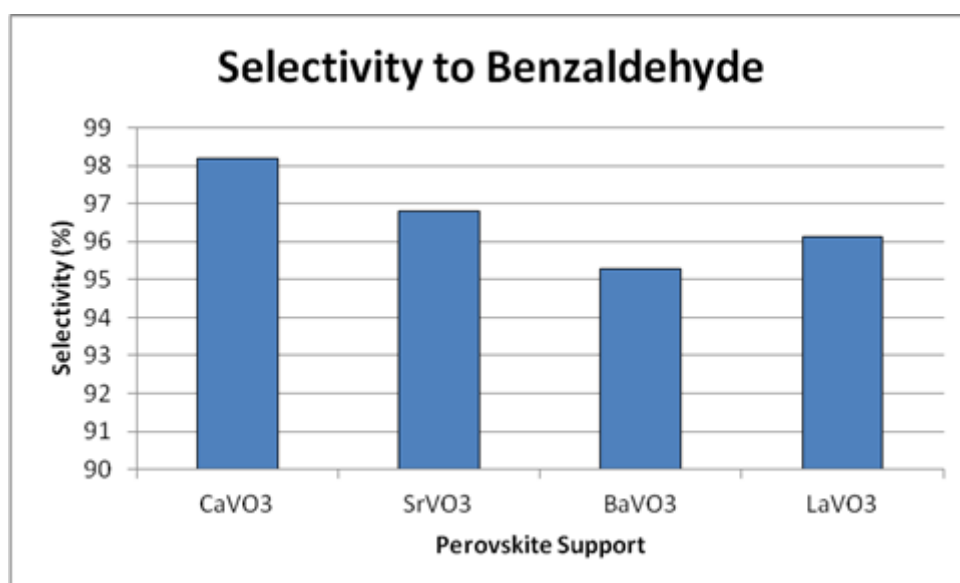


Figure 5.25 Bar graph displaying selectivity to benzaldehyde after 3h

There is a definite trend displayed as the substituted metal descends GrpII; conversion increases, but selectivity to benzaldehyde decreases (although remaining high). LaVO_3 falls between Ba and Sr in terms of both TON and selectivity. This is suggestive of greater acidic character for the BaVO_3 support than the LaVO_3 support, which is in agreement with the results from **Section 5.3**. Interestingly, the CaVO_3 material, although possessing high selectivity to benzaldehyde, was lower in conversion than that of the barium vanadate support without precious metals.

It can clearly be seen that increasing the acidic character of the support material increases the conversion, but also decreases the selectivity to benzaldehyde. The barium vanadate material proved the most active towards benzyl alcohol oxidation, but it must also be taken into account that the bare metal oxide support appeared to possess some activity. If this support conversion is directly subtracted from the total conversion, however, it is almost identical to the 0.1 %AuPd/ LaVO_3 material in activity.

5.4.1.4 Synergistic effects of Au and Pd

In previous studies by *Hutchings et. al.*¹⁹ it had been noted that in this reaction the conversion of benzyl alcohol was higher for a combined AuPd/ TiO_2 catalyst than a monometallic catalyst containing equal amounts of either Au or Pd on TiO_2 . This effect was termed ‘synergy’. Experiments were undertaken using the perovskite supports to ascertain if this effect was confined to certain supports, or if it applied across a broader range for this reaction. The catalysts were all made to a 0.1 %wt loading of precious metal, and the results are displayed in TON to take into account the differing number of moles of metal that this would produce. The results of these experiments are shown in **Figures 5.26** and **5.27**.

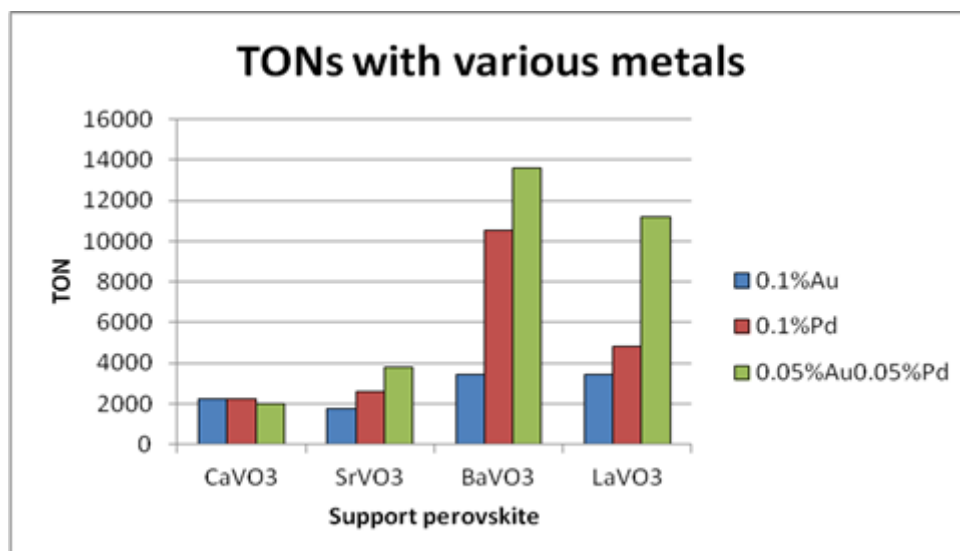


Fig 5.15 Bar chart displaying TON for benzyl alcohol after 3 h

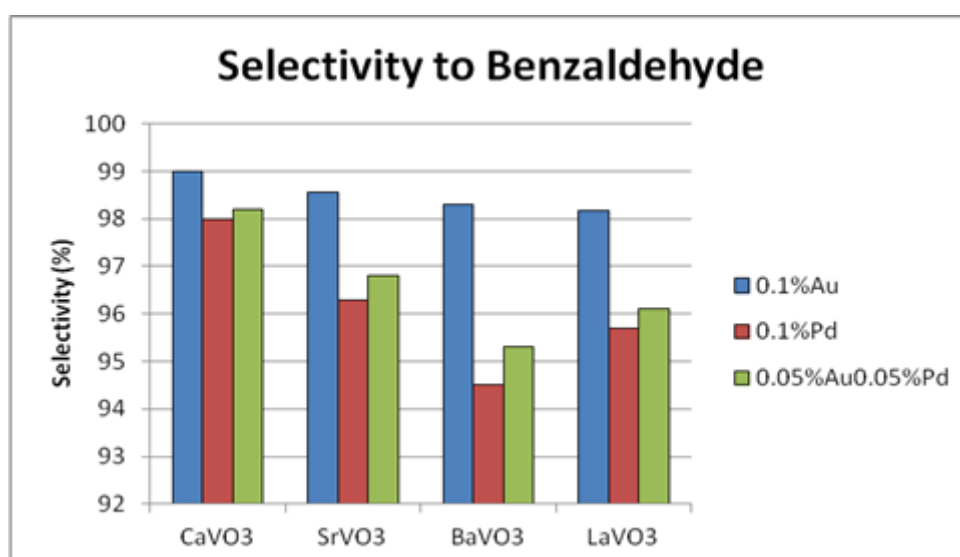


Fig 5.16 Bar chart displaying benzaldehyde selectivities after 3h

As can be seen from the results, synergy is displayed with respect to the TON for all perovskite supports except CaVO₃, but none of the supports display this with respect to the benzaldehyde selectivity. In these cases, the selectivity is observed to be between the two monometallic catalysts, and in all cases it is nearer to the value of the Pd/perovskite system than the Au/perovskite. With the exception of CaVO₃, this conforms to the phenomenon noted in the literature¹⁹. It may be that this phenomenon is linked to the acidity of the catalysts; this has not yet been assessed in literature, with only TiO₂ as a

support having been studied. Testing the effect on more basic supports such as MgO would be required to be certain.

5.5 Perovskites for Fischer-Tropsch

Given the broad range of reactions which perovskites are able to catalyse, it was decided to test whether they could be used as such in Fischer-Tropsch synthesis. The perovskite supports utilised in the benzyl alcohol reaction were all tested for activity under the conditions outlined in **Section 3.2**, but were unfortunately found to be universally inactive. Some thought was given to using them as supports, rather than active materials, but Fischer-Tropsch catalysts are generally thought to behave independently of their supporting material, so the idea was not pursued.

5.6 Conclusions

From the results in this chapter it can be concluded that substitution of more basic A metal cations into a perovskite system will increase the basicity of the perovskite. However, attention must be paid to the heat treatment and reduction temperatures to ensure that a pure perovskite phase is created.

The relationship outlined by Goldschmidt provides a useful method of determining if a perovskite phase is viable, although it does not predict at what temperature the perovskite phases will form.

The perovskite phases formed proved useful as support materials for the oxidation of benzyl alcohol, particularly given the ability to tune the acid-base characteristics of the material. There appears to be a trade-off between activity and benzaldehyde production, however, as the more acidic catalysts were more active but less selective towards benzaldehyde.

The IPA reaction proved useful for determining the relative acid-base character of the catalysts, although it is not believed to be useable to determine the absolute number of acid-base sites. Thought should be given to ammonia and CO TPD to determine the number of such sites quantitatively.

The surface areas of all perovskites created in this chapter were very low, which may have impacted their effectiveness as support materials. There are a series of methods available to increase the surface areas of perovskites, such as templating and combustion methods, and it would be beneficial to ascertain if higher surface area perovskites are more viable as support materials.

The perovskite materials tested proved inactive in Fischer-Tropsch synthesis, but this may be a factor of the metal ions used rather than perovskites as a whole. The utilisation of FT active metals such as cobalt, iron and nickel as substitution A cations in the perovskite system may change this. In such a situation the high stability of the perovskites, particularly under reducing conditions, could be useful to alleviate the problems of catalyst deactivation often suffered in FT systems.

5.7 References

1. J. M. Marin, *Advanced Materials*, 1996, **8**, 170-174.
2. F. A. Rabuffetti, P. C. Stair and K. R. Poeppelmeier, *Journal of Physical Chemistry C*, 2010, **114**, 11056-11067.
3. J. M. G. Amores, V. S. Escribano, M. Daturi and G. Busca, *Journal of Materials Chemistry*, 1996, **6**, 879-886.
4. M. Daturi, G. Busca and R. J. Willey, *Chemistry of Materials*, 1995, **7**, 2115-2126.
5. P. N. Trikalitis and P. J. Pomonis, *Applied Catalysis a-General*, 1995, **131**, 309-322.
6. W. Turek and A. Krowiak, *Applied Catalysis a-General*, 2012, **417**, 102-110.
7. P. Michorczyk, E. Sikora and J. Ogonowski, *Reaction Kinetics and Catalysis Letters*, 2008, **94**, 243-252.
8. D. Haffad, A. Chambellan and J. C. Lavalley, *Journal of Molecular Catalysis a-Chemical*, 2001, **168**, 153-164.
9. A. Gervasini, J. Fenyvesi and A. Auroux, *Catalysis Letters*, 1997, **43**, 219-228.
10. M. A. Aramendia, V. Borau, I. M. Garcia, C. Jimenez, A. Marinas, J. M. Marinas, A. Porras and F. J. Urbano, *Applied Catalysis a-General*, 1999, **184**, 115-125.
11. C. Lahousse, F. Mauge, J. Bachelier and J. C. Lavalley, *Journal of the Chemical Society-Faraday Transactions*, 1995, **91**, 2907-2912.
12. U. R. Pillai and E. Sahle-Demessie, *Applied Catalysis a-General*, 2003, **245**, 103-109.
13. A. Corma and M. E. Domine, *Chemical Communications*, 2005, 4042-4044.
14. A. Abad, A. Corma and H. Garcia, *Chemistry-a European Journal*, 2008, **14**, 212-222.
15. A. Abad, P. Concepcion, A. Corma and H. Garcia, *Angewandte Chemie-International Edition*, 2005, **44**, 4066-4069.
16. W. P. Griffith and J. M. Jolliffe, *RUTHENIUM AND OSMIUM CARBOXYLATO OXO COMPLEXES AS ORGANIC OXIDANTS*, Elsevier Science Publ B V, Amsterdam, 1991.
17. D. G. Lee and U. A. Spitzer, *Journal of Organic Chemistry*, 1970, **35**, 3589-3594.
18. M. Sankar, E. Nowicka, R. Tiruvalam, Q. He, S. H. Taylor, C. J. Kiely, D. Bethell, D. W. Knight and G. J. Hutchings, *Chemistry-a European Journal*, 2011, **17**, 6524-6532.
19. D. I. Enache, J. K. Edwards, P. Landon, B. Solsona-Espriu, A. F. Carley, A. A. Herzing, M. Watanabe, C. J. Kiely, D. W. Knight and G. J. Hutchings, *Science*, 2006, **311**, 362-365.

20. P. J. Miedziak, Q. He, J. K. Edwards, S. H. Taylor, D. W. Knight, B. Tarbit, C. J. Kiely and G. J. Hutchings, *Catalysis Today*, 2011, **163**, 47-54.
21. S. Meenakshisundaram, E. Nowicka, P. J. Miedziak, G. L. Brett, R. L. Jenkins, N. Dimitratos, S. H. Taylor, D. W. Knight, D. Bethell and G. J. Hutchings, *Faraday Discussions*, 2010, **145**, 341-356.
22. P. Miedziak, M. Sankar, N. Dimitratos, J. A. Lopez-Sanchez, A. F. Carley, D. W. Knight, S. H. Taylor, C. J. Kiely and G. J. Hutchings, *Catalysis Today*, 2011, **164**, 315-319.
23. M. S. G. Baythoun and F. R. Sale, *Journal of Materials Science*, 1982, **17**, 2757-2769.
24. Z. J. Sui, L. Vradman, I. Reizner, M. V. Landau and M. Herskowitz, *Catalysis Communications*, 2011, **12**, 1437-1441.
25. P. N. Trikalitis, T. V. Bakas, A. C. Moukarika, A. T. Sdoukos, T. Angelidis and P. J. Pomonis, *Applied Catalysis a-General*, 1998, **167**, 295-308.
26. R. D. Shannon, *Acta Crystallographica Section A*, 1976, **32**, 751-767.
27. V. M. Goldschmidt, *Naturwissenschaften*, 1926, **14**, 477-485.
28. H. D. Megaw, *Proceedings of the Physical Society of London*, 1946, **58**, 133-&.
29. T. Maekawa, K. Kurosaki and S. Yamanaka, *Journal of Alloys and Compounds*, 2006, **426**, 46-50.
30. G. Liu and J. E. Greedan, *Journal of Solid State Chemistry*, 1994, **110**, 274-289.

Chapter 6

Conclusions and future work

6.1 CoMn for Fischer-Tropsch

In this program of study we have investigated a wide range of variables in the preparation step of the CoMn catalyst supported on carbon with the overall aim of increasing CO conversion and selectivity to desirable C₂-C₄ hydrocarbons.

Our investigations have outlined an acceptable range of heat treatment temperatures, metal loadings, catalyst compositions and reduction regimes. Alteration of these parameters can, in several cases, be used to adjust both the CO conversion and selectivity patterns in the manner desired.

Of particular note was the autoreduction effect noted at 400°C when a cobalt catalyst mounted on a carbon support is heat treated in an inert atmosphere. The reduction of the catalyst to what is believed to be the phases present in the reaction (Co metal and MnO)

before a reduction step has even been performed speaks highly of the reducibility of these catalysts under these conditions.

Also noteworthy was the series of experiment showing the effect of alteration of the Co-Mn ratio in the catalyst composition. This could be demonstrably shown to reduce the α values of the catalysts with increasing Mn content, allowing for the increased production of the valuable C₂-C₄ products.

The catalysts were also seen to be highly reproducible. This allows us to use certain interesting results as a reliable baseline for future modification of the catalysts. In particular, the area of promoter addition to these catalysts is a relatively untouched area for us. Alkali promoter agents such as potassium are well documented for their ability to alter the selectivity patterns of cobalt catalysts, and precious metal additives such as ruthenium are known to aid the reducibility of cobalt.

Attempts should also be made to quantify the metal surface areas, as opposed to the surface area of the overall catalyst system. The carbon support has a very high surface area, but does not play any part in the reaction, and thus the surface area readings could be misleading as things stand. Along this line of reasoning, methods for improving the dispersion of the cobalt metal should be investigated. Literature on the subject suggests that a chelating agent such as sucrose is capable of achieving this.

6.2 CoMo for alcohol synthesis

Unfortunately, the attempted reproduction of the previous student's catalyst did not meet with any great success. However, the catalysts later prepared to test the effects of varying metal ratios performed far better than we might have expected. The first thing to be done on this front is to ensure the reproducibility of the better catalysts, such as Co:Mo 25:25. This catalyst in particular was worthy of further study, displaying as it did remarkably high total alcohol production and particularly good selectivity to ethanol. Though the conversion was below that which had previously been reported, the selectivities were so high that it actually equalled the target catalyst in terms of C₂-C₄ alcohols yield

More of an effort must be made to understand why we were unable to reproduce the original catalyst, however. If it could be ascertained why the original conversions were so much higher than ours, it may be possible to work back to the high conversion, or if not apply the knowledge to future catalysts.

As with the hydrocarbons catalysts, efforts should be made to try methods for increasing the cobalt dispersion. This is perhaps more pressing for the alcohols catalyst, as it already displays a very impressive selectivity pattern but poor conversion. The alkenes catalysts are already high-conversion, and so more effort should be made to improve their selectivities.

6.3 Perovskites as catalysts and supports

The results of the perovskites unearthed many trends which could be useful for future reactions. The conclusion that the acid-base properties of the material can be tuned could prove to be of great benefit in future reactions. It would be interesting to try a wider range of materials, but first priority should probably be given to making pure versions of the strontium and barium vanadate perovskites, so as to determine if the acid-base properties are truly as tuneable as we think they are. It would also be of great benefit to back up the IPA test data with concrete measurements of the number of acid and base sites present on the material. This could be accomplished using a temperature programmed desorption technique.

A particular failing of the perovskites as both catalysts and as supports was that of their incredibly low surface areas. Investigations should be undertaken to determine methods of increasing the surface areas of these materials, such as by templating, the combustion method, or something more exotic such as growing nanoribbons.

An attempt should also be made to link the two areas of study; perovskites and Fischer-Tropsch. It has been reported the Co-Cu perovskites can be active for the production of oxygenates, and it would be worth investigating if this could apply for other metals and reactions too.